



ПОЛИТЕХ
Санкт-Петербургский
политехнический университет
Петра Великого

Инженерно-строительный институт
Центр дополнительных профессиональных программ
195251, г. Санкт-Петербург, Политехническая ул., 29,
тел/факс: 552-94-60, www.stroikursi.spbstu.ru,
stroikursi@mail.ru

**Приглашает специалистов организаций, вступающих в СРО,
на курсы повышения квалификации (72 часа)**

Код	Наименование программы	Виды работ*
Курсы по строительству		
БС-01-04	«Безопасность и качество выполнения общестроительных работ»	п.1,2, 3, 5, 6, 7, 9, 10, 11, 12, 13, 14
БС-01	«Безопасность и качество выполнения геодезических, подготовительных и земляных работ, устройства оснований и фундаментов»	1,2,3,5
БС-02	«Безопасность и качество возведения бетонных и железобетонных конструкций»	6,7
БС-03	«Безопасность и качество возведения металлических, каменных и деревянных конструкций»	9,10,11
БС-04	«Безопасность и качество выполнения фасадных работ, устройства кровель, защиты строительных конструкций, трубопроводов и оборудования»	12,13,14
БС-05	«Безопасность и качество устройства инженерных сетей и систем»	15,16,17,18,19
БС-06	«Безопасность и качество устройства электрических сетей и линий связи»	20,21
БС-08	«Безопасность и качество выполнения монтажных и пусконаладочных работ»	23,24
БС-12	«Безопасность и качество устройства мостов, эстакад и путепроводов»	29
БС-13	«Безопасность и качество выполнения гидротехнических, водолазных работ»	30
БС-14	«Безопасность и качество устройства промышленных печей и дымовых труб»	31
БС-15	«Осуществление строительного контроля»	32
БС-16	«Организация строительства, реконструкции и капитального ремонта. Выполнение функций технического заказчика и генерального подрядчика»	33
Курсы по проектированию		
БП-01	«Разработка схемы планировочной организации земельного участка, архитектурных решений, мероприятий по обеспечению доступа маломобильных групп населения»	1,2,11
БП-02	«Разработка конструктивных и объемно-планировочных решений зданий и сооружений»	3
БП-03	«Проектирование внутренних сетей инженерно-технического обеспечения»	4
БП-04	«Проектирование наружных сетей инженерно-технического обеспечения»	5
БП-05	«Разработка технологических решений при проектировании зданий и сооружений»	6
БП-06	«Разработка специальных разделов проектной документации»	7
БП-07	«Разработка проектов организации строительства»	8
БП-08	«Проектные решения по охране окружающей среды»	9
БП-09	«Проектные решения по обеспечению пожарной безопасности»	10
БП-10	«Обследование строительных конструкций и грунтов основания зданий и сооружений»	12
БП-11	«Организация проектных работ. Выполнение функций генерального проектировщика»	13
Э-01	«Проведение энергетических обследований с целью повышения энергетической эффективности и энергосбережения»	
Курсы по инженерным изысканиям		
И-01	«Инженерно-геодезические изыскания в строительстве»	1
И-02	«Инженерно-геологические изыскания в строительстве»	2,5
И-03	«Инженерно-гидрометеорологические изыскания в строительстве»	3
И-04	«Инженерно-экологические изыскания в строительстве»	4
И-05	«Организация работ по инженерным изысканиям»	7

*(согласно приказам Минрегионразвития РФ N 624 от 30 декабря 2009 г.)

**По окончании курса слушателю выдается удостоверение о краткосрочном повышении
квалификации установленного образца (72 ак. часа)**

Для регистрации на курс необходимо выслать заявку на участие, и копию диплома об образовании по телефону/факсу: 8(812) 552-94-60, 535-79-92, , e-mail: stroikursi@mail.ru.

<http://www.engstroy.spbstu.ru> – полнотекстовая версия журнала в сети Интернет.

Бесплатный доступ, обновление с каждым новым выпуском

Инженерно-строительный журнал

НАУЧНОЕ ИЗДАНИЕ

ISSN 2071-4726, 2071-0305

Свидетельство о государственной регистрации: ПИ №ФС77-38070, выдано Роскомнадзором

Специализированный научный журнал. Выходит с 09.2008.

Включен в Перечень ведущих периодических изданий ВАК РФ

Периодичность: 8 раз в год

Учредитель и издатель:

Санкт-Петербургский политехнический университет Петра Великого

Адрес редакции:

195251, СПб, ул. Политехническая, д. 29, Гидрокорпус-2, ауд. 227А

Главный редактор:

Екатерина Александровна Линник

Научный редактор:

Николай Иванович Ватин

Технический редактор:

Ксения Дмитриевна Борщева

Редакционная коллегия:

д.т.н., проф. В.В. Бабков;
д.т.н., проф. М.И. Бальзаников;
к.т.н., проф. А.И. Боровков;
д.т.н., проф. Н.И. Ватин;
PhD, проф. М. Вельжкович;
д.т.н., проф. А.Д. Гиргидов;
д.т.н., проф. Э.К. Завадаскас;
д.ф.-м.н., проф. М.Н. Кирсанов;
D.Sc., проф. М. Кнежевич;
д.т.н., проф. В.В. Лалин;
д.т.н., проф. Б.Е. Мельников;
д.т.н., проф. Ф. Неправишта;
д.т.н., проф. Р.Б. Орлович;
Dr. Sc. Ing., professor
Л. Пакрастиньш;
Dr.-Ing. Habil., professor
Х. Пастернак;
д.т.н., проф. А.В. Перельмутер;
к.т.н. А.Н. Пономарев;
д.т.н., доцент В.В. Сергеев;
д.ф.-м.н., проф. М.Х. Стрелец;
д.т.н., проф. О.В. Тараканов;
д.т.н., проф. В.И. Травуш

Дата выхода: 21.05.2018

Содержание

Черняев А.А. Вариантное проектирование стальных балочных клеток геометрическими методами	3
Кафя М.А., Качуй А. Поведение концентрических раскосов с встроенным предохранителем по сжимающей нагрузке	16
Галямичев А.В., Кирикова В.А., Герасимова Е.А., Спринце А. Несущая способность крепления навесных фасадных систем к сэндвич-панелям	30
Туснин А.Р. Коэффициенты динамичности при повреждении опор неразрезных балок	47
Горшков А.С., Ватин Н.И., Рымкевич П.П., Кудревич О.О. Период возврата инвестиций в энергосбережение	65
Зуйков А.Л., Бакуняева В.В., Артемьева Т.В., Жажа Е.Ю. Режимы течения в классическом водомерном канале Вентури	76
Шеховцова С.Ю., Коротков А.В., Высоцкая М.А. Метод прогнозирования эффективности катионных битумных эмульсий	91
Муцанов В.Ф., Оржеховский А.Н., Зубенко А.В., Фоменко С.А. Уточненные методы расчета и проектирования инженерных сооружений	101
Ведищева Ю.С., Ананьин М.Ю., Ал Али М., Ватин Н.И. Влияние теплопроводных включений на надежность системы «сэндвич-панель – каркас здания»	116
Стручкова А.Я., Барабанщиков Ю.Г., Семенов К.В., Шайбакова А.А. Тепловыделение цемента и расчеты трещиностойкости бетонных массивов	128
Беспалов В.В., Ючер Д., Салманов И.Д., Курбанов И.Н., Купавых С.В. Деформационная совместимость каменной кладки с композитными материалами	136
Рассохин А.С., Пономарев А.Н., Фиговский О.Л. Микрокремнеземы различных типов для высокопрочных мелкозернистых бетонов	151
Самарин О.Д. Распространение температурных волн в пустотелом толстостенном цилиндре	161
Белостоцкий А.М., Акимов П.А., Негрозов О.А., Петряшев Н.О., Петряшев С.О., Щербина С.В., Каличава Д.К., Кайтуков Т.Б. Адаптивные конечноэлементные модели в системах мониторинга зданий и сооружений	169

© ФГАОУ ВО СПбПУ, 2018

На обложке: иллюстрации авторов к статьям номера

Контакты:

Тел. +7(812)535-52-47 E-mail: mce@spbstu.ru

Web: <http://www.engstroy.spbstu.ru>

<http://www.engstroy.spbstu.ru> – full-text open-access version in Internet. It is updated immediately with each new issue.

Magazine of Civil Engineering

SCHOLAR JOURNAL

ISSN 2071-4726

Peer-reviewed scientific journal

Start date: 2008/09

8 issues per year

Publisher:

Peter the Great St. Petersburg
Polytechnic University

Indexing:

Scopus, Russian Science Citation
Index (WoS), Compendex, DOAJ,
EBSCO, Google Academia, Index
Copernicus, ProQuest, Ulrich's Serials
Analysis System

Corresponding address:

227a Hydro Building, 29
Polytechnicheskaya st., Saint-
Petersburg, 195251, Russia

Editor-in-chief:

Ekaterina A. Linnik

Science editor:

Nikolay I. Vatin

Technical editor:

Ksenia D. Borshcheva

Editorial board:

V.V. Babkov, D.Sc., professor
M.I. Balzannikov, D.Sc., professor
A.I. Borovkov, PhD, professor
M. Veljkovic, PhD, professor
E.K. Zavadskas, D.Sc., professor
M.N. Kirsanov, D.Sc., professor
M. Knezevic, D.Sc., professor
V.V. Lalin, D.Sc., professor
B.E. Melnikov, D.Sc., professor
F. Nepravishhta, D.Sc., professor
R.B. Orlovich, D.Sc., professor
L. Pakrastinsh, Dr.Sc.Ing., professor
H. Pasternak, Dr.-Ing.habil.,
professor
A.V. Perelmuter, D.Sc., professor
A.N. Ponomarev, PhD, professor
V.V. Sergeev, D.Sc., associate
professor
M.Kh. Strelets, D.Sc., professor
O.V. Tarakanov, D.Sc., professor
V.I. Travush, D.Sc., professor

Contents

Chernyaev A.A. Alternative engineering of steel girder cages by geometrical methods.	3
Kafi M.A., Kachooee A. The behavior of concentric brace with bounded fuse	16
Galyamichev A.V., Kirikova V.A., Gerasimova E.A., Sprince A. Bearing capacity of facade systems fixing to sandwich panels	30
Tusnin A. Dynamic factors in case of damaging continuous beam supports	47
Gorshkov A.S., Vatin N.I., Rymkevich P.P., Kydrevich O.O. Payback period of investments in energy saving	65
Zuikov A.L., Bakunjaeva V.V., Artemyeva T.V., Zhazha E.Yu. Flow states in the classical Venturi channel water gauge	76
Shekhovtsova S.Yu., Korotkov A.V., Vysotskaya M.A. Method of forecasting the effectiveness of cationic bitumen emulsions	91
Mushchanov V.P., Orzhekhovskii A.N., Zubenko A.V., Fomenko S.A. Refined methods for calculating and designing engineering structures	101
Vedishcheva I.S., Ananin M.Y., Al Ali M., Vatin N.I. Influence of heat conducting inclusions on reliability of the system "sandwich panel –metal frame"	116
Struchkova A.Y., Barabanshchikov Yu.G., Semenov K.S., Shaibakova Al.A. Heat dissipation of cement and calculation of crack resistance of concrete massifs	128
Bespalov V.V., Ucer D., Salmanov I.D., Kurbanov I.N., Kupavykh S.V. Deformation compatibility of masonry and composite materials	136
Rassokhin A.S., Ponomarev A.N., Figovsky O.L. Silica fumes of different types for high-performance fine-grained concrete	151
Samarin O.D. The temperature waves motion in hollow thick-walled cylinder	161
Belostotsky A.M., Akimov P.A., Negrozov O.A., Petryashev N.O., Petryashev S.O., Sherbina S.V., Kalichava D.K., Kaytukov T.B. Adaptive finite-element models in structural health monitoring systems	169

© Peter the Great St. Petersburg Polytechnic University. All rights reserved.

On the cover: authors' illustrations

+7(812) 535-52-47

E-mail: mce@spbstu.ru

Web: <http://www.engstroy.spbstu.ru/eng/index.html>

doi: 10.18720/MCE.78.1

Alternative engineering of steel girder cages by geometrical methods

Вариантное проектирование стальных балочных клеток геометрическими методами

A.A. Chernyaev,
Orel State University, Orel, Russia

Канд. техн. наук, доцент А.А. Черняев,
Орловский государственный университет,
г. Орел, Россия

Key words: steel girder cages; alternative engineering; geometrical methods; structural mechanics

Ключевые слова: стальные балочные клетки; вариантное проектирование; геометрические методы; строительная механика

Abstract. Steel girder cages are widely used as plant buildings ceilings, bridge vaults, locks of hydraulic engineering constructions and other construction objects. An important task in case of their designing is the search of the most economic constructive decision with the smallest amounts of material. Therefore the great value in construction mechanics is attached to the development of methods of search of the most rational and optimal constructive solutions. The new technique of alternative engineering of steel girder cages with various cell forms, i.e. rectangular, triangular, rhombic and other, is offered. The technique is based on the principles of physicommechanical analogies and geometrical methods of construction mechanics. As a research object for a numerical example the girder cage of 12 x 6 m is considered. It has brick walls supporting. Girder profile is made of rolled sections, flooring is steel and solid. The studies showed that using a rhombic cage is the most economic.

Аннотация. Стальные балочные клетки широко используются в качестве перекрытий промышленных зданий, пролетных строений мостов, затворов гидротехнических сооружений и других объектов строительства. Важной задачей при их проектировании является поиск наиболее экономичного конструктивного решения, на выполнение которого затрачивалось бы наименьшее количества материала. Поэтому большое значение в строительной механике придают разработке методов поиска наиболее рациональных и оптимальных конструктивных решений. Предлагается новая методика вариантного проектирования стальных балочных клеток с различной в плане формой ячейки: прямоугольной, треугольной, ромбической и другой. Методика основана на использовании принципов физико-механических аналогий и геометрических методов строительной механики. В качестве объекта исследования для численного примера рассматривается балочная клетка размерами 12 x 6 м с опиранием на кирпичные стены. Сечения балок из прокатных профилей, настил стальной сплошной. Исследования показали, что наиболее экономичный вариант достигается при использовании ромбической решетки.

1. Introduction

Working platforms and many plants ceilings, bridge vaults, locks of hydraulic engineering constructions are often made in the form of steel girder cages. The design of a girder cage presents system of supporting girders of one or several directions intended for bearing existing loadings and their further transferring to columns or walls. Supporting girders are covered with steel, steel concrete or wooden flooring.

One of the major requirements when designing steel structures is metal economy as material cost makes more than a half of cost of designs. Therefore engineering of girder cages is conducted by comparison of a material capacity of various options of systems of supporting girders. Normal and complicated types of girder cages with a different spacing of flooring and minor girders and a cell are considered. The spacing of girders is set according to the existing loadings, the size of a flight, a type of flooring, purpose of the building, experience of engineering. For girders with steel flooring a usual spacing is from 0.6 m to 1.6 m, with steel concrete flooring it is from 2 m to 3.5 m, for minor girders it makes from

2 m to 5 m. Thickness of steel flooring is accepted from 6 to 40 mm. It is impossible to learn in advance what version of the project will allow the smallest material consumption. Therefore, when designing the supporting constructions the task of development of methods of search of rational and optimal constructive solutions is important [1,2].

Now computer programs of the final and element analysis of the intense deformed condition of designs are widely used as the tool of computing engineers, they are: SCAD, Nastran, Ansys, etc. [3, 4]. In tasks of alternative engineering and optimization of designs of steel girder cages numerical methods are also used [5, 6]. However, direct borrowing of universal numerical optimization methods which in some works are referred to as "search optimization methods" from mathematics leads to a problem of increase in dimension of tasks and significant growth in calculations in case of increase in number of project variables. Development of methodology of nonlinear mathematical programming should be pointed out from mathematical works on optimization methods for the purposes of designing and engineering of constructions. It requires accurate formalization in case of formulation of an optimization problem [7].

A set of methods which can be used when engineering supporting constructions is very broad: from rather universal, such as nonlinear programming and genetic algorithms, to problem-oriented [7-19]. All of them have advantages and disadvantages and means for setup which correct applying can strongly influence the speed of work of methods and even correctness of results.

In this work the new technique of alternative engineering of steel girder cages with various in the plan cell forms with the choice of the most rational constructive decision from a condition of the smallest material costs for its production is offered. The technique is based on use of the principles of physicommechanical analogies and geometrical methods of structural mechanics [20].

2. Methods

Geometrical methods of structural mechanics are based on mathematical analogy and the functional correlation, separate physicommechanical characteristics of the intense deformed status of plane elements of constructions (pressures, sags, oscillation frequencies, critical effort of loss of stability and others) in the form of plates, membranes, bar cross-sections with their geometrical parameters (sizes, angles, a ratio of the sides and so on). For this, it is necessary to choose some characteristic of a geometric shape for plates and membranes or of cross-section for the rods. And if it is proved that it is related to the parameters of the stress-strain state by some function or expression, then it is possible to study the change in the stress-strain state parameters using the chosen geometric characteristic.

The originators of geometric methods for solving some applied problems in the theory of elasticity and mathematical physics were the well-known American mathematicians G. Polia and G. Sege [21, 22]. They were the first to adapt the known isoperimetric theorem for applications in physics. The theorem states that of all flat shapes of equal perimeter the circle has the largest area. Assuming this, they have proved that of all plates of a given area with fixed contour, the circular one has the lowest fundamental frequency of vibration. In their studies, as a geometric characteristic of the shape of plates, they used the following isoperimetric quotient [22]:

$$\frac{4\pi A}{L^2}, \quad (1)$$

where A is area of a plate; L is perimeter.

As geometrical characteristics known also ones are: form coefficient [20], perimeter, inradius, circumradius, second moment of area and some other.

In this work we suggest using of mapping radiuses of the areas restricted to a circuit of plates, membranes, bar cross-sections. Mapping radiuses are the radiuses received in case of conformal mapping of plane area on an interior and exterior of a circle. They are known from the theory of conformal mapping [23, 24]. Where, the mapping of a shape (domain) onto another one, at which two curves, intersecting at an angle at the inner point of the first shape, are transformed into curves intersecting at the same angle at the inner point of the second shape, is called conformal mapping. In Figure 1 show an example of conformal mapping of a triangular domain onto a unit circle.

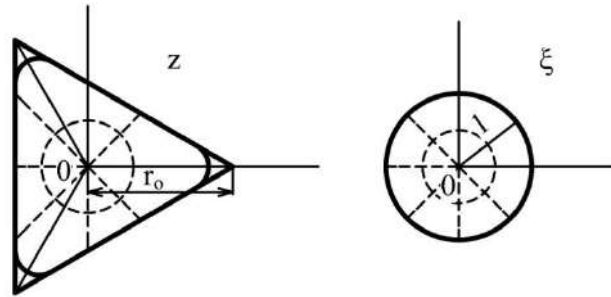


Figure 1. An example of conformal mapping of a triangular domain onto a unit circle

The mapping (Figure 1) is performed by the following function [25]:

$$z = \omega(\zeta) = 0.566,100 \cdot r_0 \cdot \zeta + 0.094,350 \cdot r_0 \cdot \zeta^4 + 0.044,929 \cdot r_0 \cdot \zeta^7 + 0.027,956 \cdot r_0 \cdot \zeta^{10} + 0.019,712 \cdot r_0 \cdot \zeta^{13} + 0.014,948 \cdot r_0 \cdot \zeta^{16}, \quad (2)$$

where z, ξ are the complex variables (the points of the complex plane); r_0 is radius of a circle circumscribed around a triangle.

2.1. Definition of terms

In case of mapping the domain z onto the interior of a circle in the plane ξ , an arbitrary point belonging to domain z shifts to the center of the circle. The circle is characterized by an internal mapping radius \dot{r} .

If in a simply-connected domain z we consider an infinitely remote point $z = \infty$, then this domain should be conformally mapped onto the outer domain of a circle in the plane ξ so that the infinitely remote point returns into itself. The radius of the circle is called the outer radius of the domain z and its length is denoted by the symbol \bar{r} [24].

2.2. Formulae

Formulas for finding internal \dot{r} and external \bar{r} mapping radiuses for some singly connected domains take the form [22, 26]:

– for a radius circle a

$$\dot{r} = a, \quad \bar{r} = a; \quad (3)$$

1.

– for the correct n -squares

$$\dot{r} = \frac{G\left(1 - \frac{1}{n}\right)}{2^{1-\frac{2}{n}} G\left(\frac{1}{2}\right) G\left(\frac{1}{2} - \frac{1}{n}\right)} L, \quad \bar{r} = \frac{G\left(1 + \frac{1}{n}\right)}{2^{1+\frac{2}{n}} G\left(\frac{1}{2}\right) G\left(\frac{1}{2} + \frac{1}{n}\right)} L, \quad (4)$$

where n is number of the sides; L is perimeter; $G(x)$ is Gamma-function;

– for random triangles with angles $\pi\alpha, \pi\beta, \pi\gamma$

$$\dot{r} = 4\pi \cdot f(\alpha) f(\beta) f(\gamma) \cdot \rho, \quad \bar{r} = \frac{A}{\pi \dot{r}} \quad (5)$$

where

$$f(x) = \frac{1}{G(x)} \left\{ \frac{x^x}{(1-x)^{1-x}} \right\}^{\frac{1}{2}}; \quad (6)$$

ρ is a long radius; A is square; x is α or β or γ ; $G(x)$ is the same that in (4).

– for isosceles triangles with angles $\alpha = \beta$ expressions (5) will take the following form:

$$\dot{r} = 4\pi \cdot f^2(\alpha) f(\gamma) \cdot \rho; \quad \bar{r} = \frac{ctg\alpha \cdot h^2}{\pi \dot{r}}, \quad (7)$$

where α is an equal base angle; h is height;

– for rectangular triangles ($\alpha = \pi/2$) from expression (5) follows

$$\bar{r} = \frac{\sin 2\alpha \cdot c^2}{4\pi \dot{r}}, \quad (8)$$

where α is angle in case of hypotenuse; c is hypotenuse;

– for rhombs with angle $\pi\alpha$

$$\dot{r} = \frac{\pi^{\frac{1}{2}}}{G\left(\frac{\alpha}{2}\right)G\left(\frac{1-\alpha}{2}\right)} L, \quad \bar{r} = \frac{\pi^{\frac{1}{2}}}{8G\left(1-\frac{\alpha}{2}\right)G\left(\frac{1+\alpha}{2}\right)} L; \quad (9)$$

where $G(x)$ and L is the same that in (4);

– for ellipses with semiaxis a and b ($a \geq b$)

$$\dot{r} = \bar{r} \left\{ \sum_{n=0}^{\infty} q^{n(n+1)} \right\}^{-1} \left\{ 1 + 2 \sum_{n=1}^{\infty} q^{n^2} \right\}^{-1}, \quad \bar{r} = \frac{a+b}{2}, \quad (10)$$

where

$$q = \frac{(a-b)^2}{(a+b)^2}; \quad (11)$$

– for rectangles with the sides a и b ($a \geq b$)

$$\dot{r} = \frac{2}{\pi} b \left(1 + 2 \sum_{n=1}^{\infty} q^{n^2} \right)^{-2}, \quad \begin{cases} \frac{a}{\bar{r}} = \pi \cos^2 \alpha \sum_{k=0}^{\infty} \frac{((2k-1)!!)^2}{2^{2k} (k+1)!k!} \cos^{2k} \alpha; \\ \frac{b}{\bar{r}} = \pi \sin^2 \alpha \sum_{k=0}^{\infty} \frac{((2k-1)!!)^2}{2^{2k} (k+1)!k!} \sin^{2k} \alpha; \end{cases} \quad (12)$$

where $q = e^{-\frac{\pi a}{b}}$, α is argument of complex numbers (circle points which images are rectangle vertexes in case of conformal mapping).

2.3. Mathematical functional correlation

Mathematical analogy and the functional correlation of mapping radiuses with characteristics of the intense deformed status of elements of constructions in the form of plates, membranes, bar cross-sections are defined in works [27, 28].

Since the stress state of a plate in bending is under consideration, then, the resulting relationship for the maximum deflection of a plate should be also considered. The maximum deflection of a plate w_{\max} is connected with mapping radiuses \dot{r} and \bar{r} by expression [27]:

$$w_{\max} \leq \pi k \left(\frac{\dot{r}}{\bar{r}} \right) \cdot \frac{qA^2}{D}, \quad (13)$$

where k – the numerical constant turning expression into equality for round plates, in case of a hinged fixing of a plate $k = 1.96$, in case of rigid restraint of a plate $k = 0.504$; q – uniformly distributed load; A – area of a plate; D – cylindrical rigidity of a plate:

$$D = \frac{Et^3}{12(1-\nu^2)} \quad (14)$$

where E – modulus of elasticity; t – thickness of a plate; ν – Poisson's coefficient.

The expression (13) shows, that maximum deflection of a plate W_{\max} is directly proportional to mapping radiuses \dot{r} and \bar{r} . It means that, the change in maximum deflection W_{\max} for plates of various shapes can be studied by defining the change in mapping radiuses \dot{r} and \bar{r} . Mapping radiuses \dot{r} and \bar{r} in expression (13) characterize the geometric shape of a plate.

3. Results and Discussion

In work [29] the technique, an algorithm (Figure 2) and the special computer program “RR Geometric Modeling” the certificate on No 2013613173 patent of Russia (fig. 3) on alternative engineering of plate and rod load-bearing units by geometrical modeling of their form from a condition of equal rigidity was developed.

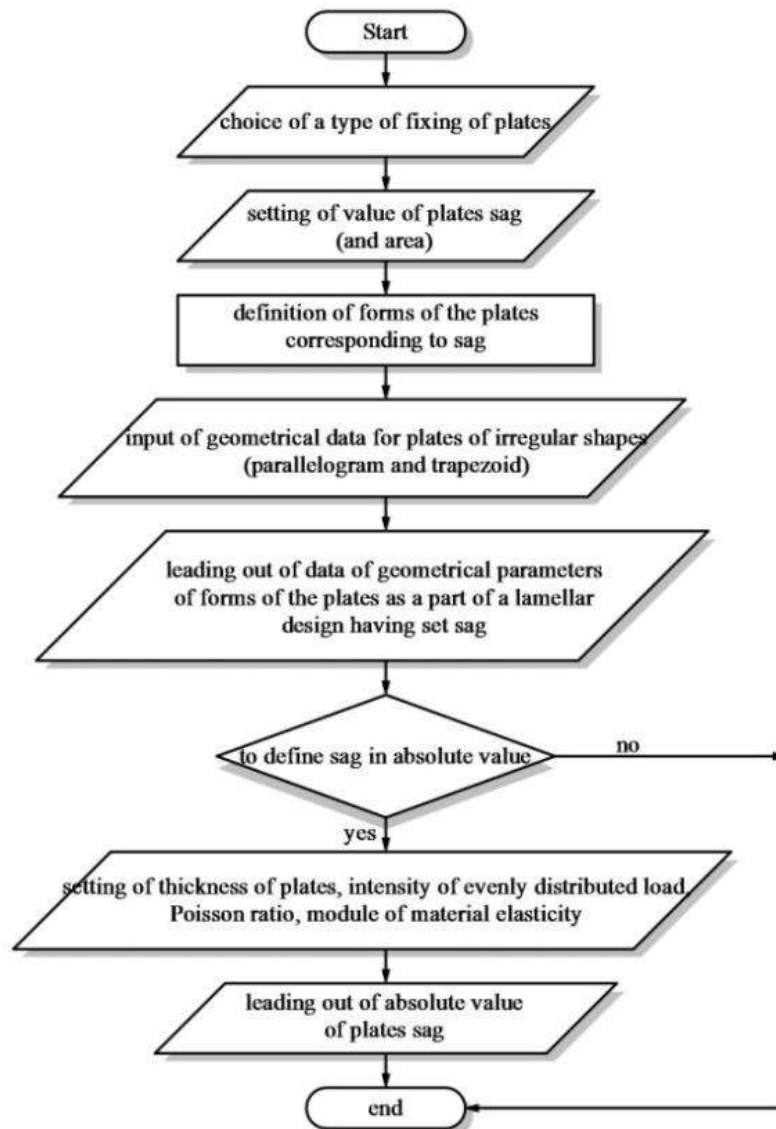


Figure 2. Algorithm of the computer program “RR Geometric Modeling”

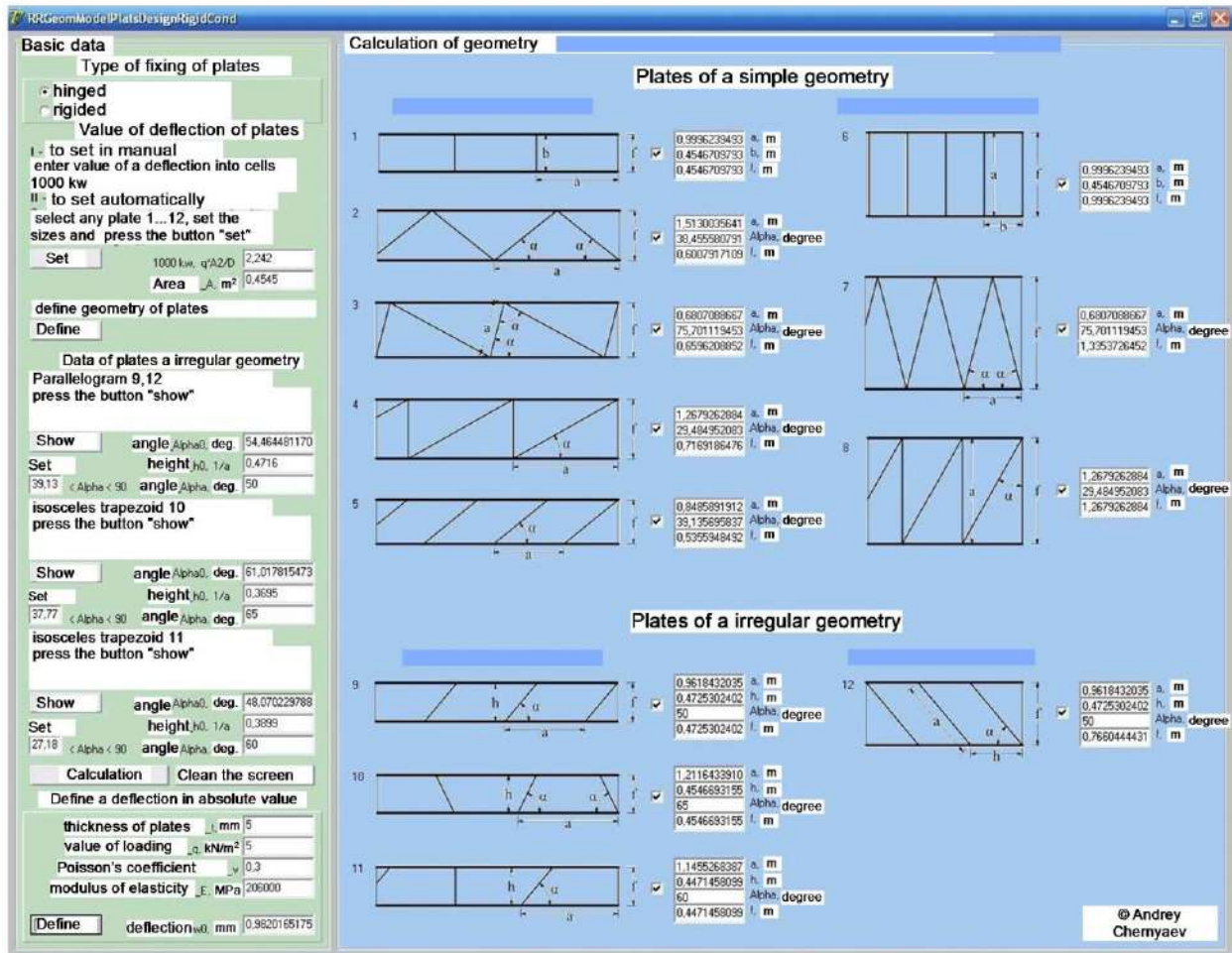


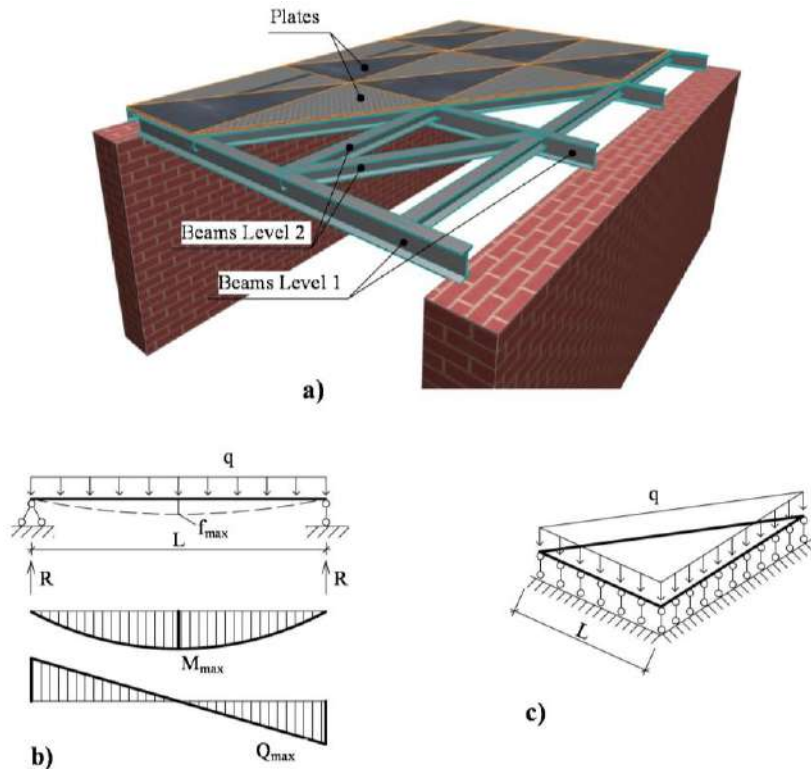
Figure 3. Working window of the computer program “RR Geometric Modeling”

The program performs the following procedure. The method of fixing of plates on a contour is chosen: either hinged fixing or tough jamming. Plates are a part of the supporting panel with two basic parallel guideways (longerons, girders). Plates loading is considered regularly distributed on the entire surface. Restriction for plates sag is set. The program considers plates of various forms in the plan (rectangular, triangular, rhombic, parallelogram, trapezoid) and determines their geometrical parameters corresponding to the set sag. In other words, the program determines geometry of plates (the sizes of sides, corners, sides ratio, etc.) of various forms which provide identical set sag to all the plates.

Let us consider use of this program and a technique [29] for alternative engineering of a steel girder cage.

The model of a steel girder cage represents a cross system of cores of the first and second levels which support plates. Girders are designed in the form of rods; the steel flooring is designed in the form of thin plates. Girders of the first level are freely based on walls, such binding is considered hinged. Girders of the second level are connected to girders of the first level by means of steel slips on bolts, such binding is considered hinged. The steel flooring is welded to flooring girders by means of semi-automatic welding. Strictly speaking, such binding is considered tough, however in calculations such binding is considered hinge fixed in safety margin of material (Figure 4).

Rods and plates under the influence of vertical loading experience the intense deformed condition of a cross bend. In case of this type of the intense deformed condition determination of the necessary sizes of bar cross-sections and plates is conducted from strength conditions (on the allowed stress) and rigidity (on the allowed deflection) [30, 31].



a) general view, b) model of flooring beams, c) model of a flooring

Figure 4 Steel girder cage supported by walls

At loading $q < 50 \text{ kN/m}^2$ flooring strength is provided and its rigidity is calculated. The maximum permissible ratio of span of beam L to its thickness t is determined by A.L. Teloyan's formula [1]:

$$\frac{L}{t} = \frac{4 \cdot n}{15} \left(1 + 72 \frac{E_1}{n^4 \cdot q} \right), \quad (15)$$

where E_1 – flooring cylindrical rigidity:

$$E_1 = \frac{E}{1 - \nu^2} = \frac{2.06 \cdot 10^4}{1 - 0.3^2} = 2.26 \cdot 10^4 \frac{\text{kN}}{\text{cm}^2},$$

where $E = 2.06 \cdot 10^4 \text{ kN/cm}^2$ – modulus of elasticity of steel; $\nu = 0.3$ – Poisson's coefficient of steel; n – quantity inverse to a limit relative flooring sag; q – uniformly distributed load of a flooring.

The equation of strength of flooring girders has a form [30]:

$$\sigma = \frac{M_{max}}{c_1 W} < R_y \gamma_c, \quad (16)$$

where σ – normal stress; M_{max} – the maximum bending moment; c_1 – coefficient considering development of plastic deformations in section; W – moment of resistance of cross section; R_y – proof strength; γ_c – condition load effect factor of a girder.

The maximum bending moment (Figure 4, b) [1]:

$$M_{max} = \frac{qL^2}{8}. \quad (16)$$

From a formula (16) we define the required moment of resistance of girder cross section:

$$W = \frac{M_{max}}{c_1 \cdot R_y \cdot \gamma_c}, \quad (18)$$

The condition of flooring girders rigidity has a form [1]:

$$f_{max} = \frac{5}{384} \cdot \frac{q \cdot L^4}{E \cdot J} < f_u. \quad (19)$$

where f_{max} – maximum deflection of beam; J – moment of inertia of girder cross section; f_u – allowed deflection.

The maximum deflection of a plate w_{max} is connected with mapping radiuses r and \bar{r} by expression (13).

Normal σ_x , σ_y , and tangent τ_{xy} stress are defined through sag w plate by means of the known formulas of the theory of elasticity [18]:

$$\begin{cases} \sigma_x = -\frac{E\gamma}{1-\nu^2} \left(\frac{\partial^2 w}{\partial x^2} + \nu \frac{\partial^2 w}{\partial y^2} \right), \\ \sigma_y = -\frac{E\gamma}{1-\nu^2} \left(\frac{\partial^2 w}{\partial y^2} + \nu \frac{\partial^2 w}{\partial x^2} \right), \\ \tau_{xy} = -\frac{E\gamma}{1+\nu} \frac{\partial^2 w}{\partial x \partial y}. \end{cases} \quad (20)$$

where $\frac{\partial^2}{\partial x^2} + \frac{\partial^2}{\partial y^2}$ – Laplacian operator; x , y , γ – working space coordinates.

We will carry out the search of versions of constructive solutions for steel girder cages in the following sequence.

1. Restriction for flooring sag is set according to existing rules [31].
2. By a formula (15), flooring thickness is defined according to a range on the operating loadings.
3. By means of formulas (20) flooring stress through a sag are defined.
4. By means of the special computer program (Figure 3) the sizes of plates of various forms in the plan are defined: rectangular, triangular, rhombic, parallelogram, trapezoid. All plates have the identical maximum stress and a sag, the identical area, but a different form and sizes.
5. Cross sections of girders of the second level are defined. For this purpose loads of girders transferred from flooring are gathered. By means of a formula (18) the required girder section is defined. Section is accepted according to a range of rolled iron. The condition of rigidity is checked (19).
6. Cross sections of girders of the first level are defined. For this purpose loads of girders transferred from above from girders of the second level and flooring are gathered. Similarly, by means of a formula (18) the required section of a girder is defined and is accepted according to a range.
7. Ceiling is done with the received variants of girder cages.
8. We determine the mass of material which is spent for each option of a girder cage. We compare material capacity and choose the variant with the smallest material consumption. This option will be the most economic.

Let us consider a numerical example. It is necessary to design a steel girder cage of a plant building with sizes in axes: length is 12 m, width is 6 m. Basic data:

Material – C245 steel, calculated resistance $R_y = 23$ MPa [30].

Flooring – solid steel in accordance with State Standard Specification 19903-74 on sheet steel.

Girder section of a flooring of the second level – equilateral angle in accordance with state standard specification 8509-93.

Girder section of a flooring of the first level – either flange beam in accordance with state standard specification 8239-89, or a channel in accordance with State Standard Specification 8240-89.

Load of ceiling – $q = 5 \text{ kN/m}^2$.

Solution.

1. According to the operating construction regulations [31] the flooring and girders sags of designs of coverings and ceilings mustn't exceed extreme value which depends on flight. For a flooring flight width, as a rule, doesn't exceed $L = 3 \text{ m}$. For this flight the permitted sag constitutes 2 cm .

2. We determine the required thickness of flooring by a formula (15):

$$\frac{L}{t} = \frac{4 \cdot n}{15} \left(1 + 72 \frac{E_1}{n^4 \cdot q} \right) = \frac{4 \cdot 150}{15} \left(1 + 72 \frac{2.26 \cdot 10^4}{150^4 \cdot 5 \cdot 10^{-4}} \right) = 297, \quad (15)$$

where $n = 150$ is quantity inverse to a limit relative sag of flooring according to [31].

So, $t = \frac{L}{297} = \frac{300}{297} = 1.01 \text{ cm}$. In accordance with State Standard Specification 19903-74 we accept $t = 10 \text{ mm}$.

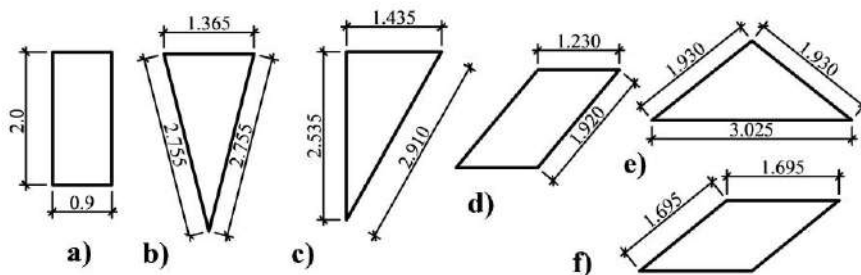
Taking into account dead load flooring load will constitute:

$$q_1 = q + g_1 = 5 + t \cdot A \cdot g_{steel} = 5 + 0.01 \cdot 1.8 \cdot 78.5 = 5 + 1.41 = 6.41 \text{ kN/m}^2,$$

where $A = 1.8 \text{ m}^2$ – we set the area of plates, $g_{steel} = 78.5 \text{ kN/m}^2$ – dead load of steel.

3. According to formulas (20) we will receive the maximum operating stress in the middle of flooring of $\sigma_x = 40.4 \text{ MPa}$, $\sigma_y = 18.5 \text{ MPa}$, $\tau_{xy} = 18.4 \text{ MPa}$.

4. With the help of the computer program "RR Geometric Modeling" (Figure 3) we determine the sizes of plates of a various form (Figure 5). All plates have identical values of the maximum tension of 40.4 MPa , sag of 2 cm and identical area $A = 1.8 \text{ m}^2$.



a) rectangular, b) isosceles triangular extended down, c) rectangular triangular, d) parallelogram, e) isosceles triangular extended across, f) rhombic

Figure 5. Plate of various forms of identical strength and rigidity

5. Loading which is transferred to flooring girders of the second level along perimeter of plates P will make:

$$q_2 = \frac{q_1 \cdot A}{P} = \frac{6.41 \cdot 1.8}{P} = \frac{11.54}{P}. \quad (21)$$

Perimeter of a rectangular plate (Figure 5, a):

$$P = (2+0.9) \cdot 2 = 5.8 \text{ m},$$

perimeter of an isosceles triangular plate (Figure 5, b):

$$P = 2.755 \cdot 2 + 1.365 = 6.875 \text{ m},$$

perimeter of a rectangular triangular plate (Figure 5, c):

$$P = 2.535 + 2.910 + 1.435 = 6.88 \text{ m},$$

perimeter of a parallelogram plate (Figure 4, d):

$$P = (1.920+1.230) * 2 = 6.3 \text{ m,}$$

perimeter of an isosceles triangular plate (Figure 5, e):

$$P = (1.930+3.025) * 2 = 6.88 \text{ m,}$$

perimeter of a rhombic plate (Figure 5, f):

$$P = 1.695 * 4 = 6.78 \text{ m.}$$

6. Loading which is transferred to flooring girders of the first level from girders of the second level will constitute:

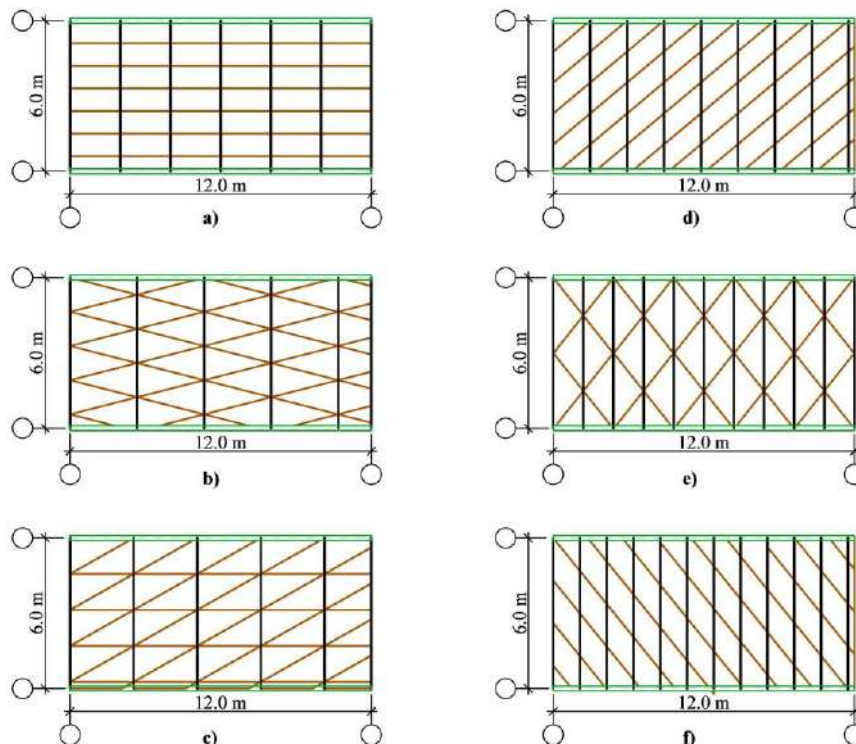
$$q_3 = \frac{Q_{max}}{n_1} \tag{22}$$

where Q_{max} – bearing reaction of girders of the second level (Figure 4, b), n_1 – spacing of flooring girders of the second level.

Results of determination of cross sections of flooring girders of the first and second levels from a condition of strength (15) in the maximum bending moment M_{max} in the middle of flight (Figure 4, b) and conditions of rigidity (16) are given in table 1. In Figure 6 the received options of girder cages are shown.

Table 1. Results of calculations

A girder cage variant (fig. 6)	Thickness of flooring t, mm	Section of girders of the second level	Section of girders of the first level	Materials consumption, kg
1	2	3	4	5
a)	10	angle 70x7	flanged beam No 24	1,679
b)		angle 90x7	flanged beam No 27	2,053
c)		angle 90x8, 75x9	flanged beam No 27	1,973
d)		angle 70x6	channel No 22	1,637
e)		angle 75x5	channel No 20	1,657
f)		angle 70x4.5	channel No 18a	1,616



a) rectangular, b) isosceles triangular extended down, c) rectangular triangular, d) parallelogram, e) isosceles triangular extended across, f) rhombic

Figure 6. Obtained options of steel girder cages with various cells

The analysis of a material consumption of the received options (column 5 of Table 1) shows that the most economic option is reached when using a rhombic cells.

The reliability of the offered new technique is confirmed by numerical studies. Test problems were solved to determine the variants of girder cages with different cells in terms of different loads. The resulting girder cages were created in the form of a finite-element plate-rod model in the SCAD program [3]. Using the built-in module for checking the bearing capacity of steel structures on the set of rules "Steel structures", the load-carrying capacity of the floor girder, secondary girders and flooring for the calculated combinations of forces from the payload and the load from its own weight was checked. The check confirmed the use of the bearing capacity of the selected cross sections and plates close to the maximum with coefficients of use of 0.9-1 depending on the number of the rolling section. A deflection was checked for the flooring. The values deduced in the SCAD program for plates of various shapes were approximately the same with an error of 5–10 %, for plates with sharp angles somewhat higher. They corresponded to the given permissible deflection. When the model was shattered by a smaller grid, a smaller error was achieved. The material capacity was automatically counted in the SCAD program [3] and manually.

4. Conclusions

1. There was offered the new technique of alternative engineering of steel girder cages with various in the plan cell forms with the choice of the most rational constructive decision on a condition of the smallest material costs for its production, on the basis of geometrical methods of structural mechanics.

2. Numerical example of alternative engineering of steel girder cage of plant building shows the possibility of real engineering of designs of this kind on the basis of the developed technique.

3. The offered technique can be used when designing this sort of constructive systems.

4. The reliability of the offered new technique is confirmed by the solution of the test problems of designing steel girder cages of various shapes for different loads and by comparing the obtained results with the results of numerical studies obtained using the SCAD Office software.

5. Shows that the most economic option is reached when using small cells.

6. It is shown that the use of a fine grid in comparison with a large grid allows saving material of steel for producing a girder cage up to 20 %.

References

1. Abasheva L.P., Kochepanova M.N. *Raschet stalnykh balochnykh kletok* [Calculation of steel girder cages]. Perm: PNIPU, 2012. 127 p. (rus)
2. Umnova O.V., Yevdokimtsev O.V. *Stalnyye balochnyye kletki: albom chertezhey* [Steel girder cages: album of drawings]. Tambov: TGTU, 2011. 36 p. (rus)
3. Konstantinov I.A., Lalin V.V., Lalina I.I. *Stroitel'naya mekhanika. Primeneniye programmy SCAD dlya resheniya zadach teorii uprugosti* [Structural mechanics. Application of the SCAD program for the solution of tasks of the theory of elasticity]. SPb: SPbGPU, 2005. 260 p. (rus)
4. Zienkiewicz O.C., Taylor R.L., Fox D.D. *The Finite Element Method for Solid and Structural Mechanics*. Elsevier, 2014. 657 p.
5. Korzhun A.V. *Avtomatizatsiya protsessa sinteza proyektnykh resheniy metallicheskih balochnykh kletok* [Automation of process of synthesis of design solutions of metal frame cages]. PhD Thesis: 05.13.12. Moscow, 2010. 160 p. (rus)
6. Dmitriyeva T.L. *Adaptivnyye mnogourovnevnyye matematicheskiye modeli v chislennoy optimizatsii plastinchatykh-sterzhnevyykh konstruksiy* [Adaptive multilevel mathematical models in numerical optimization of lamellar and rod designs]. Doctorial Thesis: abstract. 05.13.18. Moscow, 2012. 38 p. (rus)
7. Garina C.V. *Matematicheskoye modelirovaniye protsessa postroyeniya otsenok optimalnosti stroitelnykh konstruksiy*

Литература

1. Абашева Л.П., Кочепанова М.Н. Расчет стальных балочных клеток. Пермь: ПНИПУ, 2012. 127 с.
2. Умнова О.В., Евдокимцев О.В. Стальные балочные клетки: альбом чертежей. Тамбов: ТГТУ, 2011. 36 с.
3. Константинов И.А., Лалин В.В., Лалина И.И. Строительная механика. Применение программы SCAD для решения задач теории упругости. СПб: СПбГПУ, 2005. 260 с.
4. Zienkiewicz O.C., Taylor R.L., Fox D.D. The Finite Element Method for Solid and Structural Mechanics. Elsevier, 2014. 657 p.
5. Коржун А.В. Автоматизация процесса синтеза проектных решений металлических балочных клеток: дис. ... канд. техн. наук: 05.13.12. М., 2010. 160 с.
6. Дмитриева Т.Л. Адаптивные многоуровневые математические модели в численной оптимизации пластинчато-стержневых конструкций: автореф. дис. ... докт. техн. наук: 05.13.18. М., 2012. 38 с.
7. Гарина С.В. Математическое моделирование процесса построения оценок оптимальности строительных конструкций: дис. ... канд. техн. наук: 05.13.18. Саранск, 2005. 117 с.
8. Серпик И.Н., Алексейцев А.В., Швыряев М.В. Параметрическая оптимизация стальных балочных клеток // Строительство и реконструкция. № 4. 2013. С. 43–50.
9. Tusnin A.R., Prokić M. Bearing capacity of steel I-sections

- [Mathematical modeling of process of creation of estimates of an optimality of building constructions]. PhD Thesis: 05.13.18. Saransk, 2005. 117 p. (rus)
8. Serpik I.N., Alekseytsev A.V., Shvyryayev M.V. Parametricheskaya optimizatsiya stalnykh balochnykh kletok [Parametrical optimization of steel girder cages]. *Stroitelstvo i rekonstruktsiya*. 2013. No 4. Pp. 43–50. (rus)
 9. Tusnin A.R., Prokić M. Bearing capacity of steel I-sections under combined bending and torsion actions taking into account plastic deformations. *Journal of Applied Engineering Science*. 2014. No. 3. Pp. 179–186.
 10. Rybakov V.A. *Osnovy stroitelnoy mekhaniki legkikh stalnykh tonkostennykh konstruksiy* [Fundamentals of structural mechanics of easy steel thin-walled structures]. Saint-Petersburg: SPbGPU, 2015. 207 p. (rus)
 11. Lyakhovich L.S. Dual approach to solving the problems of structural optimization. *Procedia Engineering*. 2015. Vol. 111. Pp. 510–515.
 12. Martini K. Harmony search method for multimodal size, shape, and topology optimization of structural frameworks. *Journal of Structural Engineering*. 2011. Vol. 137. No. 11. Pp. 1332–1339.
 13. Agrama F.A. Multi-objective genetic optimization for scheduling a multi-storey building. *Automation in Construction*. 2014. Vol. 44. Pp. 119–128.
 14. Scherer M. Steinmann P., Denzer R. A fictitious energy approach for shape optimization. *International Journal for Numerical Methods in Engineering*. 2010. Vol. 82. No. 3. Pp. 269–302.
 15. Aslami M., Akimov P.A. Wavelet-based finite element method for multilevel local plate analysis. *Thin-Walled Structures*. 2016. Vol. 98. Pp. 392–402.
 16. Savchenko A.V., Ioskevich A.V., Khaziyeva L.F., Nesterov A.A., Ioskevich V.V. Longitudinally cross bend of a beam. The decision in various program complexes. *Construction of unique building and structures*. 2015. No. 11. Pp. 96–111. (rus)
 17. Rozin L.A. Zadachi teorii uprugosti i chislennyye metody ikh resheniya [Tasks of the theory of elasticity and numerical methods of their decision]. SPb.: SPbGPU, 1998. 260 p. (rus)
 18. Timoshenko S.P., Voynovskiy-Kriger S. *Plastinki i obolochki* [Plates and shells]. Moscow: Librokom, 2009. 636 p. (rus)
 19. Vatin N.I., Rybakov V.A. Raschet metallokonstruktsiy: sedmaya stepen svobody [Calculation of a metalwork: seventh degree of freedom]. *Stroyprofil*. 2007. No. 2. Pp. 60–63. (rus)
 20. Korobko A.V. *Geometricheskoye modelirovaniye formy oblasti v dvumernykh zadachakh teorii uprugosti* [Geometrical modeling of a form of area in two-dimensional tasks of the theory of elasticity]. Moscow: ASV, 1999. 320 p. (rus)
 21. Korobko V., Korobko A., Chernyaev A. Isoperimetric properties of the torsion rigidity of convex sections. *Procedia Engineering*. 2016. Vol. 150. Pp. 1648–1656.
 22. Polia G., Sege G. *Izoperimetricheskiye neravenstva v matematicheskoy fizike* [Isoperimetric inequalities in mathematical physics]. Moscow: KomKniga, 2006. 336 p. (rus)
 23. Driscoll T.A., Trefethen L.N. *Schwarz-Christoffel Mapping*. Cambridge University Press, 2002. 149 p.
 24. Ivanov V.I., Popov V.Yu. *Konformnyye otobrazheniya i ikh prilozheniya* [Conformal displays and their applications]. Moscow: Yeditorial, 2002. 324 p. (rus)
 25. Ovakimyan S.G. Izgib pravilnykh mnogougolnykh i ovaloobraznykh, zashchemlennykh po konturu tonkikh plit, metodom konformnogo otobrazheniya [A bend correct polygonal and the ovaloobraznykh, the thin plates jammed on a contour, method of conformal mapping]. *Trudy Yerevanskogo politekhnicheskogo instituta*. 1950. No. 4. under combined bending and torsion actions taking into account plastic deformations // *Journal of Applied Engineering Science*. 2014. № 3. Pp. 179–186.
 26. Рыбаков В.А. Основы строительной механики легких стальных тонкостенных конструкций. СПб: СПбГПУ, 2015. 207 с.
 27. Lyakhovich L.S. Dual approach to solving the problems of structural optimization // *Procedia Engineering*. 2015. Vol. 111. Pp. 510–515.
 28. Martini K. Harmony search method for multimodal size, shape, and topology optimization of structural frameworks // *Journal of Structural Engineering*. 2011. Vol. 137. No. 11. Pp. 1332–1339.
 29. Agrama F.A. Multi-objective genetic optimization for scheduling a multi-storey building // *Automation in Construction*. 2014. Vol. 44. Pp. 119–128.
 30. Scherer M. Steinmann P., Denzer R. A fictitious energy approach for shape optimization // *International Journal for Numerical Methods in Engineering*. 2010. Vol. 82. No. 3. Pp. 269–302.
 31. Aslami M., Akimov P.A. Wavelet-Based Finite Element Method For Multilevel Local Plate Analysis // *Thin-Walled Structures*. 2016. Vol. 98. Pp. 392–402.
 32. Савченко А.В., Иоскевич А.В., Хазиева Л.Ф., Нестеров А.А., Иоскевич В.В. Продольно-поперечный изгиб балки. Решение в различных программных комплексах // *Строительство уникальных зданий и сооружений*. № 11. 2015. С. 96–111.
 33. Розин Л.А. Задачи теории упругости и численные методы их решения. СПб.: СПбГПУ, 1998. 260 с.
 34. Тимошенко С.П., Войновский-Кригер С. Пластинки и оболочки. М.: Либроком, 2009. 636 с.
 35. Ватин Н.И., Рыбаков В.А. Расчет металлоконструкций: седьмая степень свободы // *Стройпрофиль*. 2007. № 2. С. 60–63.
 36. Коробко А.В. Геометрическое моделирование формы области в двумерных задачах теории упругости. М.: АСВ, 1999. 320 с.
 37. Korobko V., Korobko A., Chernyaev A., Isoperimetric Properties of the Torsion Rigidity of Convex Sections // *Procedia Engineering*, 2016. Vol. 150. Pp. 1648–1656.
 38. Полия Г., Сеге Г. Изопериметрические неравенства в математической физике. М.: КомКнига, 2006. 336 с.
 39. Driscoll T.A., Trefethen L.N. *Schwarz-Christoffel Mapping*. Cambridge University Press, 2002. 149 p.
 40. Иванов В.И., Попов В.Ю. Конформные отображения и их приложения. М.: Едиториал, 2002. 324 с.
 41. Овакимян С.Г. Изгиб правильных многоугольных и овалообразных, защемленных по контуру тонких плит, методом конформного отображения // *Труды Ереванского политехнического института*. 1950. № 4. С. 187–235.
 42. Казанцев В.П., Золотов О.А., Долгополова М.В. Электростатика на плоскости. Нормировка потенциала. Емкости уединенного проводника и линии относительно точки. Конформные радиусы // *Вестник Красноярского государственного университета. Физико-математические науки*. 2005. № 1. С. 32–38.
 43. Коробко В.И., Черняев А.А. Отношение конформных радиусов – новый аргумент геометрических методов решения двумерных задач теории упругости // *Вестник Российской академии архитектуры и строительных наук*. 2012. № 16. Т. 1. С. 149–161.
 44. Korobko V.I., Korobko A.V., Chernyaev A.A., Savin S.Y., Determination of maximum deflection at cross bending parallelogram plates using conformal radius ratio interpolation technique // *Journal of the Serbian Society for Computational Mechanics*. 2015. № 1(9). Pp. 36–45.
 45. Черняев А.А. Построение алгоритма и разработка программы для ЭВМ по вариантному проектированию

- Pp. 187–235. (rus)
26. Kazantsev V.P., Zolotov O.A., Dolgoplova M.V. Elektrostatika na ploskosti. Normirovka potentsiala. Yemkosti uyedinenного проводника i linii otnositelno tochki. Konformnyye radiusy [Electrostatics on the plane. Potential normalization. Capacities of the lonely conductor and the line concerning a point. Conformal radiuses]. *Vestnik Krasnoyarskogo gosudarstvennogo universiteta. Fiziko-matematicheskiye nauki*. 2005. No. 1. Pp. 32–38. (rus)
 27. Korobko V.I., Chernyayev A.A. Otnosheniye konformnykh radiusov – novyy argument geometricheskikh metodov resheniya dvumernykh zadach teorii uprugosti [The relation of conformal radiuses – a new argument of geometrical methods of the solution of two-dimensional tasks of the theory of elasticity]. *Vestnik Rossiyskoy akademii arkhitektury i stroitelnykh nauk*. 2012. No. 16. Vol. 1. Pp. 149–161. (rus)
 28. Korobko V.I., Korobko A.V., Chernyaev A.A., Savin S.Y., Determination of maximum deflection at cross bending parallelogram plates using conformal radius ratio interpolation technique. *Journal of the Serbian Society for Computational Mechanics*. 2015. No. 1(9). Pp. 36–45.
 29. Chernyayev A.A. Postroyeniye algoritma i razrabotka programmy dlya EVM po variantnomu proyektirovaniyu plastinchato-sterzhnevyykh silovykh konstruksiy iz usloviya zhestkosti plastin putem geometricheskogo modelirovaniya ikh formy [Creation of an algorithm and development of the computer program on alternative design of lamellar and rod power designs from a condition of rigidity of plates by geometrical modeling of their form]. *International Journal for Computational Civil and Structural Engineering*. 2016. No. 2. Pp. 147–157. (rus)
 30. СП 16.13330.2017. Стальные конструкции. Актуализированная редакция СНиП II-23-81*. М.: Минстрой России, 2017. 178 с.
 31. СП 20.13330.2016. Нагрузки и воздействия. Актуализированная редакция СНиП 2.01.07-85*. М.: Минстрой России, 2016. 96 с.

Andrey Chernyaev,
+7(920)801-84-17; chernyev87@yandex.ru

Андрей Александрович Черняев,
+7(920)801-84-17;
эл. почта: chernyev87@yandex.ru

© Chernyaev A.A., 2018

doi: 10.18720/MCE.78.2

The behavior of concentric brace with bounded fuse

Поведение концентрических раскосов с встроенным предохранителем по сжимающей нагрузке

*M.A. Kafi,
A. Kachooee,
Semnan University, Semnan, Iran*

*PhD, доцент М.А. Кафя,
PhD А. Качуй,
Университет Семнан, г. Семнан, Иран*

Key words: local fuse; concentrically braced structures; ductility; energy dissipation capacity; load bearing capacity; cyclic load

Ключевые слова: местный предохранитель; концентрически стержневые конструкции; податливость; способность к рассеиванию энергии; грузоподъемность; циклическая нагрузка

Abstract. The concentrically braced system is one of the most common lateral load-bearing systems among the steel structures. This lateral loadbearing system has various apparent forms where the main characteristic of them all is their significant stiffness and lateral strength. The main weakness of the concentrically braced system is buckling in compression. This issue causes that concentric bracings have low compressive load-bearing capacity together with undesirable ductility and limited energy dissipation capacity. In this study to solve this problem use has been made of a heuristic method. In this method a local fuse has been used in the middle of bracing where its periphery and inner circumference have been covered with an auxiliary casing within a casing. The local fuse is designed in a way that after yielding, the bracing undergoes local buckling at this area. But presence of an auxiliary element placed around the fuse prevents this local buckling and thus the bracing would exhibit almost a symmetric behavior during compressive and tensile loadings. Thus the bracing would exhibit a wide and spindle-shaped hysteresis curve under a cyclic loading with desirable ductility and high energy dissipation capacity. Also in this article a numerical study is performed utilizing ABAQUS Ver. 6.12 software to make comparison between concentric bracings with local fuse –auxiliary element (LF-AECB) and usual concentric bracings (UCB) in terms of ductility, energy dissipation capacity and loadbearing capacity. The results of numerical studies have indicated the extraordinary better performance of LF-AECB with respect to that of UCB.

Аннотация. Концентрически стержневая система является одной из наиболее распространенных среди стальных систем с поперечными несущими конструкциями. Эта система имеет различные формы, где основной их характеристикой является значительная жесткость и устойчивость против поперечной силы. Основным недостатком такой системы является изгиб при сжатии. Эта проблема приводит к тому, что концентрические раскосы имеют низкую несущую способность при сжатии вместе с нежелательной податливости и ограниченной способностью к рассеиванию энергии. В этом исследовании для решения проблемы использовался эвристический метод. Местный предохранитель использовался в середине раскоса, где его край и внутренняя окружность были покрыты вспомогательным кожухом внутри корпуса. Местный предохранитель по сжимающей нагрузке спроектирован таким образом, что после прогибания конструкции раскос подвергается местной потере устойчивости. Но наличие вспомогательного элемента, расположенного вокруг предохранителя, предотвращает это, и, таким образом, раскос будет проявлять почти симметричное поведение во время сжимающих и растягивающих нагрузок. Раскос будет иметь широкую и веретенообразную петлю гистерезиса при циклической нагрузке с оптимальной податливостью и высокой способностью рассеивать энергию. Также в этой статье проводится численное исследование с использованием ABAQUS Ver. 6.12 для того, чтобы сравнить концентрический раскос с местным предохранителем-вспомогательным элементом (LF-AECB) и обычными концентрическими раскосами (UCB) с точки зрения податливости, способности рассеивания энергии и несущей способности. Результаты численных исследований показали лучшие эксплуатационные параметры LF-AECB по сравнению с UCB.

1. Introduction

The concentric braced systems are one of the most applicable systems in steel structures. These systems due to having high stiffness and lateral load bearing with respect to other structural systems have been under focus of attention. The main weakness of these structural systems is buckling of the bracing under compressive loading. Therefore when these structures undergo a cyclic loading, they exhibit an undesirable ductility with low energy dissipation capacity. Hence, researchers from around the world have performed extensive studies to solve this problem in concentric bracings. In continuation, some of these studies are cited.

One of the solutions for enhancing ductility and energy dissipation in concentric braced structures is use of energy dissipation elements located at the intersection of bracings. In this respect application of the rings made of steel tubes as energy dissipater element at intersection with the bracing has been investigated both analytically and experimentally by Abbasnia et al. [1]. The results of these studies have shown that these bracings possess wide and stable hysteresis curves. One of the disadvantages of this system is the certain dimensions of the steel tubes incorporated in the steel rings which cause dimensional restrictions. For this purpose Andalib et al. [2], introduced steel rings made of plates as a replacement for the initial rings and in this respect they have performed an experimental and numerical study to investigate performance of the mentioned rings. The steel rings made of steel plates include two semi rings which are connected to the bracing via some connections and form a single ring. The results of Andalib et al. [2] studies exhibit wide and stable hysteresis curves for the rings made of the steel plates.

The off-center bracing system (OBS) is one of the invented systems to improve the concentric braced structures [3]. In this structural system, the tensile element is not straight and when a lateral load is exerted on the system, its initial geometry changes. Therefore the load-deformation curve of these systems is in the nonlinear geometric form. Moghaddam and Estekanchi [4] in their study on these systems found that the load-deformation diagram of OSBs follows a nonlinear hardening pattern with two yielding points. Then they subjected the single-story and two-story OBS structures to the seismic loading using this pattern. The results of these analyses indicated that the OBS structural system has a behavior similar to that of the Base Isolation system and has a good strength against lateral loads. Bazzaz et al. [5–8] have used a ductile annular steel element to enhance behavior of these systems (OBS-C systems). The results of this study have exhibited higher ductility and greater energy dissipation of this structural system with respect to the OBS system. In another study [9] which has been performed to make comparison between OBS-C systems and diagonal bracing systems with ductile steel rings i.e. DBS-C, the better behavior of OBS-C system in terms of ductility and energy dissipation capacity has been observed.

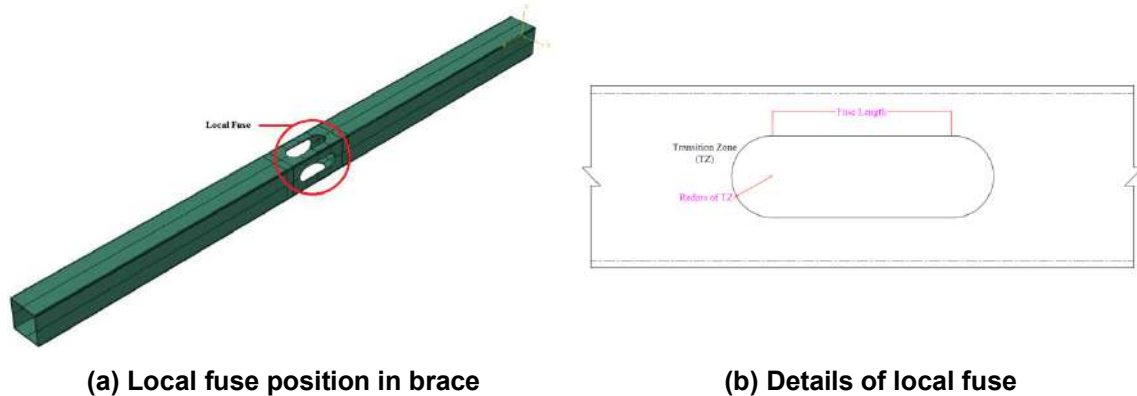
Use of two-level or multi-level control systems is another method for improving the seismic behavior of structures which has recently been under focus of attention of researchers [10–12]. The main idea in these structural systems, is combination of different control systems with various stiffness and strength values which results into desirable energy absorption in the structure for various earthquake intensities. In one of this study, Zahrai and Vosooq [11] introduced a dual system in which use has been made of the combination of vertical link beam and knee elements to maintain energy absorption. In this structural system, in order to improve the seismic performance, the vertical link beam is used as an energy absorption element in the small loads area and knee elements are used for energy absorption under intense earthquakes. Another system created for implementing the idea of two-level control systems, is the passive tube in tube control system.

Use of ductile fuse elements in the diagonals of concentric braced structures, is another method to improve their seismic behavior. Rezai et al. [13] investigated the effect of different cases of implementing local fuses on the behavior of bracing elements in an experimental study. The result of their study revealed that the fuse elements with appropriate lateral restraints exhibit a stable hysteretic response with high energy absorption and large non-elastic deformation capacity characteristics. In another studies by Legeron et al. [14] and Desjardins et al. [15], they investigated the application of local ductile fuses in the concentric bracings with single-angle section to reduce demand of the acting load on the connection to avoid the need for its strengthening. In this study the tensile capacity of the bracing has been reduced equal to the connection capacity. The Legeron et al. [14] studies showed that implementing ductile local fuses would effectively reduce the seismic load demand acting upon the bracing connections and would prevent their strengthening.

One of the other invented structural systems for improving seismic performance of the structures with concentric bracings is application of the buckling restrained brace (BRB) [16–20]. In this structural system attempt is made that using bracings which include a casing and core, the main shortcoming of the

concentrically braced structural systems which is buckling in compression is removed [16, 17 and 19]. The structures with BRBs, present symmetric and stable hysteresis curves which also have significant capacity in terms of ductility and energy dissipation. Furthermore, in the BRB structural system, the non-elastic deformations are entirely and uniformly distributed over the length of buckling restrained bracing and thus damage to other structural elements is prevented.

In this study a novel method is introduced for improving the seismic performance of concentric braced frames. In this method, use has been made of a fuse element in the middle of the bracing (Fig. 1). Design of this element is in a way that after yielding of the bracing at this point, it undergoes local buckling.

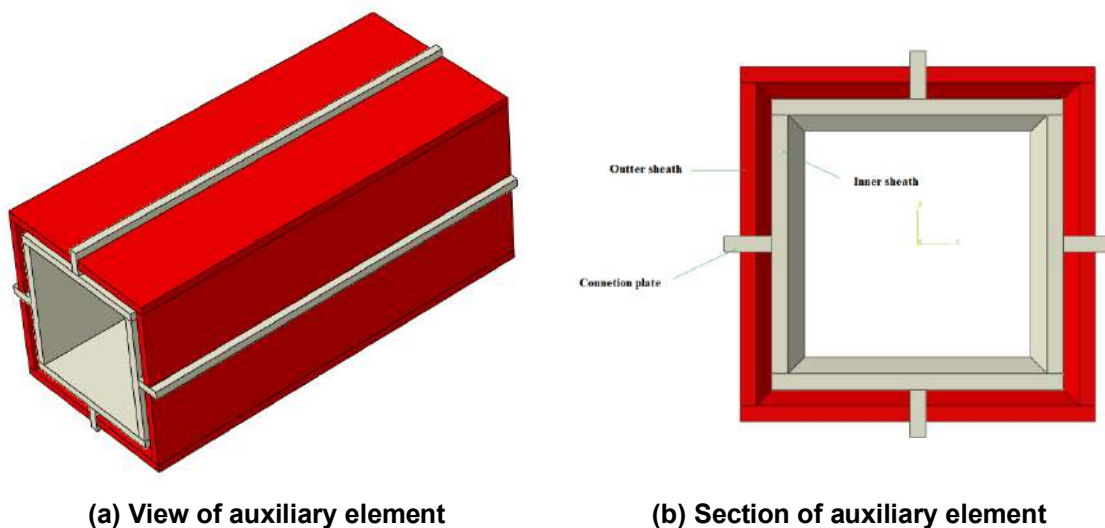


(a) Local fuse position in brace

(b) Details of local fuse

Figure 1 Local fuse in LF-AECB

To prevent local buckling of the bracing an auxiliary element in the form of casing within casing is used at the fuse area, as shown in Figure 2. This auxiliary element which covers the periphery and inner circumference of the fuse, allows the bracing to resist against local buckling of the fuse and thus prevents loss of the compressive loadbearing. This issue causes that the bracings equipped with fuses and auxiliary elements under cyclic loads to have wide and stable hysteresis curves together with desirable ductility and energy dissipation capacity. Also in this study using ABAQUS Ver. 6.12 [21] a comparison has been made between performances of the concentric bracings with local fuse-auxiliary element (LF-AECB) and usual concentric bracings (UCB), under cyclic pseudo-static loads. In continuation, a complete introduction of LF-AECB bracing and the obtained results from the numerical study will be presented.



(a) View of auxiliary element

(b) Section of auxiliary element

Figure 2 Auxiliary element in LF-AECB

2. Methods

2.1. Introduction of LF-AEBC bracing

LF-AEBC bracings are comprised of two parts. The first part is the local fuse implemented at the middle of the bracing area and the second part is the auxiliary element placed at the fuse area to prevent its local buckling. The local fuse used in the bracing, as shown in Fig. 1, is created by reducing the cross section area of the bracing and has a semi-circular transition zone to prevent stress concentration. To calculate the cross section area of the fuse, first the demand exerted load on the bracing (P_u) should be obtained from the analyses. After calculating P_u from Eq. (1), it is concluded:

$$P_u = T_{u,fuse} \quad (1)$$

where, $T_{u,fuse}$ is the ultimate tensile loadbearing capacity of the fuse. The value of $T_{u,fuse}$ could be calculated from Eq. (2):

$$T_{u,fuse} = A_{fuse} \cdot F_u \quad (2)$$

In Eq. (2), A_{fuse} and F_u are the fuse cross section area and ultimate stress of the bracing, respectively. Now regarding Eqs. (1) and (2), the fuse cross section area could be calculated from Eq. (3):

$$A_{fuse} \leq \frac{P_u}{F_{u,fuse}} \quad (3)$$

After calculating the fuse cross section area, the required cross section area of the bracing is calculated. For this purpose according to Eq. (4), the fuse ultimate tensile capacity should be taken less than 80 % of the yielding capacity of the bracing:

$$A_{fuse} \cdot F_{u,fuse} \leq 0.8 \cdot A_g \cdot F_y \quad (4)$$

In the above equation, A_g and F_y are the required cross section area and yielding stress of the bracing materials, respectively. In the above equation, the reason for selecting a coefficient value of 0.8 is to ensure lack of overall yielding of the bracing before the fuse reaches its ultimate capacity, as entire yielding of the bracing causes significant reduced stiffness after its yielding and thus according to Eq. (5), its buckling capacity also decreases proportionally. This issue causes that before the fuse reaches its ultimate loadbearing capacity, the bracing undergoes overall buckling and consequently the expected performance of LF-AEBC bracing system in terms of energy dissipation capacity and expected ductility is not happened.

$$P_{Cr} = \frac{\pi^2 \cdot E}{\lambda^2} \quad (5)$$

In the above equation, E is the materials elastic modulus and λ is the slenderness ratio of the element under compression. Regarding Eq. (4), the required cross section area could be calculated using Eq. (6):

$$A_g \geq (A_{fuse} \cdot F_{u,fuse}) / (0.8 \cdot F_y) \quad (6)$$

It should be mentioned that with respect to Eq. (1), the capacity of the bracing designed according to Eq. (6), is equal to that of the fuse and the loadbearing capacity of the bracing overall cross section area would not affect its loadbearing capacity.

In LF-AEBC bracings, the fuse length is calculated in a way that the fuse buckling occurs after its yielding, so that maximum use of the fuse capacity is utilized for dissipating the input energy to the structure. Respecting this issue, Eq. (7) should be established in LF-AEBC bracings:

$$P_{Cr,fuse} \geq T_{u,fuse} \quad (7)$$

In the above equation, $P_{Cr,fuse}$ is the fuse buckling capacity. The $P_{Cr,fuse}$ value could be calculated from Eq. (8):

$$P_{Cr,fuse} = \frac{\pi^2 \cdot E \cdot I_{min,fuse}}{L_{fuse}^2} \quad (8)$$

In the above equation, $I_{min,fuse}$ and L_{fuse} are the minimum moment of inertia and fuse length, respectively. Now respecting Eqs. (2), (7) and (8) the L_{fuse} value could be calculated from Eq. (9):

$$L_{fuse} \leq \sqrt{\frac{\pi^2 \cdot E \cdot I_{min, fuse}}{A_{fuse} \cdot F_{u, fuse}}} \quad (9)$$

The second component in LF-AEBC bracings is the auxiliary element. The auxiliary elements generally include the external and internal areas of the fuse with 1mm distance from the fuse walls so that they could not affect the fuse loadbearing capacity. The philosophy behind existence of the auxiliary element in LF-AEBC bracing is to prevent local buckling of the bracing in the fuse area. As is evident from Fig. 2, for bracings with box section, this element is comprised of one internal casing with rectangular shape and one external casing with four angle-section elements. These two casings are connected to each other by connecting plates which have passed through the fuse area. The connecting plates' lengths should be exactly equal to the fuse length plus the length of its transition areas to prevent displacement of the auxiliary element over the bracing length. The thickness of connecting plates should also be taken in a way that they do not buckle over the length. Also the length of auxiliary element should be taken at least 15cm greater than the two ends of the fuse transition area.

2.2. Introduction of the numerical models

In this study in order to investigate the effect of implementing local fuse together with auxiliary element on the behavior of concentric bracings, a numerical study utilizing ABAQUS Ver. 6.12 [21] has been conducted. Regarding that all non-elastic deformations in structures equipped with LF-AEBC bracings occur within the fuse area, in this study only the behavior of these bracings under cyclic pseudo-static displacement loads has been investigated, as the behavior of this element under cyclic load would indicate overall behavior of the structure under lateral loads. According to Figure 3, to investigate the behavior of LF-AEBC bracings and making comparison between response of these bracings and that of the concentric bracings, two models of B14 and B20-LF-AE are modeled using Solid Element and with fixed end condition in ABAQUS Ver. 6.12 [21] software. In this paper, model B14 represents the UBC and model B20-LF-AE represents the LF-AECB.

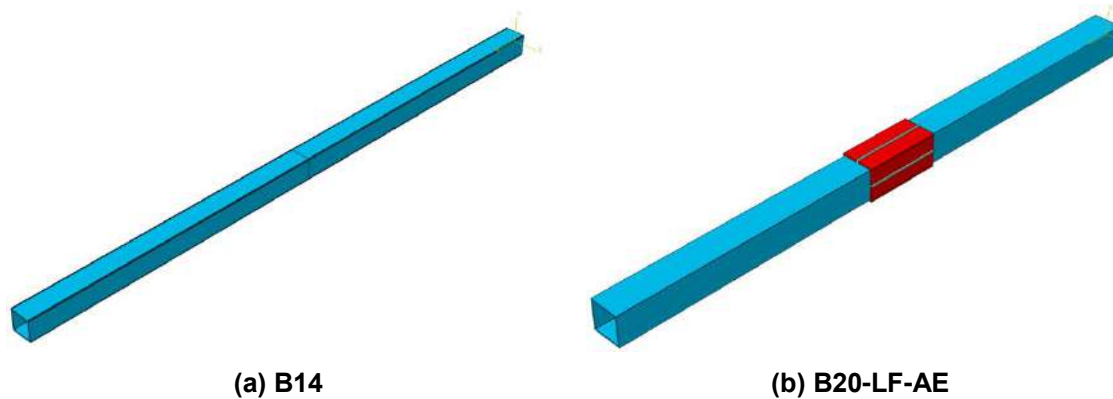


Figure 3 Analytical models

The geometric characteristics of structural models are shown in Table 1. Also the materials characteristics utilized in these models are given in Fig. 4 and Table 2. The cross section area of the local fuse implemented in model B20-LF-AE has been obtained based on Eq. (3) and assuming that P_u value is equal to 117 Tons. The local fuse length also is selected 20cm based on Eq. (9). Also transition area of the fuse is a semicircle with a radius of 45.8mm. Regarding the fuse length and the transition area length, the length of auxiliary element is taken equal to 50cm.

Table 1 Geometric characteristics of structural

Models	Brace section	Brace area	Brace length	LF length	LF area	Transition Zone radius	Inner sheath section	Outer sheath section	Connection plate section	Auxiliary element length
B14	Box 14*14*0.6	32.16	400.00	none	none	none	none	none	none	none
B20-LF-AE	Box 20*20*0.8	60.80	400.00	20.00	31.55	4.58	19.8*19.8*1	Four 11.4*11.4*1 angle member	3*1	50.00

Note: The unite of lengths and areas are Cm and Cm²

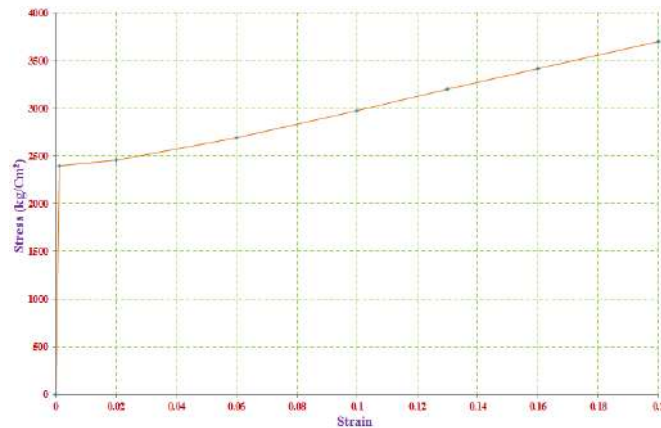


Figure 4 Strain-stress curve of steel material used in the analytical models

Table 2 Material properties used in the analytical models

Element material	Elastic Modulus	Yielding stress	Yielding strain	Final stress	Final strain
ST37	2000000	2400	0.0012	3700	0.20

Note: The unit of stresses is Kg/Cm²

Model B14 is a UCB with equal cross section and tensile capacity equal to those of B20-LF-AE bracing. This model is built to make comparison between seismic behavior of LF-AEBC bracings and that of the UCBs which have equal ultimate tensile capacities. In the next section the responses of the models are compared to each other. Also to perform pseudo static analysis of the structural models and comparing their responses, the ATC-24 loading pattern has been utilized according to Figure 5.

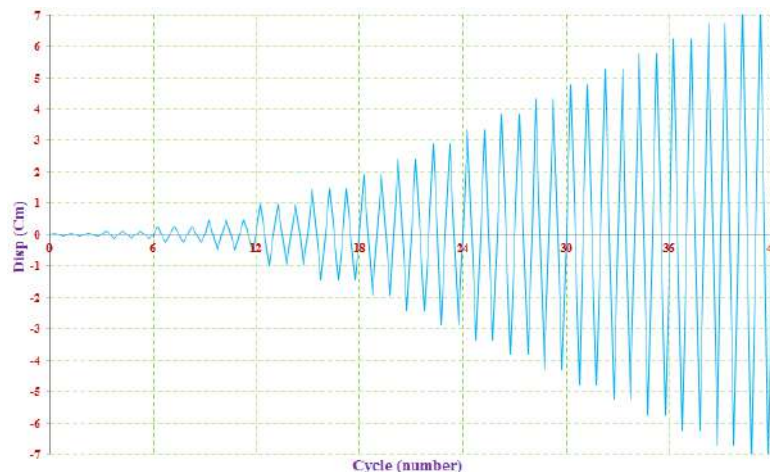


Figure 5 ATC-24 load pattern used in pseudo static analysis

3. Results and Discussion

In this section, the results obtained from analysis of models B14 and B20-LF-AE are investigated. First, the corresponding hysteresis curves of the mentioned models obtained from pseudo-static analyses are accurately investigated. Then, models B14 and B20-LF-AE are compared to each other in terms of ductility, loadbearing capacity and energy dissipation capacity.

3.1. Interpretation of model's hysteresis curves

In this section the interpretation of hysteresis curves has been presented. In Fig. 6 the hysteresis curve of model B14 has been shown. As expected, this model has yielded at 77 tons load and a corresponding displacement of 0.5cm. But contrary to what is expected, this model has buckled in the first cycle of loading after yielding. The reason for premature buckling of the bracing is related to significant reduction in the plastic stiffness of the material with respect to its elastic stiffness. Based on the theoretical calculations, the elastic buckling load of model B14 is 458 tons. Therefore its plastic buckling load would be equal to 1.3 tons, because the plastic stiffness of material is 0.003 its elastic

stiffness. Thus, as during yielding, the available load in the bracing is greater than the plastic buckling load, the bracing has immediately undergone buckling.

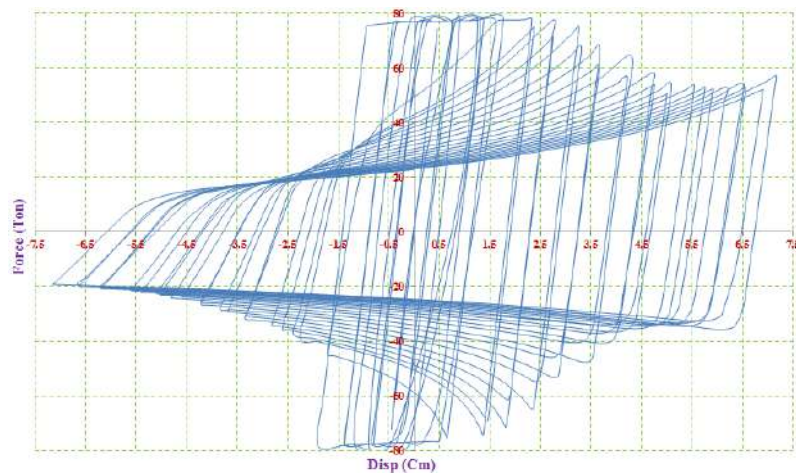


Figure 6 Hysteresis curve of B14

Also after yielding, due to hardening of the steel it was expected that model B14 would enhance its tensile loadbearing capacity with a positive slope in the hysteresis curve, but according to Figure 6, the opposite was observed. The reason for this reduction in tensile loadbearing capacity after yielding of model B14 is also related to the premature buckling of this element. This issue is explained in detail in the next section. Finally model B14 failed at the tensile load of 57 tons and the compressive load of 19 tons and the corresponding ultimate displacement of 7.2 cm in both tension and compression cases. Figure 7 shows the deformed situation of model B14 for its ultimate cyclic loading.

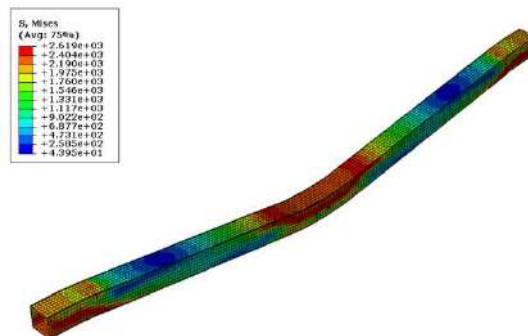


Figure 7 Deformed shape of B14 in final cyclic loading

The hysteresis curve of model B20-LF-AE has been shown in Figure 8. As seen in this figure, the hysteresis curve of this model is wide and spindle shaped which indicates desirable and good performance of this type of bracing in terms of ductility and energy dissipation capacity.

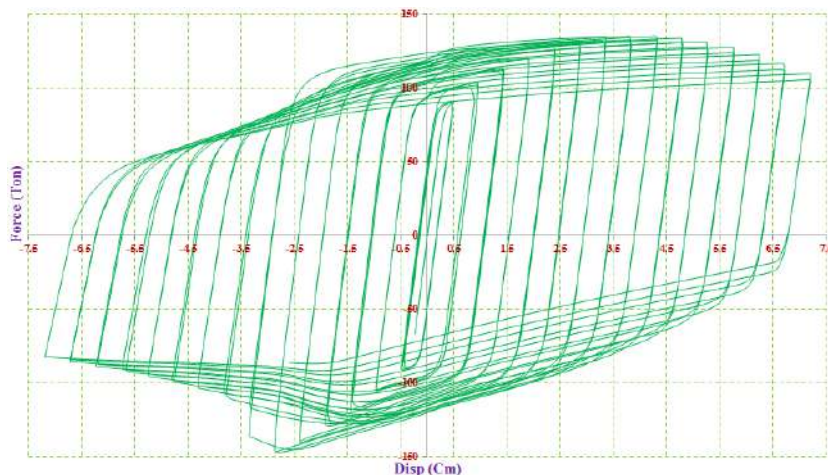


Figure 8 Hysteresis curve of B20-LF-AE

This model has yielded at 76 tons and the corresponding displacement of 0.33 cm. In this model, after yielding and due to significant reduction in the stiffness of the materials, the bracing has undergone buckling. But as was explained before this bracing has been designed in a way that firstly local buckling occurs in the fuse area and secondly, due to presence of the auxiliary element, local buckling of the fuse has been prevented. This is clearly seen in the hysteresis curve of model B20-LF-AE. According to Figure 8, after yielding no loss is seen in the loadbearing capacity of B20-LF-AE bracing and loadbearing capacity of the bracing is increasing both in the compression and tension. But increase in the loadbearing capacity has continued till the bracing has reached overall yielding of the section in the compressive load i.e. a load equal to 146 tons. In this case, as is seen also in Figure 8, the bracing has undergone loss in its compressive loadbearing capacity. The reason for this issue is that when B20-LF-AE bracing has reached its overall yielding capacity, buckling is not as local in the fuse area but in this case overall buckling of the bracing has occurred. Therefore the auxiliary element is no longer able to prevent buckling of the bracing and loss in the compressive loadbearing capacity has occurred. Correspondingly and after overall buckling of B20-LF-AE bracing, its tensile capacity has also degraded. The important issue concerning overall buckling of B20-LF-AE bracing is that loss in the loadbearing capacity in this bracing has occurred with a lower rate with respect to model B14. Finally, B20-LF-AE bracing also has failed in the tensile load of 110 tons and compressive load of 82 tons and a corresponding displacement of 7.2 cm in both compression and tension. Figures. 9 and 10, present the deformation status of B20-LF-AE bracing for the two cases of the final cycle of loading before overall buckling, and the ultimate loading cycle, respectively.

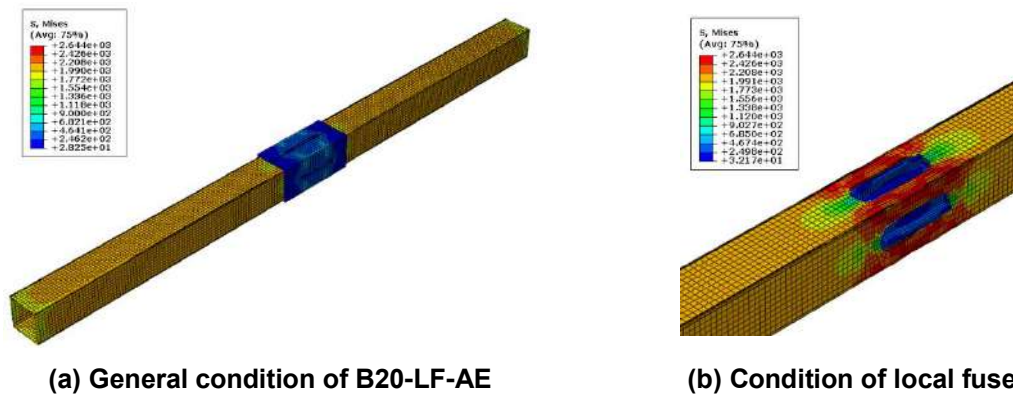


Figure 9 Deformed shape of B20-LF-AE in final cyclic loading before buckling

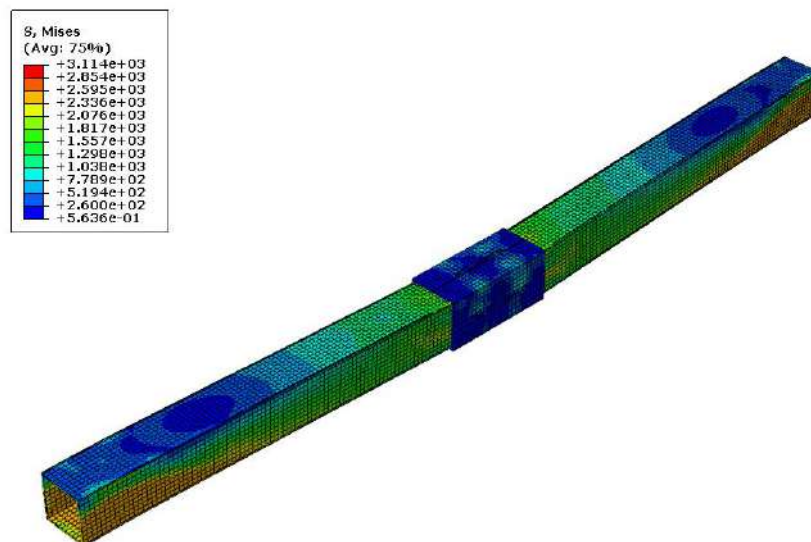


Figure 10 Deformed shape of B20-LF-AE in final cyclic loading

3.2. Comparison between loadbearing capacities of models

To make comparison between loadbearing capacities of models B14 and B20-LF-AE according to Figure 11, the envelope of hysteresis curves corresponding to these two models have been utilized. As is seen in this figure, model B20-LF-AE both in the tensile load and compressive load has far greater loadbearing capacity with respect to that of model B14. In the tension area, as was expected both models

have yielded in their expected tension capacity. But after yielding the behavior of models has been entirely different. The tensile loadbearing capacity of model B14 is reduced after yielding which is not expected. Based on the theoretical calculations, the ultimate tensile loadbearing capacity of this model should have reached 119 tons due to the steel hardening, but because of overall buckling of the bracing and permanent lateral displacement due to it, this model could not achieve its loadbearing capacity.



Figure 11 Comparison between envelope curve of analytical models

When the bracing buckles, it experiences lateral displacement. A portion of this lateral displacement remains as residual in the bracing after yielding. This issue causes that the bracing could not become perfectly straight in tension and consequently its tensile loadbearing capacity would reduce. This is clearly seen in Figure 12. This figure shows permanent lateral displacement of the middle point of the bracing with respect to the bracing length (residual relative lateral displacement) for different loading cycles.

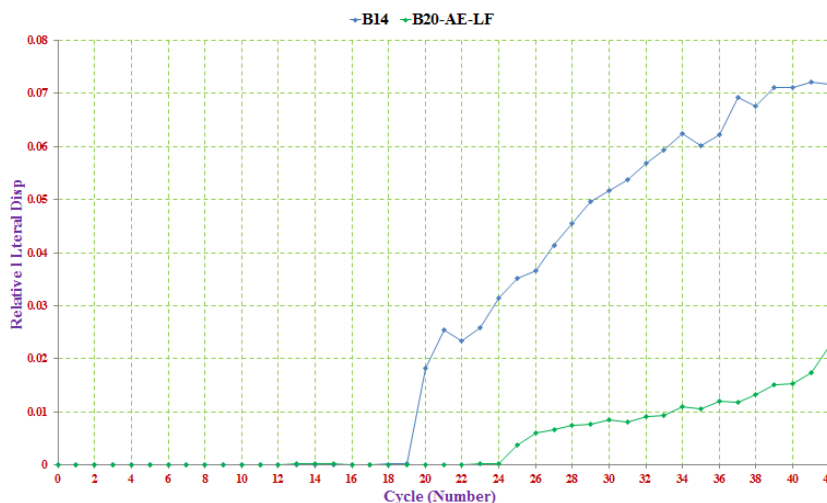


Figure 12 Comparison between residual relative lateral displacement of analytical models

As is seen in Figure 12, the B14 bracing has experienced significant residual lateral displacement from the 20th cycle on. This loading cycle corresponds to an axial displacement equal to 2.4 cm. With respect to the envelope curve of model B14 shown in Figure 11, it is observed that loss in the tensile loadbearing capacity in this model has also started from a displacement value equal to 2.4 cm and with increase in the residual lateral displacement in the next cycles its corresponding tensile force has decreased conversely. Finally, regarding Figure 11, the maximum values of tensile loadbearing capacity and ultimate tensile loadbearing capacity in B14 bracing are 77 tons and 57 tons, respectively. But concerning model B20-LF-AE, the issue is entirely different. The reason is that in this model due to the presence of auxiliary element, the fuse local buckling has been prevented after yielding and thus the bracing not only has not undergone loss in its tensile loadbearing capacity but also its tensile capacity has increased. This increase in the loadbearing capacity has continued up to a load equal to 135 tons but after it due to the overall buckling of the bracing, this model has also undergone loss in its tensile

loadbearing capacity. This issue is evident in Figure 12. As is seen in this figure, model B20-LF-AE from cycle 33 on, has experienced a significant residual relative lateral displacement (greater than 0.01 which is equivalent to a lateral displacement greater than 4cm). This cycle corresponds to an axial displacement equal to 5.3 cm, where according to the envelope curve of model B20-LF-AE shown in Figure 11, reduction in the loadbearing capacity of this model has started from this displacement and with increase in the lateral displacement in the next cycles, the corresponding tensile force has decreased, conversely. Albeit it is essential to state that the rate of reduction in the tensile loadbearing capacity in model B20-LF-AE has been considerably less than that of model B14 due to the presence of auxiliary element. This issue is also evident from Figures 11 and 12, so that according to Figure 12, the maximum residual lateral displacement in model B14 was about 29 cm whereas this value in model B20-LF-AE is 69 % less and was equivalent to 9 cm. For model B20-LF-AE also the maximum tensile capacity and ultimate tensile capacity values were 135 tons and 110 tons, respectively. These values were 75 % and 93 % greater than the corresponding values in the model B14, respectively.

As is seen in Figure 11, in the compressive area of model B14, immediately in the first cycle of loading after yielding which corresponds to a load value of 77 tons, has buckled due to reduced Post-elastic stiffness of materials. Regarding Figure 11, the maximum compressive loadbearing capacity and ultimate compressive capacity in model B14 have been 79 tons and 19 tons, respectively. For model B20-LF-AE also after yielding of the fuse, the bracing has undergone local buckling in this area. But due to presence of the auxiliary element, this buckling is prevented and compressive loadbearing capacity of the bracing is increased. Increase in the compressive loadbearing capacity in model B20-LF-AE has continued up to a load value of 146 tons, which corresponds to yielding of the overall section of the bracing in this model. But immediately after this load and due to reduced post-elastic stiffness of the materials, the bracing has undergone overall buckling. Albeit it should be noted that due to presence of the auxiliary element, the rate of reduction in the compressive loadbearing capacity in this bracing is significantly less than that of model B14. This issue could be completely observed comparing envelope curves (Fig. 11) and residual relative lateral displacements of the two models (Fig. 12). Finally and with respect to Figure 11, the maximum and ultimate compressive loadbearing capacities in model B20-LF-AE were 146 tons and 82 tons, respectively. These values were 85 % and 331 % greater than their corresponding values in model B14, respectively. In Table 3, a comparison has been made between the maximum and ultimate tensile and compressive capacity values in models B14 and B20-LF-AE.

Table 3 Loadbearing capacity of models

Models	Max Tension Capacity	Final Tension Capacity	Max Compression Capacity	Final Compression Capacity
B20-AE-LF	135	110	146	82
B14	77	57	79	19
Ratio	1.75	1.93	1.85	4.32

Note: The unite of forces are Ton

3.3. Comparison between ductility in the structural models

In this section comparison has been made between ductility in models B14 and B20-LF-AE. The ductility coefficient values have been obtained separately for the tension and compression areas. In the tension area, the ductility coefficient value, according to Eq. (10), has been calculated by the ratio of the ultimate movement, δ_u^T which is equivalent to a corresponding movement equal to 70 % of the maximum force in the bracing in the tensile area to the yielding movement, δ_y .

$$\mu^T = \frac{\delta_u^T}{\delta_y} \quad (10)$$

Based on Figure 11, the δ_y value for models B14 and B20-LF-AE are 0.5 cm and 0.33 cm, respectively. Also the δ_u^T value for both models is 7.2 cm. Thus based on Eq. (10), the tensile ductility coefficient value for models B14 and B20-LF-AE are 14.4 and 21.8, respectively. In other words in the tensile area the ductility coefficient value of model B20-LF-AE has been 1.5 times that of model B14.

In the compression area also the value of ductility coefficient, according to Eq. (11), has been calculated from the ratio of ultimate movement, δ_u^C , which is equivalent to the movement corresponding to a force equal to 70 % of the maximum force of bracing in the compressive area, to the movement corresponding to the first buckling in the model i.e., δ_{FB} .

$$\mu^C = \frac{\delta_u^C}{\delta_{FB}} \quad (11)$$

As two models have undergone buckling immediately after yielding, their δ_{FB} value is equal to their δ_y value. Also according to Figure 11, the δ_u^C values of models B14 and B20-LF-AE are 2.09 cm and 5.25cm, respectively. Then based on Eq. (11), the compressive ductility coefficient value of models B14 and B20-LF-AE are 4.18 and 15.9, respectively. In fact the ductility coefficient of model B20-LF-AE is 3.8 times of that in model B14.

Thus in general and regarding the topics discussed in this section, it is found that LF-AEBC bracings in comparison to the UCBs, exhibit considerably much better ductility. Also in Table 4, the tensile and compressive ductility coefficient values in models B14 and B20-LF-AE have been compared to each other.

Table 4 Ductility of models

Models	Yielding Disp	Final Tension Disp	Tension Ductility Ratio	First Buckling Disp	Final Compression Disp	Compression Ductility Ratio
B20-AE-LF	0.33	7.20	21.82	0.33	5.25	15.91
B14	0.50	7.20	14.40	0.50	2.09	4.18
Ratio	0.66	1.00	1.52	0.66	2.51	3.81

Note: The unite of displacements are Cm

3.4. Comparison between dissipated energy capacities by the structural models

As is in Figures 6 and 8, model B20-LF-AE having a wide and symmetric hysteresis curve, guarantees high energy absorption in this model under lateral loads. Furthermore as is seen in Figures 9 and 10, damage concentration in this model has occurred in the fuse area and this means that in the braced structures with LF-AEBC bracings under lateral loads, the main structural elements are kept safe from damage and inelastic deformations remain in the bracing and are concentrated in the fuse area. To perform a more accurate investigation of the dissipated energy in the numerical models and comparing them to each other, the cumulative dissipated energy (CDE) curves in each loading cycle for models B14 and B20-LF-AE have been shown in Figure 13.

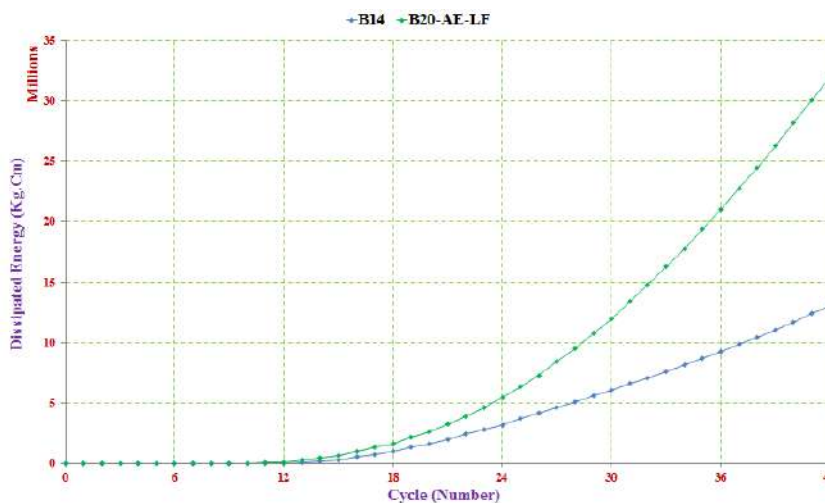


Figure 13 Comparison between cumulative dissipated energy (CDE) of analytical models

As is seen in this figure, the maximum absorbed energy by model B14 was equal to 13047 tons.cm, while this value for model B20-LF-AE was equal to 32016 tons.cm. This means that the amount of overall dissipated energy by bracing B20-LF-AE was 2.45 times of this value for the UCB in model B14. Then regarding that the design loadbearing capacity in both bracings is the same, it is concluded that LF-AEBC bracings have a much better performance in dissipating energy exerted upon the structure with respect to their corresponding UCBs. Also to investigate the effect of overall buckling on the amount of dissipated energy in the bracing, the relative dissipated energy (with respect to the displacement corresponding to each loading cycle) i.e., ECDE/Disp, in each cycle has been shown in Figure 14.

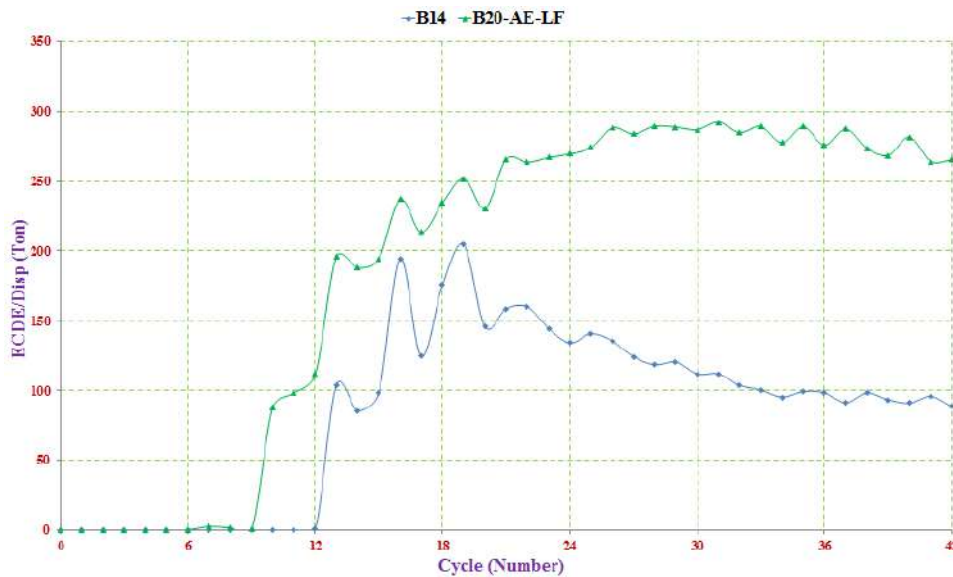


Figure 14 Comparison between ECDE/Disp of analytical models

As is seen in this curve, for model B14 up to cycle 20 of the loading, where no overall buckling has occurred, the curve has an ascending trend which indicates increase in the amount of relative dissipated energy in each loading cycle but immediately after occurrence of buckling in the 20th loading cycle, the slope of the curve has turned negative and the amount of relative dissipated energy by model B14 has decreased from this loading cycle on. For model B20-LF-AE also this issue is clearly observed. In this model up to the 33th loading cycle, where overall buckling of the bracing has not occurred, the curve has exhibited an ascending trend which indicates increase in the amount of relative dissipated energy in each loading cycle, but from this loading cycle on where overall buckling has occurred, the slope of the curve also has turned negative and the amount of relative dissipated energy in each cycle has taken a descending trend. The important issue concerning B20-LF-AE bracing is that till overall buckling of the bracing in the cycle 33, the positive slope of the curve is also decreasing. The reason of this is related to the fuse confined capacity. In fact after complete yielding of the fuse and reaching its maximum loadbearing capacity, there is no ascending trend for relative energy absorption and the slope of the curve turns zero and then negative. This case is the best and most ideal possible case for absorbing the input energy to the structure and design of LF-AEBC bracing should be in a way that this kind of energy absorption occurs in the bracing. But in this model, before the slope of the curve turns negative, due to reaching the fuse its maximum capacity, the bracing undergoes overall buckling and this factor has caused negative slope in the curve as shown in Fig. 14 and reduced relative energy absorption by the bracing in each loading cycle. Also comparing the EDCE/Disp curves for models B14 and B20-LF-AE, as shown in Figure 14, it is observed that after overall buckling, the slope of the curve for model B14 decreases with a higher rate in comparison to the slope of the curve corresponding to model B20-LF-AE. This is due to the presence of auxiliary element in model B20-LF-AE and also proves positive performance of this element in the post-buckling behavior of concentric bracings.

4. Conclusion

In this study a complete introduction to the new LF-AEBC bracings has been presented to improve the seismic performance of concentric bracings. In this respect two numerical models of B14 and B20-LF-AE, which represent UCB and LF-AEBC, respectively, have been modeled utilizing ABAQUS Ver. 6.12 [21] and are subjected to the displacement cyclic pseudo-static loading. Then the results of these analyses in terms of loadbearing capacity, ductility and energy dissipation capacity have been compared to each other. In the following the general results obtained from these analyses are presented:

- The hysteresis curve obtained from the analyses results for model B20-LF-AE is a wide spindle-shaped and stable curve. This curve indicates that LF-AEBC bracings could solve the main problem associated with concentric bracings which is buckling and ultimately present a symmetric hysteresis curve.
- Based on the results obtained from this study, the concentric bracings which have an elastic buckling capacity greater than their yielding capacity, immediately after yielding and due to considerable reduced stiffness of their materials, undergo buckling. This issue should be considered in the design of concentric bracings, otherwise design of these structures would be incorrect.

- Generally and based on the obtained results from this study, the LF-AEBC bracings have significantly greater maximum and ultimate tensile and compressive loadbearing capacities in comparison to their corresponding concentric bracings, so that the maximum and ultimate tensile loadbearing capacity of LF-AEBC bracings are about 75 % and 90 % greater than their corresponding UCB bracings, respectively. These values in the compressive area for LF-AEBC bracings are 1.85 and 4.3 times that of their corresponding UCB bracings, respectively.

- Generally and based on the results obtained from this study, the residual lateral displacement due to overall buckling of the bracing causes reduced tensile loadbearing capacity of the bracing and with increase in this displacement, the tensile capacity of the bracing decreases, conversely. It is important to consider this issue that in LF-AEBC bracings with respect to UCB bracings, the rate of reduction in tensile loadbearing capacity is much slower due to presence of the auxiliary element.

- Based on the study results, the tensile and compressive ductility coefficients in LF-AEBC bracings are about 50 % and 280 % greater than their corresponding values in UCB bracings, respectively. This issue indicates the significant impact of implementing LF-AE fuse in concentric bracings to improve ductility in these bracings.

- Based on the results of this study, the amount of dissipated energy by model B20-LF-AE was about 2.5 times of this value for model B14. This issue indicates the much better behavior of LF-AEBC bracings with respect to their corresponding UCB bracings. Also the results of this study showed that in general, the overall buckling of the bracing results into reduced relative dissipated energy in each loading cycle. This reduction occurs with a lower rate for LF-AEBC bracings with respect to UCB bracings, which is due to presence of the auxiliary element and also proves positive performance of this element in the post-buckling behavior of concentric bracings.

References

1. Abbasnia R., Vetr M.G.H., Ahmadi R., Kafi M.A. Experimental and analytical investigation on the steel ring ductility. *Sharif J. Sci. Technol.* 2008. Vol. 52. Pp. 41–48.
2. Andalib Z., Kafi M.A., Kheyroddin A., Bazzaz M. Experimental investigation of the ductility and performance of steel rings constructed from plates. *J.Construct. Steel Res.* 2014. Vol. 103. Pp. 77–88.
3. Moghaddam H., Estekanchi H. On the characteristics of off-centre bracing system. *J.Construct. Steel Res.* 1995. Vol. 35(3). Pp. 361–376.
4. Moghaddam H., Estekanchi H. Seismic behavior of off-centre bracing systems. *J.Construct. Steel Res.* 1999. Vol. 51(2). Pp. 177–196.
5. Bazzaz M., Kheyroddin A., Kafi M.A., Andalib Z. Evaluating the performance of steel ring in special bracing frame. *6th International Conference of Seismology and Earthquake Engineering*. Tehran, Iran. May, 2011.
6. Bazzaz M., Kheyroddin A., Kafi M.A., Andalib Z. Evaluation of the seismic performance of off-centre bracing system with ductile element in steel frames. *Steel Compos. Struct., Int. J.* 2012. Vol. 12(5). Pp. 445–464.
7. Bazzaz M., Kheyroddin A., Kafi M.A., Andalib Z., Esmaili H. Evaluating the seismic performance of off-centre bracing system with circular element in optimum place. *Int. J. Steel Struct.* 2014. Vol. 14(2). Pp. 293–304.
8. Bazzaz M., Andalib Z., Kafi M.A., Kheyroddin A. Evaluating the performance of OBS-C-O in steel frames under monotonic load. *Earthq. Struct., Int. J.* 2015. Vol. 8(3). Pp. 697–710.
9. Bazzaz M., Andalib Z., Kheyroddin A., Kafi M.A. Numerical comparison of the seismic performance of steel rings in off-centre bracing system steel rings in off-centre bracing system. *Steel Compos. Struct., Int. J.* 2015. Vol. 19(4). Pp. 917–937.
10. Balendra T., Yu C.H., Lee F.L. An economical structural system for wind and earthquake loads. *J. Eng.Struct.* 2001. Vol. 23. Pp. 491–501.
11. Zahrai S.M., Vosooq A.K. Study of an innovative two-stage control system: Chevron knee bracing & shear panel in series connection. *J. Struct Eng.* 2013. Vol. 47(6). Pp. 881–898.

Литература

1. Abbasnia R., Vetr M.G.H., Ahmadi R., Kafi M.A. Experimental and analytical investigation on the steel ring ductility // *Sharif J. Sci. Technol.* 2008. Vol. 52. Pp. 41–48.
2. Andalib Z., Kafi M.A., Kheyroddin A., Bazzaz M. Experimental investigation of the ductility and performance of steel rings constructed from plates // *J.Construct. Steel Res.* 2014. Vol. 103. Pp. 77–88. DOI: 10.1016/j.jcsr.2014.07.016
3. Moghaddam H., Estekanchi H. On the characteristics of off-centre bracing system // *J.Construct. Steel Res.* 1995. Vol. 35(3). Pp. 361–376.
4. Moghaddam H., Estekanchi H. Seismic behavior of off-centre bracing systems // *J.Construct. Steel Res.* 1999. Vol. 51(2). Pp. 177–196.
5. Bazzaz M., Kheyroddin A., Kafi M.A., Andalib Z. Evaluating the performance of steel ring in special bracing frame // *6th International Conference of Seismology and Earthquake Engineering*. Tehran, Iran. May, 2011.
6. Bazzaz M., Kheyroddin A., Kafi M.A., Andalib Z. Evaluation of the seismic performance of off-centre bracing system with ductile element in steel frames // *Steel Compos. Struct., Int. J.* 2012. Vol. 12(5). Pp. 445–464.
7. Bazzaz M., Kheyroddin A., Kafi M.A., Andalib Z., Esmaili H. Evaluating the seismic performance of off-centre bracing system with circular element in optimum place // *Int. J. Steel Struct.* 2014. Vol. 14(2). Pp. 293–304.
8. Bazzaz M., Andalib Z., Kafi M.A., Kheyroddin A. Evaluating the performance of OBS-C-O in steel frames under monotonic load // *Earthq. Struct., Int. J.* 2015. Vol. 8(3). Pp. 697–710.
9. Bazzaz M., Andalib Z., Kheyroddin A., Kafi M.A. Numerical comparison of the seismic performance of steel rings in off-centre bracing system steel rings in off-centre bracing system // *Steel Compos. Struct., Int. J.* 2015. Vol. 19(4). Pp. 917–937.
10. Balendra T., Yu C.H., Lee F.L. An economical structural system for wind and earthquake loads // *J. Eng.Struct.* 2001. Vol. 23. Pp. 491–501.
11. Zahrai S.M., Vosooq A.K. Study of an innovative two-stage control system: Chevron knee bracing & shear panel in series connection // *J. Struct Eng.* 2013. Vol. 47(6). Pp. 881–898.

12. Cheraghi A., Zahrai S.M. Innovative multi-level control with concentric pipes along brace to reduce seismic response of steel frames. *J.Construct. Steel Res.* 2016. Vol. 127. Pp. 120–135.
13. Rezaei M., Prion H., Tremblay R., Bouatay N., Timler P. Seismic performance of brace fuse elements for concentrically steel braced frames. *3rd Proc. of STESSA Conference.* Montréal, Canada, 2000.
14. Legeron F., Desjardins E., Ahmed E. Fuse performance on bracing of concentrically steel braced frames under cyclic loading. *J.Construct. Steel Res.* 2014. Vol. 95. Pp. 242–255.
15. Desjardins E., Legeron F., Ahmed E. Performances of ductile fuses in reducing seismic demand on connections of concentrically steel braced frames. *15th World conference on Earthquake Engineering.* Lisbon, Portugal, 2012.
16. Iwata M., Kato T., Wada A. Buckling-restrained braces as hysteretic dampers. *3rd International Conference STESSA.* Montreal, Canada, 2000.
17. Sabelli R., Mahin S., Chang C. Seismic demands on steel braced frame buildings with buckling-restrained braces. *J. Eng Struct.* 2003. Vol. 25(5). Pp. 655–666.
18. Kiggins S., Uang C.M. Reducing residual drift of buckling-restrained braced frames as a dual system. *J. Eng. Struct.* 2006. Vol. 28(11). Pp. 1525–1532.
19. Hoveidae N., Tremblay R., Rafezy B., Davaran A. Numerical investigation of seismic behavior of short-core all-steel buckling restrained braces. *J.Construct. Steel Res.* 2015. Vol. 114. Pp. 89–99.
20. Maurya A., Eatherton M.R., Matsui R., Florig S.H. Experimental investigation of miniature buckling restrained braces for use as structural fuses. *J.Construct. Steel Res.* 2016. Vol. 127. Pp. 54–65.
21. ABAQUS Ver .6.12. User's Manual, RI, USA, 2012.
12. Cheraghi A., Zahrai S.M. Innovative multi-level control with concentric pipes along brace to reduce seismic response of steel frames // *J.Construct. Steel Res.* 2016. Vol. 127. Pp. 120–135.
13. Rezaei M., Prion H., Tremblay R., Bouatay N., Timler P. Seismic performance of brace fuse elements for concentrically steel braced frames // *3rd Proc. of STESSA Conference.* Montréal, Canada, 2000.
14. Legeron F., Desjardins E., Ahmed E. Fuse performance on bracing of concentrically steel braced frames under cyclic loading // *J.Construct. Steel Res.* 2014. Vol. 95. Pp. 242–255.
15. Desjardins E., Legeron F., Ahmed E. Performances of ductile fuses in reducing seismic demand on connections of concentrically steel braced frames // *15th World conference on Earthquake Engineering.* Lisbon, Portugal, 2012.
16. Iwata M., Kato T., Wada A. Buckling-restrained braces as hysteretic dampers // *3rd International Conference STESSA,* Montreal, Canada, 2000.
17. Sabelli R., Mahin S., Chang C. Seismic demands on steel braced frame buildings with buckling-restrained braces // *J. Eng Struct.* 2003. Vol. 25(5). Pp. 655–666.
18. Kiggins S., Uang C.M. Reducing residual drift of buckling-restrained braced frames as a dual system // *J. Eng. Struct.* 2006. Vol. 28(11). Pp. 1525–1532.
19. Hoveidae N., Tremblay R., Rafezy B., Davaran A. Numerical investigation of seismic behavior of short-core all-steel buckling restrained braces // *J.Construct. Steel Res.* 2015. Vol. 114. Pp. 89–99.
20. Maurya A., Eatherton M.R., Matsui R., Florig S.H. Experimental investigation of miniature buckling restrained braces for use as structural fuses // *J.Construct. Steel Res.* 2016. Vol. 127. Pp. 54–65.
21. ABAQUS Ver .6.12. User's Manual, RI, USA, 2012.

Mohammad Ali Kafi,
00982331533755; mkafi@semnan.ac.ir

Ali Kachooee,
00989127910346; ali.kachooee@semnan.ac.ir

Мохаммад Али Кафя,
00982331533755; эл. почта: mkafi@semnan.ac.ir

Али Качуй,
00989127910346;
эл. почта: ali.kachooee@semnan.ac.ir

© Kafi M.A., Kachooee A., 2018

doi: 10.18720/MCE.78.3

Bearing capacity of facade systems fixing to sandwich panels

Несущая способность крепления навесных фасадных систем к сэндвич-панелям

A.V. Galyamichev,
V.A. Kirikova,
G.E. Gerasimova,

Peter the Great St. Petersburg Polytechnic University, St. Petersburg, Russia

A. Sprince,
Riga Technical University, Riga, Latvia

Старший преподаватель А.В. Галямичев,
студент В.А. Кирикова,
студент Е.Н. Герасимова,

Санкт-Петербургский политехнический университет Петра Великого,

г. Санкт-Петербург, Россия
д-р техн. наук, доцент А. Спринце,
Рижский технический университет, г. Рига, Латвия

Key words: facade system; sandwich panel; bracket; screw; facade

Ключевые слова: навесные фасадные системы; сэндвич-панель; кронштейн; самонарезающий винт; фасад

Abstract. The article presents results of the experimental and theoretical research of bearing capacity determination for fixings, used for bearing and supporting brackets in facade systems with the base from sandwich panel. The experiment included the consideration of several types of brackets fixing: using self-tapping screws and threaded rods, taking into account the variation in the thickness of the bearing steel plates. The required values of the research were critical longitudinal force for the pull-out from the base, deformations of the base, which lead to the disruption of sandwich-panel structural integrity. In addition, full-sized samples of the bearing bracket (the most loaded element of the facade system), installed on sandwich panel, were tested for the longitudinal (wind) and shearing (self-weight of cladding and system) load with different types of fixing. As a result, the article gives recommendations for the joints design of facade system brackets fixing to the base from sandwich panel, developed on the results of tests and theoretical studies.

Аннотация. В статье изложены результаты проведенных экспериментальных и теоретических исследований по определению несущей способности креплений несущих и опорных кронштейнов навесных фасадных систем (НФС) к основанию из стеновой сэндвич-панели. В процессе испытаний по определению несущей способности крепления НФС к стеновой сэндвич-панели ставились задачи по определению критического продольного усилия необходимого для вырывания элемента крепления или деформации основания, приводящей к нарушению целостности конструкции; испытывались полноразмерные образцы несущего (наиболее нагруженного элемента системы) кронштейна расчетной продольной (ветровой) и вертикальной (весовой) нагрузкой; измерялись величины поперечной деформации сэндвич-панели от сосредоточенной силы, вызываемой действием весовой и ветровой нагрузок, действующей на систему НФС. По результатам проведенных испытаний и теоретических исследований даются рекомендации по проектированию соединений крепежных элементов креплений навесных фасадных систем к основанию из стеновой сэндвич-панели.

1. Introduction

Nowadays, rapid progress in the field of application of energy-efficient outdoor facade systems and increased amount of work, associated with using of various fastenings combinations for these systems, lead to the need of deciding large number of questions, which appear at engineers about requirements for reliability and durability of facade connections. Insufficient volume of the conducted researches in this sphere essentially complicates qualitative designing and the subsequent normal exploitation of facade systems designs.

While researching this area, it is necessary to make a review of some works made on this theme. Questions of strength and anchor deformation from static and dynamic load, considered in the D.A. Kiselev dissertation work [1]. Author developed and proposed the practical application of the test

Галямичев А.В., Кирикова В.А., Герасимова Е.А., Спринце А. Несущая способность крепления навесных фасадных систем к сэндвич-панелям // Инженерно-строительный журнал. 2018. № 2(78). С. 30–46.

procedure, performed a comparative assessment of existing test methods, established criteria for the value of calculation load, which can act on the anchor and recommended some types of anchors for using in buildings and structures, constructed in areas with seismicity range: 7 - 9 points.

I.V. Katranov in his work [2] developed a method for testing the shear and stretching of joints with rivets or self-tapping screws, identified and classified the failures of light steel structures connections and also made practical recommendations for conducting certification tests of rivet and screw connections for shear and tension.

Articles [3, 4] show the experimental studies of the self-tapping screws work in seismic areas, in conditions of the dynamic loading effect; also authors give recommendations in the field of fastening for sandwich-panels in building areas with seismicity of 7÷9 points. A.V. Granovsky [5] developed and approved the testing method for breakout anchors from various base materials, compared the test methods that are conducted abroad and in our country and noted the advantages of testing anchors method, developed at the Kucherenko Central Scientific Institute.

M.Yu. Ananyin and Yu.S. Vedischeva [6] revealed the nature of the deformation of the fastening system on the basis of a series of preliminary numerical experiments performed with the application of a uniformly distributed static load to the system, as well as loads arising from the difference in temperatures outside and inside the building. Calculated results obtained by authors and compared with theoretical calculations, however, during the experiment, the joint operation of the sandwich panel system with the building frame was not taken into account.

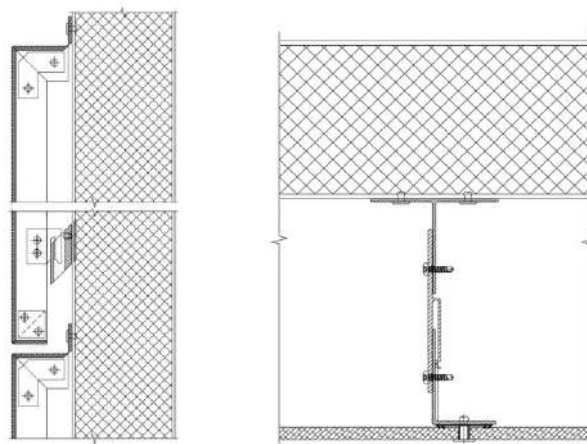
Articles of O.A. Tushina [7–9] considered fastening thin-walled Z-purlins supported by sandwich panels. In this paper she considered questions of numerical analysis of purlins in sandwich panel coverings. Numerical analysis was based on laboratory experiments and modeling of the situation in the program. The results of the theoretical study were compared with the results of the experiments. A finite-element model proposed for constructing the connection of cold-bent purlins and sandwich panels.

Paper [10] is devoted to the development of a complex geometrically nonlinear theory of three-layered shells, which also includes the influence of initial geometric imperfections. It assumed that the sandwich panel is an anisotropic material. Taking into account all features, authors developed a structural model that provides checking load bearing capacity of the three-layer panels and, in addition, ways of increasing the load capacity of the three-layer shells and plates.

In articles [11, 12], authors presented a technique of bearing capacity calculation for multilayer structures, determining stresses and deformations in sandwich panels, based on numerical simulation with taking into account design features and comparing the results of calculations with experimental data for the maximum permissible load.

Currently, there are many newly constructed and reconstructed objects with enclosing structures made from sandwich panels. To impart for these buildings new aesthetic and architectural features, it is necessary to use non-standart technologies and materials to make cladding on the surface of sandwich panel. In this regard, the constructive solution is to fix the facing materials to the body of the sandwich panel.

There are several types of these fastening (see Figs. 1, 2).



Figures 1, 2. Existing methods of fixing systems to sandwich panels (Fig. 1 (left, section) – “Hand-made” system of fixing, Fig. 2 (right, top view) – system with uniformly fixed T-profile to sandwich panel)

These two types of fixing have obvious disadvantages, due to the dependence from the cohesive joint bearing capacity between the zinc-coated steel sheet and insulation material, which will deteriorate over time due to temperature fluctuations and condensation. An example of such object with a similar fixing see on Figure 3.



Figure 3. Western speed diameter office (St. Petersburg)¹

Researched type of fastening (Figs. 4–9) have known thermal and aesthetic disadvantages, due to the presence of "cold bridges" in the insulating structure and visible self-tapping screws at internal structure. However, theme of the study was obtaining of necessary and sufficient bearing capacity of connection. Negative factors solved by the thickness of insulation and internal finishing by gypsum plasterboard sheets [13].

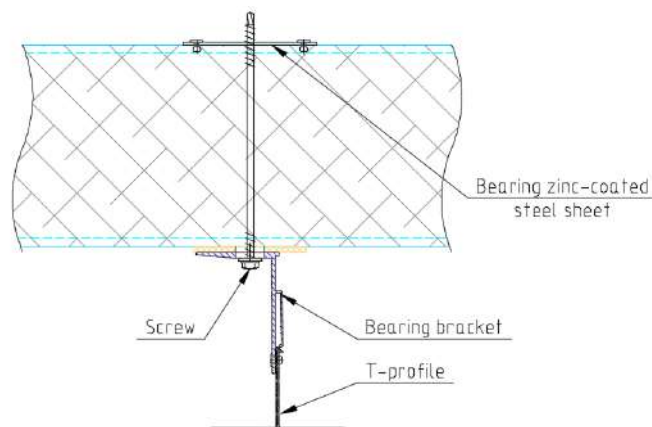


Figure 4. One of the researched types of fastening to sandwich-panel

The main aim of this article, based on the experimental and theoretical studies, is to develop:

- Method of static testing connection between the facade system elements and sandwich panels on the action of wind (longitudinal) and self-weight (shear) forces;
- Method of testing for the action of a cyclic (breakout) load;
- Investigation of strength and deformation of fastening under the action of calculation loads;
- Recommendations for different types of fastening application.

The task of the study is to determine the bearing capacity for combinations of different facade systems fastening types to sandwich panels

2. Materials and Methods

The object of a study – is connection between the bearing and supporting brackets of facade systems with sandwich panels with external and internal zinc-coated steel sheets, at least 0.5 mm thick and mineral wool insulation (total panel thickness in experimental tests was 150 mm).

¹ Photo link: <https://yandex.ru/maps/-/C6aqM-6f>

Research for defining the bearing capacity included several types of fastening to sandwich panels:

1. Fixing system by self-tapping screw [14] to the structure from the following composition: zinc-coated steel sheet with thickness 1 mm; sandwich panel $t = 150$ mm (0.5 / 0.5); steel zinc-coated sheet with thickness 1 mm. Type 1, abbreviated name "1+1" (Fig. 5).

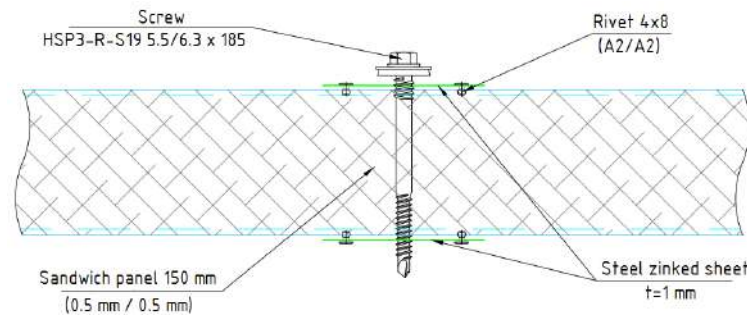


Figure 5. Experimental type of fixing (Type 1 – "1+1")

2. Fixing system by self-tapping screw to the structure from the following composition: sandwich panel $t = 150$ mm (0.5 / 0.5); zinc-coated steel sheet with thickness 1 mm from the inside. Type 2, abbreviated name "0+1" (Fig. 6).

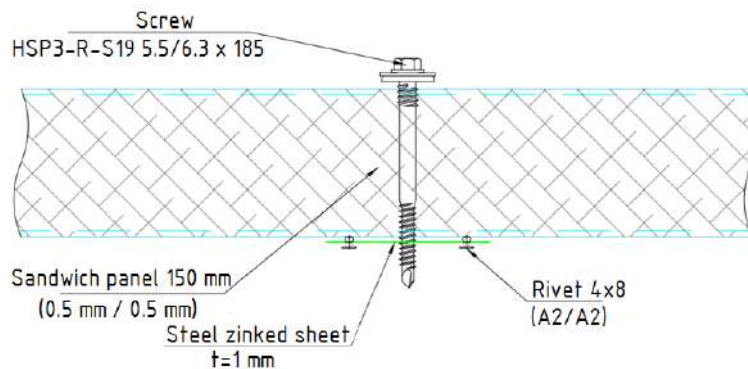


Figure 6. Experimental type of fixing (Type 2 – "0+1")

3. Fixing system by self-tapping screw to the structure from the following composition: sandwich panel $t = 150$ mm (0.5 / 0.5); zinc-coated steel sheet with thickness 2 mm from the inside. Type 3, abbreviated name "0+2" (Fig. 7).

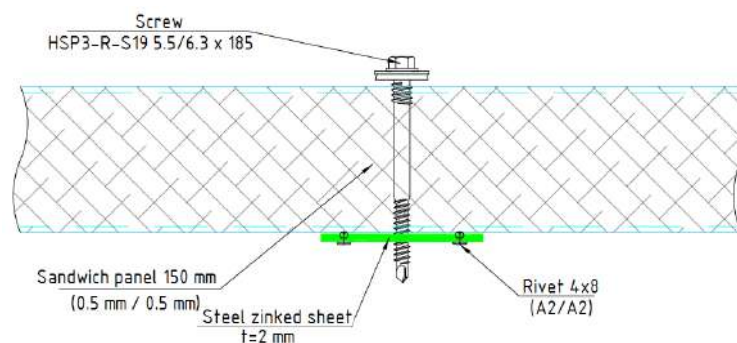


Figure 7. Experimental type of fixing (Type 3 – "0+2")

4. Fixing system by threaded rod with M8 diameter to the structure from the following composition: zinc-coated steel sheet with thickness 1 mm; sandwich panel $t = 150$ mm (0.5 / 0.5); steel zinc-coated sheet with thickness 1 mm. Type 4, abbreviated name "TR 1+1" (Fig. 8). If this connection applied on construction objects, it is necessary to use the methods of locking the threaded connection provided by the existing normative documentation

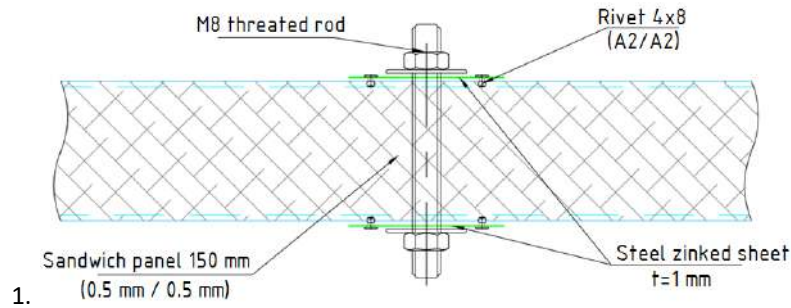


Figure 8. Experimental type of fixing (Type 4 – «Threated rod 1 + 1»)

5. Fixing system by self-tapping screw to the structure from the following composition: zinc-coated steel sheet with thickness 1 mm; sandwich panel $t = 150$ mm (0.5 / 0.5); steel plate with thickness 8 mm. Type 5, abbreviated name “1+8” (Fig. 9). This type of structure is considered to show, how system work in conditions of fixing to existing steel substructure and to restrict the limit values of thickness for supporting plates.

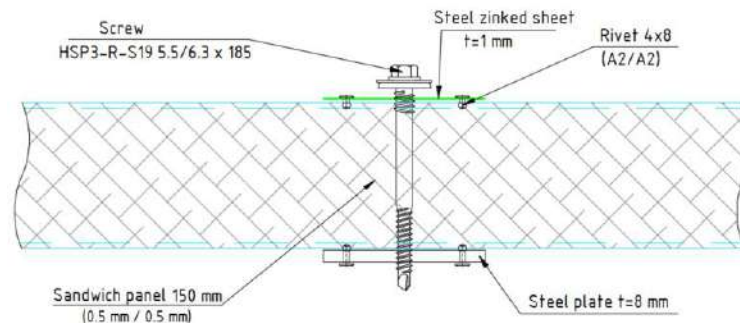


Figure 9. Experimental type of fixing (Type 5 – “1+8”)

Determination of the fastening bearing capacity of facade system brackets to the sandwich panels was performed in three stages:

I. Determination of the longitudinal force, necessary for the breakout of fixing element from the base material, or deformation, which leads to defects in the structure integrity.

II. Testing the full-sized sample of the bearing (the most loaded element of the system) bracket with the calculated wind (longitudinal) and self-weight (shear) load.

III. Determination of the sandwich panel deformation from the forces caused by the action of the weight and wind load acting on the facade system.

The essence of the first method is in test the fastening elements by the tensile load, applied to the connection element along its axis, determination the strength resistance and base deformation, setting of values for limit states. Stretching bearing capacity of the fixing elements calculated by processing the test results, must ensuring the work of the fixing element in the elastic conditions. In addition, rivet joints, installed near to the anchor, increases the bearing capacity of the joint and test must provide the most disadvantageous position of rivets.

The second method involves checking the calculated values on a full-size model in conditions of a complex stress state corresponding to the actual operation of the system and help to evaluate the accepted reliability coefficients for the design work. The principle of the test is to apply a constant vertical (weight) load to the fragment of a façade system and sequential increase of the horizontal (wind) load to determine the critical value of the applied force group. Experimental sample loaded by stages with subsequent unloading to determine the value of inelastic deformations. After evaluation of residual effects, the sample loading until the appearance of the first limit state signs on the fixing element or on the supporting base.

The third method is designed to determine the maximum possible displacements of the building base under the action of a concentrated load, evaluate the rigidity of the sandwich panel and perform a comparative analysis for compliance with the second limit state.

For the first test was applied method, given in [15].

Measuring instrument: Hydrajaws 2000, EMC 91/130364526/100613273 (Fig. 10) – hydraulic jack “hydrajaws limited”.



Figure 10. Measuring instrument (tensile machine)

On the Figure 11, shown sample of a panel, in which was installed fixing elements for test.

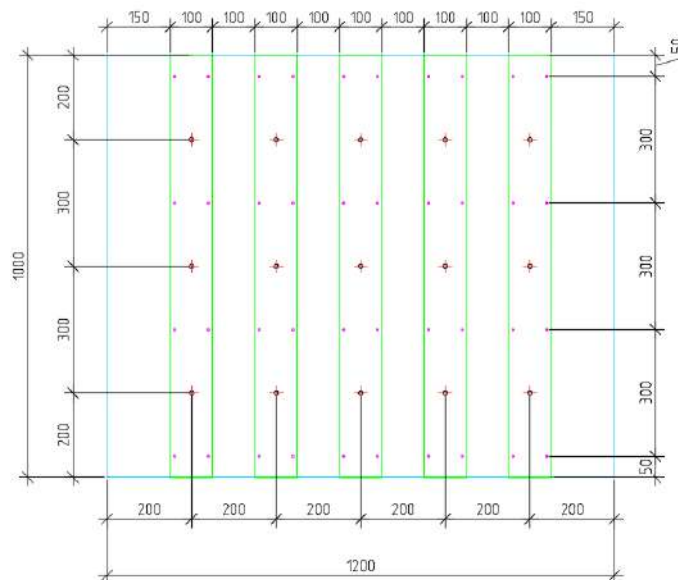
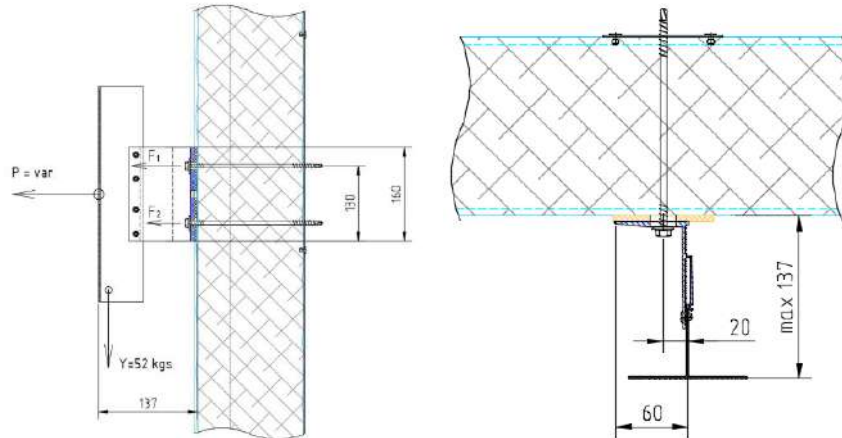


Figure 11. Sandwich panel test sample with a marking for the installation of fixings

Self-tapping screws fixed in the basis in the most disadvantageous position, implying no effect of the rivet connections on the bearing capacity required for plate mounting.

The basis for the analysis of the second testing is a comparison of the obtained values of the tearing force in full-sized modeling with the results obtained by pulling along the longitudinal axis of the fixing element during the first testing. The difference in the values lies in the fact that under operational loads, not only the longitudinal force comes to the bracket, but also the shearing loads in combination with the bending moment, caused by the effect of the weight of the liner and the subsystem. Conditions for the most disadvantageous position of system were determined during the test and include the maximum span of the system adopted on basis of [14] of 137 mm and the height of the bracket of 130 mm (Figs. 12 and 13). At this case, the specimen is the most loaded upper fixing element, as it connects with the action of bending moment. In addition, it is necessary to take into account in the calculation the eccentricity of the load application in the plan, shown in Figure 12.

To calculate the value of F_1 with taking into account action of the moment in two planes, the standards of the manufacturer of anchor technics for this type of impact should be considered.



Figures 12 and 13. Scheme for testing the fixing element in the second stage

3. Results and Discussion

3.1. The first stage of the study

Process of experimental determination of the longitudinal force, necessary for the breakout of fixing element from the base material, is shown on Figures 14 and 15.

As a result, the following parameters were found for each type of structure:

Table 1. The results of the pull out tests of structure Type 1 ("1+1")

№	Name	Applied longitudinal load (kN)	The mean square deviation of unit load values (kN)	Type of failure
1	1+1	2.17	0.000	Pull out a screw
2	1+1	2.18	0.001	Pull out a screw
3	1+1	2.59	0.192	Pull out a screw
4	1+1	2.09	0.004	Pull out a screw
5	1+1	2	0.023	Pull out a screw
6	1+1	1.88	0.074	Pull out a screw
		$N = 2.15 \text{ kN}$	$S = 0.242 \text{ kN}$	

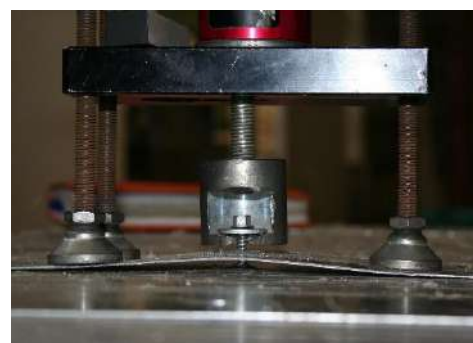


Figure 14 and 15. Process of pulling out a screw (left), hole in the plate after the pull out (right)

Average value of load [15]:

$$N = \frac{\sum_{i=1}^n N_i}{n} = \frac{12.91}{6} = 2.15 \text{ kN} \quad (1)$$

The mean square deviation of unit load values:

$$S = \sqrt{\frac{\sum_{i=1}^n (N_i - N)^2}{n-1}} = 0.242 \text{ kN} \quad (2)$$

Variation coefficient:

$$v = \frac{S}{N} = 0.11 \quad (3)$$

Design value of resistance for calculations:

$$R = \frac{N(1 - tv)}{m} \quad (4)$$

where m – Reliability coefficient of the material ($m = 1.3$ according to [14]);

t – Coefficient corresponded to the lower limit of the bearing capacity of the anchor with security 0.95 at veracity of 90 % (For 6 tests $t = 3.091$ according to [15] Table 1).

$$R = \frac{2.15 \cdot (1 - 3.091 \cdot 0.11)}{1.3} = 1.08 \text{ kN} \quad (5)$$

As fixing elements were set in laboratory, it is necessary to reduce the results by coefficient of the working conditions

$$R_c = \frac{R}{\gamma_n} = \frac{1.08}{1.1} = 0.98 \text{ kN} \quad (6)$$

Table 2. The results of the pull out tests of structure Type 2 (“0+1”)

№	Name	Applied longitudinal load (kN)	The mean square deviation of unit load values (kN)	Type of failure
1	0+1	2.68	0.375156	Pull out a screw
2	0+1	1.63	0.191406	Pull out a screw
3	0+1	1.72	0.120756	Pull out a screw
4	0+1	2.13	0.003906	Pull out a screw
5	0+1	2.32	0.063756	Pull out a screw
6	0+1	1.82	0.061256	Pull out a screw
7	0+1	2.71	0.412806	Pull out a screw
8	0+1	1.53	0.288906	Pull out a screw
		$N = 2.07 \text{ kN}$	$S = 0.47 \text{ kN}$	

Design value of resistance for calculations [15]:

$$R = \frac{2.07 \cdot (1 - 2.755 \cdot 0.22)}{1.3} = 0.6 \text{ kN} \quad (7)$$

$$R_c = \frac{R}{\gamma_n} = \frac{0.6}{1.1} = 0.55 \text{ kN} \quad (8)$$

Table 3. The results of the pull out tests of structure Type 3 (“0+2”)

№	Name	Applied longitudinal load (kN)	The mean square deviation of unit load values (kN)	Type of failure
1	0+2	3.67	0.001344	Pull out a screw
2	0+2	3.88	0.030044	Pull out a screw
3	0+2	3.58	0.016044	Pull out a screw
4	0+2	3.76	0.002844	Pull out a screw
5	0+2	3.68	0.000711	Pull out a screw
6	0+2	3.69	0.000278	Pull out a screw
7	0+2	3.79	0.006944	Pull out a screw
8	0+2	3.56	0.021511	Pull out a screw
9	0+2	3.75	0.001878	Pull out a screw
		$N = 3.71 \text{ kN}$	$S = 0.1 \text{ kN}$	

Design value of resistance for calculations [15]:

$$R = \frac{3.71 \cdot (1 - 2.645 \cdot 0.1)}{1.3} = 2.65 \text{ kN} \quad (9)$$

$$R_c = \frac{R}{\gamma_n} = \frac{2.65}{1.1} = 2.4 \text{ kN} \quad (10)$$

It was revealed in the course of experiment that the loss of the bearing capacity of joining type 4 – “Threaded rod 1 + 1” and joining type 5 – “1 + 8” does not occur. The failure was caused by delamination of sandwich panel at 4.1 kN (Figs. 16 and 17).

$$R_c = \frac{R}{\gamma_n \cdot \gamma_m} = \frac{4.1}{1.1 \cdot 1.3} = 2.87 \text{ kN} \quad (11)$$



Figures 16 and 17. Delamination of sandwich panel

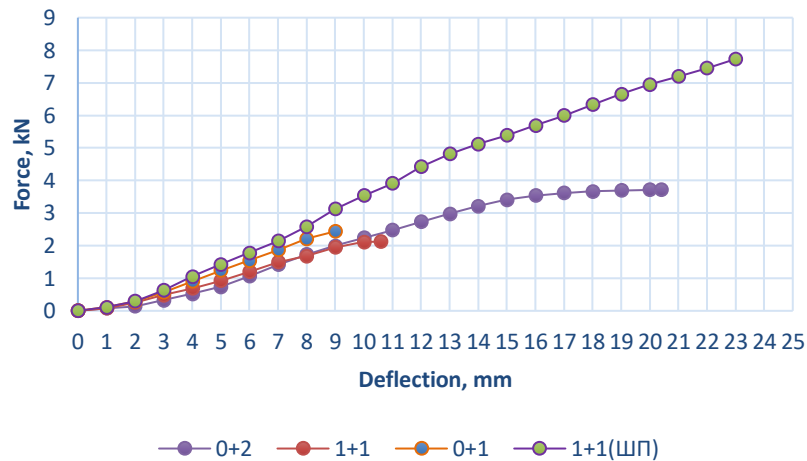


Figure 18. Dependence of deformations on the tensile force

3.2. The second stage of the study

The experimental construction is shown in Figure 19.

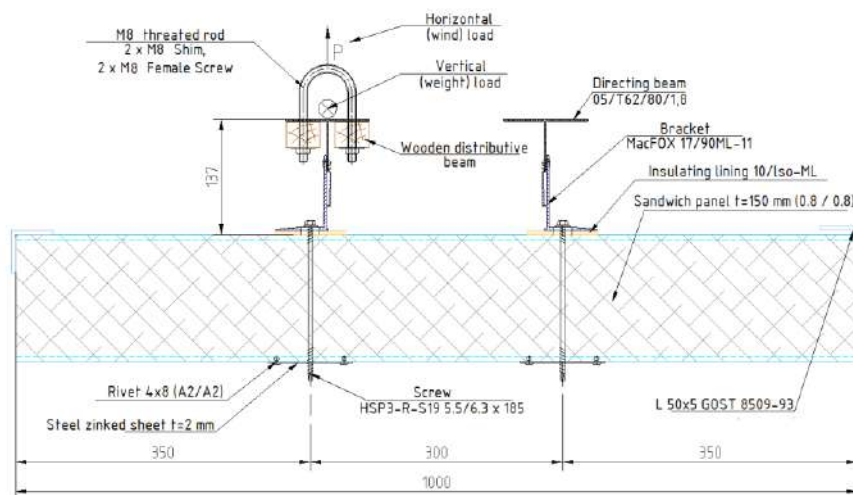


Figure 19. Scheme of the experimental structure with fixing to the plate $t = 2$ mm

Measuring instrument: strain gauge [18], accuracy class III according to [19].

Samples of joining Type 3 ("0 + 2"), Type 4 ("1 + 1") and Type 5 ("1 + 8") were not destroyed, but at a load of 595 kg the zinc sheathing began to flake off at the inner surface of the sandwich panel. This process developed most actively in the samples with fixing of the facade system by threaded rod: the large diameter of shim M8 created a local zone of stress concentration and local areas of crumpling that contributed to the flaking of the sheathing.

Table 4. The results of the tests of structures Type 1, Type 2 and Type 3

№	Number of samples	Fixing elements		Load, kg				Type of failure
		Plates	Fixing tool	Weight	Stage 1	Stage 2	Max	
1	1	1+1	Screw	52	257	314	437	Pull out
2	1	1+1	Screw	52	222	314	418	Pull out
3	1	1+1	Screw	52	222	314	418	Pull out
4	1	0+1.2	Screw	52	222	-	493	Pull out
5	1	0+1.2	Screw	52	222	-	456	Pull out
6	1	0+1.2	Screw	52	222	-	447	Pull out
7	1	0+1	Screw	52	222	-	428	Pull out

The breaking of bracket attachment to the sandwich panel occurred by pulling out the self-tapping screws from the sandwich with the simultaneous deformation of the shim of head of the self-tapping screw to the bracket.

The maximum load on stages 4, 5, 6 was higher than for 1, 2, 3 due to a small (0.2 mm) increasing of the thickness of the plate (from 1.03 to 1.22 mm).

The results of values of tensile forces in the top (F_1) and bottom (F_2) bracket fastenings, obtained during the second stage, are summarized in Table 5.

Table 5. The value of tensile force based on the calculation results

№	Type of fixing		Critical load, kN		Longitude force, kN		Type of failure
	Plates	Anchors	Weight (Y)	Wind (P)	F_1 , kN	F_2 , kN	
1	1+1	Screw	0.516	4.29	3.470	3.104	Pull out
2	1+1	Screw	0.516	4.1	3.325	2.959	Pull out
3	1+1	Screw	0.516	4.1	3.325	2.959	Pull out
4	0+1.2	Screw	0.516	4.84	3.889	3.525	Pull out
5	0+1.2	Screw	0.516	4.47	3.607	3.242	Pull out
6	0+1.2	Screw	0.516	4.39	3.546	3.181	Pull out
7	0+1	Screw	0.516	4.2	3.401	3.035	Pull out
8	1+1	Threaded rod	0.516	5.84	4.651	4.289	Delamination
9	1+8	Screw	0.516	5.84	4.651	4.289	Delamination
10	0+2	Screw	0.516	5.84	4.651	4.289	Delamination

Results of numerical determination of forces F_1 and F_2 obtained in calculation complex Hilti Profis Anchor (Fig. 20).

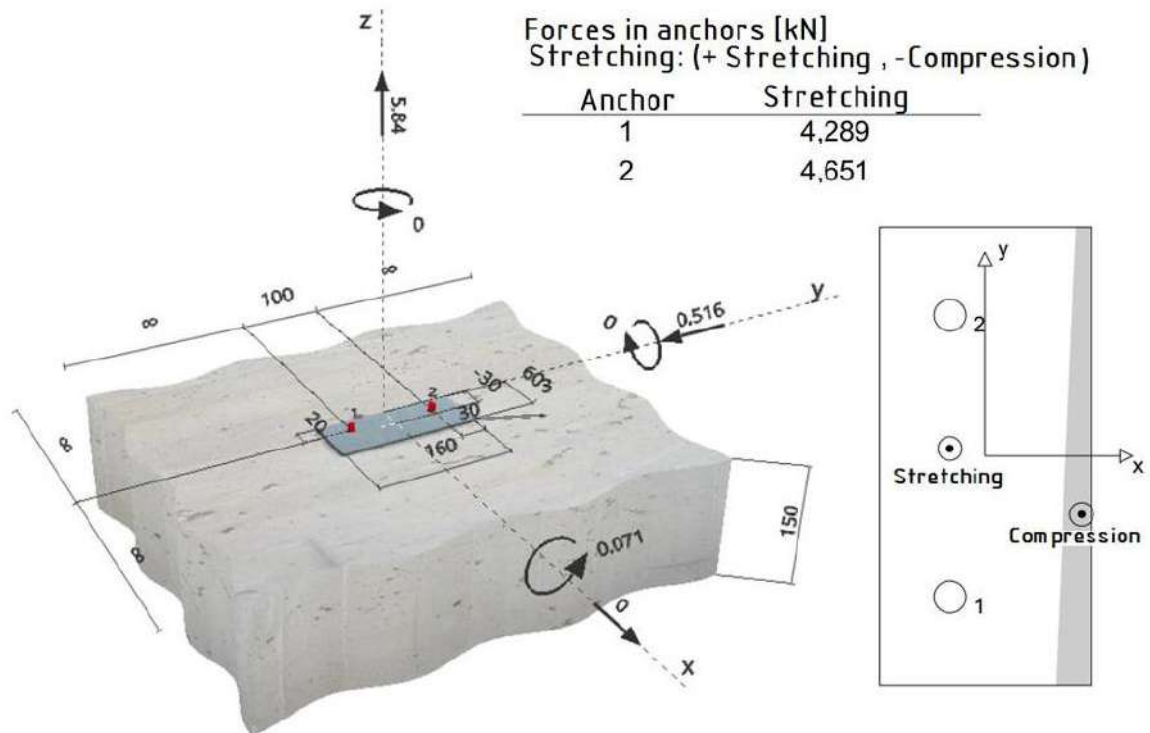


Figure 20. Design scheme, stress distribution along the base of bracket and the results of calculation (according to [21])

3.3. The third stage of the study

Experiments that are carried out to determine deformations of a wall sandwich panel impacted by load from an facade system make possible to conclude about occurred stress-strain state of structures. The experimental construction is on Figure 21.

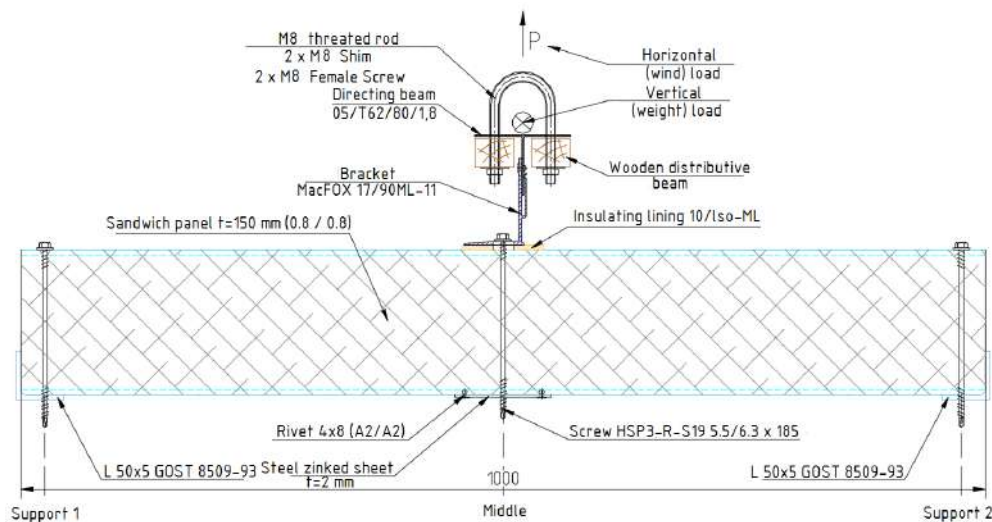


Figure 21. Scheme of the experimental structure for determination of deflections

Measuring instruments: deflectometer [20] for determining the values of displacement of considered points of structures under static loading; strain gauge [18], accuracy class III according to [19].

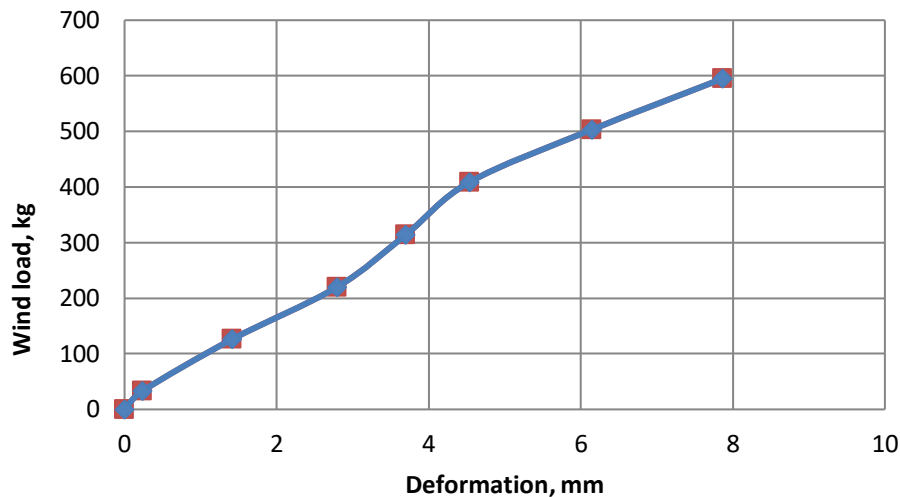


Figure 22. Averaged displacement chart

Thus, it is possible to draw a generalized conclusion about the operation of the structure for various types of fixing elements used. Table 6 gives the values of the longitudinal force of the fixing element necessary for the pulling out or deformation of the base, which causes structural integrity violation.

Table 6. Summary of the pull out tests

№	Name	Average calculative critical longitude force (kN)	Type of failure
1	0+1	0.55	Pull out
2	1+1	0.98	Pull out
3	0+2	2.4	Pull out
4	Threaded rod 1 + 1	2.87	Delamination
5	1+8	2.87	Delamination

On the basis of the obtained results, it can be concluded that self-tapping screws can be used as fixing elements of facade system to a bearing base by wall sandwich panel. In this case, the value of the bearing capacity of the joint is sufficient to resist the combined effect of peak wind loads and weight loads of the sheathing and the system within the design resistance to the breaking of the fixing element.

It is recommended to use sandwich panels with additional amplification by steel zincated plates with a thickness of at least 2 mm.

Usage of amplifying plates with a thickness of 1 mm in combination with self-tapping screw for fixing the brackets is not allowed due to considerable variation in the values of the tearing force (up to ± 0.58 kN) while testing in laboratory conditions. It is caused by small thickness of the thread of the self-tapping screw in the zincated plate and the random distribution of the thread turns while screw installation.

This conclusion is confirmed, in particular, by the limitations established in [14]: the minimum thickness of the plates in which it is allowed to install self-tapping screws HSP3 is 2 mm. The values of the tearing force obtained in experiment are close to the values of the critical force given in [14] for plates with 2 mm thick:

$$R_c^{STO} = \gamma_c \cdot \frac{F_{tn}}{\gamma_m} = 0.9 \cdot \frac{3.315}{1.3} = 2.3 \text{ kN} \quad (12)$$

$$R_c = \frac{R}{\gamma_n} = \frac{2.65}{1.1} = 2.4 \text{ kN} \quad (13)$$

The difference in the value of 0.1 kN is explained by the presence of additional steel sheets (2 x 0.5 mm) in the sandwich panel structure, for which fixing is also carried out, but due to results they have no significant effect.

As an alternative method of fixing, it is allowed to use threaded rods with a diameter of 8 mm in combination with a washer and a nut. To prevent unscrewing of the joint, it is necessary to use the methods of locking the threaded connection.

In addition, on the basis of the tests, it can be stated that the fixing of the facade system by a self-tapping screw to the bearing steel structures (on the example of a plate 8 mm thick) is permissible and reliable.

On the basis of the test, it can be concluded that it is necessary to take into account the value of the edge distance from free edge of the sandwich panel to the axis of the fixing element installed by the panel manufacturers together with the producers of self-tapping screws. This requirement is set due to the need to prevent detachment of the inner sheathing of steel zincated sheet and mineral wool insulation. It is permissible not to take into account the value of the edge distance during installing the bracket in the immediate vicinity of the sandwich panel locks, and also during fixing of system elements directly to the frame of the building.

The design value of the tearing force for the object must be taken on the basis of full-scale tests of the sample with considering possible features of sandwich panels, self-tapping screws and amplifying zincated plates. The test can be performed according to the methodological instructions described in [15].

Analysis, based on the results of pull-out tests, is confirmed by the study of static operation of full-size models. Samples fixed with self-tapping screws in the sandwich panel with amplifying zincated steel plate 2 mm thick, and samples with a threaded rod and fixing in a steel plate 8 mm thick have sufficient bearing capacity for perception of loads from façade system. The first (ultimate) limit state was obtained due to detachment of sandwich panel near free edge of panel. At the same time, the connection remains bearing capable.

Samples, which are fixed to zincated plate 1 mm thick, were destroyed during tests: first (ultimate) limit state occurred as a result of pulling the self-tapping screw out of the steel zincated plate. As in the case of pull-out testing, there was a significant variation in the values of the critical load, what confirms the thesis of the small thickness of gearing of the thread of self-tapping screw in the zincated plate and the random distribution of the thread turns while screw installation.

Analysis of cyclic loading (loading-unloading-loading) revealed no significant residual deformations and decreasing of bearing capacity of the connection in the samples, taking into account the work within the design resistance of the fixing element.

Tests indicated necessity of replacement the standard sealing EPDM shim of self-tapping screws by two shims M6 DIN 9021 due to significant deformations caused by the compression of the sealing rubber under loading (Fig. 23).



Figure 23. Difference between using of rubber and steel plates

It led to heeling of the screw, which causes additional deformations of the sample. When using double shims, such deformations were eliminated. In the design of facade systems, it is necessary to precise this requirement in working documentation.

The difference in the results in the first and second test groups is explained by the effect of the weight (shear) load on the bearing capacity of the threaded connection in fixing to the sandwich panel. This effect contributes a better gearing of the thread of the self-tapping screw to the zincated amplifying plate.

At the same time, the physical modelling demonstrated a greater bearing capacity of the joint than results of the longitudinal tearing of self-tapping screws.

In this way, when designing structures of façade system, it is recommended to adhere to calculated resistance to the tearing of the fixing elements obtained from the first test group (pulling out due to [15]), because coverings used at the construction sites have different weight characteristics and amplifying impact on the connections. The additional bearing capacity, acquired due to the weight of covering, is taken into the safety margin of the system.

The obtained values of deformation for facade system fixed to sandwich panel by self-tapping screw and a zinced plate 2 mm thick must be correlated with the requirement [22] for second (serviceability) limit state (the value of permissible deformations).

In accordance with paragraph E.2.4.3 [22], "The horizontal limit deflections of the racks and girders, as well as of wall hinged panels, from wind load, must be taken as $l / 200$, where l is the design span of the racks or panels".

Thus, for panels with a height between clutch locks 1200 mm:

$$f_{per} = \frac{1200}{200} = 6 \text{ mm} \quad (14)$$

Maximum permissible load for the "0 + 2" system:

$$R_c = 2.4 \text{ kN} \quad (15)$$

Therefore, on the basis of the deformation diagram given in Figure 22, the value of deflection under the given load will be:

$$f_{(2,4 \text{ kN})} = 3 \text{ mm} < f_{per} = 6 \text{ mm} \quad (16)$$

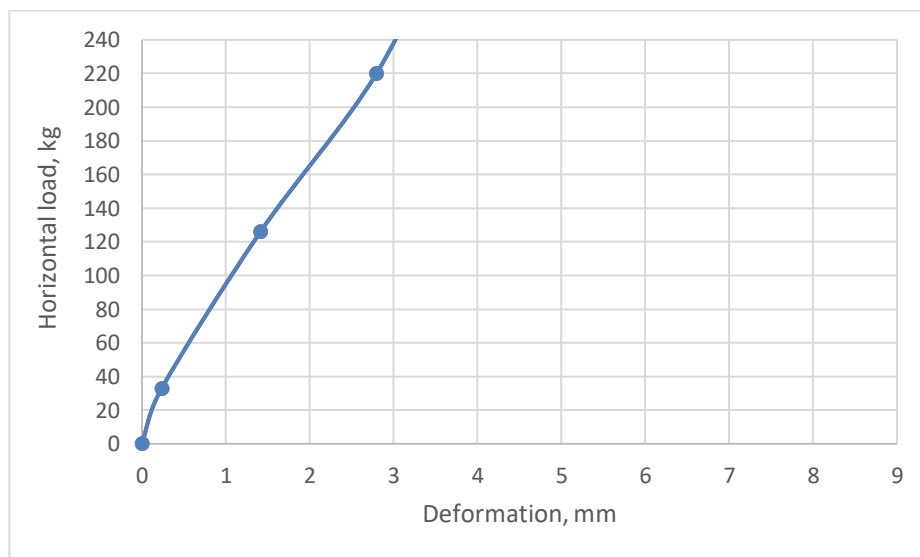


Figure 24. Enlarged graph of the averaged displacement, shown on Figure 22

In this way, it can be concluded that the fixing of facade system to the sandwich panel 150 mm thick using a self-tapping screw and a zinced plate $t=2$ mm satisfies the requirement of the second (serviceability) limit state.

4. Conclusions

According to the results of the study, it can be concluded that use of self-tapping screws as element, which provides fixing of facade system [13] to a wall sandwich panel jointly with an amplifying plate with a thickness of at least 2 mm. An alternative method of fixing is the use of self-tapping screws as fixing element with fastening to the bearing metal frame of the structure with thickness of at least 2 mm. It is also possible to replace the self-tapping screw with a M8 threaded rod fixed on both sides with a shim M8 and female screw M8, in this case, it is permissible to use amplifying plates with a thickness of at least 1 mm. Thread locking means on construction objects must be provided by the existing normative documentation.

While designing a façade system structure, it is recommended to adhere the following conditions:

- To act in accordance with the calculated value of the resistance of the fixing elements to the tearing force, obtained by the method [15].
- To replace the standard EPDM shim of self-tapping screw with double shim in the working documentation to eliminate deformations and heels associated with the compression of the rubber seal.
- To note that the application of self-tapping screws must be carried out taking into account the aggressiveness of the environment in accordance with technical certificate, and the steel and zinc elements must be protected against corrosion in accordance with [23, 24].
- To take into account the values of the edge distance between free trimmed edge of the sandwich panel and axis of the fixing element, which is set by manufacturers of panels jointly with the manufacturers of self-tapping screws.

5. Acknowledgment

The group of researchers thanks the company NordFOX and Teplant for the provided elements of facade systems and sandwich panels.

References

1. Kiselev D.A. *Prochnost i deformativnost ankernogo krepzha pri deystvii staticheskoy i dinamicheskoy nagruzok* [Strength and deformability of anchor fasteners under the action of static and dynamic loads]. Abstract PhD Thesis: 05.23.01. Moscow, 2010. 29 p. (rus)
2. Katranov I.G. *Nesushchaya sposobnost vintovykh i zaklepochnykh soyedineniy stalnykh tonkostennykh konstruksiy* [Bearing capacity of screw and riveted joints of steel thin-walled structures]. Abstract PhD Thesis. Moscow, 2011. 22 p. (rus)
3. Granovskiy A.V., Dottuyev A.I. K otsenke seysmostoykosti soyedineniy sendvich-paneley so stalnym karkasom s pomoshchyu samosverlyashchikh shurupov "HARPOON" To assess the seismic resistance of sandwich panels with a steel frame using self-drilling screws "HARPOON". *Seysmostoykoye stroitelstvo. Bezopasnost sooruzheniy*. 2012. No. 5. Pp. 54–58. (rus)
4. Granovskiy A.V., Dottuyev A.I., Krasnoshchekov G.Yu. Seysmostoykost ankernogo krepzha dlya krepeleniya sendvich-paneley k metalicheskomu karkasu [Seismic resistance of anchor fasteners for fixing sandwich panels to metal frame]. *Promyshlennoye i grazhdanskoye stroitelstvo*. 2012. No. 3. Pp. 46–48. (rus)
5. Granovskiy A.V., Kiselev D.A. Rekomendatsii po naznacheniyu metodiki ispytaniy ankerov na vyryv i opredeleniyu raschetnoy nagruzki vyryva [Recommendations for assignment of methods of pull-out tests for anchors and determination of calculated load of pull-out]. *Promyshlennoye i grazhdanskoye stroitelstvo*. 2012. No. 3. Pp. 35–37. (rus)
6. Ananin M. Yu., Vedishcheva Yu. S. K postanovke problemy o neobkhodimosti ucheta v raschete napryazhenno-deformirovannogo sostoyaniya sistemy "sendvich-panel – karkas zdaniya" krepzhenykh elementov [To the formulation of the problem of the need to take into account in the calculation of the stress-strain state of the "sandwich panel-frame of the building" system of fastening elements]. *Mezhdunarodnaya konferentsiya: sbornik tezisov (Elektronnoye izdaniye)*. Yekaterinburg: Izd-vo Federalnoye gosudarstvennoye avtonomnoye obrazovatelnoye uchrezhdeniye vysshego professionalnogo obrazovaniya Uralskiy federalnyy universitet im. pervogo Prezidenta Rossii B.N. Yeltsina, 2015. Pp. 51–55. (rus)
7. Tushina O.A. Finite element analysis of cold-formed Z-purlins supported by sandwich panels. *Applied Mechanics and Materials*. 2013. No. 464. Pp. 398–403.
8. Tushina O.A. Eksperimentalno-teoreticheskiye issledovaniya zhestkosti soyedineniya tonkostennogo gnutogo progona pokrytiya s sendvich-panelyu [Experimental theoretical studies of the stiffness of joining a

Литература

1. Киселев Д.А. Прочность и деформативность анкерного крепежа при действии статической и динамической нагрузок: автореф. дис. канд. техн. наук: 05.23.01 / Киселев Дмитрий Александрович. М., 2010. 29 с.
2. Катранов И.Г. Несущая способность винтовых и заклепочных соединений стальных тонкостенных конструкций: автореф. дис. канд. техн. наук: 05.23.01 / Катранов Иван Георгиевич. М., 2011. 22 с.
3. Грановский А.В., Доттуев А.И. К оценке сейсмостойкости соединений сэндвич-панелей со стальным каркасом с помощью самосверлящих шурупов "HARPOON" // Сейсмостойкое строительство. Безопасность сооружений. 2012. № 5. С. 54–58.
4. Грановский А.В., Доттуев А.И., Краснощечков Г.Ю. Сейсмостойкость анкерного крепежа для крепления сэндвич-панелей к металлическому каркасу // Промышленное и гражданское строительство. 2012. № 3. С. 46–48.
5. Грановский А.В., Киселев Д.А. Рекомендации по назначению методики испытаний анкеров на вырыв и определению расчетной нагрузки вырыва // Промышленное и гражданское строительство. 2012. № 3. С. 35–37.
6. Ананьин М.Ю., Ведищева Ю.С. К постановке проблемы о необходимости учета в расчете напряженно-деформированного состояния системы "сэндвич-панель – каркас здания" крепежных элементов // Международная конференция: сборник тезисов (Электронное издание). Екатеринбург: Изд-во Федеральное государственное автономное образовательное учреждение высшего профессионального образования Уральский федеральный университет им. первого Президента России Б.Н. Ельцина, 2015. С. 51–55.
7. Tushina O.A. Finite element analysis of cold-formed Z-purlins supported by sandwich panels // *Applied Mechanics and Materials*. 2013. № 464. Pp. 398–403.
8. Туснина О.А. Экспериментально-теоретические исследования жесткости соединения тонкостенного гнутого прогона покрытия с сэндвич-панелью // Научно-технический вестник Поволжья. 2014. № 5. С. 308–311.
9. Туснина О.А. Соединения кровельных сэндвич-панелей с тонкостенными гнутыми прогонами, выполняемые на вытяжных заклепках // Промышленное и гражданское строительство. 2013. № 3. С. 14–16.
10. Librescu L., Hause T. Geometrically linear/nonlinear sandwich structures with anisotropic face sheets: theory and behavior // Virginia Polytechnic Institute and State University Department of Engineering Science and

Галямичев А.В., Кирикова В.А., Герасимова Е.А., Спринце А. Несущая способность крепления навесных фасадных систем к сэндвич-панелям // Инженерно-строительный журнал. 2018. № 2(78). С. 30–46.

- thin-walled curved coating operate with a sandwich panel]. *Nauchno-tehnicheskiiy vestnik Povolzhya*. 2014. No. 5. Pp. 308–311. (rus)
9. Tushina O.A. Soyedineniya krovelnykh sendvich-paneley s tonkostennymi gnutymi progonami, vypolnyayemyye na vytyazhnykh zaklepkakh [Joints of sandwich panels with thin-walled bent purlins with the use of blind rivets]. *Promyshlennoye i grazhdanskoye stroitelstvo*. 2013. No.3. Pp. 14–16. (rus)
 10. Librescu L., Hause T. Geometrically linear/nonlinear sandwich structures with anisotropic face sheets: theory and behavior. *Virginia Polytechnic Institute and State University Department of Engineering Science and Mechanics Blacksburg, USA (ICAS 2002 congress)*.1998. Pp. 311.1–311.10.
 11. Danilov M.N., Fedorova N.N. Konechno-elementnoye modelirovaniye mnogosloynnykh ograzhdayushchikh konstruksiy [Finite element modeling of multilayer constructions]. *Izvestiya vuzov. Stroitelstvo*. 2012. No. 10. Pp. 92–100.(rus)
 12. Danilov M.N., Adishchev V.V. Konechno-elementnyy analiz povedeniya trekhslonnykh paneley pri staticheskikh i dinamicheskikh vozdeystviyakh [Application of ansys software for solving problems of dynamics of multilayer shells]. *Izvestiya vuzov. Stroitelstvo*. 2016. No. 5. Pp. 106–118. (rus)
 13. *Album tehnicheskikh resheniy "NordFOX MTH-v-100"* [Album of technical solutions "NordFOX"] (rus)
 14. *Organization Standart STO 0065-02494680-2014 Vinty samonarezayushchiye i samosverlyashchiye "Harpoon"* [Screws self-tapping and self-drilling "Harpoon"] (rus)
 15. *Organization Standart STO 44416204-010-2010 Krepleniya ankerneye. Metod opredeleniya nesushchey sposobnosti po rezul'tatam naturnykh ispytaniy* [Anchor fasteners. The method of determining the bearing capacity by the results of full-scale tests] Moscow: Izdatelstvo FGU "FCS". 2011 (rus)
 16. *Technical certificate № 4925-16 Vinty samonarezayushchiye "Harpoon"* [Technical certificate No. 4925-16 self-tapping screws "Harpoon"] Moscow: Minsroy Rossii. 2016 (rus)
 17. *Technical certificate № 3880-13 Zaklepki vytyazhnyye "Harpoon" so standartnym i shirokim bortikom tipov: A/US, A/A2, US/US, A2/A2* [Technical certificate No. 3880-13 "Harpoon" rivet with standard and wide sides of types: A/US, A/A2, US/US, A2/A2] (rus)
 18. *Certificate of verification № 0059-2015 vesy tenzometricheskiye VTB-12* [Certificate of verification No. 0059-2015 weighing strain gauge VTB-12] (rus)
 19. *State Russian Standart GOST 76-1-2011 Vesy neavtomaticheskogo deystviya. Chast 1 Metrologicheskkiye i tehnicheskkiye trebovaniya. Ispytaniya* [State Russian Standart "Non-automatic weighing instruments" - Part 1: Metrological and technical requirements – Tests (IDT)] Moscow: Standartinform. 2013. 133 p. (rus)
 20. *Certificate of verification № 0059-2015 progibomera 6-PAO* [Certificate of verification No. 0059-2015 of the 6-PAO] (rus)
 21. *Organization Standart STO 36554501-039-2014 Ankernyye krepneniya k betonu s primeneniym ankerov Hilti. Raschet i konstruirovaniye* [Anchoring attachments to concrete using Hilti anchors. Calculation and construction]. Moscow: OAO "NIC "Stroitelstvo". 2014. (rus)
 22. *Russian Set of Rules SP 20.13330.2011 Nagruzki i vozdeystviya. Aktualizirovannaya redaktsiya SNIIP 2.01.07-85** [Russian Set of Rules SP 20.13330.2011. Loads and impacts. Actualized version] Moscow. 2011. (rus)
 23. *Russian Set of Rules SP 28.13330.2012 Zashchita stroitelnykh konstruksiy ot korrozii. Aktualizirovannaya redaktsiya SNIIP 2.03.11-85* [Russian Set of Rules SP 28.13330.2012. Protection of building structures against corrosion. Updated version of SNIIP 2.03.11-85] Moscow. 2012. (rus)
 24. *Mechanics Blacksburg, USA (ICAS 2002 congress)*.1998. Pp. 311.1–311.10.
 25. Данилов М.Н., Федорова Н.Н. Конечно-элементное моделирование многослойных ограждающих конструкций // *Известия вузов. Строительство*. 2012. № 10. С. 92–100.
 26. Данилов М.Н., Адищев В.В. Конечно-элементный анализ поведения трехслойных панелей при статических и динамических воздействиях // *Известия вузов. Строительство*. 2016. № 5. С. 106–118.
 27. Альбом технических решений "NordFOX MTH-v-100"
 28. СТО 0065-02494680-2014 Винты самонарезающие и самосверлящие "Harpoon"
 29. СТО 44416204-010-2010 Крепления анкерные. Метод определения несущей способности по результатам натурных испытаний. М.: Изд-во ФГУ "ФЦС", 2011.
 30. Техническое свидетельство № 4925-16 Винты самонарезающие "Harpoon". М.: Минстрой России, 2016.
 31. Техническое свидетельство № 3880-13 Закlepки вытяжные "Harpoon" со стандартным и широким бортиком типов: A/US, A/A2, US/US, A2/A2
 32. Свидетельство о проверке № 0059-2015 весы тензометрические ВТБ-12
 33. ГОСТ OIML R 76-1-2011 Весы неавтоматического действия. Часть 1 Метрологические и технические требования. Испытания. М.: Стандартиформ, 2013. с. 133.
 34. Свидетельство о проверке № 0059-2015 прогибомера 6-ПАО
 35. СТО 36554501-039-2014 Анкерные крепления к бетону с применением анкеров Hilti. Расчет и конструирование. М.: ОАО "НИЦ "Строительство", 2014.
 36. СП 20.13330.2011 Нагрузки и воздействия. Актуализированная редакция СНиП 2.01.07-85*. М.: Минрегион России, 2011.
 37. СП 28.13330.2012 Защита строительных конструкций от коррозии. Актуализированная редакция СНиП 2.03.11-85. М.: Минрегион России, 2012.
 38. Vatin N., Havula Ja., Martikainen L., Sinelnikov A., Orlova A., Salamakhin S. Thin-walled cross-sections and their joints: tests and FEM-modelling // *Advanced Materials Research*. 2014. Vols. 945–949. Pp. 1211–1215.
 39. СП 128.13330.2012 Алюминиевые конструкции. Актуализированная редакция СНиП 2.03.06-85. М.: Минрегион России, 2012.
 40. СП 70.13330.2012 Несущие и ограждающие конструкции. Актуализированная редакция СНиП 3.03.01-87. М.: ГОССТРОЙ России, 2013.
 41. ГОСТ 22233-2001 Профили прессованные из алюминиевых сплавов для светопрозрачных ограждающих конструкций. М.: МНТКС, 2001.
 42. ТУ 5284-013-01395087-2001 Панели стеновые и кровельные бескаркасные. М.: 2012.
 43. Lange J., Berner K., Hassinen P., Heselius L., Isabel D., Käpplén S., Misiek Th., Rädél F., Tillonen A., Zupancic D. New European Recommendations for the design and application of sandwich panels – Results of the work of the Joint Committee on Sandwich Constructions // *Steel Construction*. 2013. № 6(4). Pp. 294–300.
 44. Lange J., Kurpiela A. Optimization algorithm for sandwich panels // *Nordic Steel Construction Conference*. 2012. № 5. bis 7.9.2012 Oslo, Norwegen
 45. Lange J., Kurpiela A., Berner K. Optimization of Geometry and Core Materials of Sandwich Panels with metallic Faces // *4th International Conference on Steel & Composite Structures*, Sydney, Australia, 2010.
 46. Misiek T., Käpplén S. 07.28: Fastening to face sheets of sandwich panels. ce/papers. 2017. № 1. Pp. 1746–1755. doi:10.1002/cepa.218
 47. Lange J., Renner A. Load-bearing behaviour of high-strength bolts in combined tension and shear // *Steel*

24. Vatin N., Havula Ja., Martikainen L., Sinelnikov A., Orlova A., Salamakhin S. Thin-walled cross-sections and their joints: tests and FEM-modelling. *Advanced Materials Research*. 2014. Vols. 945–949. Pp. 1211–1215.
25. *Russian Set of Rules SP 128.13330.2012* Alyuminiyevyye konstruksii. Aktualizirovannaya redaktsiya SNiP 2.03.06-85 [Russian Set of Rules SP 128.13330.2012. Aluminum structures. Updated version of SNiP 2.03.06-85]. Moscow. 2012. (rus)
26. *Russian Set of Rules SP 70.13330.2012* Nesushchiye i ograbdayushchiye konstruksii. Aktualizirovannaya redaktsiya SNiP 3.03.01-87. [Russian Set of Rules SP 70.13330.2012. Bearing and enclosing structures. Updated version of SNiP 3.03.01-87]. Moscow. 2013. (rus)
27. *State Russian Standart GOST 22233-2001* Profili pressovannyye iz alyuminiyevykh splavov dlya svetoprozrachnykh ograbdayushchikh konstruksiy // [State Russian Standart "Profiles extruded from aluminum alloys for translucent enclosing structures"]. Moscow: MNTKS. 2001. (rus)
28. *Technical Conditions TU 5284-013-01395087-2001* Paneli stenovyye i krovelnyye beskarkasnyye [Technical Conditions "Panels wall and roof frameless"]. Moscow 2012. (rus)
29. Lange J., Berner K., Hassinen P., Heselius L., Izabel D., Käpplein S., Misiek Th., Rädell F., Tillonen A., Zupancic D. New European Recommendations for the design and application of sandwich panels – Results of the work of the Joint Committee on Sandwich Constructions. *Steel Construction*. 2013. No. 6(4). Pp. 294–300.
30. Lange J., Kurpiela A. Optimization algorithm for sandwich panels. *Nordic Steel Construction Conference*. 2012. No. 5. bis 7.9.2012 Oslo, Norwegen
31. Lange J., Kurpiela A., Berner K. Optimization of Geometry and Core Materials of Sandwich Panels with metallic Faces. *4th International Conference on Steel & Composite Structures*. Sydney, Australia, 2010.
32. Misiek T., Käpplein S. 07.28: Fastening to face sheets of sandwich panels. *ce/papers*. 2017. No. 1. Pp. 1746–1755. doi:10.1002/cepa.218
33. Lange J., Renner A. Load-bearing behaviour of high-strength bolts in combined tension and shear. *Steel Construction*. 2012. Vol. 5. No. 3. Pp. 151–157.
34. Käpplein S., Misiek Th. Stabilisation of beams by sandwich panels. EASIE report D3.3 – part 1, 2011. [Online]. URL:http://www.easie.eu/page1.php?id_chapitre=91
35. Georgescu M., Ungureanu V., Dubina D. Diaphragm effect in sandwich panel roofing – Experimental approach. *Proceedings of the 6th European Conference on Steel and Composite Structures*. Budapest, Hungary. 2011. Pp. 165–170.

Alexander Galyamichev,
+7(911)811-07-19; galyamichev@yandex.ru

Victoria Kirikova,
+7(931)206-78-24; vikakirikova@yandex.ru

Ekaterina Gerasimova,
+7(921)554-48-72; katyageras17@gmail.com

Andina Sprince,
+3(716)708-91-45; andina.sprince@rtu.lv

Александр Викторович Галямичев,
+7(911)8110719;
эл. почта: galyamichev@yandex.ru

Виктория Анатольевна Кирикова,
+7(931)2067824;
эл. почта: vikakirikova@yandex.ru

Екатерина Николаевна Герасимова,
+7(921)5544872;
эл. почта: katyageras17@gmail.com

Андина Спринце,
+3(716)708-91-45;
эл. почта: andina.sprince@rtu.lv

© Galyamichev A.V., Kirikova V.A., Gerasimova E.A., Sprince A., 2018

doi: 10.18720/MCE.78.4

Dynamic factors in case of damaging continuous beam supports

Коэффициенты динамичности при повреждении опор неразрезных балок

A. Tusnin,
Moscow State University of Civil Engineering,
Moscow, Russia

Д-р техн. наук, профессор А.Р. Туснин,
Московский государственный
строительный университет, Москва,
Россия

Key words: beam; support; liveness calculations; dynamic factor; dynamic calculations; frequency; time length

Ключевые слова: балка; опора; расчет живучести; коэффициент динамичности; динамический расчет; частота; временной промежуток

Abstract. The article provides the research results of the continuous beam operation in case of the support damage. When the support is damaged, the design model of the beam is changing, the spans are increasing, and the force in the beam is increasing. Moreover, a fast removal of the support at the effect of the unaltering during the destruction of the beam concentrated or distributed force will lead to the evolvment of the vibrations and increase of the beam force. The theoretical jurisdictions are provided for the determination of dynamic factors which might be used for the determination of dynamic force based on the results of the static calculations for the damaged construction. Theoretical dynamic factors are determined for the beams loaded by the concentrated loads. The numerical computations have been performed with the use of finite-element design models. By the example of the continuous beams loaded by the concentrated and distributed forces, the consequence of the dynamic calculations for damaged beams is shown taking to account the time of the support breakdown. It is set that the maximum force values appear in the beams with time for the support damage from 0.01 to 0.1 sec. The comparison of theoretical and numerical dynamic factors is conducted. It showed a good compliance of factor values determined by different methods. The recommendations are provided for practical applications of the dynamic factor at the calculation of continuous beams.

Аннотация. В статье представлены результаты исследования работы неразрезных балок при повреждении опор. При повреждении опор изменяется расчётная схема балки, возрастают пролёты и увеличиваются усилия в балке. Кроме того быстрое исключение опоры при действии на балку не меняющейся в момент разрушения сосредоточенной или распределённой нагрузки ведёт к развитию колебаний и увеличению усилий в балке. Представлены теоретические обоснования для определения коэффициентов динамичности, которые можно использовать для определения динамических усилий по результатам статических расчётов повреждённой конструкции. Теоретические коэффициенты динамичности определены для балок нагруженных сосредоточенными нагрузками. Проведены численные расчёты с применением конечно-элементных расчётных схем. На примере неразрезных балок, нагруженных сосредоточенными и распределёнными нагрузками показана последовательность динамических расчётов повреждённых балок с учётом времени выхода опор из строя. Установлено, что максимальные значения усилий возникают в балках при времени повреждения опоры от 0,01 до 0,1 сек. Выполнено сравнение теоретических и численных коэффициентов динамичности, показавшее хорошее совпадение значений коэффициентов, полученных разными методами. Даны рекомендации для практического применения коэффициента динамичности при расчетах неразрезных балок.

1. Introduction

In Russia and other countries, a scientific direction which studies the behavior of load-bearing structures when they are damaged is developing. In the design practice, the analysis of the bearing capacity of structures in the case of damage is called the calculation of stability against progressive collapse or the calculation of survivability. The problem of studying of the bearing capacity of damaged structures is very urgent due to the adverse consequences of the destruction of buildings [1, 2]. In

Russia, such a calculation is carried out, as a rule, when designing unique buildings and structures. However, the calculation of stability with progressive collapse is also carried out for buildings of mass construction [3–5]. The purpose of the calculation of survivability is to increase the reliability of structures and to prevent the destruction of the building in case of damage to certain elements of load-bearing structures.

In the article [6] there are represented an overview of the regulatory requirements of the United States, Canada, and Europe in carrying out calculations to prevent avalanche collapse, and methods to avoid progressive collapse are analyzed.

In article [7] the problem of providing load-bearing capacity in accidents leading to damage the structures is considered as a complex of preliminary and operational measures reducing possible adverse consequences from the destruction of individual elements. The formulation of the survivability of structures is presented in [8]. Great attention is paid to resistance to the progressive destruction of frame buildings [9–11]. The authors consider the destruction schemes, and the results of calculations of the damaged structures in static and dynamic formulations are presented. In the paper [12], a simplified approach to the calculation of damaged structures is considered, which ensures an acceptable accuracy of the results. The causes of the destruction of structures and constructive measures that reduce the possibility of progressive destruction are considered in [13]. The questions of the evaluation of the ability of structures to resist to progressive destruction have been investigated in [14], where new recommendations increasing the survivability of structures are shown. The design of the joints has a significant effect on ensuring the survivability of the load-bearing system [15]. The problems of progressive collapse of steel trusses and frames are being investigated. On the example of the destruction of the large-span bridge [16], the reasons for the collapse of the span are analyzed. For a multistory steel frame [17], questions of structural behavior in the case of damage of the lower floor column are investigated, as well as the influence of the damping coefficient, which varies from 0.01 to 0.1.

Static, dynamic, linear and nonlinear calculations are successfully used to analyze load-bearing capacity of the damaged structures [18–20]. The effect of an increase of the number of floors on the decrease in dynamic effects in the framework was noted [18].

The review of literature has shown that significant studies of the work of damaged structures have been carried out. There are normative requirements for the design of structures with regard to the destruction of individual elements. There are recommendations for the selection of damaged elements, the appointment of the load and the appointment of materials. However, up to the present time there are no recommendations for designers on the calculation of damaged structures taking into account dynamic processes. One way to calculate survivability is to apply a modified long-term load with a dynamic factor that is determined by the damaged element, its failure rate and the current load. The magnitude of the dynamic factor with a fast turn-off of the element can be taken as 2, assuming an instantaneous application of the load. However, for spatial structures, local damage, even with instantaneous failure of the element, does not always lead to dynamic effects corresponding to the dynamism factor 2. In addition, the dynamic effects on the structure depend on the failure rate of the structural element. Determination of the dynamic coefficients for typical structures with different damage schemes is of great practical importance.

The aim of the study is to determine the dynamic coefficients for the concentrated and distributed load on continuous beams in the case of damage of intermediate supports.

To achieve this goal, the following tasks are solved:

1. Theoretical justification of the dynamic coefficients under the action of concentrated loads on the beam.
2. Development of a numerical technique for the dynamic calculation of continuous beams in the case of damage of supports and the action of concentrated and distributed loads.
3. Numerical studies of the dynamic coefficients of continuous beams in the case of damage of supports, including beam systems contain main and secondary beams.

2. Methods

For the purpose of theoretical justification of the dynamic factor, the simple beam construction can be used [19, 20]. Let us consider the double-span beam with a hinged support. In the midspan, the beam was subjected to a concentrated load P . Damage to the construction includes midspan support damage. The basic and damaged beams are shown in Figure 1.

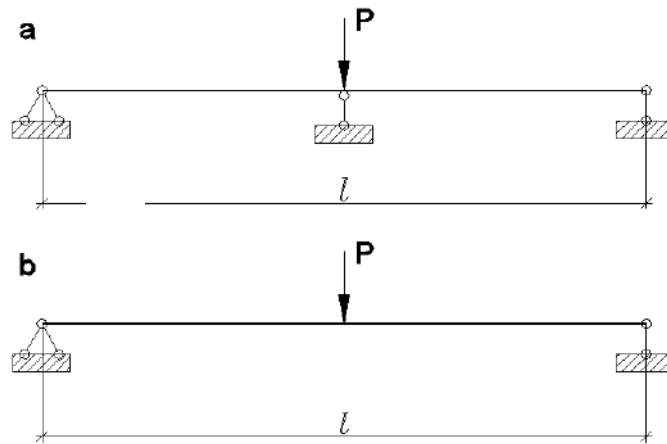


**Figure 1. Beam subjected to a concentrated load in the midspan:
a – basic construction; b – damaged construction.**

Depending on the initial position of the beam and midspan support (deflection or hogging of the beam in the support area), several types of interaction between this support and the beam are possible:

Type 1. Supporting force is zero, i.e. at the static action of the load P the beam span l due to the behavior in bending flexed to the size of deflection w_c (w_c – beam deflection on two supports from the concentrated force P), and only then an intermediate support was underpinned.

Type 2. The support was pinned under a load P_0 equal to force fraction P , at the moment of the contact of the beam with the midspan support the beam deflection is w_0 and is equal to the proportional to the load part of deflection w_c of the beam on two supports from the normal load.

Type 3. The beam supports on the intermediate support before the load is applied, initial deflection is zero.

Type 4. The beam supports on the intermediate support, herein the beam is put into the shape of initial upward buckling equal to w_c of the beam span l on two hinged supports under the action of force P .

We shall find the dynamic factor for the concentrated load, acting in each mentioned type of structural damage. To determine the dynamic factor k_d known relationship may be used [21]:

$$k_d = 1 + \sqrt{1 + \frac{2H}{w_c}}, \quad (1)$$

where H – height, with which the weight P – falls down on the beam, w_c – deflection of the beam span l of hinge-supported at each end of the static action of force P . This dependence is valid when the weight falls down on the undeformed beam, design model of which isn't changed in the process of interaction between the beam and falling weight. If the design model is changed, additional studying of the behavior of the construction is needed.

For finding the connection between force and deflection, use the following relations [21]: $P = cw_c$ and $P_d = cw_d$, where c – control stiffness (the same for static and dynamic load action), P_d – dynamic force, w_d – dynamic deflection.

2.1. Type 1

In the first type, the beam originally has the deflection equal to the full static when it is supported on two seats at the ends, and the effect of force in the middle P . The absence of the intermediate

support in case of its damaging does not affect the behavior of the beam. Therefore, the dynamic factor for the load P will be 1.

2.2. Type 2

In the first type of the damage of the construction, the part of the full load P_o is taken up through the beam deformations, and the remaining load is delivered on the intermediate support. At the initial deflection w_o prior to the beginning of interaction with the support, the fraction of the force taken up by the beam deformation is $P_o = \frac{P w_o}{w_c}$. After removing the support, the beam will be affected by the

instantly superimposed unbalanced fraction of force, equal to $\Delta P = P \left(1 - \frac{w_o}{w_c} \right)$. This part of the load will have a dynamic effect with a dynamic factor 2, as instantly superimposed to the beam. The aggregate load on the beam will be: $P_d = P_o + 2\Delta P = P \left(\frac{w_o}{w_c} + 2 - \frac{2w_o}{w_c} \right) = P \left(2 - \frac{w_o}{w_c} \right)$. The dynamic factor of the aggregate load, in this case, will be:

$$k_d = \frac{P_d}{P} = 2 - \frac{w_o}{w_c} \quad (2)$$

With the initial deflection over the midspan support, $w_o = 0.5w_c$ the dynamic factor calculated using the formula (2) will be 1.5.

2.3. Type 3

In the third type of the damage of the construction, the total load is delivered to the midspan support. After the instant removal of this support, the whole load is instantly applied to the beam, the initial height from which the weight falls (acts) P is zero, and the dynamic factor is $k_d = 2$. This result can be obtained using the formula (1), or the formula (2).

2.4. Type 4

In the fourth type of the damage of the construction (the initial deflection of the midspan support is w_c), in order to determine the dynamic factor let us consider the power U_d , which is accumulated in the system after its deformation, the strain power of preliminary hogging of the beam U_o and action A , performed by the load P after the removal of the support. The power balance of the system makes it possible to make up an equation:

$$U_o + A = U_d \quad (3)$$

where $U_o = \frac{Pw_c}{2}$ is the power accumulated in the beam when it is hogged over the midspan support by the amount w_c , $A = P(w_c + w_d)$, $U_d = \frac{P_d w_d}{2} = \frac{c w_d^2}{2} = \frac{P w_d^2}{2w_c}$, w_d – the dynamic deflection of the beam, measured from the rectilinear axis of the beam.

After the simplest transformations, we will get the quadratic equation:

$$w_d^2 - 2w_c w_d - 3w_c^2 = 0 \quad (4)$$

The solution of the quadratic equation is as follows:

$$w_{d,1,2} = w_c \pm \sqrt{w_c^2 + 3w_c^2} \quad (5)$$

The roots of the quadratic equation are:

$$w_{d_1} = 3w_c, \quad w_{d_2} = -2w_c \quad (6)$$

The second root is in contrast to the physical content of equation, therefore, $w_d = 3w_c$, and the dynamic factor is:

$$k_d = w_d / w_c = 3 \quad (7)$$

The same value of the dynamic factor was obtained using the formula (2) if the initial deflection is as follows: $w_o = -w_c$.

At the initial hogging over the midspan support $0.5 w_c$ the power accumulated with the beam:

$$U_o = 0.25Pw_c, \quad (8)$$

In case of damaging the midspan support, the work of the force P is as follows:

$$A = P(0.5w_c + w_d) \quad (9)$$

The power of the beam deformation is: $U_d = \frac{Pw_d^2}{2w_c}$

With allowance for the power balance (3), the quadratic equation may be made up:

$$w_d^2 - 2w_c w_d - 1.5w_c^2 = 0 \quad (10)$$

The solution of the quadratic equation is as follows:

$$w_{d_{1,2}} = w_c \pm \sqrt{w_c^2 + 1.5w_c^2} \quad (11)$$

The roots of the quadratic equation are:

$$w_{d_1} = 2.581w_c, \quad w_{d_2} = -0.581w_c \quad (12)$$

The second root is in contrast to the physical content of equation, therefore, $w_d = 2.581w_c$, and the dynamic factor is:

$$k_d = w_d / w_c = 2.581 \quad (13)$$

The dynamic factor obtained using the formula (2) at the initial deflection: $w_o = -0.5w_c$, is:

$$k_d = \frac{P_d}{P} = 2 - \frac{-0.5w_c}{w_c} = 2.5 \quad (14)$$

The difference between dynamic factors calculated using the formulas (13) and (14) is not too large and is approximately 3 %.

Thus, the dynamic factor depends on how the construction was formed during the construction. In the process of design and construction, the presence of the clearances between the supports and the construction should be taken into account, as well as the presence of the preliminary deflections in the process of assembling the supports. The presence of the preliminary deflection of the construction is considered to be more dangerous for design survivability.

Let us consider the behavior of the construction in the form of the continuous double-span beam, subjected to a concentrated load P in the middle of each span (Fig.2).

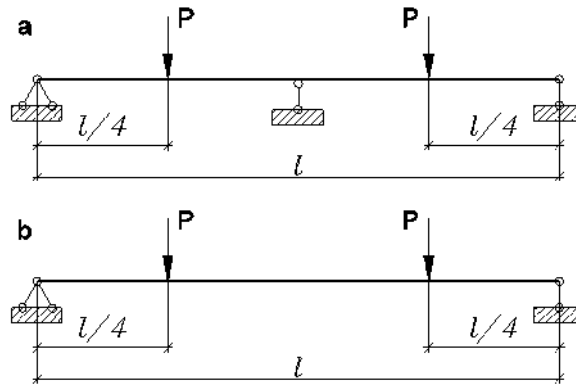


**Figure 2. Double-span beam subjected to two concentrated loads in the middle of the span:
a – basic construction; b – damaged construction**

The support reactions for the basic construction are as follows:

- at the end supports:

$$F_1 = \frac{5}{16} P; \quad (15)$$

- at the midspan supports:

$$F_2 = \frac{22}{16} P \quad (16)$$

The deflection of the beam under each concentrated load in the basic construction is:

$$w_o = \frac{7P(0.5l)^3}{768EI} = \frac{0.001139Pl^3}{EI} \quad (17)$$

The deflection of the beam under each concentrated load under the static action of the load in the damaged construction (without the midspan support), measured from the rectilinear axis of the beam is as follows:

$$w_c = \frac{l^3}{48EI} = \frac{0.02083Pl^3}{EI} \quad (18)$$

To determine the dynamic factor, consider the power balance of the system (3).

The power accumulated in the basic construction during its loading P is:

$$U_o = \frac{2Pw_o}{2} = Pw_o \quad (19)$$

The work performed by the power P in case of damaging the support is:

$$A = 2P(w_d - w_c) \quad (20)$$

The energy accumulated in the beam in case of damaging the support is:

$$U_d = \frac{2P_d w_d}{2} = \frac{2c w_d^2}{2} = \frac{2P w_d^2}{2w_c} = \frac{P w_d^2}{w_c}, \quad (21)$$

where w_d – dynamic beam deflection in the points of load application, measured from the rectilinear axis of the beam.

After the simplest transformations, we will get the quadratic equation:

$$w_d^2 - 2w_c w_d + w_c w_o = 0 \quad (22)$$

The solution of the quadratic equation is as follows:

$$w_{d_{1,2}} = w_c \pm \sqrt{w_c^2 - w_o w_c} \quad (23)$$

Taking into account the formulas (17) and (18), write down:

$$w_o = \frac{0.001139}{0.02083} w_c = 0.05468 w_c \quad (24)$$

Then:

$$w_{d_{1,2}} = w_c \pm \sqrt{w_c^2 (1 - 0.05468)} = w_c \pm 0.9723 w_c \quad (25)$$

The roots of the quadratic equation are:

$$w_{d_1} = 1.9723 w_c, \quad w_{d_2} = 0.02773 w_c \quad (26)$$

If we do not consider the second root, that is in contrast to the statement, then $w_d = 1.9723 w_c$, and the dynamic factor is:

$$k_d = w_d / w_c = 1.9723 \quad (27)$$

2.5. Computational investigation

The computational investigation is carried out using the finite element models of the damaged construction in the static and dynamic setting [22–27]. In the process of dynamic designing, the damaged element is removed, and the internal forces occurring in the element being removed are impressed upon the construction. The internal forces are impressed so as to completely replace the failed component, and then these forces are decreased to zero during the time corresponding to the breakdown of the component [22–26]. It is recommended to take the value of decrease time of the equivalent forces as 0 to 0.1 sec. It is assumed, that if the vibration period of the damaged construction coincides with the decrease time of the forces, then the dynamic factor will be maximum.

The computational investigation was carried out using the computer system Nastran. The beam was simulated with the axial finite elements “beam”. Each beam span was divided into 6 finite elements. For accounting the mass during the dynamic designing, the weight of which is equal to the actual loading, in the points of concentrated load application, the element of “mass” type is used.

The investigation of the dynamic factors is carried out for the continuous double-span beam from double-T iron 20B1 Corporate Standard of Association CHERMETSTANDART 20-93. The beam spans are 6 m, the support is hinged. The damage to the construction in the form of removing the midspan support and several types of loading are considered:

Type 1: concentrated force 48.94 kN is impressed above the midspan support upon the undeformed beam;

Type 2: concentrated force is impressed upon the beam with the span of 12 m, after the deformation of the beam by the amount of the half of deflection the midspan support is pinned under the beam, and the load is adjusted to 48.94 kN, the support reaction is 24.47 kN;

Type 3: the beam is hogged by the bearing of the midspan support by the amount equal to the half of deflection of the beam with the span of 12 m from the concentrated force of 48.94 kN, after that the concentrated force of 48.9 kN is impressed above the midspan support upon the beam, the support reaction is 73.41 kN.

The types of the constructions under investigation are presented in Figure 3. The initial position of the beam and the support being removed are stippled in Figure 3.

For each type of the damaged constructions, the frequency of the first vibration mode was calculated. When calculating the vibration mode for each type, the beam proper weight (21 kg/m) is taken into account as distributed mass, and the concentrated mass is 4894 kg (equivalent force is 48.94 kN). According to the results of the calculation, the frequency and the self-induced vibration period of the first form were: 0.712 Hz and 1.404 sec. The following time periods are considered, during which the support reactions are decreased, sec.: 0.05, 0.1, 0.14, 0.4, 0.7, 1.0, 1.404, 2.0, 3.0.

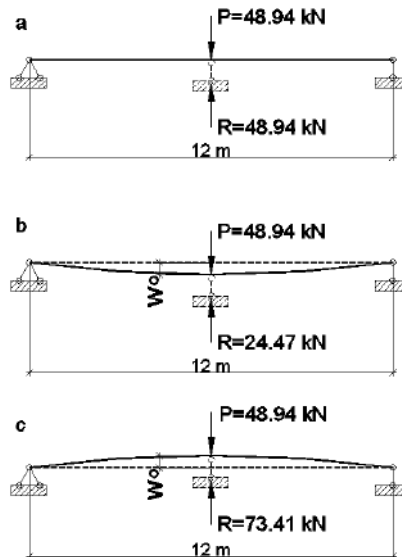


Figure 3. Diagrams of the constructions under investigation
a – type 1; b – type 2; c – type 3

When calculating the type 1 of the construction, the exterior load is constant, and the support reaction is decreasing for the predetermined time interval to zero. In types 2 and 3, the load and the support reaction vary according to the dependencies illustrated in Figure 4 (exterior load increases for 20 sec. from zero to the complete value, the support reaction increases to the complete value for the same time period and then decreases to zero for the selected time interval).

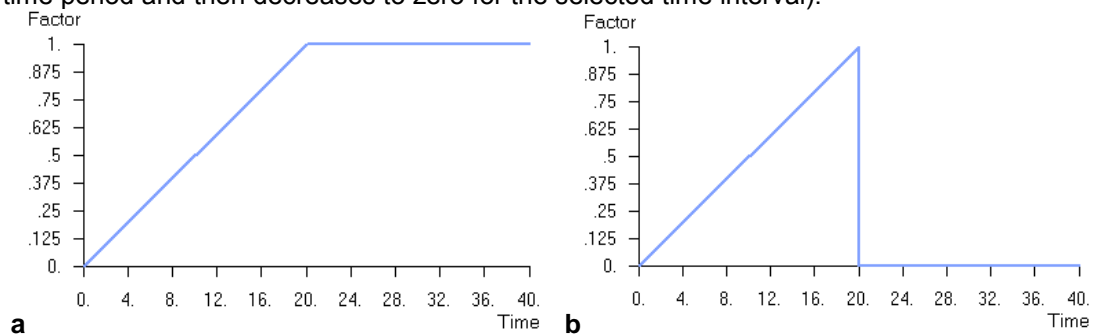


Figure 4. Change of load and support reaction during
a – load; b – support reaction

The work of beams on load at the spams of the continuous beam from the double-T iron 20B1 was numerically studied. The behavior of two constructions (fig. 5) was considered: the beam with the concentrated force in the middle of each span and beam with the uniformly distributed load.

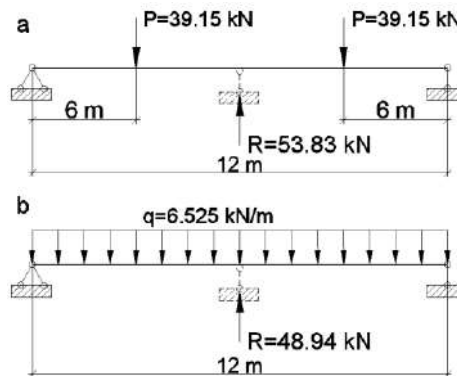


Fig.5. Diagram of the studied construction on load at the span
a – concentrated force; b – distributed force

The proper weight (21 kg/m) is taken into account at the places of the concentrated load action of the 3915 kg mass. For beams with loaded distributed force, the distributed mass which is equal to

652.5 kg/m together with the self-weight is considered. For the diagrams of the load at the spans, the frequency and the period of the first form of the self-induced vibration are: at the concentrated load – 0.794 Hz and 1.260 sec., at the distributed force – 0.812 Hz and 1.232 sec. The following time periods are considered, during which the support reactions are decreasing, sec.: 0.05, 0.1, 0.14, 0.4, 0.7, 1.0, 1.260 (for concentrated load), 1.232 (for distributed force), 2.0, 3.0.

When calculating the beams with load at the spam, the exterior load is recognized as permanent over time and the support reaction when removing the midsupport is changing during the above-mentioned time intervals in accordance with the diagram, shown in the Figure 6.

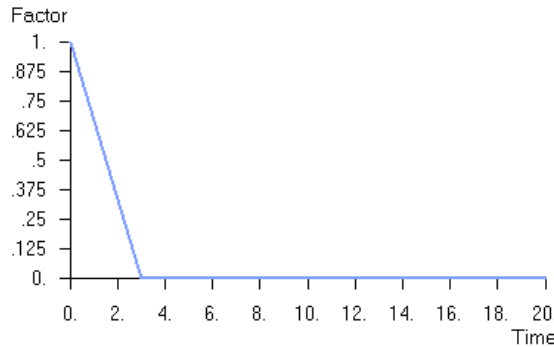


Figure 6. Change of the support reaction at the loaded beam in the spam and time interval of 3 sec

The work of three- and fourspan beams from the double-T iron 20B1 is considered in case of the damage of one of the midspans. At the Figure 7, a threespan beam from the double-T iron 20B1 is shown; a fourspan beam – at the Figure 8. At the figures, the removed supports are pointed with dot line. The support reaction value of the removed support:

for the threespan beam is $1.1 \cdot 6.525 \cdot 6 = 43.07$ kN;

for the fourspan beam is $0.929 \cdot 6.525 \cdot 6 = 36.37$ kN.

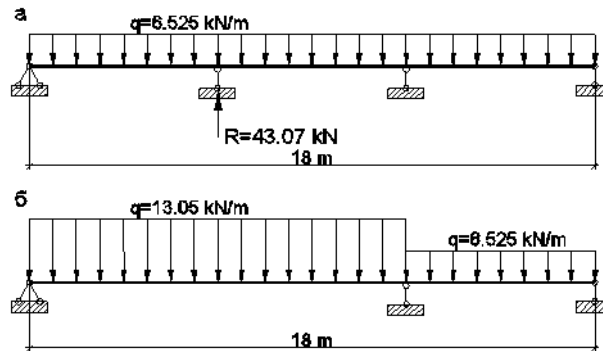


Fig.7. Design model at the destruction of the internal support of the threespan beam a – at the calculation in the dynamic setting; b – at the calculation in the static setting with $k_d=2$ for the load at the spans adjoining to the damaged support

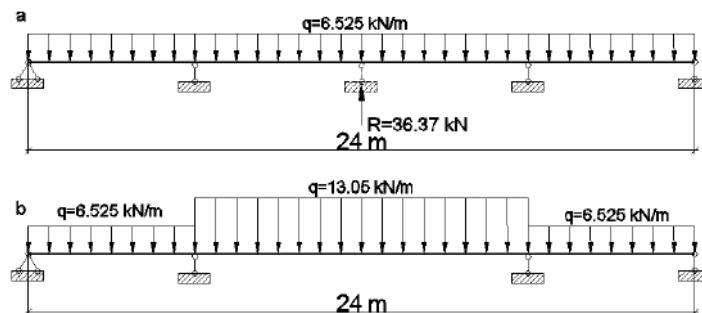


Figure 8. Design model at the destruction of internal support of the fourspan beam a – at the calculation in the dynamic setting; b – at the calculation in the static setting with $k_d=2$ for the load at the spans adjoining to the damaged support

The calculation in the dynamic setting was performed in the same manner as for the double-span beam; the time of the support reaction reduction during the removal of the midsupport is 0.05 sec.

At the static calculation, the design model with the corresponding removed support is taken into consideration. The load in the spans adjoining to the damaged span is admitted with the dynamic factor 2.

The behavior of the multispan beam which carries the secondary beams is studied at the removal of the midsupport. The main beam made of the double-T iron 20B1 is a fourspan beam, the length of each beam is 6 m. Secondary beams made of the double-T iron 10B1 have span of 6 m length and are located at the 2 m pitch. Two types of construction are studied: type 1 – secondary beams are hinged to the main beam; type 2 – secondary beams are continuous. The load on the secondary beams is 1.088 kN/m. Fig. 9 shows the design model of the continuous beam with secondary beams attached to the main beam by the hinged fastening.

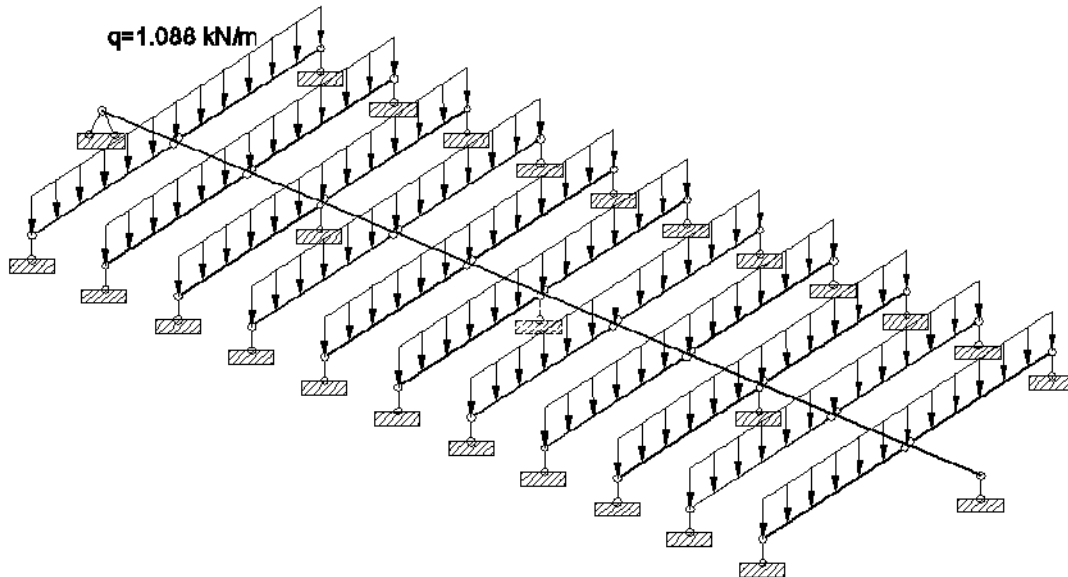


Figure 9. Design model with secondary beams attached by the hinged fastening

The midsupport reaction of the continuous beam is 40.41 kN. In case of construction damage, the midsupport is removed, and the first form frequency of the vibration is 0.706 Hz (simply supported secondary beams) and 0.759 Hz (continuous secondary beams), vibration periods are 1.416 and 1.318 sec. respectively. During the dynamic calculations, the following is taken into account: the distributed mass for the main beam – 21 kg/m; for the proper weight of the secondary beam – 8.1 kg/m, and the additional mass – $108.8 - 8.1 = 100.7$ kg/m (for consideration of dynamic action of exterior load at the support damage).

3. Results and Discussion

Figure 10 shows the relationship between the bending moment over the midspan (type 3) of double-span beam and the action of the concentrated load over the midspan (Fig. 3) at the removal of this support within 0.05 sec.

Table 1 provides the forces at the double-span beam depending on reduction time of support reaction at the damage of the midsupport. Except for the forces, Table 1 gives dynamic factors calculated as the ratio of final force in the damaged construction to the corresponding forces calculated at the static loading conditions to the damaged construction. The forces of the static load are:

$$\text{maximum bending moment: } M = 48.94 \cdot 12/4 = 146.82 \text{ kN}\cdot\text{m},$$

$$\text{maximum shear force: } Q = 48.94/2 = 24.47 \text{ kN}.$$

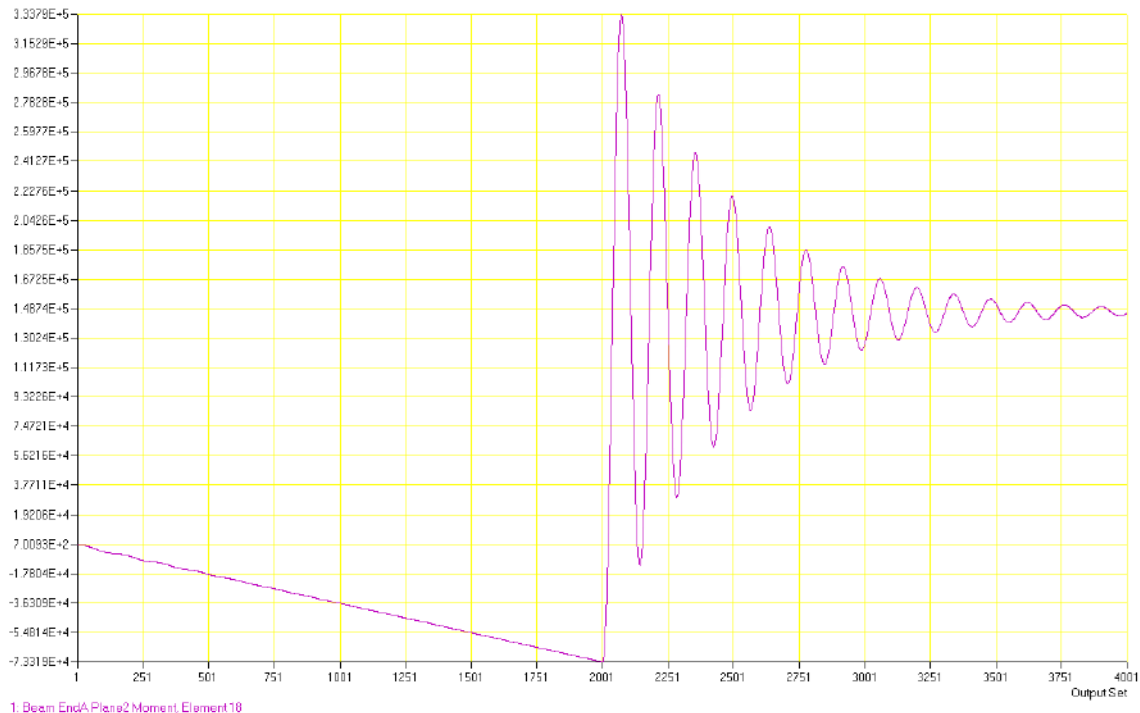


Figure 10. Change of bending moment over the midspan for type 3 of the construction

Table 1. Forces and dynamic factors at the double span beam when the middle support is damaged

Parameter	Forces and dynamic factors at the time of reaction reduction								
	0.05	0.10	0.14	0.40	0.70	1.00	1.401	2.00	3.00
1 type									
M, kN m	273.88	273.08	272.05	257.78	228.17	191.77	152.04	171.38	154.26
kd	1.87	1.86	1.85	1.76	1.55	1.31	1.04	1.17	1.05
Q, kN	45.95	45.82	45.65	43.24	38.23	32.07	25.35	28.62	25.35
kd	1.88	1.87	1.86	1.76	1.56	1.31	1.03	1.17	1.03
2 type									
M, kN m	210.25	209.95	209.43	202.14	187.49	169.30	149.43	159.10	150.54
kd	1.43	1.43	1.43	1.38	1.28	1.15	1.02	1.08	1.03
Q, kN	35.22	35.15	35.06	33.86	31.37	28.28	24.92	26.55	25.11
kdyn	1.44	1.43	1.43	1.38	1.28	1.15	1.02	1.08	1.02
3 type									
M, kN m	333.79	332.67	331.24	310.63	267.17	213.51	154.95	182.92	157.87
kd	2.27	2.27	2.26	2.12	1.82	1.45	1.06	1.25	1.08
Q, kN	56.12	55.94	55.70	52.20	44.85	35.76	25.85	30.58	26.34
kd	2.29	2.28	2.27	2.13	1.83	1.46	1.06	1.25	1.08

The computational investigation demonstrated that the less time for support reaction reduction the bigger is the dynamic factor. The studied simple constructions show that during the time of support reaction reduction equal to the period of the first frequency of self-induced vibration, the dynamic factor is close to 1. The maximum values of the dynamic factors received in numerical computation are different

from the theoretical values – from 4 to 8–12 %. Theoretical dynamic factors are a bit bigger than the numerically calculated.

Carried out numerical calculations confirmed the effectiveness of the previously proposed [22, 26] method of numerical dynamic calculation with the replacement of the damaged element by internal forces, decreasing from time to zero for a time interval from 0 to 0.1 seconds. At carrying out the numerical researches the factor of damping 0.1 is accepted. Studies have shown that using such a damping factor reduces the damping time of the oscillations, but does not affect the level of peak values of forces and displacements of the structure. This was the results obtained earlier [17] in the calculation of multi-story steel frames.

Figure 11 shows the relation of the dynamic factors to the time of support reaction reduction for the considered types of construction damage.

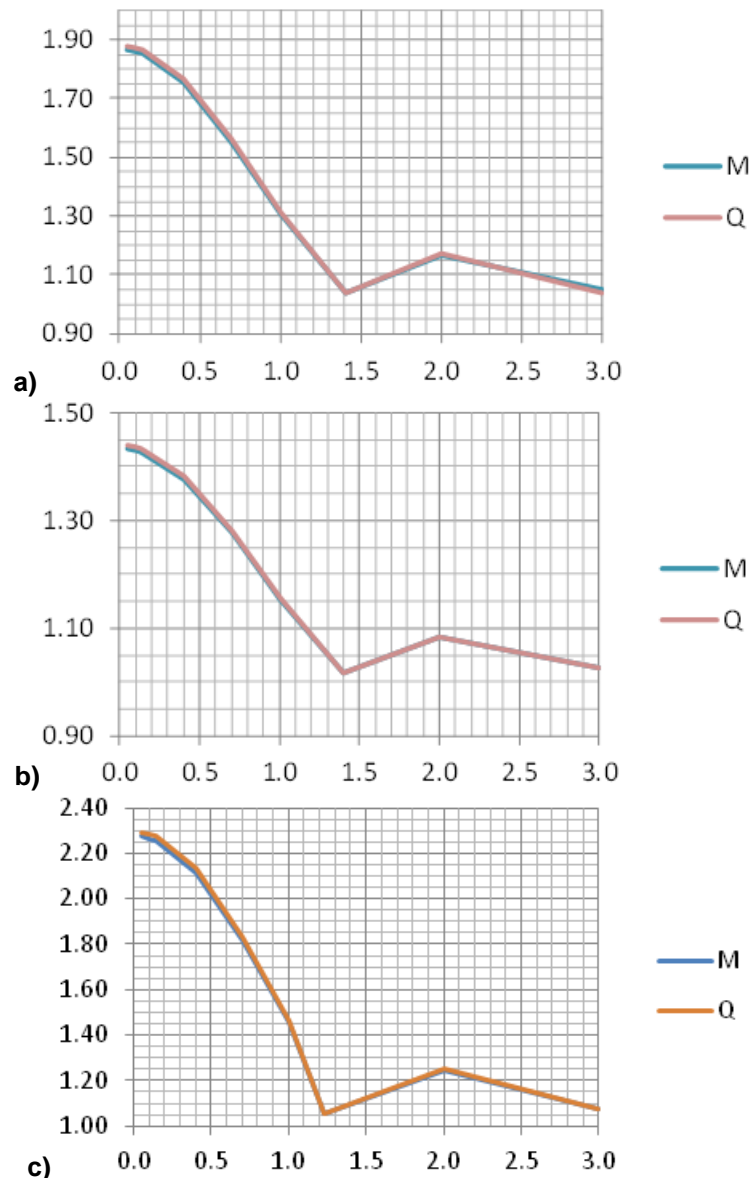


Figure 11. Relation of the dynamic factors to time of support reaction reduction

a – type 1; b – type 2; c – type 3

— M - dynamic factor for the moment
— Q - dynamic factor for the shear force

Figure 12 shows the ration of support reaction of the end supports of the doublespan beam in case of the load in the span by the concentrated loads (Fig. 5) to the removal of the support during the 0.14 sec.

Table 2 gives forces and dynamic factors of the doublespan beam loaded in the span depending on the time of support reaction reduction at the damage of midsupport. The forces of the static load at the

concentrated loads in the span are maximum bending moment: $M=39.15 \cdot 3=117.45$ kN·m, maximum shear force: $Q=39.15$ kN. At the uniformly distributed load, the static forces are $M=6.525 \cdot 12^2/8=117.45$ kN·m, $Q=6.525 \cdot 12/2=39.15$ kN.

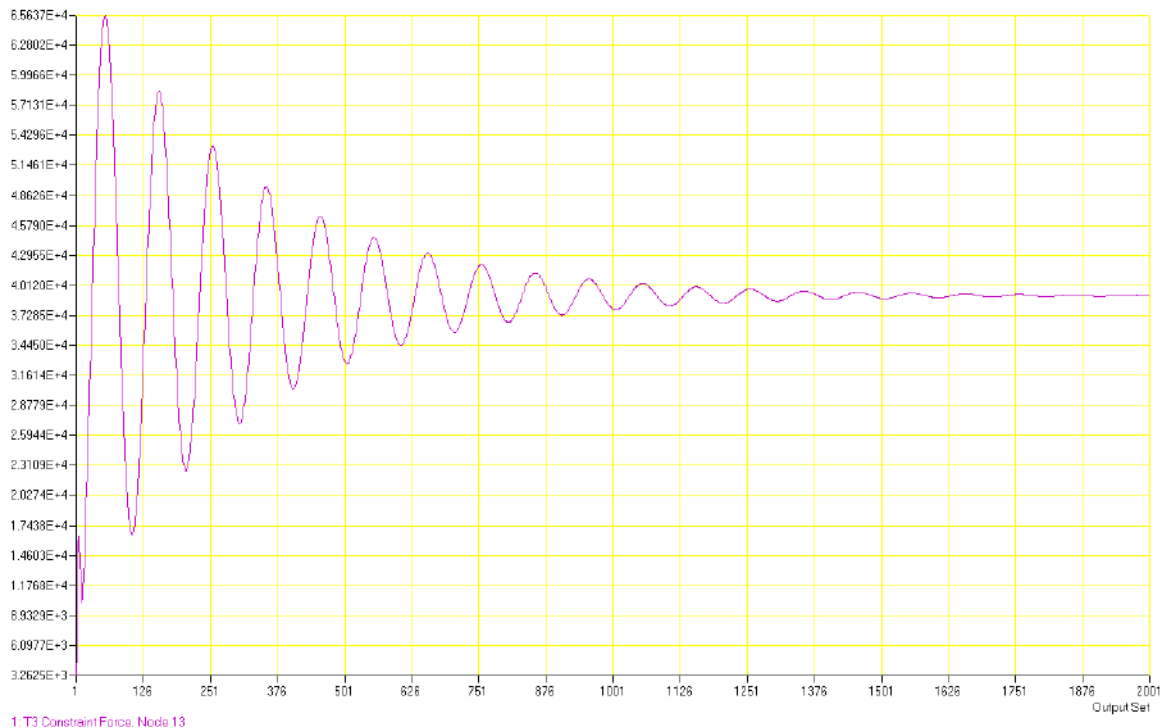


Figure 12. Change of end support reaction at the concentrated loads in the span and at the removal of the midsupport within 0.14 sec

Table 2. Forces and dynamic factors at the double span beam loaded in the span when the middle support is damaged

Parameter	Forces and dynamic factors at the time of reaction reduction								
	0.05	0.10	0.14	0.40	0.70	1.00	1.260(1.232)	2.00	3.00
Concentrated loads in the span									
M, kN m	217.97	217.38	216.07	200.93	170.39	137.05	123.39	132.90	128.57
kd	1.86	1.85	1.84	1.71	1.45	1.17	1.05	1.13	1.09
Q, kN	72.57	72.30	71.94	66.91	56.84	45.57	41.13	44.28	42.85
kd	1.85	1.85	1.84	1.71	1.45	1.16	1.05	1.13	1.09
Uniformly distributed load									
M, kN m	221.81	219.99	219.80	204.40	173.69	139.26	122.87	133.86	128.62
kd	1.89	1.87	1.87	1.74	1.48	1.19	1.05	1.14	1.10
Q, kN	66.14	65.92	65.64	61.58	53.63	44.70	40.42	43.28	41.91
kd	1.69	1.68	1.68	1.57	1.37	1.14	1.03	1.11	1.07

If the damage time of midsupport is decreasing, the dynamic factor will rise. When the time for support reaction reduction equals to the period of the first frequency of self-induced vibration, the dynamic factor is close to 1. The maximum dynamic factor at the load in the span received numerically can differ from the theoretical value which is 1.9723 no more than by 6 % (theoretical value is bigger than the numerical).

Figure 13 shows the ratio of dynamic factor to the time of support reaction reduction at the load in the span.

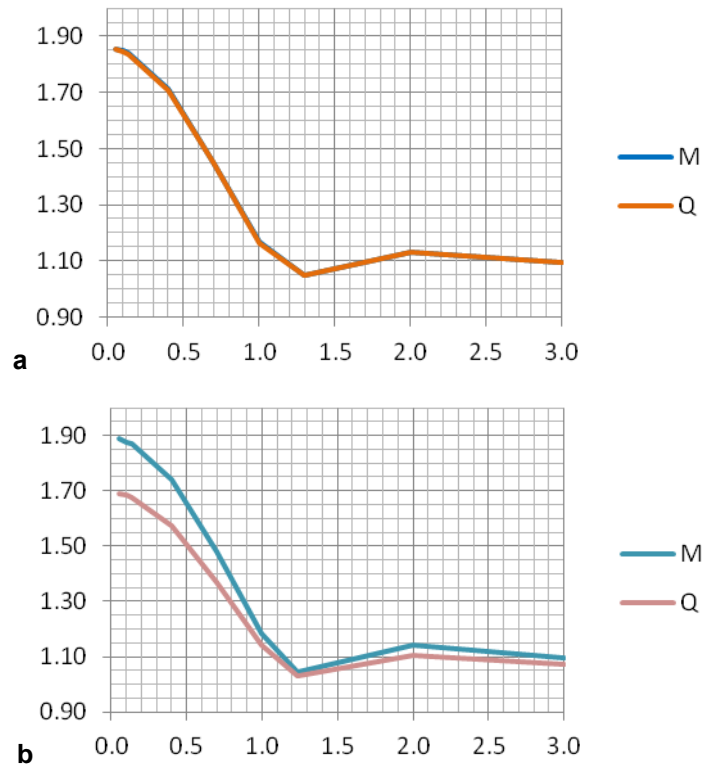


Figure 13. Ratio of dynamic factor at the load in the span to the time of support reaction reduction
a – concentrated load; b – distributed force

— M – dynamic factor for the moment
 — Q – dynamic factor for the shear force

In the threespan continuous beam (Fig. 7), the maximum bending moment appears in the part of the beam where the support was removed and comprises 141.92 kN·m according to the data of dynamic calculation, and 159.05 kN·m – according to the data of static calculations with the dynamic factor. The maximum support reaction appears in the undamaged midsupport and comprises 113.5 kN (dynamic calculations) and 139.5 kN (static calculations).

In the fourspan continuous beam (Fig. 8), the maximum bending moment appears in the area of removed support and comprises 90.32 kN·m according to the data of dynamic calculation and 110.11 kN·m – according to the data of static calculations with the dynamic factor 2. The maximum support reaction appears in the closest to the middle of the beam undamaged supports and comprises 92.54 kN (dynamic calculations) and 118.7 kN (static calculations).

The comparison of the results of the dynamic and static calculations demonstrated that the bending moment and support reactions received by the dynamic calculations are smaller than the values received by the static calculations by 11–22 %.

Table 3 provides the forces and dynamic factors in the continuous main beam and in the secondary beams (Fig. 9) depending on the time of the support reaction reduction with the damaged midspan. The forces of the static load without the dynamic factor in the damaged construction are: bending moment in the main beam in the area of the removed support is $M=26.93$ kN·m, the support reaction of the span which is closest to the damaged one is $R=34.68$ kN, in the secondary beam with the hinged fastening, the bending moment in the beam span is $M_1=4.90$ kN·m, the shear force is $Q_1=3.26$ kN, for the continuous secondary beam in the place of its attachment to the main beam $M_1=3.26$ kN·m, shear force is $Q_1=3.26$ kN.

Table 3. Forces and dynamic factors in the continuous main beam and in the secondary beams when the middle support is damaged

Parameter	Forces and dynamic factors at the time of reaction reduction								
	0.01	0.05	0.10	0.14	0.40	0.70	1.00	1.416(1.318)	2.00
Simply supported secondary beam									
M, kN m	46.80	45.68	42.31	38.43	33.78	32.11	30.23	28.07	28.44
kd	1.74	1.70	1.57	1.43	1.25	1.19	1.12	1.04	1.06
R, kN	46.18	45.60	43.69	41.59	38.19	37.13	36.14	35.54	35.19
kd	1.33	1.31	1.26	1.20	1.10	1.07	1.04	1.02	1.01
M1, kN m	6.61	6.58	6.52	6.46	6.23	5.74	5.37	4.98	5.06
kd	1.35	1.34	1.33	1.32	1.27	1.17	1.10	1.02	1.03
Q, kN	4.18	4.17	4.12	4.08	3.82	3.65	3.38	3.17	3.23
kd	1.28	1.28	1.26	1.25	1.17	1.12	1.04	0.97	0.99
Continuous secondary beam									
M, kN m	56.20	55.72	54.33	52.62	40.38	31.00	30.94	30.46	29.11
kd	2.09	2.07	2.02	1.95	1.50	1.15	1.15	1.13	1.08
R, kN	50.58	50.31	49.50	48.56	41.87	36.98	36.87	36.60	35.82
kd	1.46	1.45	1.43	1.40	1.21	1.07	1.06	1.06	1.03
M1, kN m	5.62	5.52	5.43	5.26	4.04	3.10	3.09	3.05	3.58
kd	1.72	1.69	1.67	1.61	1.24	0.95	0.95	0.94	1.10
Q, kN	6.87	6.82	6.65	6.46	4.98	3.75	3.76	3.70	3.25
kd	2.11	2.09	2.04	1.98	1.53	1.15	1.15	1.13	1.00

The final force appears in the continuous beam and secondary beams at the minimum time of support destruction. At the same moment, the dynamic factor for construction with continuous beams is bigger, than for constructions with the simply supported secondary beams.

The calculation of the damaged construction with the loaded secondary beams in the area of load damage with the dynamic factor – 2. While other secondary beams are loaded with the initial load. Basing on the static calculations, the bending moment in the beam area located over removed support was 57.12 kN·m, the reaction of support closest to the damaged one – 59.02 kN. For the secondary beams, the bending moment in the hinged secondary beams is 9.79 kN·m, in the continuous secondary beams - 6.53 kN·m. The shear force in the secondary beams is 6.53 kN.

The moment determined by the static calculation with the increased load on the beams in the area of support destruction exceeds the moment obtained by the dynamic calculation in the main beam by 2–18 %, in the secondary beam by 14–34 %, the "static" support reaction of the main beam is more "dynamic" by 14–22 %, and the "dynamic" shear force in the secondary beam takes 64–105 % of the "static" one. Thus, for a spatial construction in the form of a continuous beam to which the secondary beams are adjoined, the static calculation can be used with a load doubled in the area of damage. Such a calculation is carried out with a reserve of load-carrying capacity, with the exception of the shear force in continuous secondary beams, which in case of a static calculation with a dynamic factor of 2 is less than dynamic by no more than 5 %.

A suggestion regarding the continuous beams was not confirmed on the fact that the biggest dynamic factors should appear at the coincidence of time for construction damage with the period of the first form of vibrations of such construction. Maximum dynamic factors of such beams are determined at the time length of damage which is lower than 0.1 sec.

4. Conclusions

Depending on the initial state of the continuous double-span beam, the theoretical value of the dynamic factor varies in the range from 1 to 3. The possibility of numerical calculation of damaged constructions in a dynamic setting using the Nastran computer complex has been developed, and a numerical calculation method for the action of concentrated and distributed load has been worked out. The discrepancy between the theoretical dynamic factors and the factors determined by the numerical calculation is 4–12 %. It is revealed that in the considered constructions, the shorter the time of the midsupport destruction, the greater the dynamic factor. At the time of damage of the midsupport, equal to the period of the first form of vibrations, there are no significant values of the dynamic factors; the dynamic factors, in this case, are from 1.02 to 1.06.

For simple beam constructions (in the form of individual beams, girders, consisting of main and secondary beams) with the load capacity reserve, it is allowed to perform a static calculation in the design using loads with corresponding dynamic factors.

Taking into account the carried out studies on constructions in the form of simply supported and continuous beams, including those with secondary beams adjoining to them, in the absence of initial gaps or bends; in static calculations, it is recommended to use loads with a dynamic factor equal to 2 in the spans adjacent to the damaged support.

References

1. *Report of the Inquiry into the Collapse of Flats at Ronan Point*. Caning Town. MSO, 1968
2. Marchand K.A., Alfawakhive F. *Blast and Progressive Collapse*. AISC, 2005.
3. Strugatskiy Yu.M., Shapiro G.I. Bezopasnost moskovskikh zhilykh zdaniy massovykh seriy pri chrezvychaynykh situatsiyakh [Security of Moscow residential buildings of mass series in emergency situations]. *Industrial and Civil Engineering*. 1998. № 8. Pp. 37–41. (rus)
4. Strugatskiy Yu.M. Obespecheniye prochnosti panelnykh zdaniy pri lokalnykh razrusheniyyakh ikh nesushchikh konstruksiy [Ensuring the strength of panel buildings with local destruction of their load-bearing structures]. *Sb.: Issledovaniya nesushchikh betonnykh i zhelezobetonnykh konstruksiy sbornykh mnogoetazhnykh zdaniy*. Moscow: MNIITEP, 1980. Pp. 3–19. (rus)
5. Zenin S.A., Sharipov R.Sh., Kudinov O.V., Shapiro G.I., Gasanov A.A. Methods of calculating of large-panel buildings: how to prevent progressing collapse. *Academia. Arkhitektura i stroitel'stvo*. 2016. No. 4. Pp. 109–113. (rus)
6. Yermeyev P.G. Predotvrashcheniye lavinoobraznogo (progressiruyushchego) obrusheniya nesushchikh konstruksiy unikalnykh bolsheproletnykh sooruzheniy pri avariynnykh vozdeystviyakh [Prevention of avalanche-like (progressive) collapse of load-bearing structures of unique long-span structures during emergency operations]. *Structural Mechanics and Analysis of Constructions*. 2006. No. 2. Pp. 65–72. (rus)
7. Danilov A.I. Kontseptsiya upravleniya protsessom razrusheniya stroitel'nogo obyekt [The concept of controlling the process of destruction of a building object] // *Industrial and Civil Engineering*. 2014. No. 8. Pp. 74–77. (rus)
8. Nazarov Yu.P., Gorodetskiy A.S., Simbirkin V.N. K probleme obespecheniya zhivuchesti stroitelnykh konstruksiy pri avariynnykh vozdeystviyakh [To the problem of ensuring the survivability of building structures under emergency influences]. *Structural Mechanics and Analysis of Constructions*. 2009. No. 4. Pp. 5–9. (rus)
9. Xavier F.B., Macorini L., Izzuddin B.A.. Contribution of masonry cladding for robustness enhancement of multi-storey buildings under sudden column loss. *Proceedings of the 16th International Brick and Block Masonry Conference*. Padova, Italy, 2016.
10. Nethercot D.A. Design of building structures to improve their resistance to progressive collapse. *The Twelfth East Asia-Pacific Conference on Structural Engineering and*

Литература

1. Report of the Inquiry into the Collapse of Flats at Ronan Point, Caning Town. – MSO, 1968 (ЦИНИС, перевод 18736).
2. Marchand K.A., Alfawakhive F. *Blast and Progressive Collapse*. AISC, 2005.
3. Стругацкий Ю.М., Шапиро Г.И. Безопасность московских жилых зданий массовых серий при чрезвычайных ситуациях // *Промышленное и гражданское строительство*. 1998. № 8. С. 37–41.
4. Стругацкий Ю.М. Обеспечение прочности панельных зданий при локальных разрушениях их несущих конструкций // *Сб.: Исследования несущих бетонных и железобетонных конструкций сборных многоэтажных зданий*. М.: МНИИТЭП, 1980. С. 3–19.
5. Зенин С.А., Шарипов Р.Ш., Кудинов О.В., Шапиро Г.И., Гасанов А.А. Расчёты крупнопанельных зданий на устойчивость против прогрессирующего обрушения методами предельного равновесия и конечного элемента // *Academia. Архитектура и строительство*. 2016. № 4. С. 109–113.
6. Еремеев П.Г. Предотвращение лавинообразного (прогрессирующего) обрушения несущих конструкций уникальных большепролетных сооружений при аварийных воздействиях // *Строительная механика и расчет сооружений*. 2006. № 2. С. 65–72.
7. Данилов А.И. Концепция управления процессом разрушения строительного объекта // *Промышленное и гражданское строительство*. 2014. № 8. С. 74–77.
8. Назаров Ю.П., Городецкий А.С., Симбиркин В.Н. К проблеме обеспечения живучести строительных конструкций при аварийных воздействиях // *Строительная механика и расчет сооружений*. 2009. № 4. С. 5–9.
9. Xavier F.B., Macorini L., Izzuddin B.A. Contribution of masonry cladding for robustness enhancement of multi-storey buildings under sudden column loss // *Proceedings of the 16th International Brick and Block Masonry Conference*. Padova, Italy, 2016.
10. Nethercot D.A. Design of building structures to improve their resistance to progressive collapse // *The Twelfth East Asia-Pacific Conference on Structural Engineering and Construction*. Procedia Engineering. 2011. № 14. Pp. 1–13.
11. Yu H., Izzuddin B.A., Zha X.-X. Progressive collapse of steel-framed buildings: influence of modelling approach // *Advanced Steel Construction*. 2010. Vol. 6. № 4. Pp. 932–948.
12. Stylianidis P.M., Nethercot D.A., Izzuddin B.A.,

- Construction. Procedia Engineering.* 2011. No. 14. Pp. 1–13.
11. Yu H., Izzuddin B.A., Zha X.-X. Progressive collapse of steel-framed buildings: influence of modelling approach. *Advanced Steel Construction.* 2010. Vol. 6. No. 4. Pp. 932–948.
 12. Stylianidis P.M., Nethercot D.A., Izzuddin B.A., Elghazouli A.Y. Robustness assessment of frame structures using simplified beam and grillage models. *Engineering Structures.* 2016. Vol. 115. Pp. 78–95.
 13. Ellingwood B.R., Smilowitz R., Dusenberry D.O., Duthinh D., Lew H.S., Carino N.J. *Best Practices for Reducing the Potential for Progressive Collapse in Buildings.* National Institute of Standards and Technology, NISTIR 7396, USA. 2007.
 14. Marchand K.A., Stevens D.J. Progressive collapse criteria and design approaches improvement // *Journal of Performance of Constructed Facilities.* 2015. No. 29(5). B4015004.
 15. Stylianidis P.M., Nethercot D.A. Modelling of connection behaviour for progressive collapse analysis. *Journal of Constructional Steel Research.* 2015. Vol. 113. Pp. 169–184.
 16. Astaneh-Asl A. Progressive Collapse of steel truss bridges, the case of I-35W collapse // *Proceedings, 7th International Conference on Steel Bridges.* Guimaraes, Portugal, 2008. Pp. 1–10.
 17. Kandil K.S., Ellobody E.A.E.F., Eldehemy H. Progressive Collapse of Steel Frames. *World Journal of Engineering and Technology.* 2013. No. 1. Pp. 39–48.
 18. Белостоцкий А.М. и др. Расчеты зданий на устойчивость против прогрессирующего обрушения с учетом физической и геометрической нелинейностей [Calculations of buildings for stability against progressive caving in view of physical and geometric nonlinearities]. Теория и практика расчета зданий, сооружений и элементов конструкций. Аналитические и численные методы: Сб. трудов международной научно-практической конференции. М.: МГСУ, 2008. С. 183–193. (rus)
 19. Kaewkulchai G., Williamson E.B. Beam element formulation and solution procedure for dynamic progressive collapse analysis. *Computers & Structures.* vol.82, issues 7–8, varch 2004, pp. 639–651
 20. Canisius T.D. Robustness of structural systems – a new focus for the joint committee on structural safety (JCSS). *Applications of Statistics and Probability in Civil Engineering.* London. 2007. 8 p.
 21. Stylianidis P.M., Nethercot D.A., Izzuddin B.A., Elghazouli A.Y. Modelling of beam response for progressive collapse analysis. *Structures.* 2015. Vol. 3. Pp. 137–152.
 22. Belyayev N.M. *Soprotivleniye materialov* [Strength of materials]. Moscow, 1965. 856 p. (rus)
 23. Kudishin Yu., Drobot D. Zhivuchest konstruktсий v avariynkh situatsiyakh [Stability of structures in emergency situations]. *Metallicheskiye zdaniya.* 2008. No. 4(8). Pp. 20–22. 2008. No. 5(9). Pp. 21–23. (rus)
 24. Drobot D. Yu. Otsenka zhivuchesti Krytogo Konkobezhnogo tsentra v Krylatskom [Assessment of survivability of the Indoor Skating Center in Krylatskoye]. *Vestnik MGSU.* 2009. No. 2. Pp. 116–119. (rus)
 25. Kudishin Yu.I. Kontseptualnyye problemy zhivuchesti stroitelnykh konstruktсий [Conceptual problems of survivability of building structures]. *Vestnik MGSU.* 2009. No. 2(spec.). Pp. 28–36. (rus)
 26. Kudishin Yu.I., Drobot D.Yu. K voprosu o zhivuchesti stroitelnykh konstruktсий [To the question of the survivability of building structures]. *Structural Mechanics and Analysis of Constructions.* 2008. No. 2(217). Pp. 36–43. (rus)
 27. Kudishin Yu.I., Drobot D.Yu. Zhivuchest stroitelnykh Elghazouli A.Y. Robustness assessment of frame structures using simplified beam and grillage models // *Engineering Structures.* 2016. Vol. 115. Pp. 78–95.
 13. Ellingwood B.R., Smilowitz R., Dusenberry D.O., Duthinh D., Lew H.S., Carino N.J. *Best Practices for Reducing the Potential for Progressive Collapse in Buildings.* National Institute of Standards and Technology, NISTIR 7396, USA. 2007.
 14. Marchand K.A., Stevens D.J. Progressive collapse criteria and design approaches improvement // *Journal of Performance of Constructed Facilities.* 2015. No. 29(5). B4015004.
 15. Stylianidis P.M., Nethercot D.A. Modelling of connection behaviour for progressive collapse analysis // *Journal of Constructional Steel Research.* 2015. Vol. 113. Pp. 169–184.
 16. Astaneh-Asl A. Progressive Collapse of steel truss bridges, the case of I-35W collapse // *Proceedings, 7th International Conference on Steel Bridges.* Guimaraes, Portugal, 2008. Pp. 1–10.
 17. Kandil K.S., Ellobody E.A.E.F., Eldehemy H. Progressive Collapse of steel frames // *World Journal of Engineering and Technology.* 2013. No. 1. Pp. 39–48.
 18. Белостоцкий А.М. и др. Расчеты зданий на устойчивость против прогрессирующего обрушения с учетом физической и геометрической нелинейностей // Теория и практика расчета зданий, сооружений и элементов конструкций. Аналитические и численные методы: Сб. трудов международной научно-практической конференции. М.: МГСУ, 2008. С. 183–193.
 19. Kaewkulchai G., Williamson E.B. Beam element formulation and solution procedure for dynamic progressive collapse analysis // *Computers & Structures.* 2004. Vol. 82. No. 7–8. Pp. 639–651.
 20. Canisius T.D. Robustness of structural systems – a new focus for the joint committee on structural safety (JCSS) // *Applications of Statistics and Probability in Civil Engineering.* London. 2007. 8 p.
 21. Stylianidis P.M., Nethercot D.A., Izzuddin B.A., Elghazouli A.Y. Modelling of beam response for progressive collapse analysis // *Structures.* 2015. Vol. 3. Pp. 137–152.
 22. Беляев Н.М. Соппротивление материалов. М., 1965. 856 с.
 23. Кудишин Ю., Дробот Д. Живучесть конструкций в аварийных ситуациях // *Металлические здания.* 2008. № 4(8). С. 20–22. 2008. № 5(9). С. 21–23.
 24. Дробот Д.Ю. Оценка живучести Крытого Конькобежного центра в Крылатском // *Вестник МГСУ.* 2009. № 2. С. 116–119.
 25. Кудишин Ю.И. Концептуальные проблемы живучести строительных конструкций // *Вестник МГСУ.* 2009. № 2(спец.). С. 28–36.
 26. Кудишин Ю.И., Дробот Д.Ю. К вопросу о живучести строительных конструкций // *Строительная механика и расчет сооружений.* 2008. № 2(217). С. 36–43.
 27. Кудишин Ю.И., Дробот Д.Ю. Живучесть строительных конструкций – важный фактор снижения потерь в условиях аварийных ситуаций // *Металлические конструкции.* 2009. № 1. С. 61–72.
 28. Sanches R.A.K., Coda H.B. Flexible multibody dynamics finite element formulation applied to structural progressive collapse analysis // *Latin American Journal of Solids and Structures.* 2017. No. 14. Pp. 52–57.

konstruktsiy –vazhnyy faktor snizheniya poter v usloviyakh avariynykh situatsiy [Stability of building structures is an important factor in reducing losses in emergency situations]. *Metallicheskiye konstruktsii*. 2009. No. 1. Pp. 61–72.

28. Sanches R.A.K., Coda H.B. Flexible multibody dynamics finite element formulation applied to structural progressive collapse analysis. *Latin American Journal of Solids and Structures*. 2017. No. 14. Pp. 52–57.

Alexandr Tusnin,
+7(916)115-14-21; valeksol@mail.ru

Александр Романович Туснин,
+7(916)115-14-21; эл. почта: valeksol@mail.ru

© Tusnin A., 2018

doi: 10.18720/MCE.78.5

Payback period of investments in energy saving

Период возврата инвестиций в энергосбережение

A.S. Gorshkov,**N.I. Vatin,***Peter the Great St. Petersburg Polytechnic University, St. Petersburg, Russia***P.P. Rymkevich,***Military Space Academy named after A.F. Mozhaysky, Saint Petersburg, Russia***O.O. Kudrevich,***RUE "STROYTEHNORM", Minsk, Republic of Belarus***Канд. техн. наук, директор учебно-научного центра "Мониторинг и реабилитация природных систем"****А.С. Горшков,****д-р техн. наук, профессор Н.И. Ватин,**
*Санкт-Петербургский политехнический университет Петра Великого,**Санкт-Петербург, Россия***канд. физ.-мат. наук, профессор кафедры физики П. П. Рымкевич,***Военно-космическая академия имени**А.Ф. Можайского, Санкт-Петербург, Россия***заместитель директора О.О. Кудревич,***РУП "Стройтехнорм", г. Минск, Республика Беларусь***Key words:** civil engineering; buildings; energy resources; energy consumption; operating costs; investments; return of investments; payback period; energy efficiency; energy saving**Ключевые слова:** строительство; здания; энергетические ресурсы; энергопотребление; эксплуатационные затраты; инвестиции; окупаемость инвестиций; срок окупаемости инвестиций; энергетическая эффективность; энергосбережение

Abstract. Authors developed a mathematical model for estimating the discounted payback period of investments for reducing energy resources needed in building's development. Obtained equations allow calculating the projected payback period for investments in energy saving, taking into account the size of the investment, the estimated or actual value of the achieved energy saving effect, the dynamics of energy carriers tariff growth, the discounting of future cash flows, and also a value and a period of loan repayment. The proposed mathematical model allows to perform quickly and efficiently a comparison of various energy-saving solutions based on economic viability and choose the most optimal from them.

Аннотация. Разработана математическая модель оценки дисконтированного срока окупаемости инвестиций, направленных на уменьшение потребляемых в здании энергетических ресурсов. Получены уравнения, позволяющие выполнить расчет прогнозируемого срока окупаемости инвестиций в энергосбережение с учетом размера инвестиций, расчетного или фактического значения достигаемого энергосберегающего эффекта, величины денежного потока, достигаемого в результате реализации энергосберегающих мероприятий, динамики роста тарифов на энергоносители, дисконтирования будущих денежных потоков, а также величины и срока возврата кредитных средств. Предложенная математическая модель позволяет быстро и качественно произвести сравнение экономической эффективности различных энергосберегающих решений и выбрать из них наиболее оптимальное.

1. Introduction

Ensuring the energy efficiency of designed buildings is an important government's goal, reflected in the EPBD directive and modern energy saving requirements. However, no less urgent task is to reduce energy consumption in existing buildings. Most of the existing buildings were built before the implementation of modern energy-saving programs. For this reason, the amount of energy consumed in those buildings is much higher compared to new buildings.

One of the effective ways to reduce energy consumption in existing buildings is the implementation of a set of energy-saving measures. It can be achieved by building envelop heat insulation [1–3], improving the integrity of building structures [4, 5], implementing efficient engineering equipment [6–10], using secondary energy resources and renewable energy sources [11–15]. Energy-saving measures

usually lead to the reduction of energy consumption in buildings and, consequently, to the reduction of operating costs, for example, for heating.

However, the implementation of any energy-saving event requires investments. Investments in energy saving usually are lump-sum costs. Reduction of operating costs, achieved as a result of the implementation of a set of energy-saving measures, will take place over the next several years, i.e. the profiting component of investment is spread in time.

After a certain period of time, the total economic effect achieved as a result of the introduction of energy-saving technical solutions can reach the value of the initial investment. This time period should be considered as predictable period of their payback.

If the payback period of investments is shorter than the estimated service life or operation of the implemented technical solution, it should be considered as economically justified.

The main criteria for assessing the effectiveness of investments are:

- Simple payback period (*SPP*);
- Discounted payback period (*DPP*).
- Accounting Rate of Return (*ARR*);
- Net Present Value (*NPV*);
- Profitability Index (*PI*);
- Internal Rate of Return (*IRR*).

The above criteria for assessing the effectiveness of investment and construction processes are described in details in [16–32].

The analysis of the economic viability of investments in energy saving is presented in [6, 33–35].

In the article [33], in a case of a public school building, simple and relatively inexpensive measures aimed at energy saving are considered. The authors evaluated the environmental benefits achieved as a result of planned activities and calculated a simple payback period for investments.

The research [34] presents the results of the European project RePublic-ZEB. Its goal is the energy modernization of two existing public buildings. The aim of the research is to promote not only energy-efficient, but also cost-effective technical solutions. The research presents results as a "package of activities", calculation of energy consumption, global costs, actual payback period and CO₂ emissions.

In [35] authors investigated the energy consumption of office buildings equipped with heat pumps. Based on the analysis of the results of energy audit, the authors proposed measures for the modernization of existing heat pumps and calculated a simple payback period for investments.

The research [6] presents an economic analysis of energy-saving technologies implemented in a complex production building. The return on investment model includes combination of simple return and cost analysis of the life cycle.

In [36, 37], more complicated models of return on investment are considered.

The research [36] carried out estimates of the economic viability of energy-saving measures implemented in public buildings. The methodology is based on a sample of 36 actions. The model is designed to find conditions that ensure the profitability of the project. Financial analysis is integrated with risk analysis, which allows to evaluate the sensitivity of the results to the original model data.

In [37] the authors consider various scenarios for financing energy-saving measures aimed at reducing energy consumption in existing residential buildings, taking into account the size of the initial investment, the availability of the investor's own funds, the cost of borrowed funds, and the size of the state subsidy. The paper contains formulas for calculating net present value, simple and discounted payback period of investments.

The above-mentioned studies do not contain an assessment of the contribution of energy tariff growth. In connection with the gradual exhaustion of sources of primary energy, despite some bursts of volatility, the cost of energy carriers has a steady rising trend. This is especially valid for developing economies, where energy tariffs are constantly increasing. In St. Petersburg, the total increase in the cost of heat energy for the period from 2006 to 2016 amounted to 224 %, reaching in some years 22.4 % per year (Table 1).

Table 1. Dynamics of thermal energy tariffs growth in St. Petersburg from 2006 to 2016 with centralized heat supply

Year	Tariff value, ruble/Gcal (VAT included)	Increase in the cost of thermal energy in absolute terms, ruble/Gcal	Increase in the cost of thermal energy in relation to the previous year, %
2006	500.40		
2007	575.46	75.06	+ 15.0
2008	650.00	74.54	+ 13.0
2009	795.73	145.73	+ 22.4
2010	931.00	135.27	+ 17.0
2011	1050.00	119.00	+ 12.8
2012	1175.00	125.00	+11.9
2013	1351.25	176.25	+15.0
2014	1408.01	56.76	+4.2
2015	1541.78	133.77	+9.5
2016	1621.95	80.17	+5.2
Average in 10 years		112.16	+12.6
Total in 10 years		1121.55	+224.1

The absence of an indicator characterizing the growth of the cost of energy resources in models leads to an overestimation of the payback period of investments in energy saving. Because of this, the investments risk increases. The authors propose a mathematical model of recoupment that takes into account not only the size of investments and the discount rate of future cash flows, but also the estimated value of the growth in the cost of energy carriers.

The aim of the research is to develop a mathematical model which includes a combination of technical and economic indicators influencing both the discounted cash flow value and payback period in energy saving. The objectives of the research are to define essential factors influencing the investments payback period, to derive main defining equation, to provide the analysis of this obtained equation and to examine its properties and results.

2. Methods

Criteria for assessing the effectiveness of investment were originally developed for banking and financial sectors of the economy. Gradually, they became widespread in other areas of economic activity, including construction industry and energy.

Currently, investment in energy saving is becoming actual. This type of investment is demanded by society and in many countries is supported by the governments. The development of legislation stimulates the introduction of energy service contracts.

Despite the commonness of the basic economic laws, the construction industry has its own specifics. Incomplete accounting of variables in the mathematical model of payback or inaccurate forecast of their change within the period under consideration can lead to significant loss of the funds invested in the project and failure to achieve the forecasted profit.

In Russia, payback period of investments is defined as the ratio of the initial investment's size to the value of the estimated cash flow:

$$SPP = \frac{IC_0}{CF_1}, \quad (1)$$

where IC_0 – value of the invested capital;

CF_1 – cash flow, achieved as the result of the implementation of energy saving measures and savings in operating costs, or expected to be achieved at the stage of project development after the end of the calendar year or one full heating period.

For example, if the initial investment in energy saving is € 100,000, and the income from the energy-saving activities after the end of the first calendar year or the heating season is 10,000 euros, the simple (no-discount) payback period calculated by formula (1) is $100,000 / 10\,000 = 10$ years.

It assumes that the cash flow in formula (1) is unchanged throughout the life cycle of the building. This approach was valid for the socialist model of the economy, when tariffs for thermal energy remained unchanged for a long period of time, and the government issued loans as interest-free subsidies.

The payback period of investments, calculated according to the formula (1), was received without taking into account:

- discounting future cash flows;
- increase in the cost (tariff) for energy carriers;
- interest on the loan (when borrowed funds are used).

For this reason, the value of a simple payback period calculated by formula (1) can only be regarded as an estimate.

Therefore the goal of further research is comprehensively taking into account the limitations of equation (1) noted above and developing a mathematical model that takes into account noted above factors.

We can account discounting future cash flows for in the following amendment as:

$$CF_n = \sum_{t=1}^n \frac{CF_t}{(1+i)^n}, \quad (2)$$

where t – the calculation step (year, month, etc.);

n – number of the period under consideration;

CF_t – cash flow in t years;

i – discount rate.

While estimating future cash flows to take only discounting into consideration is not enough. In this case, the size of the annual savings of funds obtained as a result of the implementation of energy-saving activities, with each subsequent year (or heating period) will increase. Therefore, each year the amount of cash flow will increase.

Let us assume that the average annual increase in tariffs for energy carriers (in relative units) is r (for example, with an annual average tariff growth of 10 %, $r = 0.1$). Then, the annual savings of funds for any considered year n (first: $n = 1$, second: $n = 2$, third: $n = 3$, etc.), achieved by the implementation of energy-saving measures, taking into account annual tariff growth can be defined by the following expression:

$$CF_i = CF_1 \cdot (1+r)^n. \quad (3)$$

The coefficient, taking into account the estimated growth dynamics in energy tariffs r in subsequent years, in this case plays the same role as the deposit rate when opening a time deposit in the bank.

In this case, equation (2) takes the form:

$$CF_n = \sum_{t=1}^n CF_1 \cdot \frac{(1+r)^n}{(1+i)^n}. \quad (4)$$

The exponents in the numerator and denominator of expression (4) coincide, because the time interval taken to calculate the discounted value of investments and the savings achieved as a result of the implementation of energy-saving solutions coincides.

Let us introduce the following notation:

$$q = \frac{1+r}{1+i}. \quad (5)$$

Taking into account expressions (4) and (5), the total cash flow after n years from the moment implementation of a set of energy-saving activities is:

$$CF_n = CF_1 + q \cdot CF_1 + q^2 \cdot CF_1 + \dots + q^{n-1} \cdot CF_1. \quad (6)$$

Multiply the left and right sides of equation (6) by q . We get:

$$CF_n \cdot q = q \cdot CF_1 + q^2 \cdot CF_1 + \dots + q^n \cdot CF_1. \quad (7)$$

We subtract from (7) the expression (6). We get:

$$(q-1) \cdot CF_n = CF_1 \cdot [q^n - 1], \quad (8)$$

from where:

$$CF_n = CF_1 \cdot \frac{(q^n - 1)}{(q-1)} = CF_1 \cdot \frac{\left(\frac{1+r}{1+i}\right)^n - 1}{(r-i)} \cdot (1+i). \quad (9)$$

Let us substitute the received expression of the total cash flow accumulated over n years of implementation of energy saving solutions into the formula for calculating net present value:

$$NPV = -IC_0 + CF_n = -IC_0 + \sum_{t=1}^n \frac{CF_t}{(1+i)^t} = -IC_0 + CF_1 \cdot \frac{\left(\frac{1+r}{1+i}\right)^n - 1}{(r-i)} \cdot (1+i). \quad (10)$$

We equate the net present value to zero value:

$$NPV = -IC_0 + CF_1 \cdot \frac{\left(\frac{1+r}{1+i}\right)^n - 1}{(r-i)} \cdot (1+i) = 0. \quad (11)$$

This will allow to calculate the discounted payback period of investments into energy saving. In this case, the number of the considered period n turns out to be identical to the discounted payback period of investments.

We get:

$$\frac{IC_0}{CF_1} \cdot \frac{(r-i)}{(1+i)} + 1 = \left(\frac{1+r}{1+i}\right)^{DPP}, \quad (12)$$

whence it follows that the discounted payback period of investments is:

$$DPP = \frac{\ln \left[1 + \frac{IC_0}{CF_1} \cdot \frac{r-i}{1+i} \right]}{\ln \left[\frac{1+r}{1+i} \right]}. \quad (13)$$

The expression in the denominator of formula (13) can be transformed as follows:

$$\ln \left[\frac{1+r}{1+i} \right] = \ln \left[1 + \frac{r-i}{1+i} \right].$$

In this case, expression (13) taking into account (1) can be represented as:

$$DPP = \frac{\ln \left[1 + \frac{IC_0 \cdot r - i}{CF_1 \cdot 1 + i} \right]}{\ln \left[1 + \frac{r - i}{1 + i} \right]} = \frac{\ln \left[1 + SPP \cdot \frac{r - i}{1 + i} \right]}{\ln \left[1 + \frac{r - i}{1 + i} \right]}. \quad (14)$$

If the investor uses its own funds to accomplish the set of energy-saving activities, the calculation of the discounted payback period of investments into energy saving according to the formula (14) is final.

If the investor uses borrowed funds, the amount of investment in energy saving (with annuity monthly payments) should be calculated by the formula:

$$IC_l = m \cdot A \cdot IC_0, \quad (15)$$

where m – the number of loan installments periods (for example, if the loan is taken for 1 year: $m = 12$, if for 2 years: $m = 24$, etc.);

A – the annuity factor;

IC_0 – the same as in formula (1).

The annuity coefficient is calculated by the formula:

$$A = \frac{p_l \cdot (1 + p_l)^m}{(1 + p_l)^m - 1}, \quad (16)$$

where p_l – the bank's interest rate on the loan;

m – the same as in formula (15).

Then the final expression for calculating the discounted payback period of investments should be given as follows:

$$DPP = \frac{\ln \left[1 + \frac{IC_l \cdot r - i}{CF_1 \cdot 1 + i} \right]}{\ln \left[1 + \frac{r - i}{1 + i} \right]}. \quad (17)$$

Equation (14) allows to calculate the discounted payback period for investments in energy savings using the investor's own funds, equation (17) takes into account the amount of the bank loan. The amount of the loan thus increases the payback period of investments in energy saving.

The model allows to obtain the defining equation even when the investments consist of two parts: the investor's own funds and the bank loan.

3. Result and Discussion

We have obtained equations that allow calculating the discounted payback period for investments in energy saving, taking into account:

- the required investment size;
- loan repayments (if any);
- the change in the time of the cost of energy resources;
- discounting future cash flows achieved by saving money as a result of the implementation of the energy saving event or complex of activities.

As a rule, other research studies do not take into account the whole combination of the factors described above. Most of the researchers estimate the expected payback period of the investments either using simple payback period model or taking into account only discounting future cash flow.

In the most general form, the proposed mathematical model is represented by the equation (17). It allows to calculate the discounted payback period of any energy-saving measure or technical solution.

The accuracy of the mathematical model depends on the accuracy of the assessment of the energy saving potential of the planned energy-saving measure and the accuracy of the forecasted growth rates of tariffs for energy resources and discount rates.

When borrowed funds are used, we recommend to use key interest rate of the Central Bank of the country as a discount rate. When one's own funds are used while setting the value of a discount rate in formula (17) risks shall be taken into account, the numerical values of which depend on the specifics of a particular project financing.

The advantage of the presented mathematical model is that it allows to estimate the discounted payback period of investments using a single formula.

Factors that have a positive impact on reduction of the investments discounted payback period in energy saving are:

- growth of tariffs for energy carriers;
- decrease in interest rates on the loan;
- reduction of inflation and risks;
- increase of energy saving potential;
- reduction of the size of the initial investment.

Let us analyze the obtained mathematical model using the example of expression (13).

The value of the coefficient characterizing the growth dynamics of tariffs for energy resources will be taken equal to the discount rate value: $r = i$.

Under this condition, the numerator and denominator in expression (13) become equal to 0:

$$DPP = \frac{\ln \left[1 + \frac{IC_0 \cdot (r-i)}{CF_1 \cdot (1+i)} \right]}{\ln \left[\frac{1+r}{1+i} \right]} = \frac{\ln \left[1 + \frac{IC_0 \cdot (i-i)}{CF_1 \cdot (1+i)} \right]}{\ln \left[\frac{1+i}{1+i} \right]} = \frac{\ln[1]}{\ln[1]} = \frac{0}{0}. \quad (18)$$

Thus, we obtain an uncertainty of the form 0/0. We will uncover the uncertainty obtained.

We introduce an infinitesimal quantity $\varepsilon = r - i$. We expand the numerator and denominator of expression (13) in a series and leave only the first two terms of the expansion. We will receive accordingly:

$$\ln \left[1 + \frac{IC_0 \cdot (r-i)}{CF_1 \cdot (1+i)} \right] \approx \frac{IC_0}{CF_1} \cdot \frac{\varepsilon}{(1+i)} - \left(\frac{IC_0}{CF_1} \right)^2 \cdot \frac{\varepsilon^2}{2(1+i)^2}; \quad (19)$$

$$\ln \left[\frac{1+r}{1+i} \right] = \ln \left[1 + \frac{r-i}{1+i} \right] = \ln \left[1 + \frac{\varepsilon}{1+i} \right] \approx \frac{\varepsilon}{1+i} - \frac{\varepsilon^2}{2(1+i)^2}. \quad (20)$$

We transform the expression (13) to the form:

$$DPP = \frac{IC_0}{CF_1} \left\{ 1 + \frac{(r-i)}{2(1+i)} \left[1 - \frac{IC_0}{CF_1} \right] \right\}. \quad (21)$$

The second term in the curly brackets of equation (21) gives an amendment to the evaluation of the payback period of investments.

If we assume again $r = i$ we get the following:

$$DPP = \frac{IC_0}{CF_1} \left\{ 1 + \frac{(r-i)}{2(1+i)} \left[1 - \frac{IC_0}{CF_1} \right] \right\} = \frac{IC_0}{CF_1} \{1+0\} = \frac{IC_0}{CF_1} = SPP, \quad (22)$$

Then the expression for the payback period of the investment returns to the original expression (1), which is used to calculate the simple (not discounted) payback period of investments.

A deeper analysis of the mathematical model presented above shows that:

- for $r > i$, the discounted payback period, calculated by formula (18), is less than the simple (no-discount) calculated by formula (1), i.e. $DPP < SPP$;
- for $r = i$, the discounted payback period, as was shown above, becomes equal to the simple one, i.e. $DPP = SPP$;
- for $r < i$, the discounted payback period is more simple, i.e. $DPP > SPP$.

Thus, neither the growth of tariffs for energy resources nor the discount rate independently affects the payback period of investments in energy saving.

As a result, the government can create favorable, to some extent, conditions for attracting investments in energy saving.

When comparing different options for energy-saving technical solutions, the most optimal one should be one for which the discounted payback period of investments takes the least value, i.e. the following condition is fulfilled:

$$DPP_i = \frac{\ln \left[1 + \frac{IC_i \cdot (r-i)}{CF_1 \cdot (1+i)} \right]}{\ln \left[1 + \frac{r-i}{1+i} \right]} \rightarrow \min. \quad (23)$$

It should be noted that equation (23) contains several variables with time parameters. In particular, these include:

- the parameter characterizing the dynamics of changes in tariffs for heat energy;
- the rate at which discounting of future cash flows is estimated.

For long time intervals (for example, tens of years), forecasting the dynamics of changes in these variables is a difficult task. Therefore, when predicting the discounted payback period of investments invested in energy saving, one should consider not one, but several possible scenarios of behavior of the variables in equation (23), and choose the most probable scenarios from the list of obtained results.

4. Conclusions

We developed a mathematical model for estimating the discounted payback period of investments aimed at the reduction of energy resources consumed in the building. The obtained equations allow calculating the projected payback period for investments in energy conservation, taking into account the size of the investment, the estimated or actual value of the energy saving effect achieved, the growth dynamics of energy tariffs, the discounting of future cash flows, and the amount and maturity of the loan. The proposed mathematical model allows a quick and high-quality comparison of the economic viability of various energy-saving solutions and choose the most optimal one from them.

As a result of the research it is concluded that the factors positively affecting the decrease in the discounted payback period of investments in energy saving are:

- growth of tariffs for energy carriers;
- decrease in interest rates on the loan;
- reduction of inflation and risks;
- increase in energy-saving potential of the implemented technical solution;
- reduction of the amount of the initial investment.

When determining the discounted payback period of investments in energy saving, a more accurate estimate is provided not by numerical values of the coefficient characterizing the dynamics of changes in the cost of energy resources and discount rates, but by their difference ($r - i$).

If $r = i$ the discounted payback period of investments in energy saving becomes equal to a simple payback period.

The greater the positive difference between the parameters and, entering into the defining equation, the faster the investment in energy saving pays off.

With $r < i$ the risks of non-return of investment in energy saving significantly increase.

Borrowed funds also increase the discounted payback period of investments in energy saving.

The results of the research can be used by investors to assess the effectiveness of investments in energy saving more accurate, and by public authorities - to develop a set of activities to attract investment (to stimulate energy service activities).

References

1. Korniyenko S.V., Vatin N.I., Gorshkov A.S. Thermophysical field testing of residential buildings made of autoclaved aerated concrete blocks. *Magazine of Civil Engineering*. 2016. No. 4. Pp. 10–25.
2. Gorshkov A., Vatin N., Nemova D., Shabaldin A., Melnikova L., Kirill P. Using life-cycle analysis to assess energy savings delivered by building insulation. *Procedia Engineering*. 2015. No. 1(117). Pp. 1085–1094.
3. Vatin N.I., Gorshkov A.S., Nemova D.V., Staritsyna A.A., Tarasova D.S. The energy-efficient heat insulation thickness for systems of hinged ventilated facades. *Advanced Materials Research*. 2014. No. 941–944. Pp. 905–920.
4. Fuliotto R., Cambuli F., Mandas N., Bacchin N., Manara G., Chen Q. Experimental and numerical analysis of heat transfer and airflow on an interactive building façade. *Energy and Buildings*. 2010. No. 42. Pp. 23–28.
5. Vatin N.I., Petrichenko M.R., Korniyenko S.V., Gorshkov A.S., Nemova D.V. Air mode of a triple wall. *Construction of Unique Buildings and Structures*. 2016. No. 6. Pp. 102–114. (rus)
6. Kim J.J. Economic analysis on energy saving technologies for complex manufacturing building. *Resources, Conservation and Recycling*. 2017. No. 123. Pp. 249–254.
7. Zadvinskaya T.O., Gorshkov A.S. Comprehensive method of energy efficiency of residential house. *Advanced Materials Research*. 2014. No. 953–954. Pp. 1570–1577.
8. Boait P.J., Rylatt R.M. A method for fully automatic operation of domestic heating. *Energy and Buildings*. 2010. No. 42. Pp. 11–16.
9. Lauenburg P., Wollerstrand J. Adaptive control of radiator systems for a lowest possible district heating return temperature. *Energy and Buildings*. 2014. No. 11. Pp. 132–140.
10. Cheng Y., Nin J., Gao N. Thermal comfort models: a review and numerical investigation. *Building and Environment*. 2012. No. 47. Pp. 13–22.
11. Perlova E., Platonova M., Gorshkov A., Rakova X. Concept Project of Zero Energy Building. *Procedia Engineering*. 2015. No. 100. Pp. 1505–1514.
12. Rodrigues S., Voss K., Todorovich M. Energy efficiency evaluation of zero energy houses. *Energy and Buildings*. 2014. No. 83. Pp. 23–35.
13. Vasilyev G.P., Gornov V.F., Peskov N.V., Popov M.P., Kolesova M.V., Yurchenko V.A. Ground moisture phase transitions. *Magazine of Civil Engineering*. 2017. No. 6. Pp. 102–117.
14. Hewitt N.J., Huang M.J., Anderson M., Quinn M. Advanced air source heat pumps for UK and European domestic buildings. *Applied Thermal Engineering*. 2011. No. 31.

Литература

1. Корниенко С.В., Ватин Н.И., Горшков А.С. Натурные теплофизические испытания жилых зданий из газобетонных блоков // Инженерно-строительный журнал. 2016. № 4(64). С. 10–25.
2. Gorshkov A., Vatin N., Nemova D., Shabaldin A., Melnikova L., Kirill P. Using life-cycle analysis to assess energy savings delivered by building insulation // *Procedia Engineering*. 2015. № 1(117). Pp. 1085–1094.
3. Vatin N.I., Gorshkov A.S., Nemova D.V., Staritsyna A.A., Tarasova D.S. The energy-efficient heat insulation thickness for systems of hinged ventilated facades // *Advanced Materials Research*. 2014. № 941–944. Pp. 905–920.
4. Fuliotto R., Cambuli F., Mandas N., Bacchin N., Manara G., Chen Q. Experimental and numerical analysis of heat transfer and airflow on an interactive building façade // *Energy and Buildings*. 2010. № 42. Pp. 23–28.
5. Ватин Н.И., Петриченко М.Р., Корниенко С.В., Горшков А.С., Немова Д.В. Воздушный режим трехслойной стеновой конструкции // Строительство уникальных зданий и сооружений. 2016. № 6. С. 102–114.
6. Kim J.J. Economic analysis on energy saving technologies for complex manufacturing building // *Resources, Conservation and Recycling*. 2017. № 123. Pp. 249–254.
7. Zadvinskaya T.O., Gorshkov A.S. Comprehensive method of energy efficiency of residential house // *Advanced Materials Research*. 2014. № 953–954. Pp. 1570–1577.
8. Boait P.J., Rylatt R.M. A method for fully automatic operation of domestic heating // *Energy and Buildings*. 2010. № 42. Pp. 11–16.
9. Lauenburg P., Wollerstrand J. Adaptive control of radiator systems for a lowest possible district heating return temperature // *Energy and Buildings*. 2014. № 11. Pp. 132–140.
10. Cheng Y., Nin J., Gao N. Thermal comfort models: a review and numerical investigation // *Building and Environment*. 2012. № 47. Pp. 13–22.
11. Perlova E., Platonova M., Gorshkov A., Rakova X. Concept Project of Zero Energy Building // *Procedia Engineering*. 2015. № 100. Pp. 1505–1514.
12. Rodrigues S., Voss K., Todorovich M. Energy efficiency evaluation of zero energy houses // *Energy and Buildings*. 2014. № 83. Pp. 23–35.
13. Васильев Г.П., Горнов В.Ф., Песков Н.В., Попов М.И., Колесова М.В., Юрченко В.А. Фазовые переходы влаги в грунте. Учет при проектировании грунтовых теплообменников // Инженерно-строительный журнал. 2017. № 6(74). С. 102–117.
14. Hewitt N.J., Huang M.J., Anderson M., Quinn M. Advanced air source heat pumps for UK and European domestic buildings // *Applied Thermal Engineering*. 2011. No. 31.

- Pp. 3713–3719.
15. You T., Wu W., Shi W., Wang B., Li X. An overview of the problems and solutions of soil thermal imbalance of ground-coupled heat pumps in cold regions. *Applied Energy*. 2016. No. 177. Pp. 515–536.
 16. Benati S. An optimization model for stochastic project networks with cash flows. *Computational Management Science* 3. 2006. No. 4. Pp. 271–284.
 17. Demeulemeester E.L., Herroelen W.S. *Project Scheduling – A Research Handbook*. Kluwer Academic Publishers. Chichester. 2005. 375 p.
 18. Elmaghraby S.E. On the fallacy of averages in project risk management. *European Journal of Operational Research*. 2005. No. 165. Pp. 307–313.
 19. Elmaghraby S.E., Herroelen W.S. The scheduling of activities to maximize the net present value of projects. *European Journal of Operational Research*. 1990. No. 49. Pp. 35–49.
 20. Elmaghraby S.E., Kamburowski J. On project representation and activity floats. *Arabian Journal of Science and Engineering*. 1990. No. 15. Pp. 626–637.
 21. Herroelen W.S., Dommelen P.V., Demeulemeester E.L. Project network models with discounted cash flows – A guided tour through recent developments. *European Journal of Operational Research*. 1997. No. 100. Pp. 97–121.
 22. Herroelen W.S., Leus R. Project scheduling under uncertainty: Survey and research potentials. *European Journal of Operational Research*. 2005. No. 165. Pp. 289–306.
 23. Özdamar L., Dündar H. A flexible heuristic for a multi-mode capital constrained project scheduling problem with probabilistic cash inflows. *Computers and Operations Research*. 1997. No. 24. Pp. 1187–1200.
 24. Rockafellar R.T., Uryasev S. Optimization of conditional value-at-risk. *Journal of Risk*. 2000. No. 2. Pp. 21–41.
 25. Stephan K., Menassa C. Modeling the Effect of Building Stakeholder Interactions on Value Perception of Sustainable Retrofits. *J. Comput. Civ.Eng.* 2014. No. 3. Pp. 68–78.
 26. Breslau V., Fowles R.H. *Sustainability Perspectives and Trends in Corporate Real Estate*. Jones Lang LaSalle and CoreNet Global. London. 2007. 486 p.
 27. Bond S., Mitchell P. Alpha and persistence in real estate fund performance. *J. Real Estate Finance*. 2010. No. 41. Pp. 53–79.
 28. Kaplan S., Schoar A. Private equity performance: Returns, persistence, and capital flows. *J. Finance*. No. 60. Pp. 1791–1823.
 29. Sharpe W. Decentralized investment management. *J. Finance*. No. 36. Pp. 217–234.
 30. Gilemhanov R.A., Braila N.V. Methods of assessment of financial efficiency in construction projects. *Construction of Unique Buildings and Structures*. 2016. No. 10. Pp. 7–19. (rus)
 31. Leventsov A.N., Leventsov V.A. EFFECTIVE INVESTMENTS IN MODERN. *Collection: FINANCIAL SOLUTIONS OF THE XXI CENTURY: THEORY AND PRACTICE a collection of scientific papers of the 17th International Scientific and Practical Conference*. St. Petersburg Polytechnic University of Peter the Great. 2016. Pp. 235–241. (rus)
 32. Vasilyeva A.G., Dzyubenko I.B., Zavadskaya V.V., et al. Financial management of the development of economic systems: monograph. Book 13. Novosibirsk: Publishing house of CRNS, 2016. 358 p. (rus)
 33. De Santoli L., Fraticelli F., Fornari F., Calice C. Energy performance assessment and a retrofit strategies in public school buildings in Rome. *Energy and Buildings*. 2014. No. 68. Pp. 196–202.
 - buildings // *Applied Thermal Engineering*. 2011. No. 31. Pp. 3713–3719.
 15. You T., Wu W., Shi W., Wang B., Li X. An overview of the problems and solutions of soil thermal imbalance of ground-coupled heat pumps in cold regions // *Applied Energy*. 2016. No. 177. Pp. 515–536.
 16. Benati S. An optimization model for stochastic project networks with cash flows // *Computational Management Science* 3. 2006. No. 4. Pp. 271–284.
 17. Demeulemeester E.L., Herroelen W.S. *Project Scheduling – A Research Handbook*. Kluwer Academic Publishers. Chichester. 2005. 375 p.
 18. Elmaghraby S.E. On the fallacy of averages in project risk management // *European Journal of Operational Research*. 2005. No. 165. Pp. 307–313.
 19. Elmaghraby S.E., Herroelen W.S. The scheduling of activities to maximize the net present value of projects // *European Journal of Operational Research*. 1990. No. 49. Pp. 35–49.
 20. Elmaghraby S.E., Kamburowski J. On project representation and activity floats // *Arabian Journal of Science and Engineering*. 1990. No. 15. Pp. 626–637.
 21. Herroelen W.S., Dommelen P. V., Demeulemeester E.L. Project network models with discounted cash flows – A guided tour through recent developments // *European Journal of Operational Research*. 1997. No. 100. Pp. 97–121.
 22. Herroelen W.S., Leus R. Project scheduling under uncertainty: Survey and research potentials // *European Journal of Operational Research*. 2005. No. 165. Pp. 289–306.
 23. Özdamar L., Dündar H. A flexible heuristic for a multi-mode capital constrained project scheduling problem with probabilistic cash inflows // *Computers and Operations Research*. 1997. No. 24. Pp. 1187–1200.
 24. Rockafellar R.T., Uryasev S. Optimization of conditional value-at-risk // *Journal of Risk*. 2000. No. 2. Pp. 21–41.
 25. Stephan K., Menassa C. Modeling the effect of building stakeholder interactions on value perception of sustainable retrofits // *J. Comput. Civ.Eng.* 2014. No. 3. Pp. 68–78.
 26. Breslau B., Fowles R.H. *Sustainability perspectives and trends in corporate real estate*. Jones Lang LaSalle and CoreNet Global. London. 2007. 486 p.
 27. Bond S., Mitchell P. Alpha and persistence in real estate fund performance // *J. Real Estate Finance*. 2010. No. 41. Pp. 53–79.
 28. Kaplan S., Schoar A. Private equity performance: Returns, persistence, and capital flows // *J. Finance*. No. 60. Pp. 1791–1823.
 29. Sharpe W. Decentralized investment management // *J. Finance*. No. 36. Pp. 217–234.
 30. Гилемханов Р.А., Брайла Н.В. Методы оценки финансово-экономической эффективности инвестиционно-строительных проектов // *Строительство уникальных зданий и сооружений*. 2016. No. 10. С. 7–19.
 31. Левенцов А.Н., Левенцов В.А. Эффективные инвестиции в современных условиях // Сборник: ФИНАСОВЫЕ РЕШЕНИЯ XXI ВЕКА: ТЕОРИЯ И ПРАКТИКА 17-й научно-практической конференции. Санкт-Петербургский политехнический университет Петра Великого. 2016. С. 235–241.
 32. Васильева А.Г., Дзюбенко И.Б., Завадская В.В. и др. Финансовое управление развитием экономических систем. Книга 13. / Под общей редакцией С.С.Чернова. Изд. 2-е. Новосибирск, 2016. 358 с.
 33. De Santoli L., Fraticelli F., Fornari F., Calice C. Energy performance assessment and a retrofit strategies in public school buildings in Rome // *Energy and Buildings*. 2014. No. 68. Pp. 196–202.

34. Corrado V., Murano G., Paduos S., Riva G. On the Refurbishment of the Public Building Stock Toward the Nearly Zero-energy Target: Two Italian case studies. *Energy Procedia*. 2016. No. 101. Pp. 105–112.
35. Han X., Chen J., Huang C., Weng W., Wang L., Niu R. Energy audit and air-conditioning system renovation analysis on office buildings using air-source heat pump in Shanghai. *Building Services Engineering Research and Technology*. 2014. No. 35(4). Pp. 376–392.
36. Napoli G., Gabrielli L., Barbaro S. The efficiency of the incentives for the public buildings energy retrofit. The case of the Italian regions of the "objective convergence". *Valori e Valutazioni*. 2017. No. 18. Pp. 25–39.
37. Matic D., Calzada J.R., Eric M., Babin M. Economically feasible energy refurbishment of prefabricated building in Belgrade, Serbia. *Energy and Building*. 2014. <http://dx.doi.org/10.1016/j.enbuild.2014.10.041>.
34. Corrado V., Murano G., Paduos S., Riva G. On the Refurbishment of the Public Building Stock Toward the Nearly Zero-energy Target: Two Italian case studies // *Energy Procedia*. 2016. № 101. Pp. 105–112.
35. Han X., Chen J., Huang C., Weng W., Wang L., Niu R. Energy audit and air-conditioning system renovation analysis on office buildings using air-source heat pump in Shanghai // *Building Services Engineering Research and Technology*. 2014. № 35(4). Pp. 376–392.
36. Napoli G., Gabrielli L., Barbaro S. The efficiency of the incentives for the public buildings energy retrofit. The case of the Italian regions of the "objective convergence" // *Valori e Valutazioni*. 2017. № 18. Pp. 25–39.
37. Matic D., Calzada J.R., Eric M., Babin M. Economically feasible energy refurbishment of prefabricated building in Belgrade, Serbia // *Energy and Building*. 2014. <http://dx.doi.org/10.1016/j.enbuild.2014.10.041>.

Alexander Gorshkov,
+7(921)388-43-15; alsgor@yandex.ru

Александр Сергеевич Горшков,
+7(921)388-43-15; эл. почта: alsgor@yandex.ru

Nicolai Vatin,
+7(921)964-37-62; vatin@mail.ru

Николай Иванович Ватин,
+7(921)964-37-62; эл. почта: vatin@mail.ru

Pavel Rymkevich,
+7(911)224-59-13; rymkewitch@yandex.ru

Павел Павлович Рымкевич,
+7(911)224-59-13;
эл. почта: rymkewitch@yandex.ru

Olga Kydrevich,
+375(33)300-38-70; kudrevich@stn.by

Ольга Олеговна Кудревич,
+375(33)300-38-70; эл. почта: kudrevich@stn.by

© Gorshkov A.S., Vatin N.I., Rymkevich P.P., Kydrevich O.O., 2018

doi: 10.18720/MCE.78.6

Flow states in the classical Venturi channel water gauge

Режимы течения в классическом водомерном канале Вентури

A.L. Zuikov,*National Research Moscow State Civil Engineering University, Moscow, Russia***V.V. Bakunjaeva,***“SKB – Engineering” Ltd., Moscow, Russia***T.V. Artemyeva,***Moscow State Automobile and Road Technical University, Moscow, Russia***Д-р техн. наук, профессор А.Л. Зуйков,***Национальный исследовательский Московский государственный строительный университет, Москва, Россия***инженер В.В. Бакуняева,***ООО «СКБ – Инжиниринг», Москва, Россия
старший преподаватель Т.В. Артемьева,
канд. техн. наук, доцент Е.Ю. Жажа,
Московский автомобильно-дорожный государственный технический университет, Москва, Россия***Key words:** open channel flow; liquid flow rate measurement; Venturi flume; critical depth**Ключевые слова:** безнапорное течение; измерение расхода воды; лоток Вентури; критическая глубина

Abstract. The paper relates to the field of hydraulics and is devoted to the study of fluid flow states in a non-submerged Venturi channel. The aim is improvement of the method of hydraulic calculation of the classical Venturi channel. Authors applied experimental methods with the use of hi-tech certified measurement equipment allowing for digital technology-based automated collection and processing of empirical information; calculation and analytical methods. Distribution of depths, velocities and Froude numbers in flow direction inside the classical Venturi channel water gauge are obtained. The theoretical method of hydraulic calculation of the full-capacity discharge of the Venturi channel is considered, which does not contain empirical coefficients. It is established that the calculation of the full-capacity discharge of the classical Venturi channel in accordance with the current State Standard of the Russian Federation MI 2406-97 gives underestimated values of the design flow rate with the actual flow rate with a systematic error of more than -2 %, the theoretical method of hydraulic calculation of the full-capacity discharge of the Venturi channel has a relative error of ± 1 %.

Аннотация. Работа посвящена исследованию режимов течения жидкости в неподтопленном расходомерном канале Вентури. Целью является совершенствование метода гидравлического расчета классического канала Вентури. Были применены экспериментальные методы с использованием высокотехнологичного сертифицированного измерительного оборудования, позволяющего на основе цифровых технологий производить автоматизированный сбор и обработку эмпирической информации; и расчетно-аналитические. В результате были получены распределения глубин, скоростей и чисел Фруда в потоке по длине проточного тракта классического расходомерного канала Вентури. Рассмотрен теоретический не содержащий эмпирических коэффициентов метод гидравлического расчета пропускной способности канала Вентури. Установлено, что расчет пропускной способности классического канала Вентури по действующему Госстандарту РФ МИ 2406–97 даёт заниженные значения расчетного расхода относительно расхода действительного с систематической погрешностью более -2 %, теоретический метод гидравлического расчета пропускной способности канала Вентури имеет относительную погрешность ± 1 %.

1. Introduction

Attitude to water not as the main resource of life support for the population, but as an expendable material that does not have strategic value for the State and human, leads to out-of-order consumption of water, decrease in its quality in water bodies, aggravates the contradiction between water users. The priority of the use of water resources for domestic and drinking water supply purposes, declared in the Water Code of the Russian Federation, is not being fulfilled. Today, monitoring the volume of water consumption from natural sources and the return of treated wastewater to the environment has become the main function of the State hydrometric services, the implementation of which must be ensured by the

high accuracy data obtained at gauges. Of importance became the commercial accounting of water consumption [1]. The requirements for its organization are approved by the resolutions of the Government of the Russian Federation of 12.02.1999 No.167 "On Approval of the Rules for the Use of Public Water Supply and Sewage Systems in the Russian Federation", dated 10.04.2007 No. 219 "On Approval of the Regulations on Implementation of State Monitoring of Water Bodies" and dated July 29, 2013 No. 644 "On Approval of the Rules of Cold Water Supply and Sanitation and on Amending Certain Acts of the Government of the Russian Federation", as well as the Order of the Ministry of Natural Resources of Russia of 08.07.2009 No. 205 "On Approval of the Procedure for the Owners of Water Bodies and Water Users to Take into Account the Amount of Water Abstraction (withdrawal) from Water Bodies and the Volume of Discharge of Sewage and (or) Drain Water, their Quality". These documents determine that the gauges of commercial recording the volumes of clean water intake and discharge of effluents must be installed at all enterprises in the Russian Federation, without exception. Measurements of water flow in open canals and channels are governed by several State Standards, the main of which are the two regulatory documents [2, 3]: MI 2220-13 "The Flow Rate and Volume of the Waste Fluid. Gauging Procedure in Non-pressure Water Conduits by the Level of Filling with Preliminary Calibration of the Measuring Section" and MI 2406-97 "Liquid Flow in Open Channels of Water Supply and Sewerage Systems. Gauging Procedure with the Use of Standard weirs and Flumes".

According to regulatory documents, flow gauges are recognized as effective means of determining the discharges of pure and suspended load-bearing open flows in natural watercourses, reclamation canals and in domestic water supply and sewerage systems. The Venturi flume water gauge (Fig. 1) [3–9] is a typical self-cleaning flume, which is an open non-prismatic channel with vertical walls, gradually tapering downstream forming a convergent channel followed by a straightforward gorge portion, then gradually expanding downstream portion (diffuser). The Venturi flume is capable to pass fine and coarse mechanical inclusions: suspended load, sand, branches, logs and other debris. The Venturi flume hydraulics have been studied for over a hundred years [10], but even today it is of interest for the engineering and scientific community. This is reflected in a number of publications devoted to this issue with the research carried out across the entire spectrum of directions of hi-tech science from experimental to numerical and theoretical [3, 11–24]. Undoubtedly, this is due to the necessity to improve the methods for calculation of hydraulic characteristics of the Venturi flume – one of the main water gauge tools for open flows. The classical Venturi flume in the State Standard of the Russian Federation MI 2406-97 and the International Standard ISO 4359:2013 is a horizontal channel of critical depth with a free (not flooded) fluid outflow, at which the downstream water level variation (h_b) has no effect on the flow rate (Q). There are similar Standards in the most developed countries of the world, for example, U.S. ASTM D 5640-95(2014).



Figure 1. Venturi flumes: on the left – prototype (view from downstream pool); on the right – model (view from upstream pool)

Considering the Venturi flume as a channel of critical depth, the Standards declare that within a straight gorge portion there is a stream transition from a calm subcritical to a stormy supercritical flow through the critical depth h_c (Fig. 2). This statement was transferred from the previous domestic and international Standards (RPD 99-77, MI 2122-90, ISO 4359:1983, ISO 4359:1983/Cor.1:1999), based on the results of experimental studies carried out in the 60-70s of the last century on the equipment that is substantially inferior to the modern one. Since then, it has been 50 years, obviously, it's time to refine or

supplement the provisions of the current Standards, using modern hi-tech equipment, devices and instruments. Such papers began to appear recently [3, 22, 24–28].

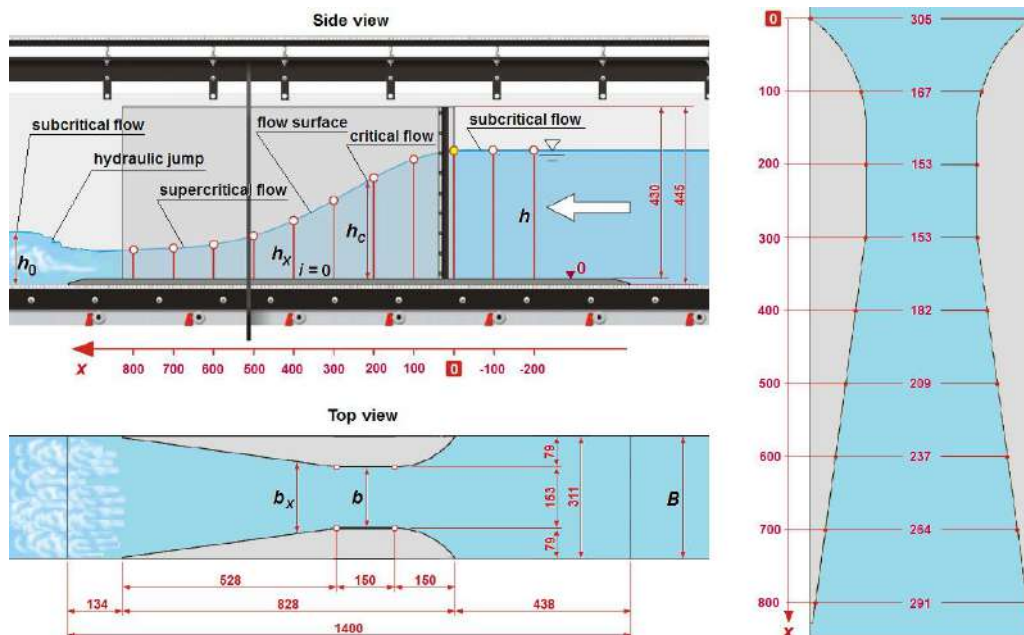


Figure 2. The laboratory model of Venturi flume (measurements in millimeters)

Objectives of the Experiments: determination of flow states within the flow path of the classical Venturi channel; determination of the position of the section in which the flow passes through a critical depth; determination of the hydraulic characteristics of the Venturi flume on the basis of experimental studies performed on hi-tech certified measurement equipment, allowing on the basis of digital technologies for automated collection and processing of empirical information; checking the provisions of the State Standard of Russia MI 2406-97; improvement of the method of hydraulic calculation of the Venturi channel.

2. Methods

2.1. Equipment, Devices and Instruments

Experimental studies of the model Venturi flume water gauge have been made in the National Research Moscow State University of Civil Engineering (NUR MGSU). The following equipment, devices and instruments have been used in the studies [24, 27 and 28]:

- HM 162 scientific research hydraulic calibrating flume [29] (manufacturer: G.U.N.T. Gerätebau GmbH, Germany) with width of cross-section $B = 311$ mm, height 450 mm and length 15.5 m with relative roughness of the walls of the flume made of hardened glass and its floor (stainless steel) produced according to the Manning design [10] $n = 0.009$;
- built-in instruments in the HM 162 flume: SHS4 80-200/40/P pump (manufacturer: Lowara S.R.L. Unipersonale, Italy) with maximal head 10 m, maximal delivery $150 \text{ m}^3/\text{h}$, power 5.5 kW; Promag 10 D electromagnetic flowmeter (manufacturer: Endress+Hauser Flowtec AG, France) with $0 - 150 \text{ m}^3/\text{h}$ range of measurement, accuracy class 0.3; GSZ-100 lifting jack system for controlling the slope of the flume (manufacturer: ZIMM Maschinenelemente GmbH & Co KG, Austria) with range of variation of slope i from -0.5% to $+1.75\%$;
- HM 162.91 digital level gauge [29] (manufacturer: G.U.N.T. Gerätebau GmbH, Germany) with range of measurement from 0 to 455 mm correct to within 0.01 mm;
- HM 162.51 model of Venturi flume (cf. Fig. 2) [30] (manufacturer: G.U.N.T. Gerätebau GmbH, Germany) with height 430 mm, width and length of the gorge portion $b = 153$ mm and $l = 150$ mm, made of plexiglass and attached on a polyvinyl chloride plate, 15 mm thick; the model is a prototype of Venturi channel water gauge, which practically corresponds to the typical design 902-9-44.87 [31] with the design maximum flow rate $Q_{\max} = 250 \text{ m}^3/\text{h}$;
- DLE 40 Professional digital laser rangefinder (manufacturer: Robert Bosch GmbH, Germany) with range of measurement from 0.05 to 40 m with accuracy within 0.5 mm.
- All the equipment is certified consistent with the Russian Laws.

2.2. Methods of the Experimental Research

1. Before performing the study the hydraulic flume HM 162 was set in horizontal position ($i = 0$) and the model of Venturi channel HM 162.51 placed in the middle part of the flume (cf. Fig. 2). The digital level gauge HM 162.91 was mounted on instrument carriage and its zero adjusted relative to the floor of the model HM 162.51. The HM 162.12 specialized software package (manufacturer: G.U.N.T. Gerätebau GmbH, Germany) was loaded into the control computer in order to record the discharge, which was measured in course of the study by an electromagnetic flowmeter Promag 10 D.

2. The forward flow rate (or discharge) Q was specified on the panel used to control the operating regime of the laboratory flume HM 162 or from the computer and the flume pump SHS4 80-200/40/P then turned on.

3. Following stabilization of the discharge with the pump turned on or with a variable operation regime of the pump (stabilization time 10 min), the value of the discharge was written to the hard disk of the control computer into a newly created data file by the HM 162.12 program. The total time needed for the measurement was 200 sec with interval between measurements 1 sec; during this period the computer system automatically executed 200 measurements. The obtained data were translated into an Excel file in the course of laboratory processing of the measurement results in which the average value of the full-capacity discharge in the course of a measurement session

$$Q = \frac{1}{k} \sum_{j=1}^k Q_j$$

and the normed standard deviation

$$\sigma = \frac{1}{Q} \sqrt{\frac{1}{k} \sum_{j=1}^k (Q_j - Q)^2}$$

were calculated, in which k is the size of the sample, $k = 200$; Q_j is the j th element of the sample. The values of Q and σ are written in Table 1.

4. The same Table 1 shows measured digital level gauge HM 162.91 values of flow depths (or water levels) h_x at 11 points x along the length of the model of Venturi flume HM 162.51 (cf. Fig. 2). The distances x were determined from the input edge of the model HM 162.51 using the digital laser rangefinder DLE 40 Professional, the same meter determined the values of the width of the Venturi flume b_x at points x . The values of x and the corresponding values of b_x are written in the title lines of Table 1.

5. Next, the discharge transmitted through the flume was changed with preliminarily selected step ΔQ and the operations from Step 3 to Step 5 repeated. The total being investigated 11 regimes of transmission discharge Q from 10.06 to 110.37 m³/h with step $\Delta Q \approx 10$ m³/h. All measured values were written in units of dimensions of the measuring instruments.

Table 1. Experimental Data

Q, m ³ /h	σ	x , mm	-200	-100	0	100	200	300	400	500	600	700	800
		b_x , mm	311	311	305	167	153	153	182	209	237	264	291
110.37	0.00245	h_x , mm	227.98	226.84	224.75	211.70	178.34	139.34	109.11	89.64	75.02	64.72	55.97
99.95	0.00273	h_x , mm	213.32	213.32	210.78	198.58	166.12	129.93	102.05	83.64	70.39	59.94	52.09
90.14	0.00262	h_x , mm	200.12	199.43	196.97	184.63	154.47	119.74	94.38	77.66	65.07	55.13	47.87
80.15	0.00201	h_x , mm	185.58	184.68	181.87	170.19	141.28	108.83	87.04	71.76	59.82	50.43	43.14
69.92	0.00226	h_x , mm	169.29	168.73	166.69	154.92	127.35	98.57	78.95	65.49	54.48	45.00	39.64
60.08	0.00235	h_x , mm	153.08	153.08	150.23	138.79	113.28	87.68	71.26	59.30	48.18	39.66	35.87
49.89	0.00251	h_x , mm	135.77	135.77	133.18	122.05	99.20	76.78	63.81	52.38	41.11	34.18	32.85
39.96	0.00224	h_x , mm	117.27	116.38	114.23	105.02	83.90	65.55	55.00	44.76	33.81	29.89	29.48
29.83	0.00427	h_x , mm	96.31	95.69	93.60	85.49	67.89	54.31	46.11	35.14	26.93	25.58	25.50
19.94	0.00394	h_x , mm	73.26	72.78	70.97	64.79	50.56	41.93	35.84	24.91	21.11	21.11	19.85
10.06	0.00689	h_x , mm	46.10	46.10	44.83	39.99	31.54	28.19	20.77	15.98	15.15	13.74	11.91

3. Results and Discussion

Laboratory processing of the measurement results was implemented in Microsoft Office Excel 2007 and the results of computations are written in Tables 2 – 4. The following quantities were calculated:

- critical depths [10, 24, 27, 28, 30] (Table 2)

$$h_c = \sqrt[3]{\frac{Q^2}{gb_x^2}},$$

where g is the gravitational acceleration, $g = 9.81$ m/sec²;

Table 2. Critical Depths

Q, m ³ /h	x, mm	-200	-100	0	100	200	300	400	500	600	700	800
	b _x , mm	311	311	305	167	153	153	182	209	237	264	291
110.37	h _c , mm	99.69	99.69	100.99	150.89	159.96	159.96	142.48	129.93	119.48	111.19	104.20
99.95	h _c , mm	93.31	93.31	94.53	141.24	149.73	149.73	133.37	121.62	111.84	104.08	97.54
90.14	h _c , mm	87.10	87.10	88.23	131.83	139.76	139.76	124.49	113.52	104.39	97.15	91.04
80.15	h _c , mm	80.54	80.54	81.59	121.91	129.24	129.24	115.12	104.98	96.54	89.84	84.19
69.92	h _c , mm	73.53	73.53	74.49	111.30	117.99	117.99	105.10	95.84	88.13	82.02	76.86
60.08	h _c , mm	66.46	66.46	67.33	100.60	106.65	106.65	94.99	86.63	79.66	74.13	69.47
49.89	h _c , mm	58.72	58.72	59.48	88.88	94.22	94.22	83.92	76.53	70.38	65.49	61.38
39.96	h _c , mm	50.64	50.64	51.30	76.65	81.26	81.26	72.38	66.00	60.70	56.48	52.93
29.83	h _c , mm	41.67	41.67	42.21	63.07	66.87	66.87	59.56	54.31	49.95	46.48	43.56
19.94	h _c , mm	31.86	31.86	32.27	48.22	51.12	51.12	45.53	41.52	38.18	35.53	33.30
10.06	h _c , mm	20.20	20.20	20.46	30.57	32.41	32.41	28.87	26.32	24.21	22.53	21.11

- Flow velocities (Table 3)

$$V = \frac{Q}{b_x h_x}; \quad (1)$$

Table 3. Flow Velocities

Q, m ³ /h	x, mm	-200	-100	0	100	200	300	400	500	600	700	800
	b _x , mm	311	311	305	167	153	153	182	209	237	264	291
110.37	V, m/sec	0.4324	0.4346	0.4472	0.8672	1.1236	1.4381	1.5439	1.6364	1.7243	1.7943	1.8823
99.95	V, m/sec	0.4185	0.4185	0.4319	0.8372	1.0924	1.3966	1.4949	1.5883	1.6643	1.7545	1.8316
90.14	V, m/sec	0.4023	0.4037	0.4168	0.8120	1.0594	1.3667	1.4576	1.5426	1.6235	1.7203	1.7974
80.15	V, m/sec	0.3858	0.3877	0.4014	0.7834	1.0300	1.3372	1.4055	1.4846	1.5705	1.6724	1.7736
69.92	V, m/sec	0.3689	0.3701	0.3820	0.7507	0.9968	1.2878	1.3517	1.4190	1.5042	1.6349	1.6837
60.08	V, m/sec	0.3506	0.3506	0.3642	0.7201	0.9629	1.2441	1.2869	1.3466	1.4616	1.5940	1.5989
49.89	V, m/sec	0.3282	0.3282	0.3412	0.6799	0.9131	1.1798	1.1934	1.2660	1.4224	1.5359	1.4498
39.96	V, m/sec	0.3044	0.3067	0.3186	0.6329	0.8647	1.1068	1.1089	1.1865	1.3852	1.4067	1.2939
29.83	V, m/sec	0.2766	0.2784	0.2902	0.5804	0.7977	0.9972	0.9873	1.1282	1.2982	1.2270	1.1166
19.94	V, m/sec	0.2431	0.2447	0.2559	0.5119	0.7160	0.8634	0.8491	1.0639	1.1071	0.9938	0.9589
10.06	V, m/sec	0.1950	0.1950	0.2045	0.4186	0.5793	0.6482	0.7396	0.8371	0.7786	0.7707	0.8066

- Froude numbers (Table 4) [10, 31, 32]

$$Fr = \frac{V}{\sqrt{gh_x}}. \quad (2)$$

Table 4. Froude Numbers

Q, m ³ /h	x, mm	-200	-100	0	100	200	300	400	500	600	700	800
	b _x , mm	311	311	305	167	153	153	182	209	237	264	291
110.37	Fr	0.2891	0.2913	0.3012	0.6017	0.8495	1.2300	1.4922	1.7450	2.0100	2.2519	2.5403
99.95	Fr	0.2893	0.2893	0.3003	0.5998	0.8557	1.2371	1.4940	1.7534	2.0028	2.2881	2.5623
90.14	Fr	0.2871	0.2886	0.2998	0.6034	0.8606	1.2610	1.5148	1.7673	2.0321	2.3392	2.6228
80.15	Fr	0.2859	0.2880	0.3005	0.6063	0.8749	1.2941	1.5211	1.7694	2.0501	2.3777	2.7263
69.92	Fr	0.2863	0.2877	0.2987	0.6090	0.8918	1.3096	1.5359	1.7703	2.0576	2.4606	2.7000
60.08	Fr	0.2861	0.2861	0.3000	0.6171	0.9135	1.3414	1.5391	1.7656	2.1260	2.5555	2.6954
49.89	Fr	0.2844	0.2844	0.2985	0.6214	0.9256	1.3594	1.5083	1.7660	2.2399	2.6524	2.5539
39.96	Fr	0.2838	0.2870	0.3010	0.6235	0.9531	1.3802	1.5096	1.7906	2.4053	2.5977	2.4060
29.83	Fr	0.2846	0.2874	0.3029	0.6337	0.9775	1.3661	1.4680	1.9215	2.5258	2.4493	2.2325
19.94	Fr	0.2868	0.2896	0.3067	0.6421	1.0166	1.3461	1.4320	2.1521	2.4327	2.1839	2.1729
10.06	Fr	0.2900	0.2900	0.3083	0.6684	1.0415	1.2326	1.6384	2.1142	2.0197	2.0993	2.3599

By results of measurement and processing of the experimental data the hydraulic characteristics of flows inside Venturi flume have been constructed. They are presented in Figures 3–5.

Figure 3 shows a grid consisting of two families of intersecting curves: the first family shown by black dots and lines reflects the experimental data of flow depth measurements lengthwise the flow path of the examined Venturi flume $h_x = f(x)$ (cf. Table 1). The second family (blue lines) shows the calculated values of the critical depths $h_c = f(x)$ (cf. Table 2). To the right of the graph opposite the experimental curves, the values of the corresponding flow rates Q are indicated in black. The flow rates corresponding to the blue lines of critical depths are indicated in blue for maximum and minimum values in the chart field. The points of intersection of curves $h_x = f(x)$ and $h_c = f(x)$ are shown in red. These points show the positions of the critical depths on the free surface lines of the stream at various flow rates through the Venturi flume. The red envelope curve is drawn along these points. To the right of this curve there are calm subcritical flow states, below there are stormy supercritical ones, and the red envelope curve corresponds to the critical flows.

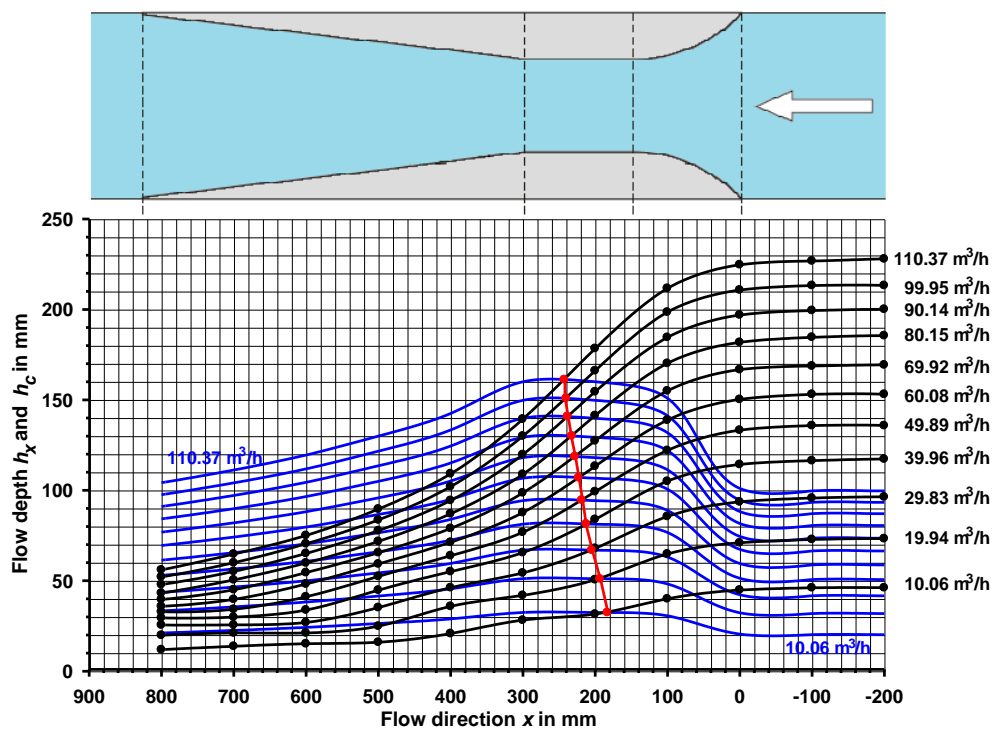


Figure 3. Water levels in the flow direction (profiles) for different flow rates

According to the data obtained (cf. Fig. 3), it can be asserted that in the classical Venturi flume with free (not flooded) fluid outflow, regardless of the flow rate, the flow passes a critical depth always within the gorge portion with parallel vertical walls. And the position of the critical section corresponds to the

middle of the gorge. Just a minor displacement of the critical depth range in one direction or another from the middle of the gorge depends on the flow parameters (on the flow rate passed), in particular, with an increase in the flow rate, the critical depth shifts slightly toward the diffuser. These studies, as well as studies carried out earlier [24], have shown that the flow inevitably passes the critical section within the gorge length of a multiple (3 to 5 times) less than in accordance with the regulations of the State Standard of Russia MI 2406-97. Thus, the length of the rectilinear gorge portion, recommended in MI 2406-97, is unreasonably overestimated that accordingly leads to unreasonable hydraulic losses in the entrance section of the Venturi flume. This distorts the hydraulics of the classic flume, according to which the hydraulic losses in its inlet section should be reduced to the utmost, and ideally reduced to zero. This is exactly what is observed in the studied channel [24], in which the hydraulic losses at the inlet section to the critical cross-section are negligible and lie in the range of accuracy of hydraulic studies. The authors believe that the Venturi open channel can be performed as a pressure flow gauge nozzle of the same name where the smooth confusor terminates with a gorge section, immediately followed by a smooth diffuser. In this case, the gorge will be the dividing cross-section, and hydraulic losses at the inlet to be virtually eliminated. The fact of formation of a flow with critical depth in a dividing cross-section is well known from hydraulics of structures [10, 27, 28]. However, this assumption requires experimental verification.

Since the flow with critical depth is physically unstable [10], the flow passes the critical section in a rapid fall with a sharp change of depth in the form of a waterfall. The fall of the depth below the critical one with formation of supercritical flow in the horizontal channel should cause subsequent flow braking, which is what happens. However, this is imperceptible for flows with a large discharge and, therefore, with a high inertia, but is very noticeable in the flows of low inertia with low flow rate. Explicit the flow braking we can be observed in the diffuser of the flume. Change in the flow velocities along the flow channel of the Venturi flume is shown in the graphs of Fig. 4 ($V = f(x)$) – Table 3).

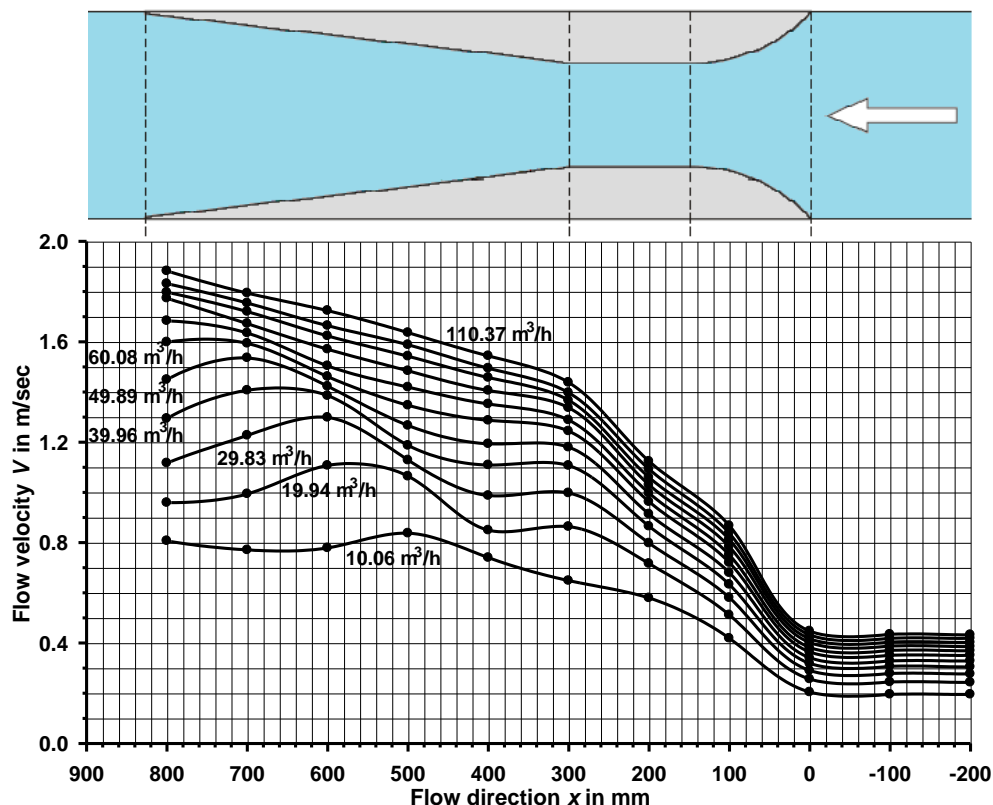


Figure 4. Flow velocities in the flow direction for different flow rates

In Figure 4 one can see significant fluctuations in the flow rates within the diffuser. This phenomenon is typical for the flows with low rates and is manifested in the wavy nature of the free surface. Such a surface can be seen in the photo on the left in Figure 1, made from the downstream side, where the entire section of the diffuser with surface waves are clearly visible. The phenomenon is associated with many factors, including flooding in the downstream h_0 and the possible formation of a hydraulic jump (cf. Fig. 2). However, this does not affect to the flow within the gorge section and, hence, does not affect to the main hydraulic characteristic of the Venturi flume: its discharge-head characteristic

$Q - h$. Thus, the Venturi flume remains a channel of critical depth regardless the flow nature within the diffuser.

Figure 5 shows the change in the Froude numbers in the direction of flow for all flow states being investigated ($Fr = f(x)$ – Table 4). As is well known [10] the Froude number shows the flow state: accordingly with $Fr < 1$, the flow is calm subcritical, with $Fr = 1$ – transient critical flow and with $Fr > 1$ – stormy supercritical flow. Therefore, in the figure, the red horizontal line shows the value $Fr = 1$, which, being a boundary state, separates the subcritical flow states from the supercritical ones. What lies beneath this red boundary line, refers to subcritical states, what is above – to supercritical states. Also red lines are allocated zone of critical depths in the gorge of the Venturi flume. Thus, the graphs in Figure 5 show the change of flow states lengthwise the classical (not flooded) Venturi flume: in the upstream portion of the flume and in its confusor (converging portion) the flow is calm subcritical, in the middle section of the flume gorge, regardless of the flow rate passed, the flow features the critical flow state and supercritical flow in the diffuser.

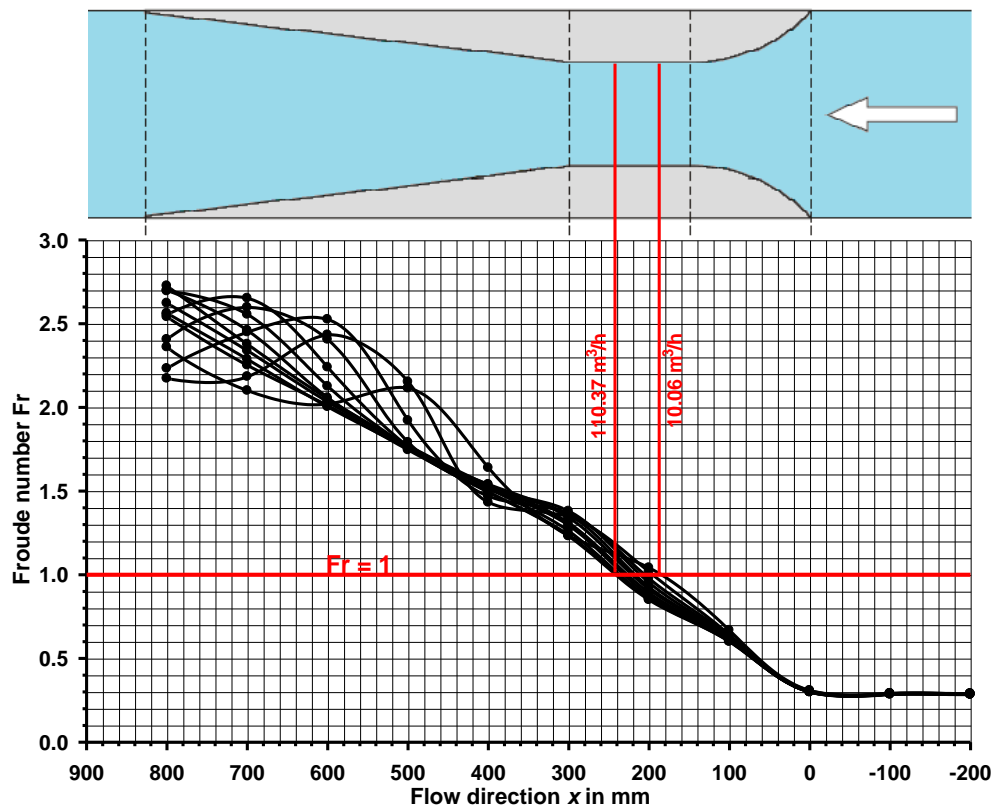


Figure 5. Froude numbers in the flow direction for different flow rates

According to the graphs in Figure 5 we also note important noteworthy features. Upstream of the inlet to the Venturi flume, the Froude numbers are always less than unity and have the same value ($Fr = C = \text{const}$) for all the flow rates passed through the flume. Hence, according to Eq. (2) the flow velocity in the upstream pool can be written as

$$V = C\sqrt{gh},$$

where h is upstream water level.

On the other side consistent with Eq. (1) we have

$$Q = VBh = CB\sqrt{gh}^{1.5},$$

where B is the width of the upstream channel.

Thus, the Froude number in the upstream pool, equal to $Fr = C = \text{const}$, can be considered as a flow coefficient of the classical Venturi channel. And this coefficient remains constant over the entire range of flow rates, which is an important property of the flow gauge.

A linear increase the Froude numbers along the length of the flow path is observed on the section from the entrance facet of the Venturi flume confusor to the exit from its rectilinear gorge. Here the flow

Zuikov A.L., Bakunjaeva V.V., Artemyeva T.V., Zhazha E.Yu. Flow states in the classical Venturi channel water gauge. *Magazine of Civil Engineering*. 2018. No. 2. Pp. 76–90. doi: 10.18720/MCE.78.6.

undergoes a drastic change from calm subcritical with Froude numbers less than unity ($Fr < 1$) to stormy supercritical with $Fr > 1$, bypassing critical state at $Fr = 1$ in the middle of the gorge. In the area of smooth linear growth of Froude numbers the hydraulic losses are negligible. The picture changes in the diffuser of the flume where the flow state stormy supercritical ($Fr > 1$), but the nature of changing the Froude numbers at low flow rates (for the investigated flume its less than $60 \text{ m}^3/\text{h}$ – cf. Fig. 4) does not follow linear law. Here the flow has a wavy free surface and is accompanied by significant hydraulic losses. The Venturi flume remains a classical channel of critical depth while the supercritical flow state in the diffuser is maintained or within its limits the supercritical flow by hydraulic jump passes into the subcritical one. But, if there is the subcritical flow in the gorge, then the Venturi flume loses the properties of a channel of critical depth and in flume is establishes the flooded mode of fluid outflow [3]. The methods of hydraulic calculation of the Venturi channel with a flooded outflow state are fundamentally different from those described in the State Standard of the Russian Federation MI 2406-97.

The Russian State Standard presents semi-empirical formula for use in hydraulic calculation of the full-capacity discharge of the classical Venturi flume

$$Q = \frac{2}{3} \sqrt{\frac{2}{3}} C_D C_V \sqrt{g b h^{1.5}}, \quad (3)$$

where C_D and C_V are empirical coefficients; b is width of gorge portion; h is upstream water level.

Empirical coefficient C_D takes into account the hydraulic losses on the section between the upstream pool and the gorge. In the document the coefficient is approximated by empirical dependence

$$C_D = \left(1 - 0.006 \frac{l}{b}\right) \cdot \left(1 - 0.003 \frac{l}{h}\right)^{1.5}, \quad (4)$$

where l is the length of the gorge portion of the Venturi flume.

In article [3], one of the authors of which was a developer of the State Standard of Russia MI 2406-97, this coefficient is determined by equality

$$C_D = \frac{1}{\sqrt{\alpha}} \left(1 - \frac{h_w}{E}\right)^{1.5}, \quad (5)$$

where α is the Coriolis (Saint-Venant) coefficient; h_w is hydraulic losses on the section between the upstream pool and gorge portion; E is unit energy of flow in the head race of the Venturi flume

$$E = h + \frac{\alpha V^2}{2g}.$$

According to empirical dependence (4), the coefficient C_D is less, and the hydraulic losses h_w are the greater, the longer is the gorge. It was noted above that the length of the gorge according to the regulations of the State Standard of Russia MI 2406-97 is unreasonably overestimated in the authors' opinion, at such a length, significant hydraulic losses are quite possible. But on the inlet section of the Venturi flume under study the hydraulic losses are negligible in comparison with the accuracy of hydraulic studies and engineering calculations, so they can be neglected by putting $h_w = 0$ in Eq. (5). In addition, in the incidence sections and all-round compression of the flow in the conditions of increasing velocities of turbulent flow, the boundary layer near the walls breaks down. As a result, the velocities are aligned over the flow cross-section, and the Coriolis coefficient α approaches the unity [10, 24, 27, 28, 30]. All of the above, according to Eq. (5), allows us to put $C_D = 1$.

Empirical coefficient C_V takes into account the relationship between the unit energy of flow and water level in upstream pool. The values of C_V coefficient are presented in Table 4 in the Appendix of the State Standard MI 2406-97 depending on $C_D b/B$ parameter. In article [3] the coefficient is written in explicit form

$$C_V = \left(\frac{E}{h}\right)^{1.5}$$

and the equation for its calculation is given

$$C_V^{2/3} = 1 + \frac{1}{2} \left(\frac{2}{3} \right)^3 C_V^2 \left(\frac{b}{B} \right)^2. \quad (6)$$

Further in article [3] it is stated that it is rather difficult to find the solution of equation (6) in general form relative to C_V , that is why the authors solve it obviously graphically or by iteration method. Having no objections against using any methods, including graphical and iteration ones, we nevertheless should like to note that this equation has rigorous analytical solution. Let us rewrite it in the form

$$C_V^2 - 2 \left(\frac{3}{2} \right)^3 \left(\frac{B}{b} \right)^2 C_V^{2/3} + 2 \left(\frac{3}{2} \right)^3 \left(\frac{B}{b} \right)^2 = 0. \quad (7)$$

Equating now $C_V^{2/3} = y$, we reduce Eq. (7) to classical cubic Cardano equation of $y^3 + py + q = 0$ form [32], in which

$$p = -2 \left(\frac{3}{2} \right)^3 \left(\frac{B}{b} \right)^2 < 0 \quad \text{and} \quad q = 2 \left(\frac{3}{2} \right)^3 \left(\frac{B}{b} \right)^2.$$

But if $p < 0$ and the sum

$$\left(\frac{p}{3} \right)^3 + \left(\frac{q}{2} \right)^2 = \left(- \left(\frac{3}{2} \right)^2 \left(\frac{B}{b} \right)^2 \right)^3 + \left(\left(\frac{3}{2} \right)^3 \left(\frac{B}{b} \right)^2 \right)^2 = \left(\frac{3}{2} \right)^6 \frac{B^4}{b^4} \left(1 - \frac{B^2}{b^2} \right)$$

is also less than zero, as $B > b$, the cubic Eq. (7) has a trigonometric solution with three real roots

$$\left(C_V^{2/3} \right)_{1,2,3} = 2 \sqrt{-\frac{p}{3}} \cos \left(\frac{\beta + 2n\pi}{3} \right) = 3 \frac{B}{b} \cos \left(\frac{\beta + 2n\pi}{3} \right), \quad (n = 0, 1, 2),$$

where

$$\cos(\beta) = -\frac{q}{2} \sqrt{-\left(\frac{3}{p} \right)^3} = -\frac{b}{B}.$$

The sought solution must satisfy the condition $1 \leq C_V^{2/3} \leq 1.5$, as $C_V^{2/3} = E/h = 1 + 0.5\alpha(\text{Fr})^2$, where the Froude number in the upstream pool for a calm subcritical flow is always less than unit ($\text{Fr} < 1$). The analysis showed that the solution of the cubic Eq. (7) is its third root corresponding to $n = 2$

$$C_V^{2/3} = 3 \frac{B}{b} \cos \left\{ \frac{1}{3} \left[\arccos \left(-\frac{b}{B} \right) + 4\pi \right] \right\} = 3 \frac{B}{b} \sin \left[\frac{1}{3} \arcsin \left(\frac{b}{B} \right) \right]$$

or

$$C_V = 3 \frac{B}{b} \sqrt{3 \frac{B}{b} \sin^{1.5} \left[\frac{1}{3} \arcsin \left(\frac{b}{B} \right) \right]}. \quad (8)$$

Substituting the values of the coefficients C_D and C_V in Eq. (3) we find

$$Q = 2 \sqrt{\frac{B}{b}} \sin^{1.5} \left[\frac{1}{3} \arcsin \left(\frac{b}{B} \right) \right] \sqrt{2g} B h^{1.5}.$$

This theoretical formula not containing empirical coefficients was obtained by us earlier in [24] and underwent experimental verification, which showed that the calculation errors were $\pm 1\%$. The formula can be rewritten in the traditional form for weirs

$$Q = mB \sqrt{2gh}^{1.5}, \quad (9)$$

where m is a theoretical flow coefficient of the classical Venturi flume water gauge

$$m = 2\sqrt{\frac{B}{b}} \sin^{1.5} \left[\frac{1}{3} \arcsin \left(\frac{b}{B} \right) \right]. \quad (10)$$

It can be seen that for $b/B = 1$ we have $m = 0.5^{0.5}$, and for $b/B \rightarrow 0$, respectively $m \rightarrow 0$. We note that the flow coefficient is proportional to the Froude number of upstream flow $m = 0.5^{0.5} Fr$.

The traditional form of the flow formula (9), in which the depth (h) and the width along the flow front (B) are measured in the same section, is more logical than the form of equation (3) from the State Standard of Russia MI 2406-97, in which the depth of the flow (h) is measured in the upstream pool, but its width (b) is measured in the gorge of the flume. Eq. (10) allows us to compare the full-capacity discharge of the Venturi channel with the capacity of other water gauges and select the best variant of water meter or the optimal ratio b/B .

The comparison of the experimental data with the results of calculations using the semi-empirical methodology of the State Standard of Russia MI 2406-97 and theoretical Eqs. (8), (9) and (10) are summarized in Table 5 and presented graphically in Figure 6. The first two columns of Table 5 show the experimental values (cf. Table 1) of the upstream water levels and the flow rates passed through the flume. The values of the upstream water levels (or flow depths) h are measured in the cross-section of the hydraulic flume HM 162 at a distance $x = -200$ mm before the entrance edge of the confusor of the Venturi channel. The experimental values of flow rates in Table 5, in Figure 6 and further in the text are denoted as Q_0 , in contrast to the calculated values of Q . The next four columns of Table 5 show the calculated values: of coefficients C_D (Eq. (4)), obtained as per the regulations of the State Standard of Russia MI 2406-97, of parameters $C_D \cdot b/B$, of coefficients C_V , which are presented in Table 4 in the Appendix of Russian State Standard MI 2406-97, and of flow rates Q . The following column shows the deviations of the calculated values of flow rates Q from their actual values Q_0

$$\Delta = \frac{Q - Q_0}{Q_0} = \frac{Q}{Q_0} - 1; \quad (11)$$

underneath Table 5 shows the value of the root-mean-square error of the calculation method as a whole

$$\sigma = \sqrt{\frac{1}{k} \sum_{j=1}^k \Delta^2}, \quad (12)$$

where k is the size of the sample, $k = 11$.

The last four columns of Table 5 give the calculated theoretical values: of coefficients C_V (Eq. (8)), of coefficients m (Eq. (10)), of full-capacity discharges of the Venturi channel Q (Eq. (9)) and of deviations Δ (Eq. (11)) of flow rates Q from their actual values Q_0 . Underneath Table 5 shows the value of the root-mean-square error of the theoretical calculation method σ (Eq. (12)).

The following dimensions of the Venturi flume under study have been used in the calculations (cf. text above and Fig. 2): width and length of the gorge portion, respectively $b = 153$ mm and $l = 150$ mm, width of the cross-section upstream channel $B = 311$ mm.

Table 5. Full-Capacity Discharge of the Venturi Flume

Initial data		Russian State Standard MI 2406-97					Theoretical Eqs. (8), (9) and (10)				
h , mm	Q_0 , m ³ /h	C_D	$C_D \cdot b/B$	C_V	Q , m ³ /h	Δ	C_V	m	Q , m ³ /h	Δ	
227.98	110.37	0.9912	0.4876	1.0600	107.40	-0.02688	1.0612	0.20094	108.47	-0.01717	
213.32	99.95	0.9910	0.4875	1.0600	97.19	-0.02765	1.0612	0.20094	98.18	-0.01772	
200.12	90.14	0.9908	0.4874	1.0600	88.29	-0.02051	1.0612	0.20094	89.21	-0.01027	
185.58	80.15	0.9905	0.4873	1.0599	78.82	-0.01667	1.0612	0.20094	79.67	-0.00610	
169.29	69.92	0.9902	0.4871	1.0599	68.64	-0.01823	1.0612	0.20094	69.41	-0.00728	
153.08	60.08	0.9897	0.4869	1.0598	59.00	-0.01807	1.0612	0.20094	59.68	-0.00664	
135.77	49.89	0.9892	0.4866	1.0598	49.25	-0.01293	1.0612	0.20094	49.85	-0.00081	
117.27	39.96	0.9884	0.4863	1.0597	39.50	-0.01157	1.0612	0.20094	40.02	0.00146	
96.31	29.83	0.9872	0.4856	1.0595	29.35	-0.01589	1.0612	0.20094	29.78	-0.00150	
73.26	19.94	0.9850	0.4846	1.0592	19.43	-0.02573	1.0612	0.20094	19.76	-0.00901	
46.10	10.06	0.9796	0.4819	1.0585	9.64	-0.04242	1.0612	0.20094	9.86	-0.01997	
						$\sigma = 0.02308$					$\sigma = 0.01101$

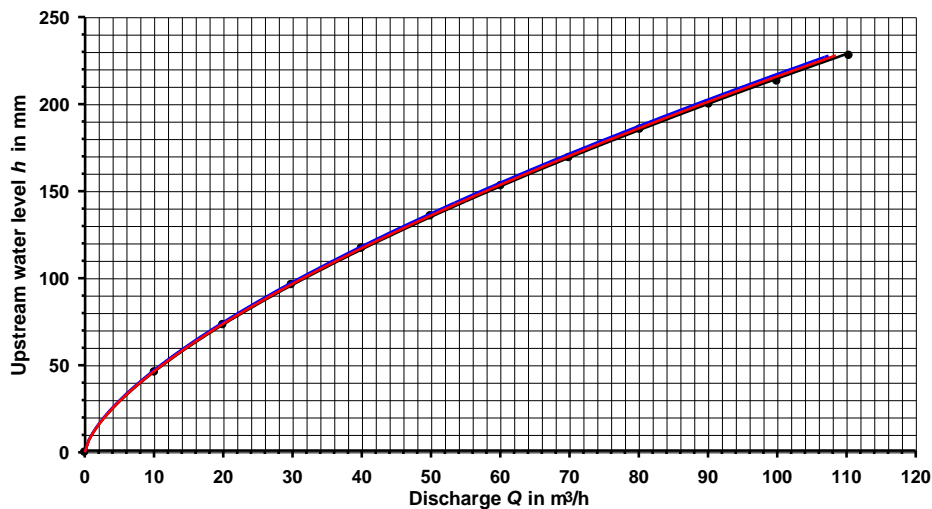


Figure 6. Discharge-head characteristics of the Venturi channel: the black points and line $Q_0 - h$ are drawn from the experimental data, the blue line $Q - h$ is calculated by the method of Russian State Standard MI 2406-97 and the red line $Q - h$ is calculated from Eqs. (9) and (10)

The obtained results show that the semi-empirical method for calculating the full-capacity discharge of the Venturi channel water gauge by formula (3) from the State Standard of Russia MI 2406-97 has a relative error exceeding 2 % ($\sigma = 0.02308$ – see Table 5). Moreover, according to the received data, this error is systematic, by which the calculated values of flow rates Q are always less than their actual values Q_0 . The same was noted in a previously published paper [24]. Underestimation of the volumes of water resources consumed and wastewater discharge is undoubtedly beneficial directly to water users, but it is not beneficial to the State and population of the country as a whole. Therefore, the situation when the State Standard has a systematic error cannot be considered admissible. The analysis allows us to conclude that this systematic error is associated with overstating the hydraulic losses in the confuser and gorge area of the Venturi channel to the critical cross-section. It is established that the theoretical solution (Eqs. (9) and (10)) obtained that does not have empirical coefficients provides a higher accuracy of the received hydrometric information in relation to the State Standard, and it has a relative error of about $\pm 1\%$ ($\sigma = 0.01101$ – cf. Table 5 and [24]). This error is not systematic. Eqs. (9) and (10) work equally well at high and low flow rates, therefore the limitation in the State Standard of Russia MI 2406-97, which regulates the minimum water level in the upstream pool $h_{\min} = 0.1$ m, can be removed. On the whole, the studies performed make it possible to conclude that the theoretical method of hydraulic calculation of the classical Venturi channel water gauge, which meets the modern requirements of engineering practice, can be recommended for inclusion in the new edition of the State Standard of the Russian Federation MI 2406-97.

4. Conclusions

1. The use of hi-tech certified measurement equipments on the basis of digital technologies allows us to obtain empirical information of high accuracy, the analysis of which allows us to clarify, supplement or review the recommendations of existing normative documents, to prepare them in a new edition, partially or completely excluding empirical coefficients. This is especially true for the State hydrometric services, which take into account and control the use of water resources and discharge of waste water into the environment.

2. In the classical Venturi channel with free fluid outflow, regardless of the flow rate, the flow passes the cross-section with critical depth always within a short gorge with parallel vertical walls. It is established that the length of the gorge can be prescribed 3 to 5 times less than specified in the State Standard MI 2406-97.

3. In the upstream pool of the Venturi channel and in its confuser part the flow is calm subcritical with Froude numbers $Fr < 1$, in the middle section of the gorge the flow is critical ($Fr = 1$), in the diffuser the flow is stormy supercritical ($Fr > 1$). The Froude number in the upstream pool of the classical Venturi channel is directly proportional to its flow coefficient $m = 0.5^{0.5} Fr$ and remains constant over the entire range of flow rates, which is an important property of the flow gauge. The flow with critical depth is physically unstable, so the flow passes the critical section in a rapid fall with a sharp change of depth in the form of a waterfall. As long as in the diffuser the flow state is supercritical or within it the flow is transiting from supercritical to subcritical in the hydraulic jump form, the Venturi flume remains a classical

channel of the critical depth. If the subcritical flow is set along the entire length of the gorge, then the Venturi flume loses the properties of a channel of critical depth and the flooded mode of fluid outflow establishes therein.

4. On the section from the entrance facet of the confusor of the classical Venturi channel to the exit from its rectilinear gorge a linear increase in the Froude numbers is observed in the flow direction. In this area of smooth linear growth of the Froude numbers the hydraulic losses are negligible and lie in the range of accuracy of the hydraulic studies. Therefore, coefficient C_D , taking into account the hydraulic losses in the area between the upstream pool and the critical cross-section of the gorge of the Venturi channel, is equal to unity.

5. Coefficient C_V , which takes into account the ratio of the specific energy of the flow in the upstream pool to the water level in it E/h , depends only on the ratio of the width of the gorge of the Venturi flume to the width of the upstream channel b/B and is determined by Eq. (8), but does not depend on parameter $C_D \cdot b/B$, as stated in Standard MI 2406-97. The coefficient varies from $C_V \rightarrow 1$ at $b/B \rightarrow 0$ to $C_V = 1.5^{1.5}$ at $b/B = 1$.

6. It was established that, using the Russian State Standard MI 2406-97, the calculation of the full-capacity discharge of the classical Venturi channel water gauge always give the understated values of the design discharge relative to the values of the discharge which in fact passed through the channel. The systematic error of calculations in accordance with State Standard MI 2406-97 is more than -2% .

7. As a result of the research, the method of hydraulic calculation of the classical Venturi channel was obtained that meets the to-date requirements of engineering practice. This method is based on theoretical formula (10) for calculating flow coefficient m . Formula (10) is free from empirical coefficients. It is established that the flow coefficient of the classical Venturi channel varies from $m \rightarrow 0$ at $b/B \rightarrow 0$ to $m = 0.5^{0.5}$ at $b/B = 1$.

8. When specifying and revising the State Standard MI 2406-97, it is recommended to include in the new edition the theoretical method of hydraulic calculation of the flow rate of the classical Venturi channel water gauge based on Eqs. (9) and (10), taking the relative error of the theoretical method equal to $\pm 1\%$.

5. Acknowledgments

The authors are grateful to PhD, Director of "PNP SIGNUR" Ltd. Michail Shafranovsky for his suggestion to conduct the research reported here. "PNP SIGNUR" Ltd. has been sponsoring the manuscript from the project dated 10.06.2016 No. K.398-16 "Conducting tests of ultrasonic flow meter EHO-R-03 on Venturi flume".

References

1. Sadchikova G.M., Mamolina A.P. Osobennosti izmerenija rashoda zhidkostej v otkrytyh kanalah [Features of measuring the flow of liquids in open channels]. *Materialy IX Mezhdunarodnoj nauchno-prakticheskoy konferencii "Sovremennye instrumental'nye sistemy, informacionnye tehnologii i innovacii"* [Proceedings of the IX international scientific and practical conference "Modern instrument systems, information technologies and innovations"]. Kursk. Southwestern State University, 2012. Pp. 191–193. (rus)
2. Vjaz'min U.A., Korneev V.N., Loitsker O.D., Mordjasov M.A., Nikitin V.I., Shafranovsky M.N. Novaja redakcija metodiki izmerenij rashoda i ob'ema zhidkosti v beznapornyh vodovodah MI 2220-13 [New edition of the measurement procedure for flow and volume of liquid in non-pressure water conduits MI 2220-13]. *Water Supply and Sanitary Technique*. 2013. No. 8. Pp. 76–78. (rus)
3. Yegorov N.L., Loitsker O.D., Shafranovsky M.N. Izmerenie rashoda zhidkosti s pomoshh'ju lotkov Venturi pri svobodnom i zatoplennom istechenii [Measuring liquid flow rate with Venturi flume at free and submerged flow]. *Water Supply and Sanitary Technique*. 2016. No. 1. Pp. 66–71. (rus)
4. Filippov V.N., Zinov'ev A.P., Ryzhov G.I., Zinov'ev S.A., Ryzhova S.A. *Oborudovanie i tehnologii ochistki stochnyh vod, primery raschetov na JeVM* [Equipment and technologies for wastewater treatment, examples of

Литература

1. Садчикова Г.М., Мамолина А.П. Особенности измерения расхода жидкостей в открытых каналах // *Материалы IX-ой Международной научно-практической конференции «Современные инструментальные системы, информационные технологии и инновации»*. Курск. Юго-Западный государственный университет. 2012. С. 191–193.
2. Вязьмин Ю.А., Корнеев В.Н., Лойцкер О.Д., Мордясов М.А., Никитин В.И., Шаfranовский М.Н. Новая редакция методики измерений расхода и объема жидкости в безнапорных водоводах МИ 2220-13 // *Водоснабжение и санитарная техника*. 2013. № 8. С. 76–78.
3. Егоров Н.Л., Лойцкер О.Д., Шаfranовский М.Н. Измерение расхода жидкости с помощью лотков Вентури при свободном и затопленном истечении // *Водоснабжение и санитарная техника*. 2016. № 1. С. 66–71.
4. Филиппов В.Н., Зиновьев А.П., Рыжов Г.И., Зиновьев С.А., Рыжова С.А. Оборудование и технологии очистки сточных вод, примеры расчетов на ЭВМ. Уфа: Издательство УГНТУ, 2003. 300 с.
5. Fonseca P., Marques N. Uncertainty estimation and calibration of operational flumes. STAR Global Conference 2017. Berlin. 2017. 20 p.
6. Gill T., Niblack M. Flow Measurement with Long-Throated Flumes under Uncertain Submergence. Venturi Flume

Зуйков А.Л., Бакуняева В.В., Артемьева Т.В., Жажа Е.Ю. Режимы течения в классическом водомерном канале Вентури // *Инженерно-строительный журнал*. 2018. № 2(78). С. 76–90.

- computer calculations]. Ufa: USPTU, 2003. 300 p. (rus)
5. Fonseca P., Marques N. Uncertainty estimation and calibration of operational flumes. *STAR Global Conference 2017*. Berlin. 2017. 20 p.
 6. Gill T., Niblack M. *Flow Measurement with Long-Throated Flumes under Uncertain Submergence. Venturi Flume Report*. U.S. Department of the Interior Bureau of Reclamation. Yuma Area Office. Yuma, AZ, 2009. 14 p.
 7. Hager W. H. *Wastewater Hydraulics. Theory and Practice*. Springer-Verlag Berlin Heidelberg. Berlin, 2010. 652 p.
 8. Samani Z., Magallanez H. Simple flume for flow measurement in open channel. *Journal of Irrigation and Drainage Engineering*. 2000. Vol. 126(2). Pp. 127–129.
 9. Surhone L.M., Tennoe M.T. Henssonow S.F. *Venturi Flume*. Betascript Publishing. 2011. 80 p.
 10. Cone M.V. The Venturi Flume. *Journal of Agricultural Research*. 1917. Vol. IX. № 4. Pp. 115–129.
 11. Castro-Orgaz O. Hydraulic design of Khafagi flumes. *Journal of Hydraulic Research*. 2008. Vol. 46. Pp. 691–698.
 12. Castro-Orgaz O., Chanson H. Near-critical free-surface flows: Real fluid flow analysis. *Environmental Fluid Mechanics*. 2011. Vol. 11. Pp. 499–516.
 13. Chanson H. A discussion to “Explicit equations for critical depth in open channels with complex compound cross-sections”. *Flow Measurement and Instrumentation*. 2013. Vol. 29. Pp. 65–66.
 14. Dabrowski W., Polak U. Flow rate measurement by flumes. *Fourteenth International Water Technology Conference, IWTC 14 2010*. Cairo. 2010. 13 p.
 15. Dufresne M., Vazquez J. Head-discharge relationship of Venturi flumes: From long to short throats. *Journal of Hydraulic Research*. 2013. Vol. 51. Pp. 465–468.
 16. Farsiroto E.D., Kotsopoulos S.I. Free surface flow over river bottom sill: Experimental and numerical study. *Environmental Processes*. 2015. Vol. 2. Pp. 133–139.
 17. Gill T., Einhellig R. Submerged Venturi flume. *Proceedings of SCADA and Related Technologies for Irrigati – A USCID Water Management Conference*. Vancouver. WA. 2005. Pp. 281–290.
 18. Howes D.J., Burt C.M., Sanders B.F. Subcritical contraction for improved open-channel flow measurement accuracy with an upward-looking ADVN. *Journal of Irrigation and Drainage Engineering*. 2010. Vol. 136. Pp. 617–626.
 19. Igo S.W., N'wuitcha K., Palm K., Mihaescu L., Bathiébo D.J. Numerical simulation of turbulent forced convection in a Venturi channel with fully developed flow at the inlet. *Advances in Applied Science Research*. 2014. Vol. 5(2). Pp. 359–367.
 20. Maghrebi M.F., Ball J.E. New method for estimation of discharge. *Journal of Hydraulic Engineering*. 2006. Vol. 132. No. 10. October. Pp. 1044–1051.
 21. Raskar V.B. New technique for measurement of discharge in open channel flow. *International Journal for Science and Research in Technology*. Vol. 3. No. 2. February. 2017. Pp. 18–21.
 22. Yegorov N.L., Loitsker O.D. Vlijanie umen'shenija dliny podvodjashhego uchastka lotka Venturi na pogreshnost' izmerenij rashoda zhidkosti [Effect of reducing the length of the inlet section of the Venturi tray on the measurement error of the liquid flow rate]. *Water Supply and Sanitary Technique*. 2012. No. 6. Pp. 70–74. (rus)
 23. Zerihun Y.T. A Numerical study on curvilinear free surface flows in Venturi flumes. *Fluids*. 2016. No. 1(3). 21.
 24. Zuikov A.L., Bakunjaeva V.V. Analiticheskij metod gidravlicheskogo rascheta rashodomernogo kanala Venturi [The analytical method of hydraulic calculation of the flow meter Venturi channel]. *Hydrotechnical Construction*. 2017. No. 9. Pp. 47–56. (rus)
 25. Filippov E.G., Brakeni A. Ispol'zovanie vodoslivo s porogom treugol'nogo profila dlja izmerenija rashodov vody Report. U.S. Department of the Interior Bureau of Reclamation. Yuma Area Office. Yuma, AZ, 2009. 14 p.
 7. Hager W.H. *Wastewater Hydraulics. Theory and Practice*. Springer-Verlag Berlin Heidelberg. Berlin, 2010. 652 p.
 8. Samani Z., Magallanez H. Simple flume for flow measurement in open channel // *Journal of Irrigation and Drainage Engineering*. 2000. Vol. 126(2). Pp. 127–129.
 9. Surhone L.M., Tennoe M.T. Henssonow S.F. *Venturi Flume*. Betascript Publishing. 2011. 80 p.
 10. Cone M.V. The Venturi Flume // *Journal of Agricultural Research*. 1917. Vol. IX. № 4. Pp. 115–129.
 11. Castro-Orgaz O. Hydraulic design of Khafagi flumes // *Journal of Hydraulic Research*. 2008. Vol. 46. Pp. 691–698.
 12. Castro-Orgaz O., Chanson H. Near-critical free-surface flows: Real fluid flow analysis // *Environmental Fluid Mechanics*. 2011. Vol. 11. Pp. 499–516.
 13. Chanson H. A discussion to “Explicit equations for critical depth in open channels with complex compound cross-sections” // *Flow Measurement and Instrumentation*. 2013. Vol. 29. Pp. 65–66.
 14. Dabrowski W., Polak U. Flow rate measurement by flumes // *Fourteenth International Water Technology Conference, IWTC 14 2010*. Cairo. 2010. 13 p.
 15. Dufresne M., Vazquez J. Head-discharge relationship of Venturi flumes: From long to short throats // *Journal of Hydraulic Research*. 2013. Vol. 51. Pp. 465–468.
 16. Farsiroto E.D., Kotsopoulos S.I. Free surface flow over river bottom sill: Experimental and numerical study // *Environmental Processes*. 2015. Vol. 2. Pp. 133–139.
 17. Gill T., Einhellig R. Submerged Venturi flume // *Proceedings of SCADA and Related Technologies for Irrigati – A USCID Water Management Conference*. Vancouver. WA. 2005. Pp. 281–290.
 18. Howes D.J., Burt C.M., Sanders B.F. Subcritical contraction for improved open-channel flow measurement accuracy with an upward-looking ADVN // *Journal of Irrigation and Drainage Engineering*. 2010. Vol. 136. Pp. 617–626.
 19. Igo S.W., N'wuitcha K., Palm K., Mihaescu L., Bathiébo D.J. Numerical simulation of turbulent forced convection in a Venturi channel with fully developed flow at the inlet // *Advances in Applied Science Research*. 2014. Vol. 5(2). Pp. 359–367.
 20. Maghrebi M.F., Ball J.E. New method for estimation of discharge // *Journal of Hydraulic Engineering*. 2006. Vol. 132. № 10. October. Pp. 1044–1051.
 21. Raskar V.B. New technique for measurement of discharge in open channel flow // *International Journal for Science and Research in Technology*. 2017. Vol. 3. № 2. February. Pp. 18–21.
 22. Егоров Н.Л., Лойцкер О.Д. Влияние уменьшения длины подводящего участка лотка Вентури на погрешность измерений расхода жидкости // *Водоснабжение и санитарная техника*. 2012. № 6. С. 70–74.
 23. Zerihun Y.T. A Numerical study on curvilinear free surface flows in Venturi flumes // *Fluids*. 2016. № 1(3). 21.
 24. Зуйков А.Л., Бакуняева В.В. Аналитический метод гидравлического расчета расходомерного канала Вентури // *Гидротехническое строительство*. 2017. № 9. С. 47–56.
 25. Филиппов Е.Г., Бракени А. Использование водосливов с порогом треугольного профиля для измерения расходов воды в открытых руслах и каналах // *Проблемы устойчивого развития мелиорации и рационального природопользования: Материалы юбилейной международной научно-практической конференции (Костяковские чтения)*. М.: ВНИИА, 2007. Том 2. С. 338–343.
 26. Лойцкер О. Д. Гидравлический расчет измерительных водосливов с порогом треугольного профиля // *Водоснабжение и санитарная техника*. 2014. № 3.

- v otkrytyh ruslah i kanalah [Use of weirs with threshold of triangular profile for measurement of discharges of water in open streams and conduits]. *Problemy ustojchivogo razvitiya melioracii i racional'nogo prirodopol'zovanija. Materialy jubilejnoy mezhdunarodnoj nauchno-prakticheskoy konferencii (Kostjakovskie chtenija)* [Problems of stable development of reclamation and rational resource management. Proceedings of international scientific-practical jubilee conference (Kostyakov session)]. Moscow: VNIIA, 2007. Vol. 2. Pp. 338–343. (rus)
26. Loitsker O.D. Gidravlicheskiy raschet izmeritelnykh vodostivov s porogom treugolnogo profilya [Hydraulic design of measuring weirs with a triangular profile chute]. *Water Supply and Sanitary Technique*. 2014. No. 3. Pp. 70–73. (rus)
 27. Zuikov A.L. Hydraulics of the classical Crump weir water gauge. *Power Technology and Engineering*. 2017. Vol. 30. No. 6. Pp. 611–619.
 28. Зуиков А.Л. Особенности гидравлики классического водослива-водомера Крампа // Гидротехническое строительство. 2016. № 10. С. 50–59.
 29. Linke U. HM 162. *Experimental Flume 309x450mm*. G.U.N.T Gerätebau GmbH. Hamburg, 2013. 52 p.
 30. Kellow M. HM 162.51. *Venturi Flume*. G.U.N.T Gerätebau GmbH. Hamburg, 2013. 59 p.
 31. Типовой проект 902-9-44.87. Водоизмерительные лотки Вентури. Госстрой СССР. Введен в действие 22.10.1987. Дата обновления 05.05.2017. Альбом I. 31 с.
 32. Korn G.A., Korn T.M. *Mathematical Handbook for Scientists and Engineers: Definitions, Theorems and Formulas for Reference and Review*. Publisher Dover Publications. 2000. 1151 p.

Andrey Zuikov,
+7(499)374-38-75; zuikov54@mail.ru

Viktorija Bakunjaeva,
+7(906)720-63-70; vbakunyaeva@yandex.ru

Tatiana Artemyeva,
+7(916)3970809; ArtemyevaTV@yandex.ru

Elena Zhazha,
+7(903)7416327; эл. почта: l-jaja@mail.ru

Андрей Львович Зуиков,
+7(499)374-38-75; эл. почта: zuikov54@mail.ru

Виктория Владимировна Бакуняева,
+7(906)720-63-70;
эл. почта: vbakunyaeva@yandex.ru

Татьяна Валентиновна Артемьева,
+7(916)3970809; эл. почта:
ArtemyevaTV@yandex.ru

Елена Юрьевна Жажа,
+7(903)7416327; эл. почта: l-jaja@mail.ru

© Zuikov A.L., Bakunjaeva V.V., Artemyeva T.V., Zhazha E.Yu., 2018

doi: 10.18720/MCE.78.7

Method of forecasting the effectiveness of cationic bitumen emulsions

Метод прогнозирования эффективности катионных битумных эмульсий

S. Yu. Shekhovtsova,

National Research Moscow State Civil Engineering University, Moscow, Russia

A. V. Korotkov,

LLC GAZPROMNEFT - BITUMEN MATERIALS, St. Petersburg, Russia

M. A. Vysotskaya,

V.G. Shukhov Belgorod State Technological University, Belgorod, Russia

Канд. техн. наук, ассистент

С.Ю. Шеховцова,

Национальный исследовательский Московский государственный строительный университет, г. Москва, Россия

начальник управления разработки технологий и контроля качества

А.В. Коротков,

ООО "Газпромнефть-битумные материалы", г. Санкт-Петербург, Россия

канд. техн. наук, доцент М.А. Высоцкая,

Белгородский государственный технологический университет

им. В.Г. Шухова, г. Белгород, Россия

Key words: bitumen emulsion; emulsifier; surface-active substances; surface tension; interfaces

Ключевые слова: битумная эмульсия; эмульгатор; поверхностно-активные вещества; поверхностное натяжение; межфазные границы

Abstract. Approbation of the procedure for predicting the production of effective bitumen emulsions at the stage of water phase preparation and also predicting the compatibility of the mineral aggregate and the surface-active substance used to emulsify the bitumen was carried out. As criteria characterizing the optimal composition of water phases, the following indicators were proposed: the surface tension of the water solutions under investigation and the wetting contact angle. The study of the dynamics of changes in the properties of the water phase and surface tension at the interface of the "water phase—mineral substrate" system during the emulsifier concentration change made it possible to establish that in the range of the emulsifier content for the bitumen emulsion recommended by the manufacturer, there are ineffective concentrations, the effect and variability of which is manifested in case of contact with mineral materials of different nature. The possibility of early prediction of the compatibility of the emulsifier used to prepare the bitumen emulsion and the mineral material, which will interact with the production emulsified binder, was evaluated.

Аннотация. Проведена апробация метода прогнозирования получения эффективных битумных эмульсий на стадии подготовки водной фазы, а также прогнозирования совместимости минерального заполнителя и поверхностно-активного вещества, используемого для эмульгирования битума. В качестве критериев, характеризующих оптимальные составы водных фаз, предложены показатели: поверхностного натяжения исследуемых водных растворов и краевого угла смачивания. Изучение динамики изменения свойств водной фазы и поверхностного натяжения на границе раздела системы «водная фаза—минеральная подложка» при изменении в ней концентрации эмульгатора, позволило установить, что в рекомендуемом производителем интервале содержания эмульгатора для битумной эмульсии, существуют неэффективные концентрации, действие и изменчивость которых проявляется при контакте с минеральными материалами различной природы. Произведена оценка возможности раннего прогнозирования совместимости эмульгатора, используемого для приготовления битумной эмульсии и минерального материала, который будет взаимодействовать с производственным эмульгированным вяжущим.

1. Introduction

The present moment can be attributed to the era of high-tech and economical technical solutions in virtually all segments of the economy. These factors determine the increased interest of various fields in emulsions – dispersed heterogeneous colloidal systems. In road construction, as well as in the production of protective coatings and adhesives in the construction industry, the bitumen emulsion is also a popular and relevant type of binder. This is due to the fact that emulsions combine many advantages.

However, it is a heterogeneous – inhomogeneous system, consisting of heterogeneous phases, differing in composition and properties, and separated by the interface. Therefore, it is difficult to develop and produce an emulsion, regardless of the field of its application, which consists in the correct choice of surface-active substances, as well as their concentrations to exclude or reduce the destruction processes and increase the kinetic stability of the entire system. As practice shows, the calculation of the amount of surface-active substances that is necessary for the stabilization of heterogeneous systems is often carried out experimentally without justification from the point of view of the colloidal system.

In the road construction segment, bitumen road cationic emulsions (BRCE) are the most common ones; they most often refer to the type of oil-in-water emulsions when bitumen is dispersed in the water phase [1–4]. To ensure this process, it is necessary to equalize the surface tension of two phases – bitumen and water. For this purpose, a certain amount of emulsifier is introduced into the water phase. It must be taken into account that the properties of colloidal dispersions depend significantly on the nature of the interface between the dispersion phase and the dispersed medium. Despite the large surface-to-volume ratio, the amount of surface-active substances required for a significant change in the volumetric properties of colloidal disperse systems is very small [5]. In this case, each emulsifier has a minimum limit of its concentration, at which emulsification is possible. A large amount of surface-active substances is an undesirable factor contributing to a slowing down of the emulsion breakdown rate – the time for which the adhesion-cohesive bonds will reach the level necessary for the formation of the composition structure, and also leading to an increase in the cost of production and the total cost of production [6].

These factors contribute to the fact that at the present time, when developing the formulation of bitumen emulsions and determining the optimum content of surface-active substances in them, test batches of emulsified binder with various surface-active substance concentrations are prepared. With the subsequent study of the main processing and operational characteristics of the prepared disperse systems. At this, such selection is long, energy-intensive and resource-intensive, and also does not take into account the specifics of a particular type of the aggregate that will contact the emulsion. The importance of the compatibility of the mineral substrate with the bitumen emulsion was noted in the study [7], where it is proposed to optimize the choice of the emulsifier in accordance with the type of mineral material used in the composition in order to achieve the maximum efficiency of preparation and use of the bitumen emulsion. The efficiency is evaluated on the system "stone material-bitumen emulsion".

Based on the foregoing, the goal of scientific research was formulated, it consists in developing the procedure for predicting the efficiency of cationic bitumen emulsions at the early stage of their selection. To do this, it is necessary to solve the problem of identifying algorithms for determining the effective content of the emulsifier in the water phase, to ensure the production of stable cationic bitumen emulsions, and also to predict the compatibility of the mineral aggregate and surface-active substances used to emulsify the bitumen.

2. Methods

In this study, the procedure is tested for determining the effective content of an emulsifier in the water phase for the preparation of stable cationic bitumen emulsions, and also predicting the compatibility of the mineral aggregate and surface-active substances used for the emulsification of bitumen. The following indicators were taken as criteria characterizing the optimum concentrations of emulsifiers in the water phase: surface tension of the solutions under study and their wetting contact angle for substrates of red granite and white marble.

The proposed method is based on the study of the dynamics of changes in the properties of the water phase and the interface of the "water phase – mineral substrate" when its surface-active substance concentration changes.

The choice of substrate type is explained by the opposite of their chemical properties. Granite refers to acid rocks, and marble to basic ones. In this connection, it can be assumed that the manifestation of the properties of the water phase upon contact with these mineral materials will be different. The substrates of the rocks used were previously prepared: sawn to plates, washed, dried, ground, then washed again and dried.

The surface tension of the water phases was studied on the Lauda TVT 2 instrument, which allows to determine the dynamic parameters of the surface and interfacial tension of liquids by the drop volume method [8]. The method is based on an accurate measurement of the volume of droplets when they fall from the dosing capillary. The value of surface or interfacial tension is calculated on the basis of the volume of droplets, depending on whether droplets form in the air, or in another, immiscible phase (oil). Measuring of droplets accurate to microliter provides high accuracy and reproducibility of measurement results.

To study the wetting contact angle, there were used droplets (Fig. 1), which were obtained with a digital camera. The wetting angle was calculated using the droplet height and width values obtained experimentally [9].

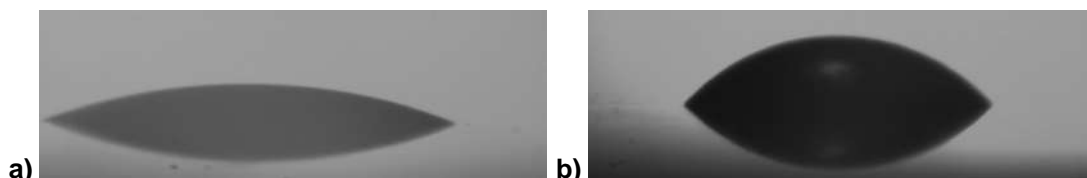


Figure 1 Form of the water phase droplet with the REDICOTE EM-44 emulsifier on the substrate of a) marble, b) granite

The contact angle of wetting is a characteristic of the hydrophilicity or hydrophobicity of the surface, and also serves as a characteristic of the adsorption that occurs when the water phase and the mineral substrate come into contact. Such contact, in some cases, can be accompanied by chemical interaction of liquids and minerals, ion exchange, and also dissolution and electrokinetic phenomena [5].

3. Results and Discussion

The experiment was performed on cationic emulsifiers produced by AkzoNobel: REDICOTE E-11 and REDICOTE EM-44. The choice of additives is justified by the difference in the mechanism of their action on the emulsion. In accordance with the manufacturer's product specification, REDICOTE EM-44 is a liquid emulsifier for bitumen cationic road emulsions with a rapid breakdown rate (EBKD B), which also acts as an adhesive additive. The recommended concentration for quick-breaking emulsions is 0.12–0.25 %, REDICOTE E-11 is a liquid emulsifier for bitumen road cationic emulsions with a slow decay rate (EBDK M), its recommended concentration in the water phase is 0.6–1.5 %. The basis for the production of REDICOTE additives is polyamines [4, 10–12].

The laboratory studies performed earlier [13] made it possible to determine the serrated profile dependencies of the surface tension and the wetting contact angle of the water phase on the emulsifier concentration in its composition. It was assumed that in the manufacturer's recommended range of emulsifier content for the bitumen emulsion, there are inefficient concentrations, the effect and variability of which is manifested by contact with mineral materials of different nature.

To confirm or refute the suggested hypothesis, there were chosen a number of concentrations of emulsifiers in the water phase with a minimum surface tension for industrial tests. This factor should lead to the formation of effective adsorption layers stabilizing the bitumen emulsion.

The composition and properties of water phases prepared in industrial conditions are shown in Table 1.

Table 1. Compositions and properties of the water phase

Emulsifier type							
REDICOTE E-11				REDICOTE EM-44			
No of composition	content, %		PH of the water phase	No of composition	content, %		PH of the water phase
	emulsifier	acid			emulsifier	acid	
1	0.15	0.07	2.21	9	0.10	0.13	2.08
2	0.20	0.07	2.19	10	0.15	0.16	2.08
3	0.25	0.08	2.14	11	0.25	0.20	2.05
4	0.60	0.10	2.04	12	0.30	0.21	2.07
5	0.80	0.08	2.16	13	0.40	0.48	2.05
6	1.01	0.08	2.15	14	0.50	0.60	2.00
7	1.30	0.08	2.10	15	0.60	0.69	1.90
8	1.51	0.09	2.19	16	0.80	0.91	1.93

Note: Compositions No. 1–12 are prepared using hydrochloric acid (HCl), formulations No. 13–16 using orthophosphoric acid (H₃PO₄)

Шеховцова С.Ю., Коротков А.В., Высоцкая М.А. Метод прогнозирования эффективности катионных битумных эмульсий // Инженерно-строительный журнал. 2018. № 2(78). С. 91–100.

To obtain stable bitumen emulsions, the pH of the water phase should be in the range of 1.5–2.5. The achievement of the specified parameters was carried out by varying the acid: orthophosphoric and hydrochloric one, depending on the emulsion obtained (slow-breaking or quick-breaking emulsion).

Surface tension is the determining factor of many manufacturing processes, including the emulsification of bitumen. Thus, at very low values of the surface tension at the interface of two phases, spontaneous emulsification of the system is possible [14].

According to the generally accepted opinion [5, 11, 14, 15], if the system is heterogeneous, the interface necessarily exists between the phases. And although the "interface surface" is noted most often, in reality it is a definite transition layer of finite thickness. With the passage of time, after the phases come in contact, there is a mutual diffusion of the molecules. As a result, the equilibrium distribution of the components in the volumes of the contacting phases and at the interface is gradually achieved [15].

Two types of the emulsifier were considered for the preparation of quick- and medium- (EM-44), as well as slow-breaking (E-11) emulsions. Disintegration is a controlled emulsion breaking, resulting from a disruption of the structure of the emulsifier adsorption layers or with a decrease in their stabilizing ability. Thus, due to the difference in the mechanism of the effect of the emulsifier on the emulsion breakdown rate, the intensity of mutual diffusion of the water phase components and the disruption of the structure of the adsorption layers will change when the surface-active substance is changed, leading to changes in the surface tension of the system.

In accordance with the data of Table. 1, the surface tension dynamics was studied as a function of the emulsifier concentration and the lifetime of the water phase solution Figure 2.

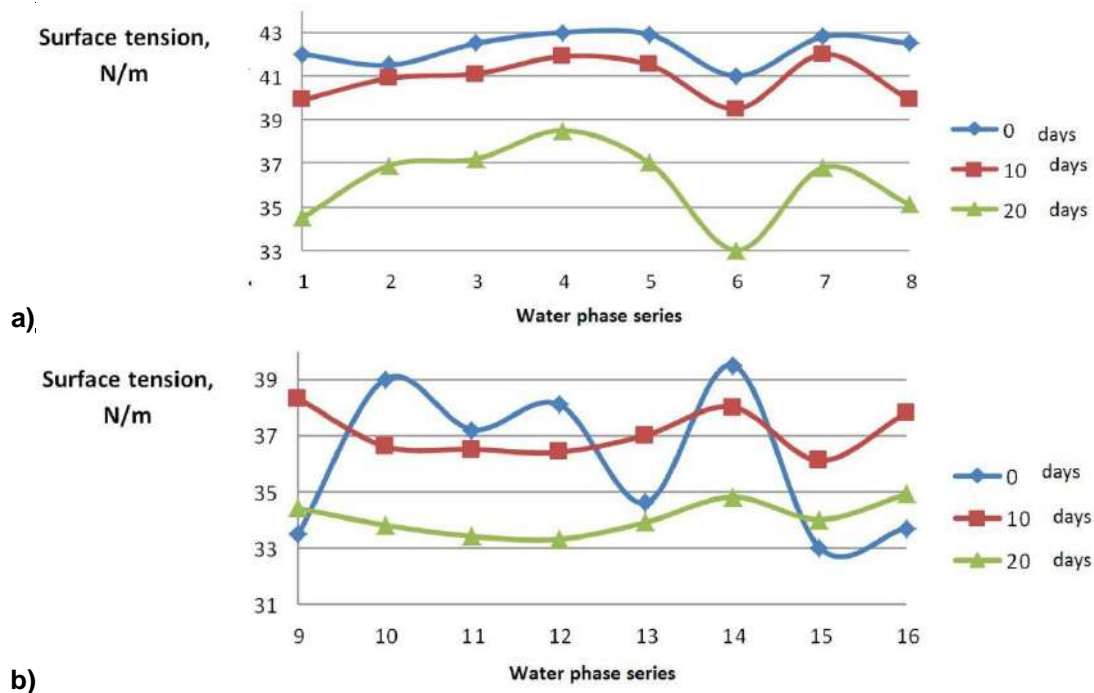


Figure 2. Surface tension of the water phase prepared on the emulsifier a) REDICOTE E-11, b) REDICOTE EM-44

The exposure time was 0 days, which corresponds to the test of the freshly prepared water phase, and also 10 and 20 days. To eliminate the effect of moisture and evaporation, tubes with ground glass stoppers were stored in a dark place at a constant temperature.

As you can see at the Figure 2 the dynamics of the water phase surface tension in time on the basis of REDICOTE E-11 and REDICOTE EM-44 emulsifiers is opposite. So, with the passage of time, the effectiveness of the REDICOTE E-11 emulsifier in the water phase increases which can be judged by the reduction of its surface tension and the detection of a clear extremum in Figure 2a. According to the data obtained, the most effective composition is water phase series No.6 with an emulsifier concentration of 1.01 %. At the same time, regardless of the exposure time of the solution, the nature of the surface tension dependencies on the emulsifier concentration (compositions No. 1–8), Figure 2a, varies insignificantly, which indicates that the selection of stable slow-breaking emulsions is possible already at an early stage of the selection of the water phase. When considering the system "water-

emulsifier REDICOTE EM-44" Figure 2b, the surface tension of the water phase having an initially sinusoidal nature of the variation of the dependencies on the emulsifier concentration over time takes a smoothed out form. Obviously, this effect can be explained from the point of view of the functionality of emulsifiers. In connection with this, when selecting the compositions of bitumen emulsions, it is necessary to take into account that the stabilizing capacity of emulsifiers in the water phase for quick-breaking emulsions is short, while the "viability" and efficiency of the "water-emulsifier" system for slow-breaking emulsions grows in time, which confirms the dependencies established earlier [13].

When investigating the spreading ability of the water phases under study, depending on the concentration and type of the emulsifier on the surface of mineral materials, interesting dependences were recorded (Figure 1), which were used to assess the possibility of early prediction of the compatibility of the emulsifier used to prepare the bitumen emulsion and mineral material which will subsequently interact with the production emulsified binder. Therefore, to study the wetting contact angle, as before, substrates were used: white marble and red granite. To verify the reproducibility and reliability of the experiment, substrates were selected from different batches of materials, it is displayed as two lines in Figures 3–4. It is obvious that the substitution of the substrate affected the changes in the wetting contact angle. However, the general pattern within one type of stone material was preserved.

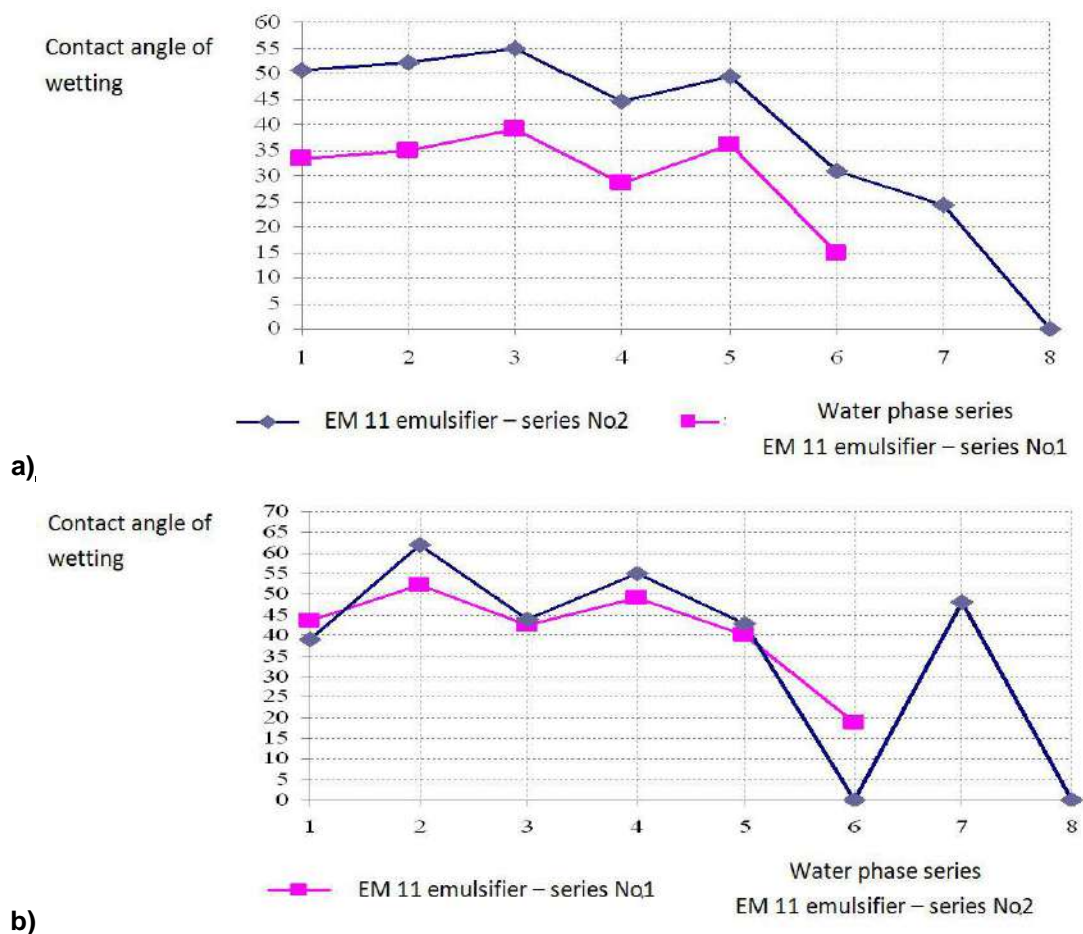


Figure 3. Dynamics of the contact angle of wetting with a water phase prepared on REDICOTE E-11, a mineral substrate of: a) white marble, b) granite

In the process of setting up the experiment, data were obtained confirming the provisions of the developed hypothesis, as described in previous works [13, 16].

In the general case, upon contact of different phases on the interface, a monolayer is formed. Upon contact of the water phase with the mineral substrate, the monomolecular layer is formed due to adsorption of the surface-active substances from the solutions under study. With an increase in the emulsifier concentration in the water phase, the monomolecular layer can transform into a polymolecular surface layer [9], as a result of which the properties of the mineral surface vary significantly. And it can be accompanied by the transformation of mineral substrates from hydrophilic to hydrophobic ones in case of contact with various emulsifiers, which subsequently leads to hetero-alescence of bitumen particles from bitumen emulsions on the mineral surface [7]. This phenomenon is based on the selective adsorption of

the emulsifier in points of contact with the mineral surface from the water phase. In the system "mineral substrate – cationic emulsifier" adsorption occurs due to physical processes, such as electrostatic attraction and bonding on the surface of the hydrocarbon chain of the emulsifier. Electrostatic forces are created due to the attraction of the positively charged polar groups of the emulsifier ions and the negatively charged point of the mineral material ions when the critical concentration is exceeded, which depends on the nature of the stone substrate and the pH of the medium [7]. These connections can be of various types. Electrostatic characteristics of the mineral surface and properties of the water phase are the most significant parameters that initiate adsorption processes of the emulsifier in the system.

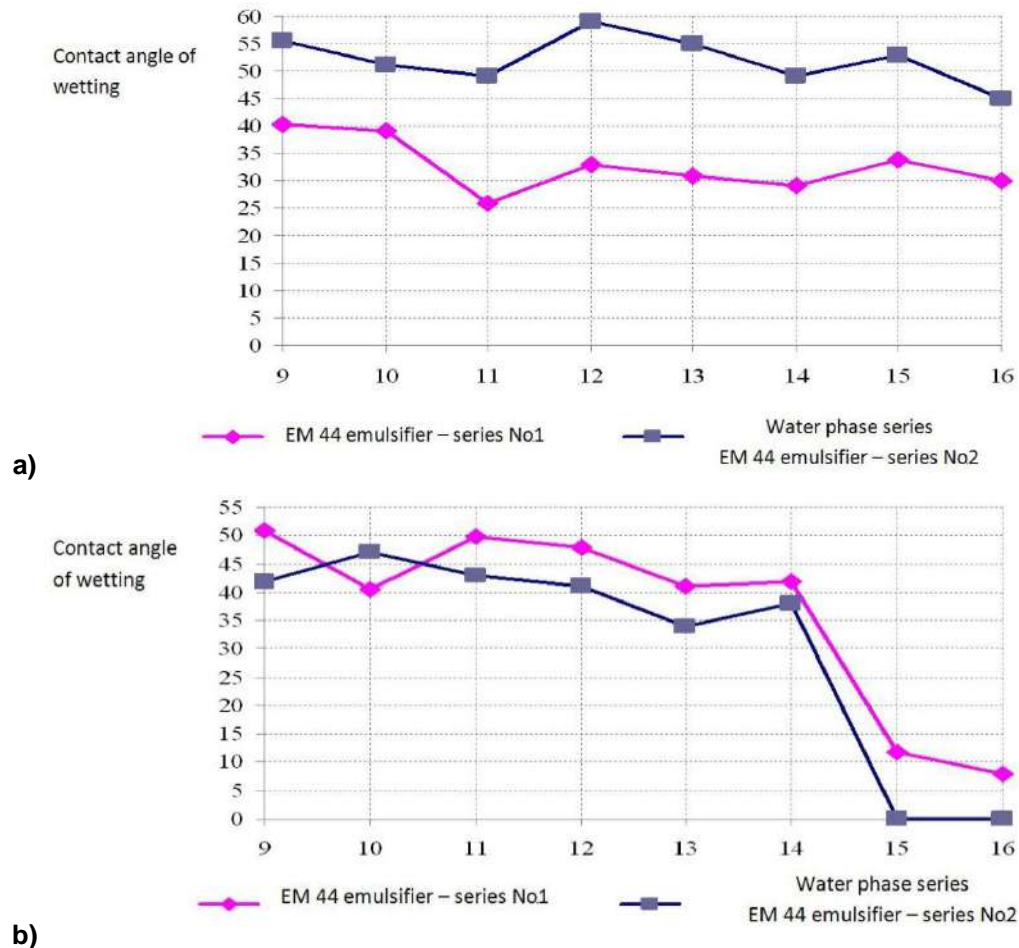


Figure 4. Dynamics of the contact angle of wetting with a water phase prepared on REDICOTE EM-44, a mineral substrate of: a) white marble, b) granite

Also, it is necessary to note a high correlation of the results on the surface tension of the water phase prepared on the REDICOTE E-11 emulsifier, with the data obtained in studying the wetting contact angle on granite. And the similarity of trend lines in Figures 2a and 3a rises as the exposure time of the water phase increases. What is natural, in view of the fact that the emulsifier under consideration relates to the cationic one according to the mechanism of action and is intended for efficient work when combined with mineral materials of acidic nature, including granite.

The most significant differences in the dependences of the wetting contact angle on the concentration of the emulsifier, Figure 4, obtained on various mineral substrates, are observed at high concentrations of the emulsifier (0.6–0.8 %). In this case, upon contact with the granite substrate, a full spread of the droplet of the water phase occurs. Which is more than understandable, since, in accordance with the manufacturer's recommendations [4, 9], the concentration range for the preparation of the medium-breaking emulsion is 0.25–0.6 %.

Analysis and comparison of the obtained data showed that in accordance with the proposed method for prediction of the properties of bitumen emulsion compositions, the graphs show the most effective concentrations corresponding to the series of water phases on the emulsifier REDICOTE E-11 – No. 6 and No. 8, on REDICOTE EM-44 – No. 9, 11 and 13, and also No. 15 and No. 16. Such a choice is justified by the low interfacial tension at the interface of the phases of the "water solution- surface-active substances" system, which predetermines the high dispersity of the emulsion prepared on its basis, and

the small values of the wetting contact angle of the mineral substrate surface show high compatibility of the system "water phase – stone material". Thus, it can be assumed that bitumen emulsions prepared using the indicated series of water phases will be kinetically stable, with the presence of adsorption layers of the emulsifier that inhibit the flocculation and coalescence of emulsion droplets and will be characterized by the relative one-dimensionality of the droplets of disperse systems [17–20].

One of the main methods for studying the structural features and properties of the bitumen emulsion is optical microscopy [18], which allows one to obtain an image of particles of emulsified bitumen without overlapping one another.

In this connection, at the next stage of the experiment, in order to study the structural features under production conditions, experimental batches of bitumen emulsions were prepared and samples of emulsified binder were selected, the surface-active substance content of which, according to the performed studies (Figures 2–4), was effective (compositions No. 6 and 13) and ineffective (compositions No. 7 and 14). The choice of compositions is justified by a lower content of emulsifier, which determines the economic effectiveness of the studied compositions. The evaluation was carried out using the MICMED-1 microscope, using the transmitted-light brightfield method, the essence of which is as follows: in the absence of the specimen, a light beam from the condenser passing through the lens gives a uniformly illuminated field near the focal plane of the eyepiece, in the presence of an absorptive element in the specimen, partial absorption and partial dispersion of light shone upon it occurs, which makes it possible to obtain an image of the emulsified bitumen in the volume. The transfer of the image to the computer monitor and the preservation of the pictures were carried out by a special camera for the DCM 310 microscope (with a resolution of 3 MPix). The samples were examined under a microscope at the magnification factor of 400. The obtained photos were processed and saved using the image editor "AxioVision". The results of the study are shown in Figures 5, 6.

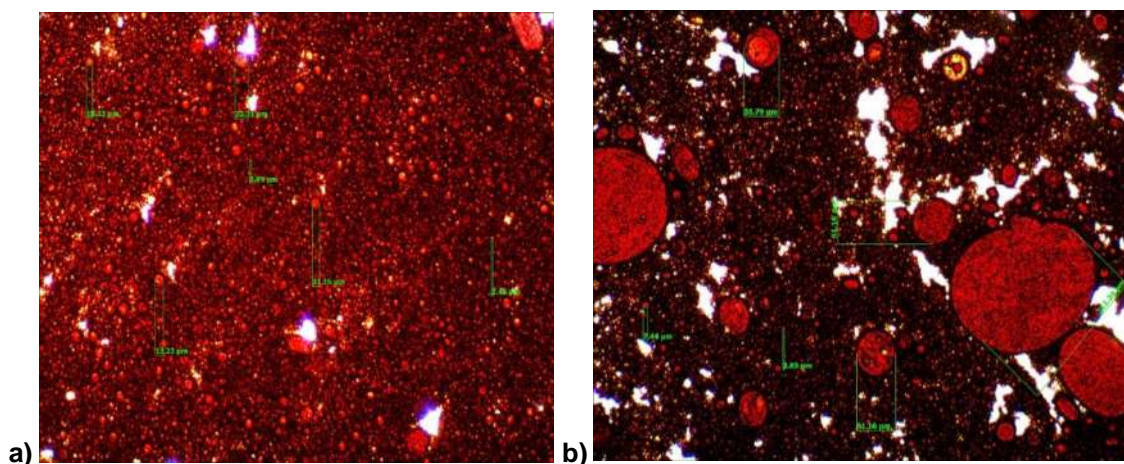


Figure 5. Microphotography of the structure of the bitumen emulsion on the REDICOTE E-11 emulsifier with the concentration: a) 1.01 % series No. 6, b) 1.30% series No. 7

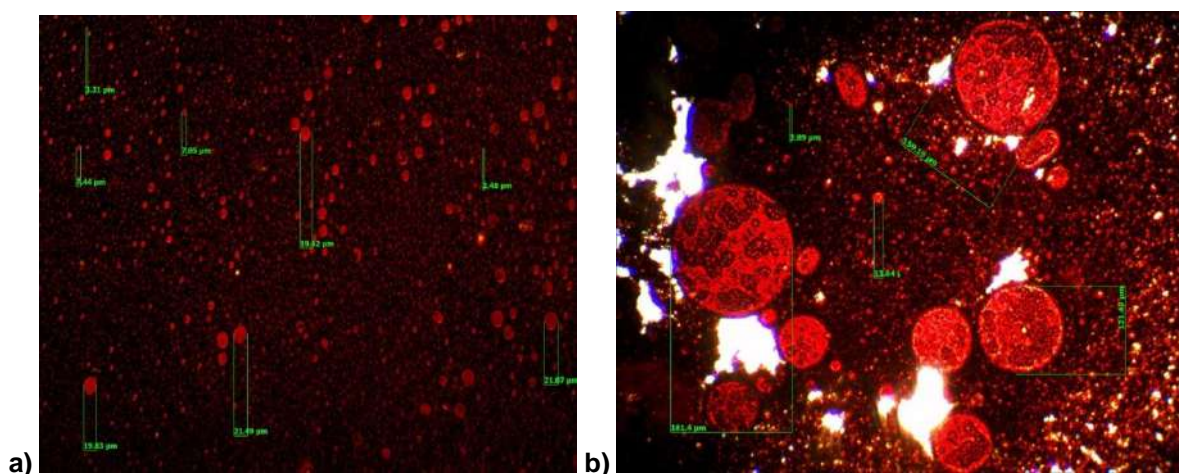


Figure 6. Microphotography of the structure of bitumen emulsion on the REDICOTE EM-44 emulsifier with concentration: a) 0.40 % series No. 13, b) 0.50 % series No. 14

As can be seen, the emulsions, Figures 5a and 6a, prepared on effective water phases from series No. 6 and No. 13, are characterized by homogeneity of the particle size distribution in geometrically correct shape, which will have a positive effect on their stability. The emulsions, Figures 5b and 6b, prepared on solutions with a high content of emulsifier, which, according to preliminary tests of water phases (Figures 2–4), were attributed to ineffective, are characterized by a different scale of structure, a coalescence effect is observed, which is evidence of low efficiency of the adsorption layers of the emulsifier. As a result, this system becomes unstable.

To ensure the production of an effective bitumen emulsion, it must be characterized by structural stability, that is, by property retention in time, but at the same time it must break upon contact with the surface of mineral materials at a certain rate due to technological requirements, providing strong adhesion-cohesive bonds to the surface to be applied.

Structural stability and consistency of bitumen emulsions were studied by the nature of the change in their properties for seven days (Table 2). The emulsion breakdown rate upon contact with the mineral material was evaluated by determining the breakdown index. This method, performed in accordance with Russian State Standard GOST R 55420-2013 (EN 13808: 2011), allows one to study the degree of the emulsion breakdown and consists in determining the maximum amount of the disperse quartz filler of a strictly defined granulometric and mineralogical composition that is mixed with the standard amount of the emulsion. The larger the value of this index is, the slower the breakdown proceeds. Table 2 presents data on the determination of the stability and breakdown index of bitumen emulsions.

Table 2. Stability and breakdown index of bitumen emulsions

Emulsifier type							
REDICOTE E-11				REDICOTE EM-44			
No of composition	When stored after 7 days		Breakdown index*	No of composition	When stored after 7 days		Breakdown index *
	Storage stability according to screening residue N 014, %	Segregation resistance, method A, %			Storage stability according to screening residue N 014, %	Segregation resistance, method A, %	
GOST R 55420-2013	EBDK M			GOST R 55420-2013	EBDK B		
	0.30	5	>80		0.30	5	20-50
6	0.20	3	82.3	13	0.20	2	48.30
7	0.31	4	84.2	14	0.32	5	64.70

* The breakdown index was determined using powder quartz

Analyzing the obtained results, it can be seen that compositions No. 7 (slow-breaking) and composition No. 14 (quick-breaking) cationic bitumen emulsions are characterized by unsatisfactory structural stability, which agrees with the preliminary results on the study of water phases (Figures 2–4).

Thus, as a result of the conducted study, an algorithm was developed for the method of early prediction of the efficiency of cationic bitumen emulsions, which consists in studying the change in surface tension as a function of the concentration of the emulsifier at the initial time of the "life" of the water phase solution, in connection with the established constancy of the character of changes in the studied factors in the time of exposure of the solution. And in the subsequent study of the wetting contact angle of the investigated water phases of the surface of mineral materials of different nature depending on the concentration and type of the emulsifier. This allows us to select the optimal ratio of the components of the water phase already at the early stage of preparation of bitumen emulsions and to predict the compatibility and activity of the interaction of the emulsified binder with the mineral substrate, to rank the mineral material by the efficiency of the interaction with the bitumen emulsion, which provides for obtaining improved and stable composite indicators. It makes the procedure of early prediction particularly relevant. Because at the present moment [5, 6], when developing the formulation of bitumen emulsions and determining the optimum content of surface-active substances in them, test laboratory batches of emulsified binders with different concentrations of surface-active substances are prepared, which is a long, energy and resource intensive process, and it also does not take into account the specifics of a particular type of aggregate, which will be in contact with the emulsion, and therefore, to evaluate the performance of the composite, it is necessary to perform a number of additional tests to assess the compatibility of bitumen emulsions with the mineral aggregate.

4. Conclusions

1. Thus, it has been established and confirmed that the proposed method for studying the dynamics of changes in the properties of the water phase and the interface of the "water phase-mineral substrate" with a change in the surface-active substance concentration allows for the determination of optimal concentrations of various emulsifiers at the early stage for the preparation of effective cationic bitumen emulsions. In the work, at the stage of preparation of the water phase, optimum concentrations of emulsifier were selected, composition No. 6 (REDICOTE E-11 – 1.01 %) and No. 13 (REDICOTE EM-44 – 0.40 %), the use of which allowed obtaining effective bituminous emulsions characterized by structural stability.

2. It has been found that, under certain optimal concentrations of emulsifiers, a higher degree of structuredness of the prepared bitumen emulsion is observed, it is expressed in a more homogeneous and uniform distribution of particles throughout the volume and the possibility of regulating the production breakdown rate, which indicates the sedimentative and aggregative stability of the emulsion. The ability to predict the effectiveness of cationic bitumen emulsions at the stage of the water phase preparation can significantly reduce the time and material funds in the process of their production, while improving the quality of the final product, which is an actual and promising direction for ensuring the development of the road construction industry.

References

Литература

- Ikem V.O., Menner A., Bismarck A. High internal phase emulsions stabilized solely by functionalized silica particles. *Angewandte Chemie International Edition*. 2008. Vol. 47. Pp. 8277–8279.
- Sun G., Li Z. Ngai T. Inversion of particle-stabilized emulsions to form high-internal-phase emulsions. *Angewandte Chemie International Edition*. 2010. Vol. 49. Pp. 2163–2166.
- Bibette J., Leal-Calderon F., Schmitt V., Poulin P. Emulsion Science. Basic Principles. An Overview. *Springer Tracts in modern physics*. 2002. Vol. 181. P. 140.
- Ronald M., Luis F.P. Asphalt emulsions formulation: State-of-the-art and dependency of formulation on emulsions properties. *Construction and Building Materials*. 2016. Vol. 123. Pp. 162–173.
- Gustafsson H., Holmberg K. Emulsion-based synthesis of porous silica // *Advances in Colloid and Interface Science*. 2017. Vol. 247. Pp. 426–434.
- Barboy V.M., Glazman Yu.M., Rebinder P.A. О термодинамически равновесных двухфазных дисперсных системах [On thermodynamically equilibrium two-phase disperse systems]. *Colloid Journal*. 1970. Vol. 32. No. 4. Pp. 480–492. (rus)
- Skorikov S.V., Iozikova YU.G. Kationnyy emul'gator emk-1 dlya bitumnykh emul'siy [Cationic emulsifier emk-1 for bitumen emulsions]. *Scientific Journal of Construction and Architecture*. 2015. No. 1(37). Pp. 88–98. (rus)
- Chevalier Y., Bolzinger M.-A. Emulsions stabilized by solid nanoparticles: pickering emulsions. *Colloids Surf A*. 2013. No. 439. Pp. 23–34.
- Summ B.D., Soboleva O.A. Static and kinetic regular trends in preferential wetting. *Moscow University Chemistry Bulletin*. 2006. Vol. 61. No. 5. Pp. 1–3.
- Kim V., Voskobojnikov E.S., Kubagushev I.G., Frolov Y.G. effect of electrolytes and surfactants on hydrodynamic characteristics and aggregation of polyacrylonitrile in dimethylformamide. *Colloid Journal*. 1994. Vol. 56. No. 4. Pp. 594–596.
- Kotomin A.A., Petel'skii M.B., Mashchenko E.I., Yakimchuk O.D., Abramzon A.A. temperature dependence of the detergency of sodium alkyl benzenesulfonate and compositions thereof. *Russian Journal of Applied Chemistry*. 2002. Vol. 75. No. 7. Pp. 1128–1131.
- Esquena J., Nestor J, Vilchez A, Aramaki K., Solans C. Preparation of mesoporous/macroporous materials in highly concentrated emulsions based on cubic phases by a single-step method. *Langmuir*. 2012. Vol. 28. Pp. 12334–12340.
- Коротков А.В., Высоцкая М.А. Изучение физико-химических свойств водной фазы катионных битумных
- Ikem V.O., Menner A., Bismarck A. High internal phase emulsions stabilized solely by functionalized silica particles // *Angewandte Chemie International Edition*. 2008. Vol. 47. Pp. 8277–8279.
- Sun G., Li Z. Ngai T. Inversion of particle-stabilized emulsions to form high-internal-phase emulsions // *Angewandte Chemie International Edition*. 2010. Vol. 49. Pp. 2163–2166.
- Bibette J., Leal-Calderon F., Schmitt V., Poulin P. Emulsion Science. Basic Principles. An Overview // *Springer Tracts in modern physics*. 2002. Vol. 181. P. 140.
- Ronald M., Luis F.P. Asphalt emulsions formulation: State-of-the-art and dependency of formulation on emulsions properties // *Construction and Building Materials*. 2016. Vol. 123. Pp. 162–173.
- Gustafsson H., Holmberg K. Emulsion-based synthesis of porous silica // *Advances in Colloid and Interface Science*. 2017. Vol. 247. Pp. 426–434.
- Барбой В.М., Глазман Ю.М., Ребиндер П.А. О термодинамически равновесных двухфазных дисперсных системах // *Коллоидный журнал*. 1970. Т. 32. № 4. С. 480–492.
- Скориков С.В., Лозикова Ю.Г. Катионный эмульгатор ЕМК-1 для битумных эмульсий // *Научный журнал строительства и архитектуры*. 2015. № 1(37). С. 88–98.
- Chevalier Y., Bolzinger M.-A. Emulsions stabilized by solid nanoparticles: pickering emulsions // *Colloids Surf A*. 2013. № 439. Pp. 23–34.
- Summ B.D., Soboleva O.A. Static and kinetic regular trends in preferential wetting // *Moscow University Chemistry Bulletin*. 2006. Vol. 61. № 5. Pp. 1–3.
- Kim V., Voskobojnikov E.S., Kubagushev I.G., Frolov Y.G. effect of electrolytes and surfactants on hydrodynamic characteristics and aggregation of polyacrylonitrile in dimethylformamide // *Colloid Journal*. 1994. Vol. 56. № 4. Pp. 594–596.
- Kotomin A.A., Petel'skii M.B., Mashchenko E.I., Yakimchuk O.D., Abramzon A.A. temperature dependence of the detergency of sodium alkyl benzenesulfonate and compositions thereof. *Russian Journal of Applied Chemistry*. 2002. Vol. 75. № 7. Pp. 1128–1131.
- Esquena J., Nestor J, Vilchez A, Aramaki K., Solans C. Preparation of mesoporous/macroporous materials in highly concentrated emulsions based on cubic phases by a single-step method // *Langmuir*. 2012. Vol. 28. Pp. 12334–12340.
- Коротков А.В., Высоцкая М.А. Изучение физико-химических свойств водной фазы катионных битумных

Шеховцова С.Ю., Коротков А.В., Высоцкая М.А. Метод прогнозирования эффективности катионных битумных эмульсий // *Инженерно-строительный журнал*. 2018. № 2(78). С. 91–100.

- Pp. 12334–12340.
13. Korotkov A.V., Vysotskaya M.A. Izucheniye fiziko-khimicheskikh svoystv vodnoy fazy kationnykh bitumnykh emulsiy [Investigation of the physicochemical properties of the aqueous phase of cationic bitumen emulsions]. *Bulletin of the Belgorod State Technological University named after V.G. Shukhov*. 2013. No. 6. Pp. 10–12. (rus)
 14. Idrisov M.R., Abdullin A.I. Bitumnyye emulsii v dorozhnom stroitelstve [Bitumen emulsions in road construction]. *Bulletin of Kazan Technological University*. 2011. Vol. 14. No. 23. Pp. 124–129. (rus)
 15. Silva B.F.B., Rodriguez-Abreu C., Vilanova N. Recent advances in multiple emulsions and their applications as templates. *Current Opinion in Colloid and Interface Science*. 2016. Vol. 25. Pp. 98–108.
 16. Qian C., McClements D.J. Formation of nanoemulsions stabilized by model food-grade emulsifiers using high-pressure homogenization: Factors affecting particle size. *Food Hydrocolloids*. 2011. Vol. 25. Pp. 1000–1008.
 17. Chen Y., Ballard N., Gayet F., Bon S.A. High internal phase emulsion gels (HIPE-gels) from polymer dispersions reinforced with quadruple hydrogen bond functionality. *Chemical Communications*. 2012. Vol. 48. Pp. 1117–1119.
 18. Murafa A.V., Makarov D.B., Nureyev M.A., Khozin V.G. Bitumen latex emulsion mastics for waterproofing and sealing use. *Polymer Science Series D*. 2013. Vol. 6. No. 1. Pp. 48–50.
 19. Kemalov A.F., Kemalov R.A. Practical aspects of development of universal emulsifiers for aqueous bituminous emulsions. *World Applied Sciences Journal*. 2013. Vol. 6. Pp. 858–862.
 20. Barbeta A., Cameron N.R. Morphology and surface area of emulsion-derived (PolyHIPE) solid foams prepared with oil-phase soluble porogenic solvents: Span 80 as surfactant. *Macromolecules*. 2004. Vol. 37. Pp. 3188–3201.
 - эмульсий // Вестник Белгородского государственного технологического университета им. В.Г. Шухова. 2013. № 6. С. 10–12.
 14. Идрисов М.Р., Абдуллин А.И. Битумные эмульсии в дорожном строительстве // Вестник Казанского технологического университета. 2011. Т. 14. № 23. С. 124–129.
 15. Silva B.F.B., Rodriguez-Abreu C., Vilanova N. Recent advances in multiple emulsions and their applications as templates // Current Opinion in Colloid and Interface Science. 2016. Vol. 25. Pp. 98–108.
 16. Qian C., McClements D. J. Formation of nanoemulsions stabilized by model food-grade emulsifiers using high-pressure homogenization: Factors affecting particle size // Food Hydrocolloids. 2011. Vol. 25. Pp. 1000–1008.
 17. Chen Y., Ballard N., Gayet F., Bon S. A. High internal phase emulsion gels (HIPE-gels) from polymer dispersions reinforced with quadruple hydrogen bond functionality // Chemical Communications. 2012. Vol. 48. Pp. 1117–1119.
 18. Murafa A.V., Makarov D.B., Nureyev M.A., Khozin V.G. Bitumen latex emulsion mastics for waterproofing and sealing use // Polymer Science Series D. 2013. Vol. 6. № 1. Pp. 48–50.
 19. Kemalov A.F., Kemalov R.A. Practical aspects of development of universal emulsifiers for aqueous bituminous emulsions // World Applied Sciences Journal. 2013. Vol. 6. Pp. 858–862.
 20. Barbeta A., Cameron N.R. Morphology and surface area of emulsion-derived (PolyHIPE) solid foams prepared with oil-phase soluble porogenic solvents: Span 80 as surfactant // Macromolecules. 2004. Vol. 37. Pp. 3188–3201.

Svetlana Shekhovtsova,
+7(980)374-97-04; SHehovtsovaSYU@mgsu.ru
Aleksey Korotkov,
+7(921)922-51-61; Korotkov.AV@gazprom-neft.ru
Marina Vysotskaya,
+7(920)561-95-16; roruri@rambler.ru

Светлана Юрьевна Шеховцова,
+7(980)374-97-04;
эл. почта: SHehovtsovaSYU@mgsu.ru
Алексей Викторович Коротков,
+7(921)922-51-61;
эл. почта: Korotkov.AV@gazprom-neft.ru
Марина Алексеевна Высоцкая,
+7(920)561-95-16; эл. почта: roruri@rambler.ru

© Shekhovtsova S.Yu., Korotkov A.V., Vysotskaya M.A., 2018

doi: 10.18720/MCE.78.8

Refined methods for calculating and designing engineering structures

Уточненные методы расчета и проектирования инженерных сооружений

*V.P. Mushchanov,
A.N. Orzhekhovskii,
A.V. Zubenko,
S.A. Fomenko,*

*Donbas National Academy of Civil Engineering
and Architecture, Makiyivka, Donetsk region,
Ukraine*

*Д-р техн. наук, проректор по научной
работе, заведующий кафедрой*

*В.Ф. Мущанов,
ассистент А.Н. Оржеховский,
ассистент А.В. Зубенко,
ассистент С.А. Фоменко,
Донбасская национальная академия
строительства и архитектуры, Макеевка,
Донецкая область, Украина*

Key words: vertical cylindrical tank; rigid bus;
frame-cantilever coating; design; calculating

Ключевые слова: вертикальный
цилиндрический резервуар; жесткая ошиновка;
рамно-консольное покрытие; проектирование;
расчет

Abstract. В статье рассмотрено совершенствование методов расчета различных конструкций инженерных сооружений, которое осуществляется на основных этапах проектирования: 1) формирование нагрузок (для конструкций вертикальных цилиндрических резервуаров); 2) совершенствование проектных решений (для конструкций жесткой ошиновки); 3) оценка надежности принятых проектных решений вероятностно-статистическим методом (на примере рамно-консольных покрытий над трибунами стадионов). Основной целью исследования, проведенного при решении первой проблемы, является улучшение метода нормирования ветровой нагрузки на поверхности цилиндрического резервуара объемом 20000–50000 м³ с учетом типа крыши (провисающей мембраны) и блочности (группа из 4 резервуаров). Решение второй задачи рассмотрено на примере новых демпфирующих устройств для уменьшения колебаний, создаваемых ветровым потоком конструкции для конструкции жесткой ошиновки балочного типа. В нормативных документах формулируются только общие требования, но в то же время нет конкретных рекомендаций по рациональному определению размеров осцилляторов и данных об эффективности их применения. Третья проблема решена на примере оценки надежности проектно-конструкторских решений рамно-консольных покрытий над трибунами стадионов с учетом случайного характера основных факторов проектирования.

Аннотация. The enhancement of calculation of different structures for engineering constructions which is carried out on the main stages of design, has been considered in this paper: 1) the formation of loads (for structures of vertical cylindrical tanks); 2) improving the design solutions (for structures of rigid bus); 3) assessing the reliability of the adopted design decisions by probabilistic and statistical methods (on the example of frame-cantilever coatings above the stands of stadiums). The main aim of the research carried out in solving the first problem is to improve the method for normalizing the wind load on the surface of a cylindrical tank with a volume of 20000–50000 m³, taking into account the type of roof (sagging membrane) and the block arrangement (a group of 4 tanks). The solution of the second problem has been considered on the example of new damping devices to reduce oscillations generated by the wind flow of the rigid jumper construction of girder type. The normative documents formulate only general requirements, but at the same time, there are no specific recommendations on rational sizing of oscillation dampeners and data on their application efficiency. The the third problem has been solved on the example of reliability estimation of design project solutions of frame-consol cover structures over stadium tribunes, taking into account the casual character of the main design factors.

1. Introduction

Most of the researches aimed at improving the energy efficiency of buildings are closely related to arrangements for thermal modernization, usage of modern thermal insulating materials and improving the efficiency of utilities system.

However, the solution of energy efficiency problem is impossible without the improvement of technological solutions throughout the whole process chain “energy generation – transportation – consumption”.

The methods of calculating and designing the structures for engineering constructions of the fuel and energy complex play an important part in this scheme. Such methods should ensure the creating of effective constructive forms which would meet all reliability requirements for high responsibility of buildings.

The enhancement of calculation of different structures for engineering constructions which is carried out on the main stages of design, has been considered in this paper:

- 1) the formation of loads (for structures of vertical cylindrical tanks);
- 2) improving the design solutions (for structures of rigid bus);
- 3) assessing the reliability of the adopted design decisions by probabilistic and statistical methods (on the example of frame-cantilever coatings above the stands of stadiums).

The main aim of the research carried out in solving the first problem is to improve the method for normalizing the wind load on the surface of a cylindrical tank with a volume of 20–50 thousand m³, taking into account the type of roof (sagging membrane) and the block arrangement (a group of 4 tanks). Existing methods for calculating the wind load on buildings and structures, using aerodynamic formulas were developed in the early 70-ies in the V.A. Kucherenko Central Scientific Research Institute for Building Structures based on the works of A. Davenport and A. Vaiz and implemented in SNiP II-6-74 [1]. In 1985, with the release of SNiP 2.01.07-85 [2], expressions describing the dynamic response of structures under the action of the wind were simplified [3]. The main theoretical information on building aerodynamics and methods for determining the wind load on buildings and structures have been presented in the works [4–6]. In works of Ye.V. Gorokhov [7], R.I. Kinash [8], Y. Uematsu [9], Y. Zhao [10], Y. Zhang [11, 12] the issues of wind effects on buildings and structures and experimental simulation of the interaction of wind flow with engineering constructions in a wind tunnel have been considered. In books of P.G. Ereemeev [13, 14] the results of model experimental studies of wind and snow loads on technically complex large-span coatings with complex geometry have been presented. The research of numerical modeling of wind influences has been considered in studies of A. Michalski, T. Okaze, K. Togbenou, A. Mochida [15–18] and others. At the same time, the issues of the normalization of wind loads on reservoirs in the form of a sagging roof and block arrangement (a block of 4 tanks [19]) remain open and require further study.

The solution of the second problem has been considered on the example of new damping devices to reduce oscillations generated by the wind flow of the rigid jumper construction of girder type. The normative documents [20, 21] formulate only general requirements in the form of parameter values of strain-stress state of a designed construction and general recommendations in the form of oscillation suppression methods which are able to furnish these requirements. At the same time, there are no specific recommendations on rational sizing of oscillation dampeners and data on their application efficiency.

The solution of the third problem is devoted to the development of the existing heart of the reliability theory and probability calculation of enhanced responsibility constructions. In this case this problem has been solved on the example of reliability estimation of design project solutions of frame-consol cover structures over stadium tribunes, taking into account the casual character of the main design factors. In spite of the fact that the basic problems of the reliability theory have been solved in the works of A.R. Rzhantsyn [22], V.V. Bolotin [23], V.D. Raizer [24], the peculiar features of different influences have been considered in the works of S.F. Pichugin [25], A.V. Perelmuter [26], S.A. Timashev [27], A.M. Ayzen [28], V.P. Mushchanov [29–32], M. Krejsa, P. Janas [33] and others, the practical realization problems of the requirements given in the normative documents [34–36] are often unsolved.

The main motivation that prompted the authors to carry out this research is the desire to ensure an increase in the efficiency and reliability of the industrial structures of the fuel and energy complex and engineering facilities used by improving the calculation, design and construction procedures.

In this regard, the main purpose of this study is to clarify certain provisions for the calculation, design and construction of structures of engineering structures in the form of vertical cylindrical tanks, rigid buses of open switchgears and stationary canopies over the stands of stadiums.

Objectivity and reliability of the obtained results is confirmed by good conformity between the data of theoretical and experimental studies and their implementation in design practice.

2. Methods

General methods used in the performance of all problems given in the report are:

- calculus of approximations of constructional mechanics (method of finite-elements – MFE) with the use of universal program complexes “SCAD Office”[32], “LIRA”;
- method of physical simulation with the use of the similarity theory;
- methods of mathematical statistics (while processing the results of experimental and numerical simulation);

Additionally used:

- a. while solving the first problem – calculus of approximations of finite volumes (MFV) of simulation of turbulent flows with the use of program complex “SolidWorksFlowSimulation” [37];
- b. while solving the second problem – the methods of mathematical physics and the methods of harmonic analysis (while processing data of field dynamic tests of structures with the help of vibrating machine) [38];
- c. while solving the third problem – trial and error methods of investigation, and specifically destructive methods of definition of material strength characteristics.

3. Results and Discussion

3.1. Perfection of normalizing loads on structures of vertical cylindrical reservoirs

Some experimental and computational investigations have been done to solve this problem. The experimental investigations have been carried out in the meteorological wind tunnel MWT-1. While performing these investigations the main similarity parameter is Reynolds number:

$$R_e = \frac{L \cdot U(z_e)}{\nu} \quad (1)$$

where L – diameter; $\nu = 1.5 \cdot 10^{-5} \text{ m}^2/\text{s}$ – kinematic air viscosity, $U(z_e) = 14.9 \text{ m/s}$ – peak wind velocity, $U(z_e)$.

Similarity condition of aerodynamic processes in the field and on the model is the geometrical similarity. To supply this similarity, corresponding sizes of field structures l_H and models l_M must be corresponded to the single scale of linear dimensions

$$M_l = \frac{l_M}{l_H} \quad (2)$$

According to the plan of experimental investigations of the reservoir model M 1:320 in the wind tube MWT-1 DonNACEA foresaw the definition of coefficients of the wind pressure (C_p) in 49 supporting points on the reservoir (Fig. 3). In the process of investigations the dependence $C_{pi} = f(\beta)$ is defined within $\beta = 0 \dots 360^\circ$ in increments of $\Delta\beta = 10^\circ$. The results have been presented on 6 directions ($\beta = 0^\circ, 45^\circ, 90^\circ, 150^\circ, 180^\circ, 270^\circ$) (Fig. 1).

Calculus investigations were conducted with the use of the finite volume method (MFV) of simulating turbulent flows with the use of program complex “SolidWorksFlowSimulation”. As the test calculations of Japanese Institute showed, the size of calculation domain in vertical direction for isolated structures had to be minimum $5H$. While investigating groups of structures it should be necessary to use the blockage coefficient. This coefficient is equal to cross area of structure – cross area of computational domain ratio. The coefficient mustn't be more than 3 %. In our case for the group when the height of the structure is 78 mm the blockage percent will be 2.09 %. The width of the calculation domain must be given, so that the blockage coefficient would be less than 3 %. The distance along the flow to the structure must be minimum $5H$. The distance behind the structure must be $\geq 15H$. The scheme of the domain is shown in Figure 2.

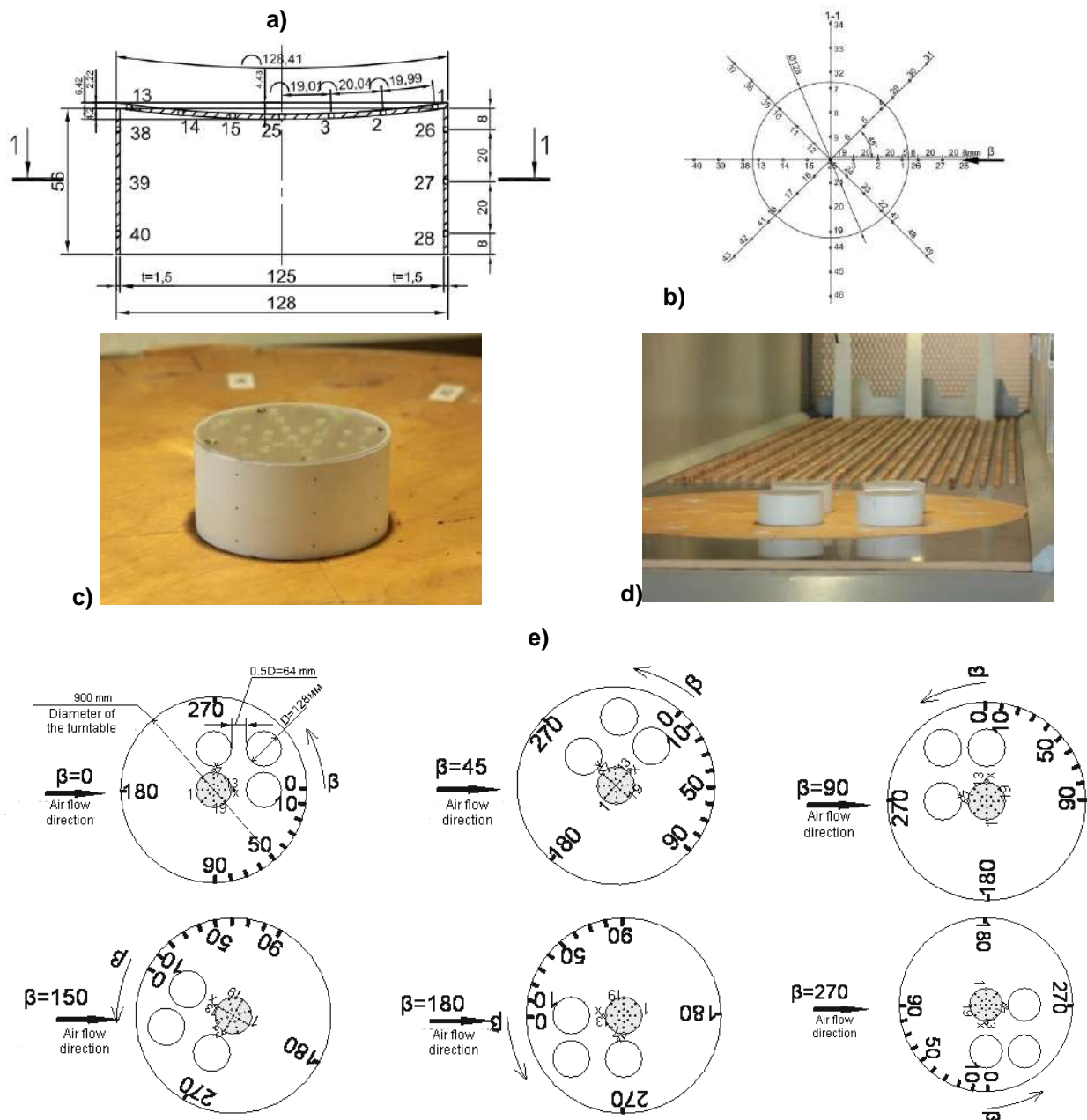


Figure 1. Conducting experimental investigations: a – cross section of model; b – scheme of disposition of draining points; c – single model with draining taps; d – simulation of the group of reservoirs; e – schemes of conducting experiment

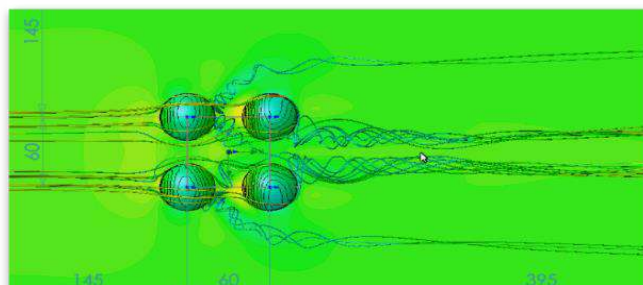


Figure 2. Visualisation of numerical investigation results

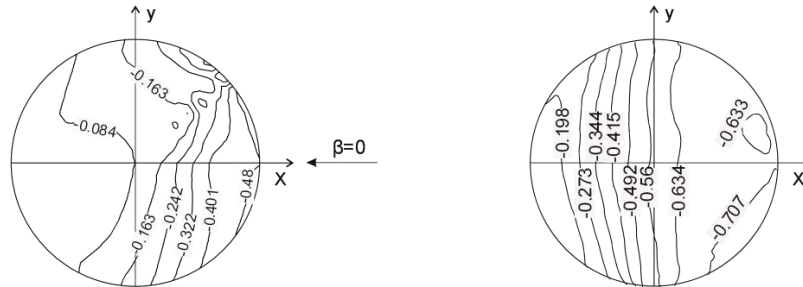
Figure 3 shows the data of the contrastive analysis of results of numerical and experimental investigations for the reservoir with the overhanging roof coating (single and in the group).

Model with overhanging roof ($Re = 1.13E + 05$)
Isofields of coefficient distribution on the roof covering

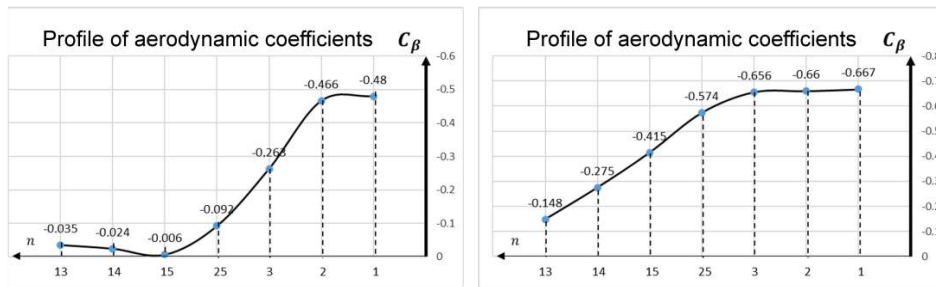
Experimental method

Numerical method in
calculative program

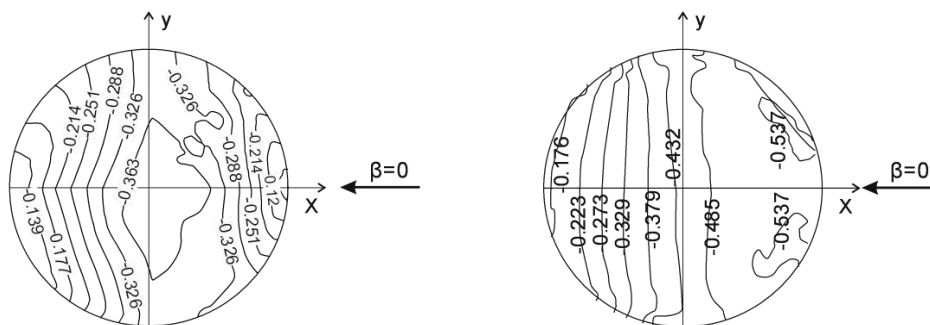
a)



Coefficient distribution profile on the roof covering



b)



3.2 New approaches to the oscillation compression of girder electricity supply constructions

The tasks of creating new rational damping devices and perfecting existing ways of oscillation suppression of rigid jumper constructions of open distribution devices in the wind flow are being considered nowadays. The rigid jumper is applied for transmission and distribution of electricity between high-voltage apparatuses both within open distributional devices (ODD) and close distributional devices (CDD) of quick-repaired factory-assembled transformer substations (see Figure 4). Known methods of wind resonance particles exclusion:

- the usage of elements having small bays;
- placing mould cores or wires into the pipes;
- installation of spiraling (screw-shaped) helical spoiler ailerons, this results in the asynchronous vortex separation along the length of cylinder;
- frequency drop of characteristic vibrations (for example, by installation of busbar overhauling weight);
- dampers in the shape of half-socked pipes, covering up to 40 per cent of the busbar length, this reduces the amplitude of wind vibration by several times;
- structural damping – energy dissipation at the site of busbar mounting (special structure of busbar clamp).



Figure 4. Outdoor switch gear construction having rigid busbar 110-750kV SJSC (ZAO) "ZETO"

Without revealing details of advantages and disadvantages, arguments of efficiency of one or another oscillation suppression method it will have been given the results of theoretic and experimental investigations, carried out by the authors for "dampener on ligament" (Figures 5–8).

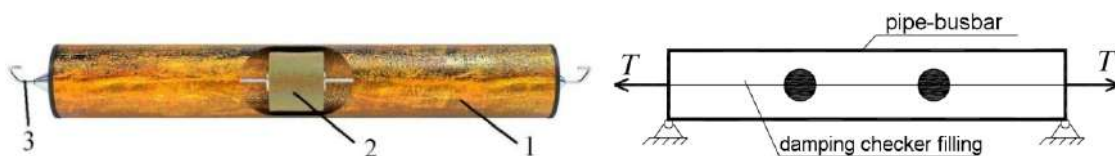


Figure 5. "Dampener on ligament" structure of bending vibrations of pipe-busbar: 1 – pipe-busbar; 2 – damping checker filling; 3 – contact wire dropper

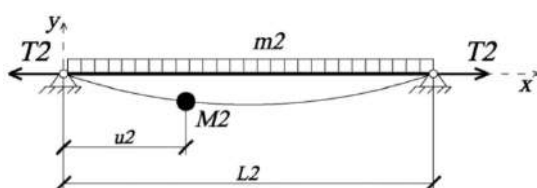


Figure 6. Design model of broaching construction (pipes)

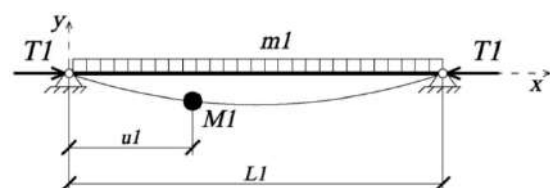


Figure 7. Design model of dampener on ligament

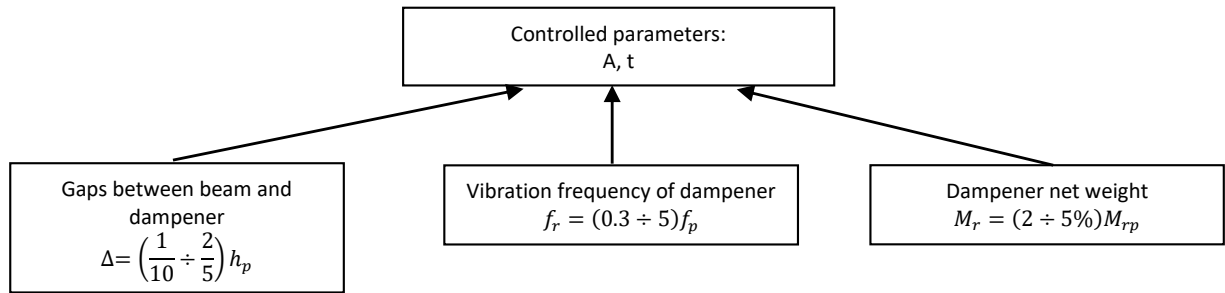


Figure 9. Numerical experiment controlled parameters

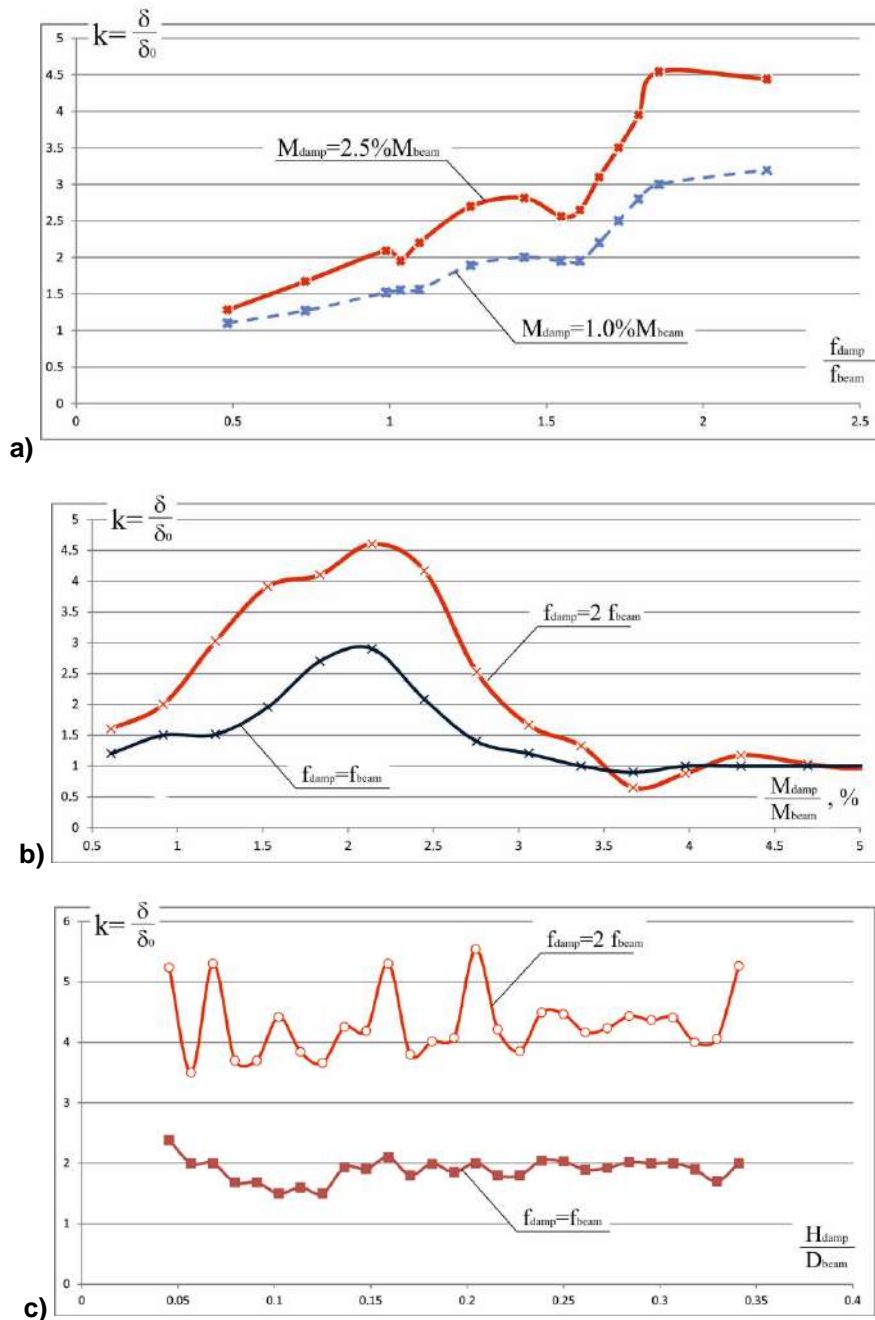


Figure 10. Change in the performance criterion k of the “thread-based damper” on affecting factors change: a) on damper natural vibration frequency change; b) on damper weight change; c) on damper dimensions change

3.3 Probabilistic approaches to design reliability assurance of space framed structures being designed (by the example of the framed and cantilever structures of stadium stands roofs)

In terms of structural concepts, 36 % of the five-star stadium stands roofs are beam roofs and framed cantilever ones, 14 % of them are steel cable and beam roofs, 18 % of them are suspended shells and structures, 25 % of them are bar structures, 7 % of them are suspended roofs (cable nets and membrane shells). On the grounds of the survey made we can draw a conclusion that the framed cantilever roofs for stadium stands are more widely used in the world practice nowadays. It has also been identified that structural erection imperfections have negative effect on the structures further serviceability. The failure ratio resulted from these defects is high enough and cannot be neglected. The methods of erection procedure are of great concern for improving the erection procedure quality. The structural design variants of the stands roofs under consideration are given in Figure 11 and Table 1.

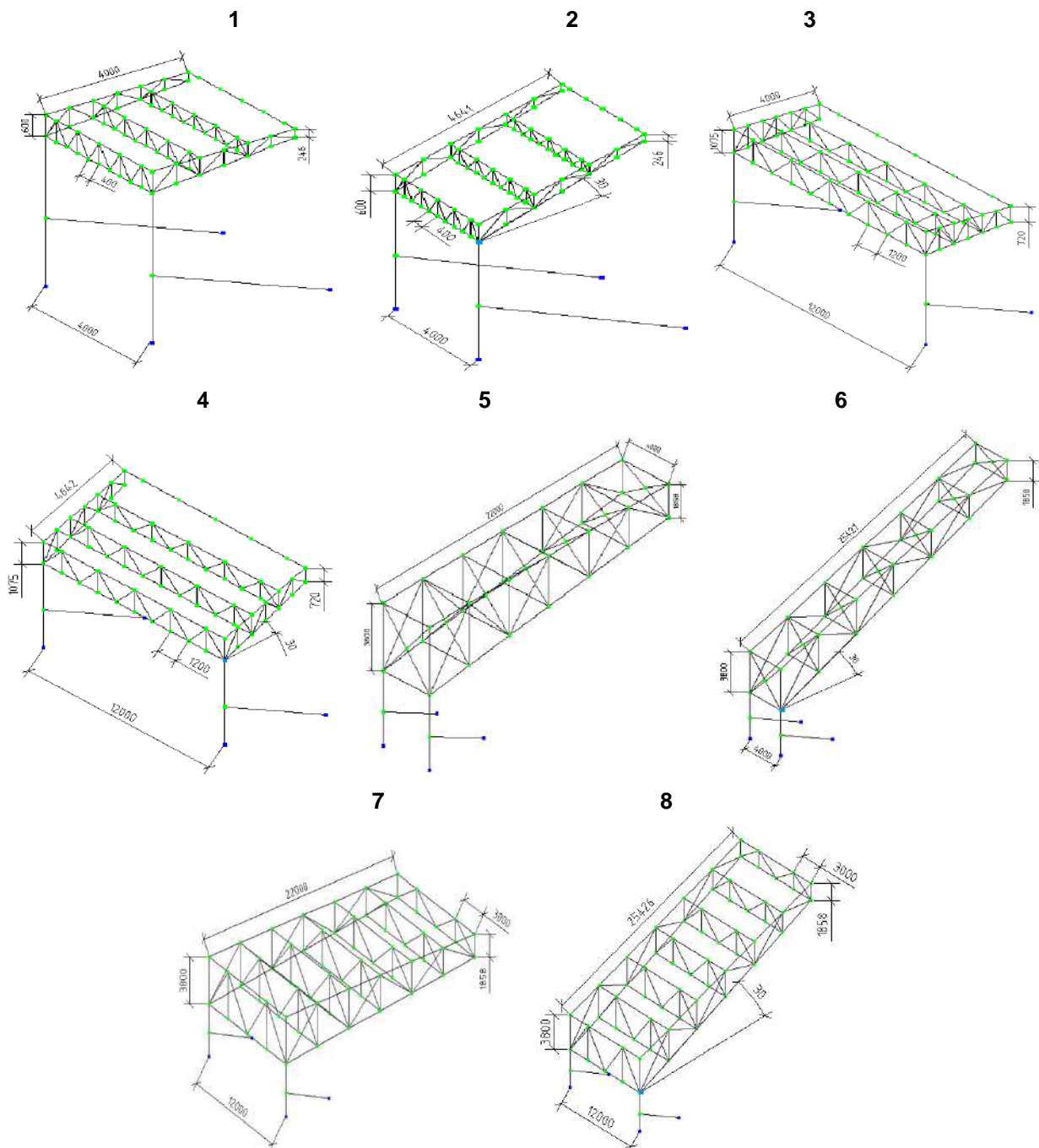


Figure 11. Design Diagram for Simulation Experiment

At the first stage the aggregate of the system bar elements to be recalculated is formed. It is more appropriate to make calculations for the most critical components as the system is redundant. For this purpose the iterative geometrically and structurally nonlinear structural analysis is made. As a result, the list of successively unserviceable members is being formed. The procedures of this stage are similar to those demonstrated in Figure 12. Following on from the data obtained, the group of the most critical structural members is selected to make recalculation of the condition load effect factor.

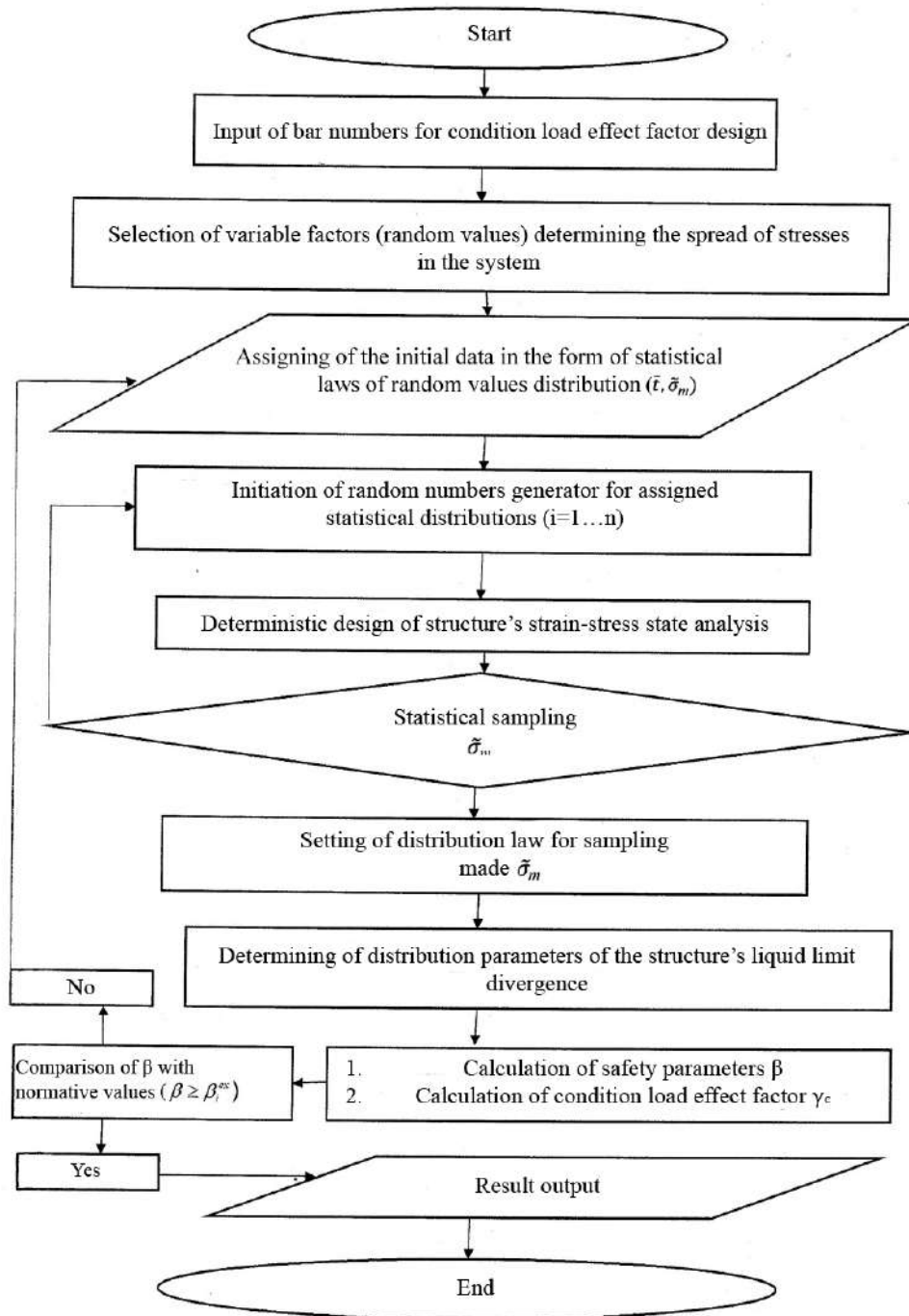


Figure 12. Control flow chart of condition load effect factor and cross section choice for framed and cantilever roofs over stadiums

The iterative structural analysis with regard to random values given is made for the elements selected in the previous stage. Hence, the sample collection of stresses for the group of bars in question is being formed. The sampling should be over the 10^4 to 10^8 range. The second random value in the analysis is the random value of the strength of constructional material (liquid limit). Two generalized

random values obtained are processed by mathematical statistics methods (their distribution law and density). Handling the density, laws and characteristics of distribution, the probable failure of the members selected is analyzed. The reliability characteristics obtained are compared to the normative values according to the importance of the structure. If the reliability requirements are satisfactory, the analysis is finished. If the reliability is not provided, the particular reliability factors are recalculated and the required probabilistic mean value of stress in the structural members is defined taking into account the required bars area. The structure with redefined cross section area is recalculated according to the algorithm described before. Iterations continue until the reliability conditions of the members considered are satisfied.

Table 1. Combinations of variable parameters of the system

Variant	Angle of Dip α (Degrees)	Framing Space H (m)	Overhanging Length L (m)
1	0	4	4
2	30	4	4
3	0	12	4
4	30	12	4
5	0	4	22
6	30	4	22
7	0	12	22
8	30	12	22

The condition load effect factor is defined as:

$$\gamma_c = 1 - \frac{\gamma_m \left(\frac{\bar{\sigma}^p}{1 - \mu_\sigma k_\sigma} - \sigma_0^p \right)}{\bar{R}_y^n (1 - \mu_r k_r)}; \tag{5}$$

where: γ_m – particular reliability factor for material strength; $\bar{\sigma}^p$ – mean square deviation of stresses in the structural member; μ_σ, μ_r – probabilistic mean value of stress in the structural members and probabilistic random mean value of strength of material (liquid limit), correspondingly; k_σ, k_r – variation coefficients of two random values considered; \bar{R}_y^n – normative value of design strength of structure’s material; σ_0^p – design value of stress in the structural member, derived from the deterministic structural design.

Whereas it is necessary to correct the condition load effect factor values, the simulation experiment for framed cantilever roofs over stadium stands has been made. The purpose of the experiment was to find the correct mathematical model connecting the condition load effect factor and the system’s initial variable parameters such as: the overhanging length of cantilever girder (L), the base cantilever frame space (H) and the understressing ratio of the cross section (due to product mix grading and designing requirements) (Table 2).

Table2. Analysis of Generalized Parameters of Durability and Carrying Capacity Allowances

No. Diagram	Safety Parameters		Failure Probability		Allowance ($\beta_{max} - \beta_{min}$)
	β_{min}	β_{max}	$P_{f min}$	$P_{f max}$	Δ
1	4.47	7.01	$0.824 \cdot 10^{-4}$	$0.773 \cdot 10^{-8}$	2.54
2	4.49	6.98	$0.772 \cdot 10^{-4}$	$0.259 \cdot 10^{-7}$	2.49
3	4.52	7.12	$0.835 \cdot 10^{-4}$	$0.528 \cdot 10^{-8}$	2.6
4	4.89	7.48	$0.568 \cdot 10^{-6}$	$0.156 \cdot 10^{-8}$	2.59
5	5.01	7.81	$0.986 \cdot 10^{-6}$	$0.257 \cdot 10^{-9}$	2.8
6	3.57	5.72	$0.378 \cdot 10^{-4}$	$0.956 \cdot 10^{-8}$	2.15
7	3.22	5.03	$0.267 \cdot 10^{-4}$	$0.887 \cdot 10^{-6}$	1.81
8	3.08	5.01	$0.399 \cdot 10^{-4}$	$0.892 \cdot 10^{-6}$	1.93

The relationship of the condition load effect factor, the overhanging length and the framing space takes the form of the equation:

$$\gamma_c = 0.9969 + 0.00191 \cdot H + 0.00295 \cdot L - 0.001025 \cdot H \cdot L, \quad (6)$$

where H – base frame space (m); L – overhanging length (m).

The application of the above mentioned estimations is quite difficult due to the certain mathematical complexity in use. For this reason in design practice these techniques are difficult to implement. It is therefore suggested to make integrated assessment of reliability and durability according to safety parameters spread assessment (failure range) β for upper and lower limits of the system reliability.

3.4 Discussion

For constructions of vertical cylindrical tanks on the basis of numerical simulation, the values of aerodynamic coefficients for wind influence on the roof of a vertical cylindrical reservoir in the form of a sagging shallow shell, both separately standing and located in the group, were obtained and experimentally confirmed. The testing of models on standard tanks with a convex spherical roof confirmed their adequacy and good conformation with the norms of a number of countries. However, further dissemination of the results to other reservoirs is needed, which is the task of further research.

For the design of a rigid bus the theoretical and experimental results obtained allowed us to justify the rational parameters of devices for damping the oscillations for the first time. Recommendations for their use are given in the regulatory documents of a number of countries [20, 21], but they do not contain any specific recommendations for design. Theoretically, the results obtained are confirmed by studies for systems of one mass [38]. At the same time, it is planned to expand the field of application of the results obtained, including for beam systems with a different cross-section.

The results of studies of the reliability of canopy structures above the tribunes of the cantilevered frame with through cross-section made it possible to propose for the design practice new values of the operating conditions coefficient γ_d for the elements of compressed chords that were absent in the standards [34–36] and provide, the most rational way the required level of reliability of this design with increased responsibility. In this regard, further research requires the question of rethinking the values of the reliability coefficients for the responsibility of the construction, the structure of which is rather complicated and contradictory.

4. Conclusions

1. The specified values of wind pressure aerodynamic coefficients for four reservoirs have been obtained by simulation modeling. It is to provide the specified assessment of the strain-stress state analysis of the structures compared to National Building Codes and Eurocodes applied nowadays.

2. On the grounds of theoretical and experimental research a new method of bending vibrations damping of rigid bar structures has been developed – “a thread-based damper”. It allows to reduce vibration amplitudes in subresonance mode much simpler compared to the common compatibles. The rational parameters of the damper under consideration have been obtained

3. For the first time, on the grounds of the failure analysis of the steel framed and cantilever roofs over stadium stands it has been suggested the structural design algorithm taking into account the geometrical and structural non-linear conditions of the system. The algorithm provides the required reliability level for critical structures.

References

1. Gosstroy SSSR. SNiP II-6-74. *Nagruzki i vozdeystviya* [Building regulations II-6-74. Loads and effects]. Moscow: Stroyizdat, 1976. 58 p. (rus)
2. Gosstroy SSSR. SNiP 2.01.07-85. *Nagruzki i vozdeystviya* [Building regulations 2.01.07-85. Loads and effects]. Moscow: Stroyizdat, 1988. 36 p. (rus)
3. *Nagruzki i vozdeystviya. Aktualizirovannaya redaktsiya SNiP 2.01.07-85*: SP 20.13330.2011* [Loads and effects. Updated version of Building regulations 2.01.07-85*: Set of rules 20.13330.2011]. Moscow: Gosstandart, 2011. 80 p. (rus)
4. Holmes J.D. *Wind Loading of Structures*. London and New

Литература

1. Госстрой СССР. СНиП II-6-74. *Нагрузки и воздействия*. М: Стройиздат, 1976. 58 с.
2. Госстрой СССР. СНиП 2.01.07-85. *Нагрузки и воздействия*. М: Стройиздат, 1988. 36 с.
3. *Нагрузки и воздействия. Актуализированная редакция СНиП 2.01.07-85*: СП 20.13330.2011*. М: Госстандарт, 2011. 80 с.
4. Holmes J.D. *Wind Loading of Structures*. London and New York: Taylor & Francis, 2007. 433 p.
5. Поддаева О.И., Кубенин А.С., Чурин П.С. *Архитектурно-строительная аэродинамика*. М.: Изд-во МИСИ - МГСУ,

Mushchanov V.P., Orzhekhovskii A.N., Zubenko A.V., Fomenko S.A. Refined methods for calculating and designing engineering structures. *Magazine of Civil Engineering*. 2018. No. 2. Pp. 101–115. doi: 10.18720/MCE.78.8.

- York: Taylor & Francis, 2007. 433 p.
5. Poddaeva O.I., Kubenin A.S., Churin P.S. *Arhitekturno-stroitel'naya aerodinamika* [Architectural and construction aerodynamics]. Moscow: Izdatelstvo MISI - MGSU, 2015. 88 p. (rus)
 6. Kondrov Ya.V., Pripadchev A.D., Gorbunov A.A. *Aerodinamika zhylykh i promyshlennykh ob"ektov s vysokoy parusnost'yu* [Aerodynamics of residential and industrial facilities with high windage]. *Materialy Vserossiyskoy nauchno-metodicheskoy konferentsii (Universitetskiy kompleks kak regional'ny tseñtr obrazovaniya, nauki i kul'tury)* [Proceedings of conference]. Orenburg: Izdatelstvo OGU, 2017. Pp. 116–119 (rus)
 7. Gorokhov Ye.V., Kuznetsov S.G. *Eksperimentalnyye metody opredeleniya vetrovykh nagruzok na zdaniya i sooruzheniya* [Experimental methods of determination of the wind loading on building and structures]. Donetsk: Nord-Press, 2009. 169 p. (rus)
 8. Kinash R.I., Kopylov A.E. *Issledovanie aerodinamicheskikh parametrov sistemy iz dvuh krugovykh tsilindrov* [Investigation of aerodynamic parameters of a system of two circular cylinders]. *Vestnik Donbasskoy natsionalnoy akademiiy stroitelstva i arhitekturyi*. 2007. No. 6(68). Pp. 32–40. (rus)
 9. Uematsu Y., Koo C. Wind-tunnel study of wind loads on circular cylindrical structures. *Journal of Wind Engineering*. 2008. No. 33. Pp. 17–25. (jap)
 10. Zhao Y. Wind loads on large cylindrical open-topped tanks in group. *Journal of Thin-Walled Structures*. 2014. No. 78. Pp. 108–120.
 11. Zhang Y. Comparison of microburst-wind loads on low-rise structures of various geometric shapes. *Journal of Wind Engineering and Industrial Aerodynamics*. 2014. No. 133. Pp. 181–190.
 12. Zhang Y. *Study of microburst-like wind and its loading effects on structures using impinging-jet and cooling-source approaches* [Online]. Syst. requirements: AdobeAcrobatReader. URL: <http://lib.dr.iastate.edu/cgi/viewcontent.cgi?article=4194&context=etd> (date of reference: 15.06.2017).
 13. Ereemeev P.G. *Prostranstvennyye tonkolistovyye metallicheskie konstruksii pokryitiy*. Nauchnoe izdanie [Dimensional metal thin sheet constructions of coverages. Scientific edition]. Moscow: Izdatelstvo ASV, 2006. 560 p. (rus)
 14. Ereemeev P.G. *Sovremennyye stalnyye konstruksii bolsheproletnykh pokryitiy unikalnykh zdaniy i sooruzheniy* [Modern steel constructions of long-span coverages of unique building and structures]. Moscow: Izdatelstvo ASV, 2009. 336 p. (rus)
 15. Michalski A., Gawenat B., Gellenne Ph., Haug E. Computational wind engineering of large umbrella structures. *Journal of Wind Engineering and Industrial Aerodynamics*. 2015. Vol. 144. Pp. 96–107.
 16. Okaze T., Takano Y., Mochida A., Tominaga Y. Development of a new $k-\epsilon$ model to reproduce the aerodynamic effects of snow particles on a flow field. *Journal of Wind Engineering and Industrial Aerodynamics*. 2015. Vol. 144. Pp. 118–124.
 17. Togbenou K., Li Y., Chen N., Liao H. An efficient simulation method for vertically distributed stochastic wind velocity field based on approximate piecewise wind spectrum. *Journal of Wind Engineering and Industrial Aerodynamics*. 2016. Vol. 151. Pp. 48–59.
 18. Ndione J., Yoshino H., Mochida A. New Method of Coupling Multizone and CFD for Building Simulation // *Journal of Asian Architecture and Building Engineering*. 2008. Vol. 7. No. 1. Pp. 125–129.
 19. Державний комітет України по нафті і газу. *Проектування складів нафти і нафтопродуктів з тиском насичених парів не вище 93,3 кПа ВБН В 2.2-58.1-94*. Київ, 1994. 150 с.
 20. СОУ 40.1-32385941-38:2011 *Загальні технічні вимоги до проектування та експлуатації конструкцій жорсткої ошиновки у відкритих розподільчих установках напругою від 110 до 750 кВ*. Київ: Об'єднання енергетичних підприємств «ГРІФРЕ», 2011. 21 с.
 21. СОУ 40.1-32385941-39:2011 *Проектування жорсткої ошиновки у відкритих розподільчих установках напругою від 110 до 750 кВ*. Київ: Об'єднання енергетичних підприємств «ГРІФРЕ», 2011. 84 с.
 22. Ржаницын А.Р. *Теория расчета строительных конструкций на надежность*. М.: Стройиздат, 1978. 2015. 88 с.
 6. Кондров Я.В., Припадчев А.Д., Горбунов А.А. *Аэродинамика жилых и промышленных объектов с высокой парусностью* // *Материалы Всероссийской научно-методической конференции (Университетский комплекс как региональный центр образования, науки и культуры)*. Оренбург: Изд-во ОГУ, 2017. С. 116–119.
 7. Горохов Е.В., Кузнецов С.Г. *Экспериментальные методы определения ветровых нагрузок на здания и сооружения*. Донецк: Норд-Пресс, 2009. 169 с.
 8. Кинаш Р.И., Копылов А.Е. *Исследование аэродинамических параметров системы из двух круговых цилиндров* // *Вестник Донбасской национальной академии строительства и архитектуры*. 2007. № 6(68). С. 32–40.
 9. Uematsu Y., Koo C. Wind-tunnel study of wind loads on circular cylindrical structures // *Journal of Wind Engineering*. 2008. № 33. Pp. 17–25. (jap)
 10. Zhao Y. Wind loads on large cylindrical open-topped tanks in group // *Journal of Thin-Walled Structures*. 2014. № 78. Pp. 108–120.
 11. Zhang Y. Comparison of microburst-wind loads on low-rise structures of various geometric shapes // *Journal of Wind Engineering and Industrial Aerodynamics*. 2014. № 133. Pp. 181–190.
 12. Zhang Y. *Study of microburst-like wind and its loading effects on structures using impinging-jet and cooling-source approaches* [Электронный ресурс]. Систем. требования: AdobeAcrobatReader. URL: <http://lib.dr.iastate.edu/cgi/viewcontent.cgi?article=4194&context=etd> (дата обращения: 15.06.2017).
 13. Еремеев П.Г. *Пространственные тонколистовые металлические конструкции покрытий*: Научное издание. М.: Изд-во АСВ, 2006. 560 с.
 14. Еремеев П.Г. *Современные стальные конструкции большепролетных покрытий уникальных зданий и сооружений*. М.: Изд-во АСВ, 2009. 336 с.
 15. Michalski A., Gawenat B., Gellenne Ph., Haug E. Computational wind engineering of large umbrella structures // *Journal of Wind Engineering and Industrial Aerodynamics*. 2015. Vol. 144. Pp. 96–107.
 16. Okaze T., Takano Y., Mochida A., Tominaga Y. Development of a new $k-\epsilon$ model to reproduce the aerodynamic effects of snow particles on a flow field // *Journal of Wind Engineering and Industrial Aerodynamics*. 2015. Vol. 144. Pp. 118–124.
 17. Togbenou K., Li Y., Chen N., Liao H. An efficient simulation method for vertically distributed stochastic wind velocity field based on approximate piecewise wind spectrum // *Journal of Wind Engineering and Industrial Aerodynamics*. 2016. Vol. 151. Pp. 48–59.
 18. Ndione J., Yoshino H., Mochida A. New Method of Coupling Multizone and CFD for Building Simulation // *Journal of Asian Architecture and Building Engineering*. 2008. Vol. 7. No. 1. Pp. 125–129.
 19. Державний комітет України по нафті і газу. *Проектування складів нафти і нафтопродуктів з тиском насичених парів не вище 93,3 кПа ВБН В 2.2-58.1-94*. Київ, 1994. 150 с.
 20. СОУ 40.1-32385941-38:2011 *Загальні технічні вимоги до проектування та експлуатації конструкцій жорсткої ошиновки у відкритих розподільчих установках напругою від 110 до 750 кВ*. Київ: Об'єднання енергетичних підприємств «ГРІФРЕ», 2011. 21 с.
 21. СОУ 40.1-32385941-39:2011 *Проектування жорсткої ошиновки у відкритих розподільчих установках напругою від 110 до 750 кВ*. Київ: Об'єднання енергетичних підприємств «ГРІФРЕ», 2011. 84 с.
 22. Ржаницын А.Р. *Теория расчета строительных конструкций на надежность*. М.: Стройиздат, 1978.

- nasy'cheny'x pariv ne vy'shhe 93,3 kPa VBN V 2.2-58.1-94 [Designing of oil and oil products with a pressure of saturated vapor no higher than 93.3 kPa VBN V 2.2-58.1-94]. Kiev, 1994. 150 p. (ukr)
20. *SOU 40.1-32385941-38:2011* Zagal'ni texnichni vy'mogy' do proektuvannya ta ekspluatatsiyi konstrukcij zhorstkoyi oshy'novky' u vidkry'ty'x rozpodil'chy'x ustanovkax naprugoyu vid 110 do 750kV [General technical requirements for the design and operation of hardwall structures in open-circuit switching installations from 110 to 750 kV]. Kyiv: Union of Power Enterprises "GRIFRE", 2011. 21 p. (ukr)
 21. *SOU 40.1-32385941-39:2011* Proektuvannya zhorstkoyi oshy'novky' u vidkry'ty'x rozpodil'chy'x ustanovkax naprugoyu vid 110 do 750kV [Designing of a hard bushing in open distribution installations with voltage from 110 to 750 kV]. Kyiv: Union of Power Enterprises "GRIFRE", 2011. 84 p. (ukr)
 22. Rzhaniysin A.R. *Teoriya raschyota stroitelnykh konstruktsiy na nadyozhnost* [The theory of calculating building structures for reliability]. Moscow: Stroyizdat, 1978. 239 p. (rus)
 23. Bolotin V.V. *Metodyi teorii veroyatnostey i teorii nadyozhnosti v raschYotah sooruzheniy* [Methods of probability theory and reliability theory in the calculations of structures]. Moscow: Stroyizdat, 1981. 351 p. (rus)
 24. Rayzer V.D. *Teoriya nadezhnosti sooruzheniy. Nauchnoe izdanie* [Theory reliability of structures. Scientific edition]. Moscow: Izdatelstvo ASV, 2010. 384 p. (rus)
 25. Pichugin S.F. *Nadyozhnost stalnykh konstruktsiy proizvodstvennykh zdaniy*. [Reliability of industrial building steel structures]. Moscow: Izdatelstvo ASV, 2011. 456 p. (rus)
 26. Perelmutter A.V. *Izbrannye problemy nadezhnosti i bezopasnosti stroitelnykh konstruktsiy. Nauchnoe izdanie* [Selected problems of reliability and safety of building structures. Scientific edition]. Moscow: Izdatelstvo ASV, 2007. 254 p. (rus)
 27. Timashev S.A. *Nadezhnost bolshih mekhanicheskikh sistem* [Reliability of large mechanical systems]. Moscow: Nauka, 1982. 184 p. (rus)
 28. Ayzhen A.M., Rotshteyn D.M. K veroyatnostnoy otsenke snegovoy nagruzki [To the probabilistic estimation of the snow load]. *Stroitel'naya mehanika i raschet sooruzheniy*. 1981. No. 5. Pp. 7–9. (rus)
 29. Gorokhov Ye., Mushchanov V., Pryadko Iu. Ensuring the required level of reliability during the design stage of latticed shells with a large opening. *Journal of Civil Engineering and Management*. 2015. Vol. 21. No. 3. Pp. 282–289.
 30. Gorokhov Ye., Mushchanov V., Pryadko Iu. Reliability provision of rod shells of steady roofs over stadium stands at stage of design work. *Procedia Engineering*. 2013. Vol. 57. Pp. 353–363.
 31. Mushchanov V., Gorokhov Ye., Vardanyan A., Kashchenko M., Nemova D. Particular futures of calculation and design of long-span membrane roofs. *Procedia Engineering*. 2015. Vol. 117. Pp. 990–1000.
 32. Priadko I.N., Mushchanov V.P., Bartolo H., Vatin N.I., Rudnieva I.N. Improved numerical methods in reliability analysis of suspension roof joints. *Magazine of Civil Engineering*. 2016. No. 5(65). Pp. 27–41.
 33. Krejsa M., Janas P., Krejsa V., Application of the DOProC method in solving reliability problems. *Applied Mechanics and Materials*. 2016. No. 821. Pp. 717–724.
 34. *DBN V 1.2-14-2009*. Zagal'ni pry'ncy'py' zabezpechennya nadijnosti ta konstrukty'vnoyi bezpeky' budivel', sporud, budivel'ny'x konstrukcij ta osnov [General principles of maintenance of reliability and constructive safety of buildings, structures, building constructions and bases]. 239 с.
 23. Болотин В.В. Методы теории вероятностей и теории надежности в расчетах сооружений. М.: Стройиздат, 1981. 351 с.
 24. Райзер В.Д. Теория надежности сооружений. Научное издание. М.: Изд-во АСВ, 2010. 384 с.
 25. Пичугин С.Ф. Надежность стальных конструкций производственных зданий: Монография. М.: Изд-во АСВ, 2011. 456 с.
 26. Перельмутер А.В. Избранные проблемы надежности и безопасности строительных конструкций. Научное издание. М.: Изд-во АСВ, 2007. 254 с.
 27. Тимашев С.А. Надежность больших механических систем. М.: Наука, 1982. 184 с.
 28. Айзен А.М., Ротштейн Д.М. К вероятностной оценке снеговой нагрузки // Строительная механика и расчет сооружений. 1981. № 5. С. 7–9.
 29. Gorokhov Ye., Mushchanov V., Pryadko Iu. Ensuring the required level of reliability during the design stage of latticed shells with a large opening // *Journal of Civil Engineering and Management*. 2015. Vol. 21. No. 3. Pp. 282–289.
 30. Gorokhov Ye., Mushchanov V., Pryadko Iu. Reliability provision of rod shells of steady roofs over stadium stands at stage of design work // *Procedia Engineering*. 2013. Vol. 57. Pp. 353–363.
 31. Mushchanov V., Gorokhov Ye., Vardanyan A., Kashchenko M., Nemova D. Particular futures of calculation and design of long-span membrane roofs // *Procedia Engineering*. 2015. Vol. 117. Pp. 990–1000.
 32. Прядко Ю.Н., Мушчанов В.Ф., Бартоло Х., Ватин Н.И., Руднева И.Н. Усовершенствование численных методов расчета надежности узлов висячих покрытий // Инженерно-строительный журнал. 2016. № 5(65). С. 27–41.
 33. Krejsa M., Janas P., Krejsa V., Application of the DOProC method in solving reliability problems // *Applied Mechanics and Materials*. 2016. No. 821. Pp. 717–724.
 34. ДБН В 1.2-14-2009. Загальні принципи забезпечення надійності та конструктивної безпеки будівель, споруд, будівельних конструкцій та основ. К.: Мінрегіонбуд України, 2009. 49 с.
 35. ГОСТ Р 54257-2010. Надежность строительных конструкций и оснований. Основные положения и требования. М.: Стандартинформ, 2011. 20 с.
 36. Eurocode. Basis of structural design: EN 1990:2002+A1. Brussels: Management Centre, 2002. 116 p.
 37. Mushchanov V.P., Zubenko G.V., Moskalenko I.V. Numerical simulation of wind pressure on a vertical cylindrical tank surface // *Metal constructions*. 2013. No. 3. Pp. 173–182.
 38. Денисов Е.В., Фоменко С.А. Особенности применения конструкций жесткой ошиновки в открытых распределительных устройствах // Металлические конструкции. 2011. Т. 17. № 1. С. 13–23.

- Kiev: Minregionbud Ukrayiny, 2009. 49 p. (ukr)
35. *Russian State Standard GOST R 54257-2010. Nadyozhnost stroitelnykh konstruktsiy i osnovaniy. Osnovnyie polozheniya i trebovaniya* [Reliability of building structures and foundations. Basic provisions and requirements]. Moscow: Standartinform, 2011. 20 p. (rus)
 36. *Eurocode. Basis of structural design: EN 1990:2002+A1*. Brussels: Management Centre, 2002. 116 p.
 37. Mushchanov V.P., Zubenko G.V., Moskalenko I.V. Numerical simulation of wind pressure on a vertical cylindrical tank surface. *Metal Constructions*. 2013. No. 3. Pp. 173–182.
 38. Denisov E.V., Fomenko S.A. Osobennosti primeneniya konstruktsiy zhestkoy oshinovki v otkrytykh raspredelitel'nykh ustroystvakh [Features of application of rigid bus designs in outdoor switchgears]. *Metal Constructions*. 2011. Vol. 17. No. 1. Pp. 13–23.

Volodymyr Mushchanov,
+380503680804; volodymyr.mushchanov@mail.ru

Anatoly Orzhekhovskii,
+380958785180; aorzhehovskiy@bk.ru

Anna Zubenko,
+380508159347; zubienko_anna@mail.ru

Serafim Fomenko,
+380503680804; fomenko_sa@mail.ru

Владимир Филиппович Мущанов,
+380503680804;
эл. почта: volodymyr.mushchanov@mail.ru

Анатолий Николаевич Оржеховский,
+380958785180;
эл. почта: aorzhehovskiy@bk.ru

Анна Васильевна Зубенко,
+380508159347;
эл. почта: zubienko_anna@mail.ru

Серафим Александрович Фоменко,
+380503680804; эл. почта: fomenko_sa@mail.ru

© Mushchanov V.P., Orzhekhovskii A.N., Zubenko A.V., Fomenko S.A., 2018

doi: 10.18720/MCE.78.9

Influence of heat conducting inclusions on reliability of the system “sandwich panel – metal frame”

Влияние теплопроводных включений на надежность системы «сэндвич-панель – каркас здания»

**I.S. Vedishcheva,
M.Y. Ananin,**

Ural Federal University named after first president of Russia B.N. Yeltsin, Ekaterinburg, Russia

M. Al Ali,
Technical University in Košice, Košice, Slovak Republic

N.I. Vatin,
Peter the Great St. Petersburg Polytechnic University, St. Petersburg, Russia

**Старший преподаватель Ю.С. Ведищева,
канд. техн. наук, доцент, заведующий
кафедрой М.Ю. Ананьин,**

Уральский федеральный университет им. первого Президента России Б.Н.Ельцина, Екатеринбург, Россия

М. Ал Али,
Технический университет г. Кошице, г. Кошице, Словакия

д-р техн. наук, профессор Н.И. Ватин,
Санкт-Петербургский политехнический университет Петра Великого, г. Санкт-Петербург, Россия

Key words: sandwich panel; temperature field; energy efficiently; thermal bridges; enclosing structures; throat forming screws; heat conduction inclusions

Ключевые слова: сэндвич-панель; температурное поле; энергоэффективность; мостики холода; ограждающая конструкция; самонарезающие винты; теплопроводные включения

Abstract. The paper presents results of numerical research oriented to the influence of heat conducting inclusions on thermo-technical properties of vertical and horizontal sandwich panels. Sandwich panels consist of flat steel sheets and thermal insulation core (from foam polystyrene, foam polyurethane and rock wool). Thread forming screws, which cross the sandwich panel through its depth, and connect the sandwich panel to frame, creates the heat conducting inclusions. The numerical analysis is carried out using software ANSYS. Based on the numerical analysis results, the regression equations for calculation of minimal values of temperature on an internal surface of a vertical sandwich panel are easy to obtain. The analysis of thermal field of the “sandwich panel – metal frame” system shown that the hygiene requirements are not complied. Proposed solution allows the reduction of the influence of heat conducting inclusions on thermo-technical properties.

Аннотация. Представлены результаты численного исследования влияния теплопроводных включений, на теплотехнические свойства стеновых сэндвич-панелей вертикальной и горизонтальной разрезки с плоскими металлическими обшивками и эффективным утеплителем (пенополистирольным, пенополиуретановыми, минераловатным). В качестве теплопроводных включений рассматриваются самонарезающие винты, прорезающие тело панели, с помощью которых панель крепится к каркасу здания – ветровым ригелями или колоннам. Исследование выполняется в программном комплексе ANSYS путем моделирования сэндвич-панели с теплопроводными включениями и, действующего на нее теплового поля, вызванного разностями температур внутреннего и наружного воздуха. По результатам проведения многофакторного численного эксперимента решены уравнения регрессии для вычисления минимального значения температуры на внутренней поверхности ограждающей конструкции, состоящей из панелей вертикальной и горизонтальной разрезки. На основе данных численного эксперимента проводится анализ температурного поля системы «сэндвич-панель – каркас здания». Показано, что при существующей системе крепления сэндвич-панели к каркасу здания не соблюдаются гигиенические требования, регламентирующие температурный перепад между внутренней поверхностью ограждающей конструкции и температурой внутреннего воздуха в помещении.

Ведищева Ю.С., Ананьин М.Ю., Ал Али М., Ватин Н.И. Влияние теплопроводных включений на надежность системы «сэндвич-панель – каркас здания» // Инженерно-строительный журнал. 2018. № 2(78). С. 116–127.

Сделаны выводы о возможности выпадения конденсата водяного пара на внутренней поверхности ограждающих конструкций общественных зданий и промышленных зданий с сухим и нормальным влажностным режимом и внутри сэндвич-панели. Предложен вариант утепления мест крепления сэндвич-панели к каркасу здания.

1. Introduction

Energy saving is the most important task for all industries, including the construction sector. Energy saving in the construction sector is a complex of measures aimed at reducing heat losses during a building life cycle. Design of energy efficient and energy saving structures is the priority area of modern science and technology. It is general knowledge, that the building loses most quantity of heat energy through windows and a ventilation system. However, the building loses more heat energy through a solid wall and roof than considered in the thermo-technical calculation.

Energy efficiency of buildings is a very topical task, so many researches and studies focus on this issue. Some authors compared the different types of external wall insulation in the context of their influence on energy saving and environmental pollution [1]. Other authors describe the tools used to analyze economic life cycle and different facade systems of the building model with the point of energy efficiently and life cycle optimization [2].

The improvement of building economic efficiency is possible by reducing the cost of heating and ventilation process by increasing resistance to heat transfer of building enclosing structures. Reducing the influence of possible "thermal bridges" on the overall resistance to heat transfer achieves these goals. Analysis and studies for the improvement of enclosing structures of buildings are presented in many researches and papers. The possibility of wetting the core of the sandwich panels due to the "thermal bridges" existing is shown in paper [3, 4]. "Thermal bridges" influence can be estimated through the thermotechnical uniformity coefficient. In paper [5] the method of thermotechnical uniformity coefficient evaluation by analyzing thermo grams are accounted. In other way this influence can be estimated through the reduced total thermal resistance [6, 7]. Evaluation of thermal performance of building envelope using the thermo vision control was carried out in papers [8–10]. In [11] non-stationary heat transfer through exterior building envelope was described. Evaluation of efficient of an energy-saving measures complex was carried out in [12–14].

Generally, the cause of heat loss and humidification of wall elements is due to the presence of heat conducting inclusions, which are inevitable for some types of wall. Sandwich panels are in active use as enclosing constructions for different types of buildings [15]. The sandwich panel is a multi-layer structural element consisting of thermal insulation located between flat or profiled metal sheets and fixed to the buildings bearing structure by means of threaded screws. These screws often create "thermal bridges" cross the sandwich panel system.

Thermo-technical properties of sandwich panels are a subject of researches carried out by many authors [13, 16–19]. Mentioned researches focus on the thermo-technical bending analysis of sandwich panels, their non-linear thermal behavior and temperature-bending dependence, using various methods and mathematical equations.

Action of external load together with temperature changes of the surrounding environment affect the global bearing capacity of the structure, so the thermo-technical properties of individual structural elements, including enclosing constructions, can also influence this bearing capacity. The research of some authors was oriented to polymer foam core exposed to elevated temperature and possible changes of sandwich structures behavior, other authors dealt with sandwich panels subjected to compression and/or bending load from the stability and serviceability point of view [20–23]. Therefore, loads and temperature changes are essential in the analysis of sandwich panels' behavior.

The development of computer technologies and software environments allow the researchers for more sophisticated and effective approaches for the solving of challenge tasks and simulations using different FEM based mathematical models and numerical analysis. Researchers, using the mentioned possibilities, can create 3D models of composite structures consisting of materials with different properties in various directions and investigate the behavior of individual layers and elements from the thermal, deflection, stiffness point of view and so on [24–31].

The purpose of this research is the numerical study of thermo-technical behavior of sandwich panels consisting of two flat steel sheets and core from different materials, such as polystyrene foam, polyurethane foam and rock wool and the investigation of the sandwich panels and frame elements

humidity due to the external and internal temperature differences. The thermo-technical behavior is undergoing investigation using CAE-software with thermal field simulation.

The objective of this study is to investigate the influence of fasteners on the thermal behavior of the wall of the sandwich panels.

2. Methods

2.1. Types of sandwich panels

The numerical analysis of this study covered two types of sandwich panels: the first type named vertical sandwich panel has vertical size more than horizontal size (Figure 1) and the second type named horizontal sandwich panel has vertical size less than horizontal size (Figure 2).

The two types of sandwich panels mounting are existed: with use of vapor and vibration barrier films and without it. For this research we considered the variant without vapor and vibration barrier films.

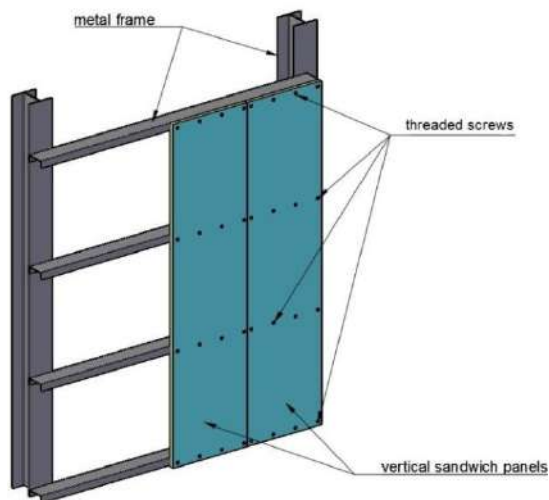


Figure 1. Vertical sandwich panels

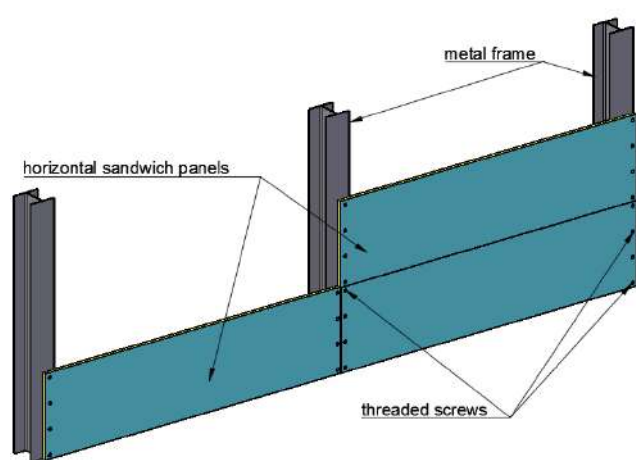


Figure 2. Horizontal sandwich panels

2.2. The determination of the temperature values and humidity near fastening elements

Sandwich panels were: width 1.2 m; length 6.0 m; steel sheet's thickness 0.5 mm; core thickness 100 mm. Next analysis covers a part of sandwich wall structure at the connection of the four sandwich panels. Dimensions of considered part were 1.2 x 6.0 m (Figure 3).

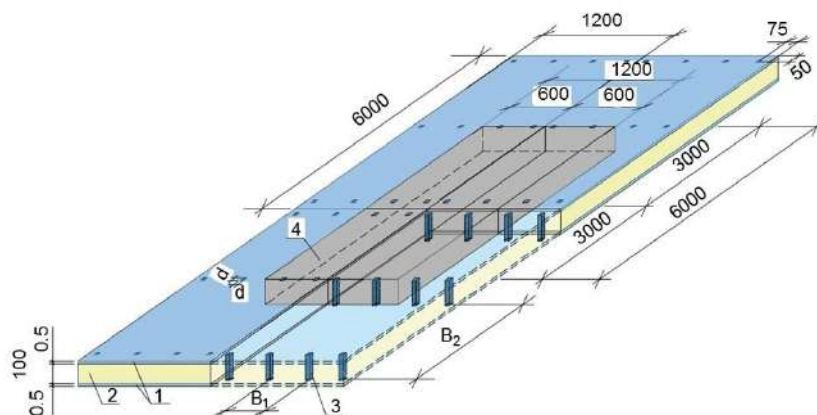


Figure 3. Part of sandwich wall structure: 1 – steel sheets, 2 – core, 3 – threaded screws, 4 – considered part of the wall

The transverse spacing of the screws (B_1) was 350 mm for both types of the sandwich panels (vertical and horizontal sandwich panels). The longitudinal spacing of the screws (B_2) for vertical sandwich panels was 1475 mm, for horizontal sandwich panels as 6000 mm.

The joint profile between panels wasn't included in this numerical model because its thermal losses are less than thermal losses through screws.

Presented values of different coefficients in this paper are actual for the time of numerical analysis and modeling realization. The model of sandwich panel core was isotropic material. This material's characteristics are: heat transfer coefficient (λ_c); 0.05 W/(m·°C); specific heat 0.84 J/(kg·°C); density 110 kg/m³. For the purpose of finite element mesh simplification, the connecting screws had square cross-sections without threads. This solution does not affect the target or expected results of the thermo-technical analysis. Screws had dimension 6.3 mm and density 7871 kg/m³ for steel [32] in the model. The heat transfer coefficient of the screws was 44.5 W/(m·°C). Material of steel sheets had the following characteristics: heat transfer coefficient 58 W/(m·°C); specific heat 482 J/(kg·°C); density 7871 kg/m³.

ANSYS 3D finite elements model consisted of 8-nodes thermal solid elements (SOLID 70). Temperature was the only element's degree of freedom in each node. The Boolean operations had allowed creating the correct model. The model's finite hexagon sweep-elements mesh size was 0.014 m.

Convection on areas is the boundary condition. The external sheet had following parameters: film coefficient 23 W/(m²·°C), bulk temperature -35 °C. The internal sheet parameters were: film coefficient 8.7 W/(m²·°C), bulk temperature 20 °C.

The ANSYS temperature field calculation gave node temperature volumes on the external surface (τ_{ext}) and internal surface (τ_{int}) of the structure and gave possibility to determine the average value of the temperatures for both of them.

In addition, temperature data processing included comparison of the:

- minimal values of temperatures on the internal surface of sandwich panel (τ_{int}^{\min}) and the dew point temperatures for two types of buildings: industrial buildings and public places;
- the indoor temperature and temperature of the internal surface of enclosing structure with the temperature gradient, given by Russian national standard [33].

The temperature field near the lengthwise connecting screws also underwent investigation.

2.3. The numerical complete multivariable analysis

Complete multivariable analysis resulted in the equations for calculation of minimal values of temperature on the internal surface of vertical and horizontal sandwich panels. Sandwich panels had: flat steel sheets of thickness 0.5 mm; varied core thickness from 50 mm to 150 mm; heat transfer coefficient from 0.03 W/(m·°C) to 0.05 W/(m·°C). The transverse spacing between screws (B_1) varied from 300 to 500 mm and the longitudinal spacing between screws (B_2) varied from 1500 to 6000 mm. Because the diameter of screws (d) may be also varied according to environment conditions, their diameters in the analysis varied from 5 to 8 mm.

3. Results and Discussion

The numerical analysis results gave the regression equations for the calculation of minimal values of temperature on the internal surfaces of vertical and horizontal sandwich panels:

$$\tau_{int,vert}^{\min} = 21.372 - 1.527 \cdot d - 24.812 \cdot \lambda_c \quad (1)$$

$$\tau_{int,hor}^{\min} = 21.36 - 1.522 \cdot d - 25.125 \cdot \lambda_c \quad (2)$$

Differences between calculation results according to equations 1 and 2 are minimal from the accuracy point of view, so the both equations are applicable.

Figures 4, 5 illustrate the area near fitting location of the sandwich panel to metal frame for analysis of the temperature values on the internal surface of panel (Figures 4, 5).

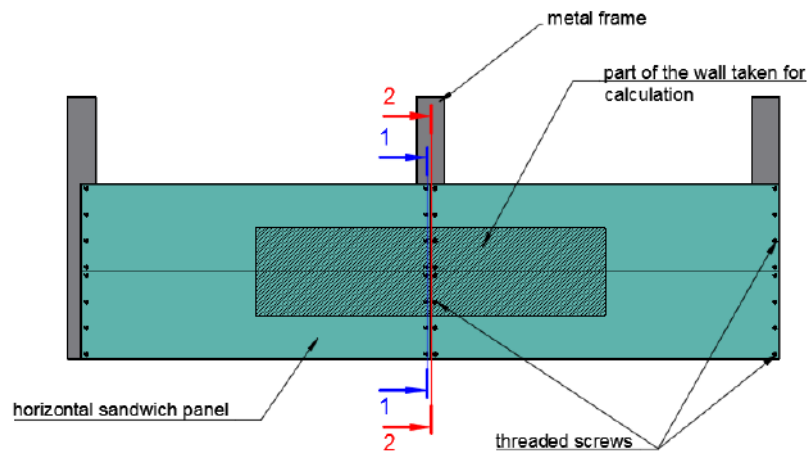


Figure 4. The cross sections of the horizontal sandwich panels with the area for analysis

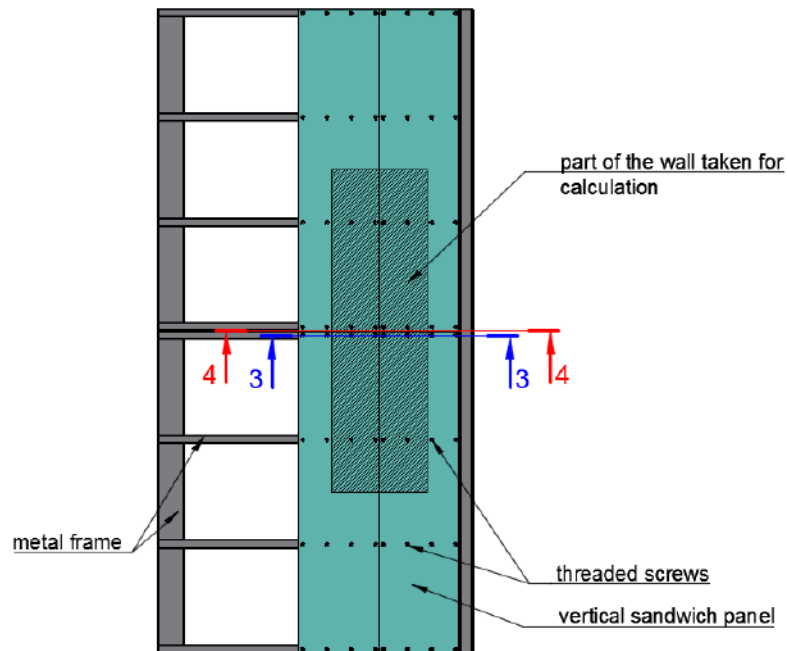


Figure 5. The cross sections of the vertical sandwich panels adopted for analysis

The diagrams (Figures 6–9) show temperature distribution (t , °C) by panel length direction (L , meters). The diagrams demonstrate that the thermal gradient exceeds the requirements values for some types of buildings:

- the green lines ($\Delta t_n(1)$) in the diagrams show the lower limit of standard temperature gradient between internal surface of enclosing structure and indoor temperature for public buildings;
- the red lines ($\Delta t_n(2)$) show the lower limit of standard temperature gradient between internal surface of enclosing and indoor temperature for industrial buildings of dry and normal humidity conditions;
- the violet lines represent the dew point temperature (t_d) for values of relative humidity (φ) 60 %;
- the blue lines represent the dew point temperature (t_d) for values of relative humidity (φ) 55 %;
- the orange lines represent the dew point temperature (t_d) for values of relative humidity (φ) 50 %.

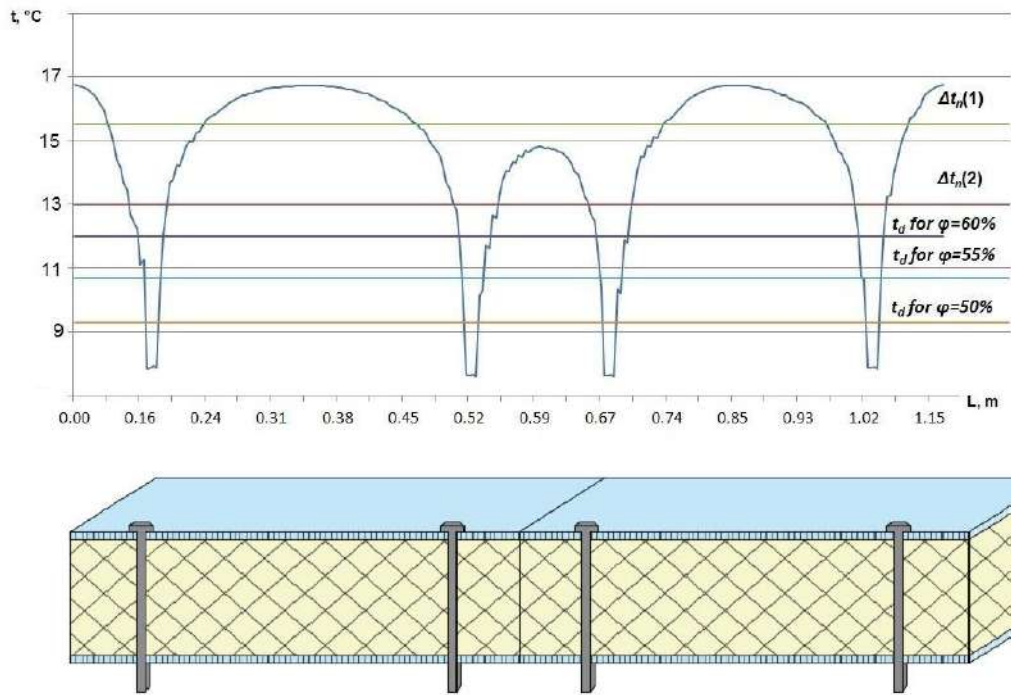


Figure 6. Diagram of temperature distribution along the internal surface of the horizontal sandwich panel. The cross section passes through the screws (section 1-1 Figure 4)

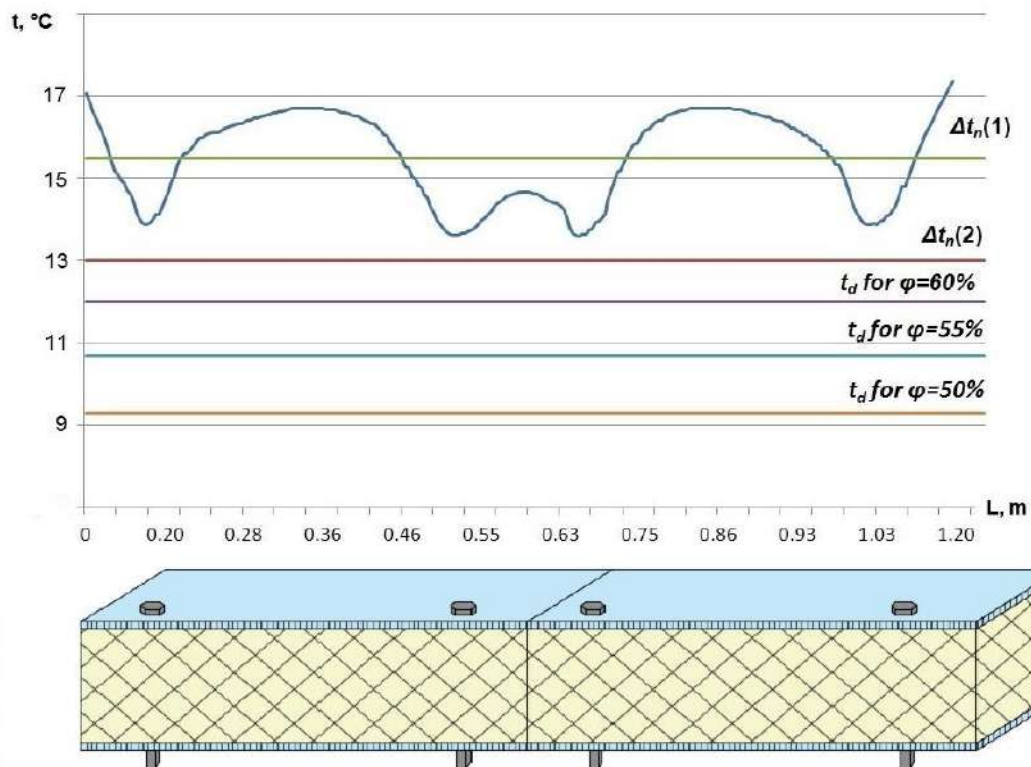


Figure 7. Diagram of temperature distribution along the internal surface of the horizontal sandwich panel. The cross section is at the junction of sandwich panels (section 2-2 Figure 4)

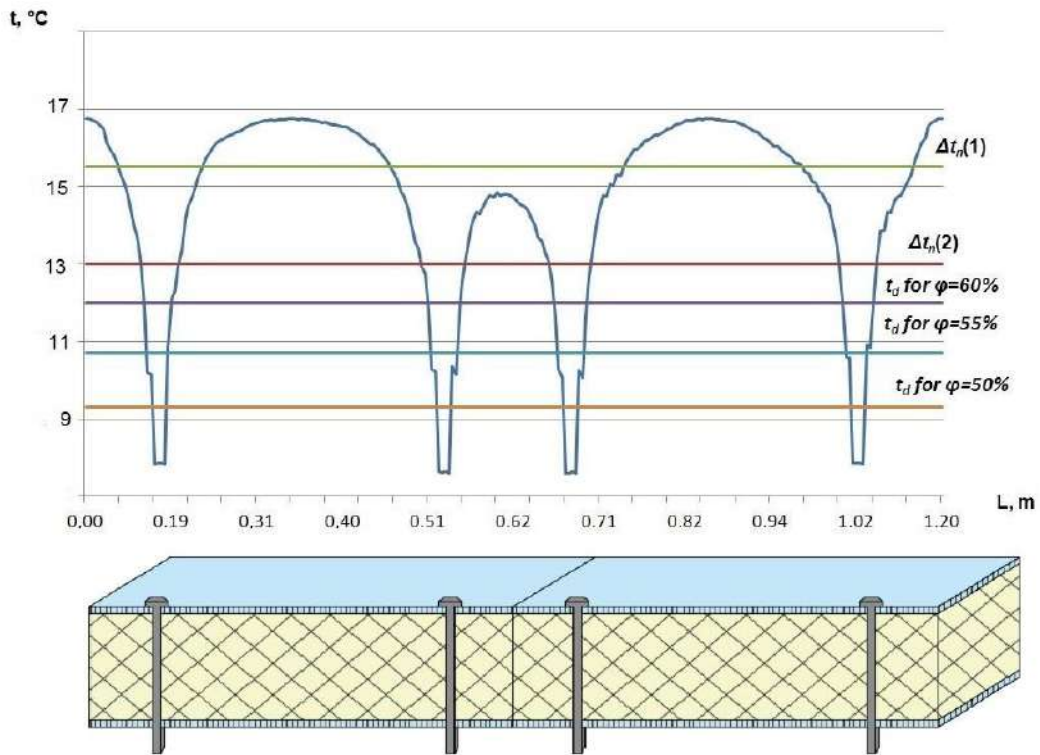


Figure 8. Diagram of temperature distribution along the internal surface of the vertical sandwich panel. The cross section passes through the screws (section 3-3 Figure 5)

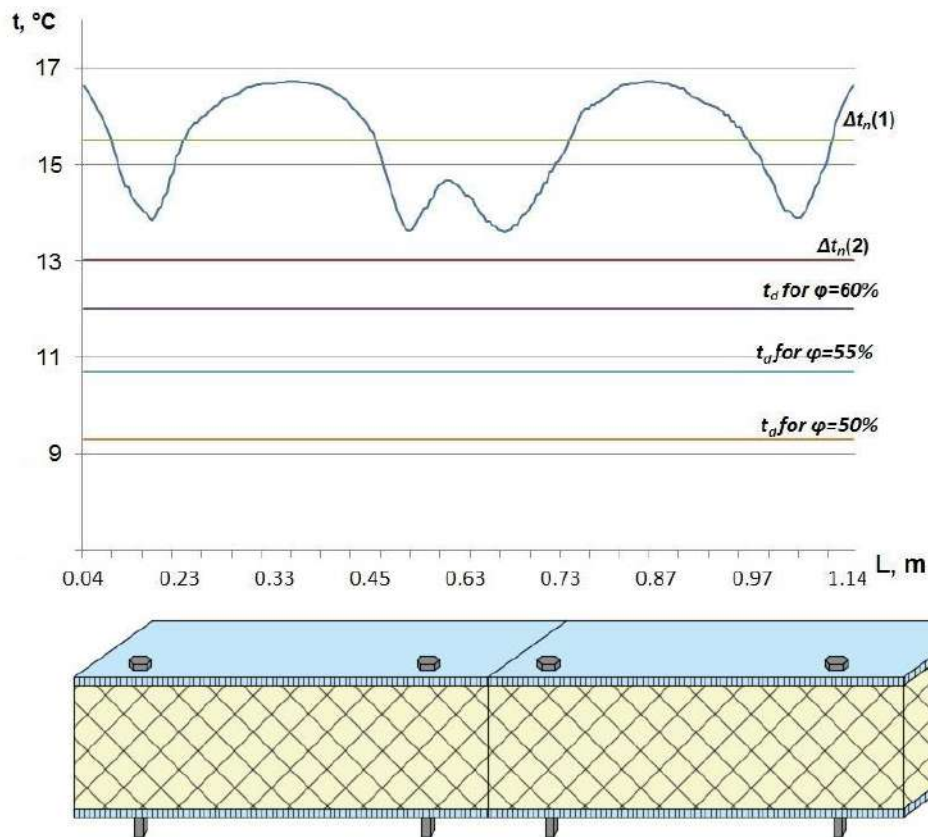


Figure 9. Diagram of temperature distribution along the internal surface of the vertical sandwich panel. The cross section is at the junction of sandwich panels (section 4-4 Figure 5)

The analysis of the thermal field on the internal surface of sandwich panels showed that the thermal gradient between internal surface of enclosing structure, in the case of both horizontal and vertical sandwich panels, and indoor temperatures exceed the nominal values [33] at the bonding locations of panels to frame for public buildings and for industrial buildings of dry and normal humidity conditions.

Obtained results show that temperature on an internal surface of an enclosure structure is less than the dew point temperature for considered parameters – the indoor temperature ($t_{int} = 20\text{ °C}$) and for the relative humidity is $\varphi = 50\%$, $\varphi = 55\%$ and $\varphi = 60\%$. If the value of element temperature less than dew point temperature on the surface of the element than condensation of water vapor is possible. So, condensate formation is possible on an internal surface of enclosure structures.

Based on the results obtained by numerical simulations, following facts became clear: condensate formation is possible on the internal surface of sandwich panels bonded to the frame due to existence of thermally conductive elements. Areas with temperatures less than the rated temperature tend to appear on sandwich panel surface. The width of these areas was 62 mm for industrial buildings of dry and normal humidity indoor conditions, and the width of these areas can achieve 200 mm for public buildings with indoor temperature less than the rated.

In order to eliminate the negative influence of possible condensation on the internal surface of enclosure structure we should use the corrosion protection of fitting locations of sandwich panels to metal frame.

Diagrams for analyzing the humidity conditions of the area near the screws, distribution of temperature values along the screw for places on the surface of screw and near it (Figures 10, 11).

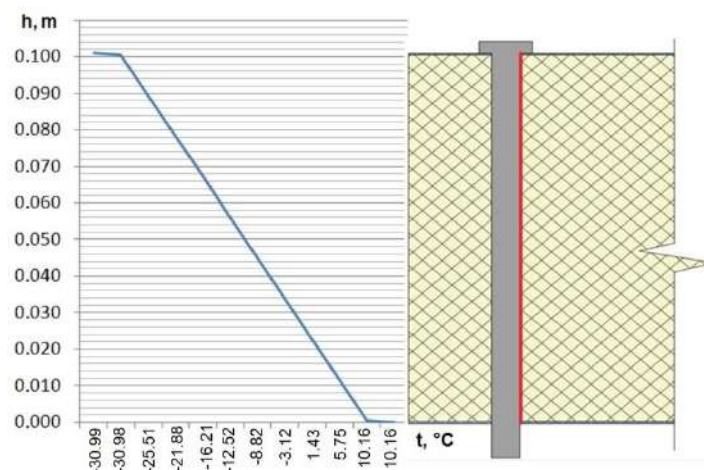


Figure 10. The distribution diagram of temperature values along the screw on surface of screw

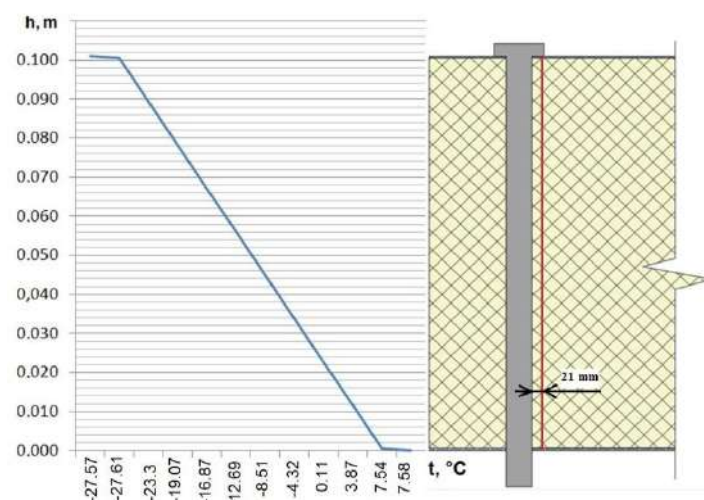


Figure 11. The distribution diagram of temperature values along the screw near screw

The diagrams show that the temperature values at areas located near the screw are less than the dew point temperatures. Therefore, the humidification process at areas located near the screws can be monitored. It follows that besides the internal surfaces, insulation cores of the sandwich panels can be exposed to humidification process. This process results in the reduction of thermal insulation and also in the reduction of sandwich panel life-cycle, because the insulation core is moisture-laden and the steel sheets are exposed to the corrosion process. In addition screws and frame are also exposed to the corrosion process.

Therefore, reduction of thermal insulation properties of sandwich panels, corrosion process of screws, sandwich panel steel sheets and frame, as well as the exceeding of temperature gradient result in the reduction of the construction life-cycle and comfort of people living in the building. Usage of additional thermal insulation at connection locations of sandwich panels to frame by mounting of panel strips with an additional thermal insulation layer may solve the above-mentioned problem. The new type of joint thermal insulation is necessary. One possibility is that we can use a thermal insulation tube when we screw fasteners into sandwich panel (Figure 12).

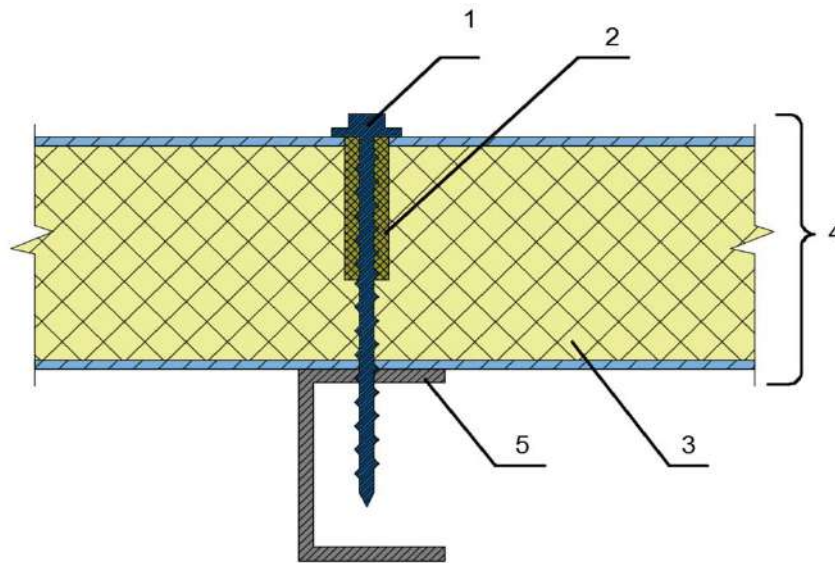


Figure 12. The alternative to thermal insulation at connection location of a sandwich panel to frame: 1 – screw, 2 – thermal insulation tube, 3 – sandwich panel core, 4 – sandwich panel, 5 – frame element

Nylon and plastic expansion bolt shield can work like a thermal insulation tube. According to thermo-technical analysis of sandwich panel with plastic expansion bolt shield thermal insulation tube the temperature gradient between the internal surface of the enclosing structure (the sandwich panel) and the indoor temperature does not exceed the standard temperature gradient near the bolt. In this case, the temperature values near the screw are less than the dew point temperature. This solution is useful to prevent condensate formation in the core near the screw.

Influence of the influence of heat conducting inclusions on thermal properties of sandwich panels can estimate with use reduced total thermal resistance. Author of follow papers [7, 30] had simulated sandwich panel thermo behavior with use other software and obtained thermal fields of roof sandwich panels with screw connections. The results shown that thread forming screws reduce the overall thermal resistance of sandwich panel. Influence of heat conducting inclusions was estimate through the reduced total thermal resistance without temperature values on constructions. This method is useful for practical evaluation by designers and engineers. Both of these methods should be considered together for different engineers tasks.

4. Conclusions

Following the above presented results and analysis, gave possibility to make following conclusions:

1. The equation for calculation of minimal values of temperature on an internal surface of a vertical sandwich panel was obtained.

2. The thermal field of a blank wall from vertical and horizontal sandwich panels was analyzed.
3. For affixing sandwich panels to a frame with thread forming screws with diameter 6.3 mm, the Russian building code hygiene requirements are not complied:
 - 3.1. The temperature gradient between an internal surface of an enclosure structure on affixing locations of a sandwich panel to a frame and the indoor temperature are more than requirements for public buildings and for industrial buildings with dry and normal humidity conditions.
 - 3.2. The temperature on internal surfaces of an enclosure structure is less than the dew point temperature in the fastening points of the sandwich panel to the frame.
4. Thermal insulating effectiveness of sandwich panels is less than designed and sandwich panel steel sheets and thread forming screws and frame elements are in danger of corrosion process. These facts reduce the life cycle of these constructions.
5. Proposed to use nylon and plastic expansion bolt shield like a thermal insulation tube, which makes it possible to reduce the influence of heat conducting inclusions on thermal technical properties.

5. Acknowledgement

This paper is supported by the project ITMS "26220220124": "Research into Filler-Beam Deck Bridges with Encased Beams of Modified Sections".

References

1. Vilcekova S., Sedlakova A., Kridlova Burdova E., Vojtus Ja. Comparison of environmental and energy performance of exterior walls. *Energy Procedia: 6th International Building Physics Conference, IBPC 2015*. 2015. Vol. 78. Pp. 231–236.
2. Kovacic I., Waltenbereger L., Gourlis G. Tool for life cycle analysis of facade-systems for industrial buildings. *Journal of Cleaner Production*. 2016. Vol. 130. Pp. 260–272.
3. Ananin M.Yu., Vedishcheva I.S.. Chislennyye issledovaniya teplotekhnicheskikh svoystv sendvich-paneley [The numerical study of teplotekhnicheskikh properties of sandwich panels]. *Stroitelstvo i obrazovaniye*. 2011. No. 14. Pp. 34–39. (rus)
4. Ananin M.Yu., Vedishcheva I.S. Mnogofaktornoye chislennoye issledovaniye teplotekhnicheskikh svoystv sendvich-paneley vertikalnoy razrezki [Multiply-factor numerical research of heat engineering properties sandwich panels of vertical position]. *Akademicheskyy vestnik UralNIIProyekt RAASN*. 2012. No. 2. Pp. 80–84. (rus)
5. Vasilyev G.P., Lichman V.A., Yurchenko I.A., Kolesova M.V. Method of evaluation of thermotechnical uniformity coefficient by analyzing thermograms. *Magazine of Civil Engineering*. 2016. No. 6. Pp. 60–67.
6. Gaysin A.M., Samokhodova S.Yu., Paymetkina A.Yu., Nedoseko I.V. Cravnitel'naya otsenka udelnykh teplopoter cherez elementy naruzhnykh sten zhilykh zdaniy, opredelyayemykh po razlichnym metodikam [Comparative assessment of specific heat losses through elements of external walls of residential buildings determined by different methods]. *Zhilishchnoye stroitelstvo*. 2016. No. 5. Pp. 36–39. (rus)
7. Tushina O.A. Otsenka teplozashchitnykh svoystv pokrytiy iz sendvich-paneley [Assessing the heat-shielding properties of sandwich panel surfaces]. *Science Review*. 2013. No. 9. Pp. 269–274.
8. Korniyenko S.V., Vatin N.I., Gorshkov A.S. Thermophysical field testing of residential buildings made of autoclaved aerated concrete blocks. *Magazine of Civil Engineering*. 2016. No. 4. Pp. 10–25.
9. Korniyenko S.V. Mnogofaktornaya otsenka teplovogo rezhima v elementakh obolochki zdaniya [Multifactorial forecast of thermal behavior in building envelope elements]. *Magazine of Civil Engineering*. 2014. No. 8(52). Pp. 25–37. (rus)
10. Korniyenko S. Evaluation of thermal performance of residential building envelope. *Procedia Engineering*. 2015.

Литература

1. Vilcekova S., Sedlakova A., Kridlova Burdova E., Vojtus Ja. Comparison of environmental and energy performance of exterior walls // *Energy Procedia: 6th International Building Physics Conference, IBPC 2015*. 2015. Vol. 78. Pp. 231–236. <https://doi.org/10.1016/j.egypro.2015.11.617>
2. Kovacic, I., Waltenbereger, L., Gourlis, G. Tool for life cycle analysis of facade-systems for industrial buildings // *Journal of Cleaner Production*. 2016. Vol. 130. Pp. 260–272. <https://doi.org/10.1016/j.jclepro.2015.10.063>
3. Ананьин М.Ю., Ведищева Ю.С.. Численные исследования теплотехнических свойств сэндвич-панелей // *Строительство и образование*. 2011. № 14. С. 34–39.
4. Ананьин М.Ю., Ведищева Ю.С.. Многофакторное численное исследование теплотехнических свойств сэндвич-панелей вертикальной разрезки. // *Академический вестник УралНИИПроект РААСН*. 2012. №2. С. 80–84.
5. Васильев Г.П., Личман В.А., Юрченко И.А., Колесова М.В. Метод оценки коэффициента теплотехнической однородности из анализа термограмм // *Инженерно-строительный журнал*. 2016. № 6(66). С. 60–67. DOI: 10.5862/MCE.66.6
6. Гайсин А.М., Самоходова С.Ю., Пайметкина А.Ю., Недосеко И.В. Сравнительная оценка удельных теплопотерь через элементы наружных стен жилых зданий, определяемых по различным методикам // *Жилищное строительство*. 2016. № 5. С. 36–39.
7. Туснина О.А. Оценка теплозащитных свойств покрытий из сэндвич-панелей // *Научное обозрение*. 2013. № 9. С. 269–274.
8. Корниенко С.В., Ватин Н.И., Горшков А.С. Натурные теплофизические испытания жилых зданий из газобетонных блоков // *Инженерно-строительный журнал*. 2016. № 4(64). С. 10–25. DOI: 10.5862/MCE.64.2
9. Корниенко С.В. Многофакторная оценка теплового режима в элементах оболочки здания // *Инженерно-строительный журнал*. 2014. № 8(52). С. 25–37.
10. Korniyenko S. Evaluation of thermal performance of residential building envelope // *Procedia Engineering*. 2015. № 117(1). Pp. 191–196.
11. Korniyenko S.V. The experimental analysis and calculative assessment of building energy efficiency // *Applied Mechanics and Materials*. 2014. № 618. Pp. 509–513.
12. Vatin N., Gorshkov A., Nemova D., Tarasova D. Energy efficiency of facades at major repairs of buildings // *Applied*

Vedishcheva I.S., Ananin M.Y., Al Ali M., Vatin N.I. Influence of heat conducting inclusions on reliability of the system "sandwich panel –metal frame". *Magazine of Civil Engineering*. 2018. No. 2. Pp. 116–127. doi: 10.18720/MCE.78.9.

- No. 117(1). Pp. 191–196.
11. Gorshkov A.S., Rymkevich P.P. Diagrammnyy metod opisaniya protsessa nestatsionarnoy teploperedachi [A diagram method of describing the process of non-stationary heat transfer]. *Magazine of Civil Engineering*. 2015. No. 8. Pp. 68–82. (rus)
 12. Vatin N., Gorshkov A., Nemova D., Tarasova D. Energy efficiency of facades at major repairs of buildings. *Applied Mechanics and Materials*. 2014. No. 633-634. Pp. 991–996.
 13. Korniyenko S.V. The experimental analysis and calculative assessment of building energy efficiency. *Applied Mechanics and Materials*. 2014. No. 618. Pp. 509–513.
 14. Meyntser S.V. Bystrovozvodimyye zdaniya promyshlennogo naznacheniya [Prefabricated building of industrial purpose]. *Magazine of Civil Engineering*. 2009. No. 6. Pp. 9–11. (rus)
 15. Li D., Deng Z., Chen G., Xiao H., Zhu L. Thermomechanical bending analysis of sandwich plates with both functionally graded face sheets and functionally graded core. *Composite Structures*. 2017. No. 1692017. Pp. 29–41.
 16. Frostig Y., Thomsen O.T. Non-linear thermal response of sandwich panels with a flexible core and temperature dependent mechanical properties. *Composites: Part B*. 2008. Vol. 39. Pp. 165–184.
 17. Frostig Y., Thomsen O.T. Non-linear behaviour of foam cored curved sandwich panels subjected to thermo-mechanical loading. *ICCM-17*. Edinburgh, Scotland. 2009.
 18. Frostig Y., Thomsen O.T. Non-linear thermo-mechanical behaviour of delaminated curved sandwich panels with a compliant core. *International Journal of Solids and Structures*. 2011. Vol. 48. Pp. 2218–2237.
 19. Zhang S. *Thermomechanical interaction effects in polymer foam cored sandwich structures*: PhD Thesis, University of Southampton, name of the University School or Department, 2013.
 20. Al Ali M., Tomko M., Demjan I. Experimental investigation and theoretical analysis of polystyrene panels with load bearing thin-walled cold-formed elements. *Applied Mechanics and Materials: Trends in Statics and Dynamics of Constructions*. Pfaffikon: Trans Tech Publications Ltd. 2015. Vol. 769. Pp. 145–152.
 21. Sedláková A., et al. Optimal construction solutions of the external wall structures. *Interdisciplinarity in Theory and Practice*. 2015. No. 8. Pp. 157–163.
 22. Lobanov D.S., Vildeman V.E., Babin A.D., Grinev M.A. Experimental research into the effect of external actions and polluting environments on the serviceability of fiber-reinforced polymer composite materials. *Mechanics of Composite Materials*. 2015. No. 1(51). Pp. 69–76.
 23. Četković M., Vuksanović G. Thermal analysis of laminated composite and sandwich plate using layer wise finite element. *Construction of Unique Buildings and Structures*. 2014. No. 5(20). Pp. 7–14.
 24. Petrov S.M. *Nesushchaya sposobnost i deformativnost trekhslonnykh paneley s obshivkami iz metallicheskih i kompozitsionnykh materialov i legkimi zapolnitelyami* [Bearing capacity and deformation of sandwich panels with skins of metal and composite materials and light fillers]: PhD Thesis. Moscow State University of Civil Engineering. Moscow, 2013. (rus)
 25. Seemann R., Krause D. Numerical modelling of nomex honeycomb cores for detailed analyses of sandwich panel joints. *11th World Congress on Computational Mechanics, WCCM 2014, 5th European Conference on Computational Mechanics, ECCM 2014 and 6th European Conference on Computational Fluid Dynamics, ECFD 2014*. 2014. Pp. 2547–2558.
 26. Cernescu A., Romanoff J., Remes H., Faur N., Jelovica J. Equivalent mechanical properties for cylindrical cell honeycomb core structure // *Composite Structures*. 2014. No. 108(1). Pp. 866–875.
 27. Горшков А.С., Рымкевич П.П., Ватин Н.И. Моделирование процессов нестационарного переноса тепла в стеновых конструкциях из газобетонных блоков // *Инженерно-строительный журнал*. 2014. № 8(52). С. 38–48.
 28. Мейнцер С.В. Быстровозводимые здания промышленного назначения. // *Инженерно-строительный журнал*. 2009. № 6 С. 9–11.
 29. Li D., Deng Z., Chen G., Xiao H., Zhu L. Thermomechanical bending analysis of sandwich plates with both functionally graded face sheets and functionally graded core // *Composite Structures*. 2017. № 1692017. Pp. 29–41.
 30. Frostig Y., Thomsen O.T. Non-linear thermal response of sandwich panels with a flexible core and temperature dependent mechanical properties // *Composites: Part B*. 2008. Vol. 39. Pp. 165–184.
 31. Frostig Y., Thomsen O.T. Non-linear behaviour of foam cored curved sandwich panels subjected to thermo-mechanical loading // *ICCM-17* Edinburgh, Scotland. 2009.
 32. Frostig Y., Thomsen O.T. Non-linear thermo-mechanical behaviour of delaminated curved sandwich panels with a compliant core // *International Journal of Solids and Structures*. 2011. Vol. 48. Pp. 2218–2237.
 33. Zhang S. *Thermomechanical interaction effects in polymer foam cored sandwich structures*: PhD Thesis, University of Southampton, name of the University School or Department, 2013.
 34. Al Ali M., Tomko M., Demjan I. Experimental investigation and theoretical analysis of polystyrene panels with load bearing thin-walled cold-formed elements // *Applied Mechanics and Materials: Trends in Statics and Dynamics of Constructions*. Pfaffikon: Trans Tech Publications Ltd. 2015. Vol. 769. Pp. 145–152.
 35. Sedláková A., et al. Optimal construction solutions of the external wall structures // *Interdisciplinarity in Theory and Practice*. 2015. № 8. Pp. 157–163.
 36. Lobanov D.S., Vildeman V.E., Babin A.D., Grinev M.A. Experimental research into the effect of external actions and polluting environments on the serviceability of fiber-reinforced polymer composite materials // *Mechanics of Composite Materials*. 2015. № 1(51). Pp. 69–76.
 37. Четкович М., Вуксанович Дж. Термический анализ ламинированных композитных и сэндвич-панелей с применением многослойного конечного элемента // *Строительство уникальных зданий и сооружений*. 2014. № 5(20). С. 7–14. (англ.)
 38. Петров С.М. Несущая способность и деформативность трехслойных панелей с обшивками из металлических и композиционных материалов и легкими заполнителями: дисс. Москва. канд. техн. наук. Московский государственный строительный университет, Москва, 2013.
 39. Seemann R., Krause D. Numerical modelling of nomex honeycomb cores for detailed analyses of sandwich panel joints // *11th World Congress on Computational Mechanics, WCCM 2014, 5th European Conference on Computational Mechanics, ECCM 2014 and 6th European Conference on Computational Fluid Dynamics, ECFD 2014*. 2014. Pp. 2547–2558.
 40. Cernescu A., Romanoff J., Remes H., Faur N., Jelovica J. Equivalent mechanical properties for cylindrical cell honeycomb core structure // *Composite Structures*. 2014. No. 108(1). Pp. 866–875.
 41. Горшков А.С., Рымкевич П.П., Ватин Н.И. Моделирование процессов нестационарного переноса тепла в стеновых конструкциях из газобетонных блоков // *Инженерно-строительный журнал*. 2014. № 8(52). С. 38–48.

Ведищева Ю.С., Ананьин М.Ю., Ал Али М., Ватин Н.И. Влияние теплопроводных включений на надежность системы «сэндвич-панель – каркас здания» // *Инженерно-строительный журнал*. 2018. № 2(78). С. 116–127.

26. Cernescu A., Romanoff J., Remes H., Faur N., Jelovica J. Equivalent mechanical properties for cylindrical cell honeycomb core structure. *Composite Structures*. 2014. No. 1(108). Pp. 866–875.
27. Gorshkov A.S., Rymkevich P.P., Vatin N.I. Simulation of non-stationary heat transfer processes in autoclaved aerated concrete-walls. *Magazine of Civil Engineering*. 2014. No. 8(52). Pp. 38–48.
28. Tusnina O. A finite element analysis of cold-formed Z-purlins supported by sandwich panels. *Applied Mechanics and Materials*. 2014. Vol. 467. Pp. 398–403.
29. Tusnina O. An influence of the mesh size on the results of finite element analysis of Z-purlins supported by sandwich panels. *Applied Mechanics and Materials*. 2014. Vol. 475–476. Pp. 1483–1486.
30. Tusnina O.A., Tusnin A.R. Programmnyy kompleks dlya teplotekhnicheskogo rascheta stroitelnykh konstruksiy [A computing program for the thermal analysis of building structures]. *Promyshlennoye i grazhdanskoye stroitelstvo* [Industrial and Civil Engineering]. 2014. No. 4. Pp. 76–79. (rus)
31. *Tekhnicheskyy katalog. Stroitelnyye trekhsloynnyye sendvich-paneli. Chast 1. Tekhnicheskkiye kharakteristiki* [The technical catalogue. Construction sandwich panel. Part 1. Specifications]. Obninsk: OOO «Rukki Rus», 2016. Pp. 24.
32. SP 50.13330.2012 Teplovaya zashchita zdaniy. Aktualizirovannaya redaktsiya SNiP 23-02-2003 [Thermal protection of buildings. The updated edition of SNiP 23-02-2003]. M: Minregion Rossii [[The Ministry Of Regional Development], 2012. 96 p.
33. Tusnina O.A. Soyedineniya krovelnykh sendvich-paneley s tonkostennymi gnutymi progonami, vypolnyayemyye na vytyazhnykh zaklepkakh [Joints of Sandwich Panels with Thin-Walled Bent Purlins with the Use of Blind Rivets]. *Promyshlennoye i grazhdanskoye stroitelstvo* [Industrial and Civil Engineering]. 2013. No. 3. Pp. 14–16. (rus)
28. Tusnina O. A finite element analysis of cold-formed Z-purlins supported by sandwich panels // *Applied Mechanics and Materials*. 2014. Vol. 467. Pp. 398–403.
29. Tusnina O. An Influence of the mesh size on the results of finite element analysis of Z-purlins supported by sandwich panels // *Applied Mechanics and Materials*. 2014. Vol. 475–476. Pp. 1483–1486.
30. Туснина О.А., Туснин А.Р. Программный комплекс для теплотехнического расчета строительных конструкций // *Промышленное и гражданское строительство*. 2014. № 4. С. 76–79.
31. Технический каталог. Строительные трехслойные сэндвич-панели. Часть 1. Технические характеристики. Обнинск: ООО «Рукки Рус», 2016. 24 с.
32. СП 50.13330.2012 Тепловая защита зданий. Актуализированная редакция СНиП 23-02-2003. М: Минрегион России, 2012. 96 с.
33. Туснина О.А. Соединения кровельных сэндвич-панелей с тонкостенными гнутыми прогонами, выполняемые на вытяжных заклепках // *Промышленное и гражданское строительство*. 2013. № 3. С. 14–16.

Iuliia Vedishcheva,
+7(903)080-50-00; j.s.vedishcheva@urfu.ru

Michail Ananin,
+7(912)211-81-34; m.y.ananin@urfu.ru

Mohamad Al Ali,
00421905359228; mohamad.al.ali@tuke.sk

Nikolai Vatin,
+7(921)964-37-62; vatin@mail.ru

Юлия Сергеевна Ведищева,
+7(903)080-50-00;
эл. почта: j.s.vedishcheva@urfu.ru

Михаил Юрьевич Ананьин,
+7(912)211-81-34; эл. почта: m.y.ananin@urfu.ru

Мохамад Ал Али,
00421905359228;
эл. почта: mohamad.al.ali@tuke.sk

Николай Иванович Ватин,
+7(921)964-37-62; эл. почта: vatin@mail.ru

© Vedishcheva I.S., Ananin M.Y., Al Ali M., Vatin N.I., 2018

doi: 10.18720/MCE.78.10

Heat dissipation of cement and calculation of crack resistance of concrete massifs

Тепловыделение цемента и расчеты трещиностойкости бетонных массивов

*A.Y. Struchkova,
Yu.G. Barabanshchikov,
K.S. Semenov,
A.A. Shaibakova,
Peter the Great St. Petersburg Polytechnic
University, St. Petersburg, Russia*

*Студент А.Я. Стручкова,
д-р техн. наук, профессор
Ю.Г. Барабанщиков,
канд. техн. наук, доцент К.В. Семенов,
студент А.А. Шайбакова,
Санкт-Петербургский политехнический
университет Петра Великого,
г. Санкт-Петербург, Россия*

Key words: thermal stressed state; thermal cracking resistance; massive concrete and reinforced concrete structures; hydration of cement; building period

Ключевые слова: термонапряженное состояние; термическая трещиностойкость; массивные бетонные и железобетонные конструкции; гидратация цемента; строительный период

Abstract. In this paper, the problems of thermal cracking resistance of massive concrete and reinforced concrete structures during the building period are considered. The calculation results of a research on the effect of hardening temperature on the process of heat dissipation process of concrete are given. The analysis of the thermal stressed state of a massive foundation plate with a fixed thickness of thermal insulation was carried out, the values of the minimum thicknesses of the surface thermal insulation ensuring cracking resistance of structure were obtained. Calculations are performed at various plate heights taking into account the effect of hardening temperature on heat dissipation and without this account. The conducted research demonstrates that not taking into account the effect of hardening temperature on the process of heat dissipation in problems of ensuring cracking resistance of concrete and reinforced concrete massifs leads to a noticeable increase in the required thickness of the necessary thermal insulation.

Аннотация. В настоящей работе рассматриваются вопросы термической трещиностойкости массивных бетонных и железобетонных конструкций в период строительства. Представлены результаты расчетного исследования по оценке влияния температуры твердения на процесс тепловыделения бетона. Проведен анализ термонапряженного состояния массивной фундаментной плиты при фиксированной толщине теплоизоляции, получены значения минимальных толщин поверхностной теплоизоляции, обеспечивающих трещиностойкость конструкции. Расчеты выполнены при различных высотах плиты с учетом влияния температуры твердения на тепловыделение и без данного учета. Проведенное исследование показывает, что не учет влияния температуры твердения на процесс тепловыделения в задачах обеспечения трещиностойкости бетонных и железобетонных массивов приводит к заметному увеличению требуемой толщины необходимой теплоизоляции.

1. Introduction

Calculations of thermal cracking resistance of the massive concrete and reinforced concrete structures during the building period are based on thermal stressed state definition and thermal field irregularity inside of these structures [1–5]. In the design and construction of massive concrete and reinforced concrete structures, much attention is paid to the regulation of the temperature regime of the concrete mix during the construction period [6–9]. This is due to the fact that the reaction of cement hydration during the hardening of concrete leads to the release of a noticeable amount of heat which gives rise to the temperature of concrete [10–14]. The resulting irregular thermal fields in the structure

generate tensile thermal stresses, first on the surface of the structure and then in its central zones, and are the main cause of the formation of thermal cracks [15–17].

Using a complex of special structural and technological measures for the erection (covering the surface of the structure with thermal insulation, peripheral concrete electric cable, forced cooling of the concrete mix, pipe cooling of the plate), it is possible to ensure the absence of thermal cracks in the building period in the construction [18–20]

Calculations of the thermal stressed state of concrete plates in the building period and the assessment of cracking resistance are classified as complex problems in the mechanics of a solid deformed body. Some researchers close to solution of these problems in a simplified variant. The influence of the hardening temperature on the heat dissipation of concrete [21–24] and its deformation characteristics is not taken into account in part of the techniques used in practical calculations at the present time.

The purpose of this work is to estimate the influence of the hardening temperature on the process of heat dissipation of massive concrete and reinforced concrete structures in the calculations of the thermal stressed state and cracking resistance in the building period and the calculation justification for the need for such accounting

2. Methods

Calculation of the thermal stressed state of a concrete foundation slab during the hardening period is carried out with the help of the TERM software developed by the staff on the Structural Mechanics and Building Structures department of the Institute of Civil Engineering at the Peter the Great St.Petersburg Polytechnic University [25]. The program takes into account the influence of temperature on the thermophysical and deformative characteristics of concrete. In order to estimate the cracking resistance of the concrete foundation slab, we would use the deformation criterion suggested by P.I. Vasiliev [13]. According to this criterion, concrete elongation deformations, determined in view of the concrete creep factor and variable deformation modulus, should not exceed the ultimate concrete elongation.

Considering horizontal mats sizes significantly exceed their height, we can study a one-dimensional structural model for the mat central part with the reasonable degree of accuracy. In this model, stress and temperature are functions of the vertical coordinate space.

Consider B35 foundation slab (thickness varies from 1.0 to 3.0 m) with the cement consumption of 340 kg/m³. The concrete bedding layer B12.5 with the grade foundation supports the foundation slab. Thermal and physical characteristics of the concrete B35 are defined by the concrete thermal conductivity $\lambda = 2.67 \text{ W/(m}\cdot\text{°C)}$ and thermal capacity $c = 1.0 \text{ kJ/(kg}\cdot\text{°C)}$. The air temperature is 20 °C, the concrete mix is 20 °C. The top surface of the slab is open – it does not have a special thermal insulation.

The heat dissipation process follows the I.D. Zaporozhets equation [26]. The equation parameters I.D. Zaporozhets gets from experimental evidence on concrete heat dissipation.

$$Q(\tau) = Q_{\max} \left[1 - (1 + A_T \tau) \right]^{-\frac{1}{m-1}} \quad (1)$$

where Q_{\max} – is limit to which heat dissipation of concrete tends;

A_T – the heat release coefficient characterizing the rate of heat release at a constant temperature T;

m – the order of the water hydration reaction, which depends on the type of additives used for portland cement (from 1.1 to 2.3)

The effect of hardening temperature on the heat release of concrete is carried out using the temperature function:

$$f_T = 2^{\frac{T_1 - T_2}{\varepsilon}},$$

where ε – the characteristic temperature difference.

When the the temperature function $T_1 - T_2 = \varepsilon$ is $f_T = 2$, that is when the temperature is raised by ε degrees, the rate of heat dissipation will increase by 2 times.

Struchkova A.Y., Barabanshchikov Yu.G., Semenov K.S., Shaibakova Al.A. Heat dissipation of cement and calculation of crack resistance of concrete massifs. *Magazine of Civil Engineering*. 2018. No. 2. Pp. 128–135. doi: 10.18720/MCE.78.10.

In this paper there is suggested the hypothesis of "reduced time" according to which at times of equal heat dissipation $Q_1 = Q_2$, where Q_1, Q_2 are the heat dissipations at temperatures respectively T_1, T_2 . The ratio of the rates of heat dissipation as well as the corresponding terms τ_2 and τ_1 remains constant throughout the process and equal to the temperature function:

$$\frac{(\partial Q / \partial \tau)_1}{(\partial Q / \partial \tau)_2} = \frac{\tau_2}{\tau_1} = f_T = const$$

The parameters of the heat dissipation process were determined experimentally: heat-liberation value of cement $q = Q / C = 482.2$ kJ/kg; $A_{20} = 2.12 \cdot 10^{-6}$ c⁻¹. The cement consumption C is 340 kg/m³.

As shown in [22] it is possible to neglect the influence of the hardening temperature on the remaining thermophysical characteristics of concrete (thermal diffusivity, heat capacity, thermal conductivity) in calculations of the thermal stressed state of massive concrete and reinforced concrete structures during the building period.

3. Results and Discussion

3.1. Investigation of the effect of temperature hardening on the heat dissipation process

We will illustrate the results of calculations using a 2.0 m thick plate as an example. The graph of the temperature changes in the control points of the slab (top surface, bottom surface and center) is shown in Figure 1

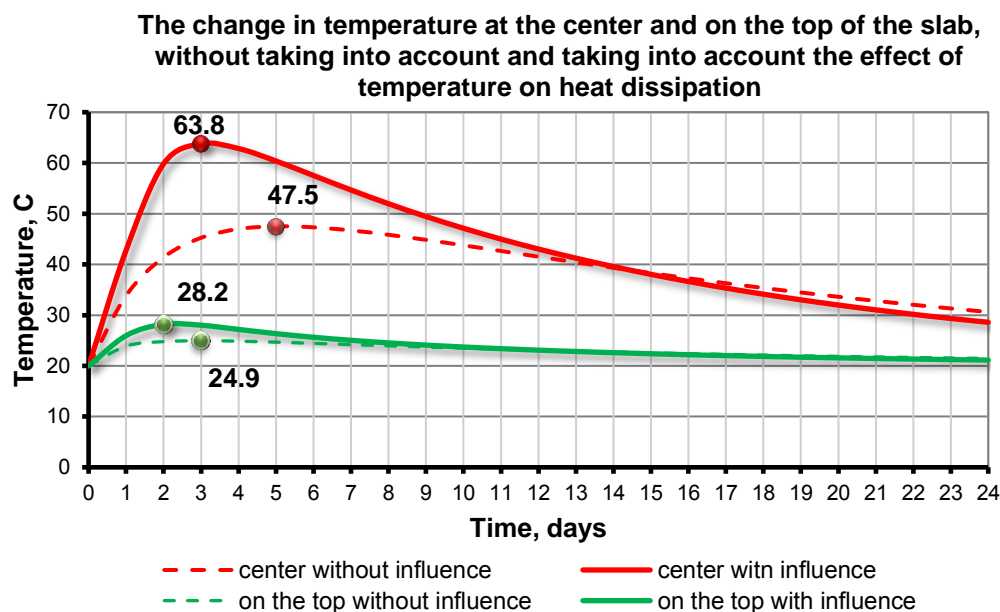


Figure 1. The graph of the temperature dependence in the center and on the top of the slab (solid line with the influence of temperature of hardening, dash line without of such influence)

Analysis of the results shows the following:

1. The nature of the change in temperature in the center and on the upper surface of the base slab in time is the same in both cases.
2. Without taking into account the influence of the hardening temperature on the process of heat generation (dash lines), the maximum temperature in the center of the slab is reached on the 5th day from the moment of laying the mixture and is 47.5 °C, and on the upper surface – on 3-rd day and is 24.9 °C.
3. Accounting for the effect of temperature (solid line) gives a peak at 63.8 °C in the center of the slab for 3rd day, and on the upper surface, the peak occurs on 2nd day and is 28.2 °C.

In such a way ignoring the influence of the hardening temperature on the heat dissipation process leads to an underestimation of the temperature in the center of the plate (by 26 %) and on the upper

surface (by 12 %). The moment of formation of the peak of temperature rise in the structure shifts to an earlier period (from 5 days to 3 days).

Figure 2 shows the graphs of the stress changes at the reference points of the foundation slab (the upper surface and the center) ignoring and taking into account the effect of hardening temperature on the heat dissipation of concrete.

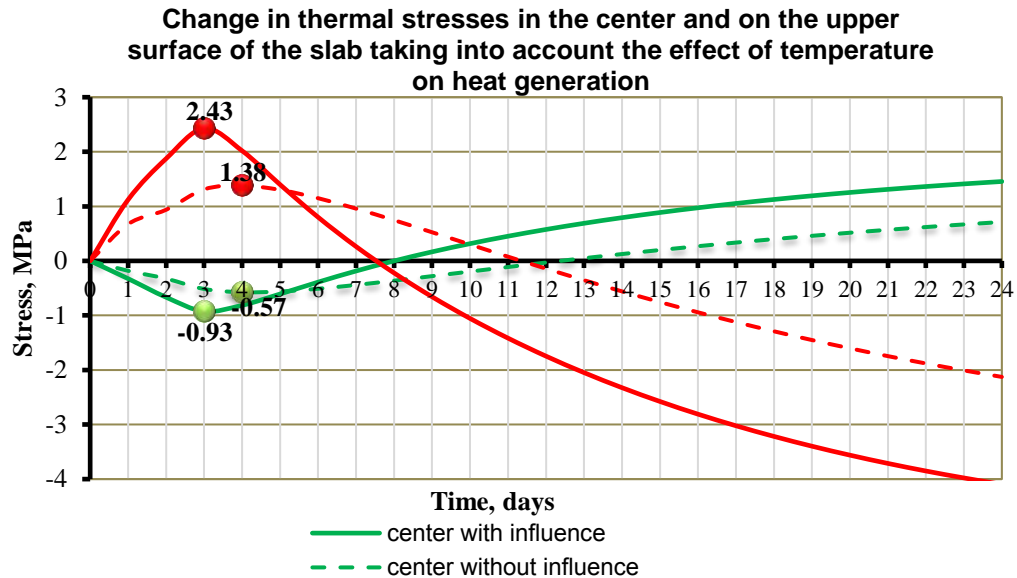


Figure 2. The graph of the dependence of thermal stresses in the center and on the top surface of the slab on time without taking into account and taking into account the effect of hardening temperature on heat dissipation

Analysis of the results shows the following:

1. The character of the change in thermal stresses in the center and on the upper surface of the slab is the same.

2. The maximum stresses at the peak of exothermic warming without taking into account the effect of hardening temperature on the heat dissipation (red dash line) are observed on 4-th day: tensile stresses on the slab surface are 1.38 MPa, compressive in the center are 0.57 MPa. In the first day cracks on the surface of the slab are observed – the criterion for cracking resistance is not satisfied by 35 %. The thickness of the surface layer of thermal insulation ensuring the absence of cracks is 0.5 cm, (coefficient of heat conductivity $\lambda = 0.03 \text{ W / m} \cdot \text{°C}$).

3. Taking into account the effect of hardening temperature on the process of heat dissipation, the maximum stresses are observed on 3-rd day: tensile at the slab surface – 2.43 MPa, compressive in the center of the slab – 0.93 MPa. The formation of cracks is observed in the first day (the criterion is not satisfied by 61 %). The thickness of the surface layer of thermal insulation, ensuring the absence of cracks is 6.1 cm, (coefficient of heat conductivity $\lambda = 0.03 \text{ W / m} \cdot \text{°C}$).

In such a way ignoring the influence of the hardening temperature on the heat dissipation process leads to an underestimation of tensile stresses on the upper surface of the slab by 43 %, and compressive in the center of the plate by 38 %. In addition, dangerous tensile stress at earlier times (shift for one day). The calculation results are close to the actual data [9].

With an increase in the thickness of the foundation slab, an increase in the hardening temperature in the center, on the upper and lower surfaces of the slab was observed, and the thermal stresses at these control points also increased. (Figures 3, 4).

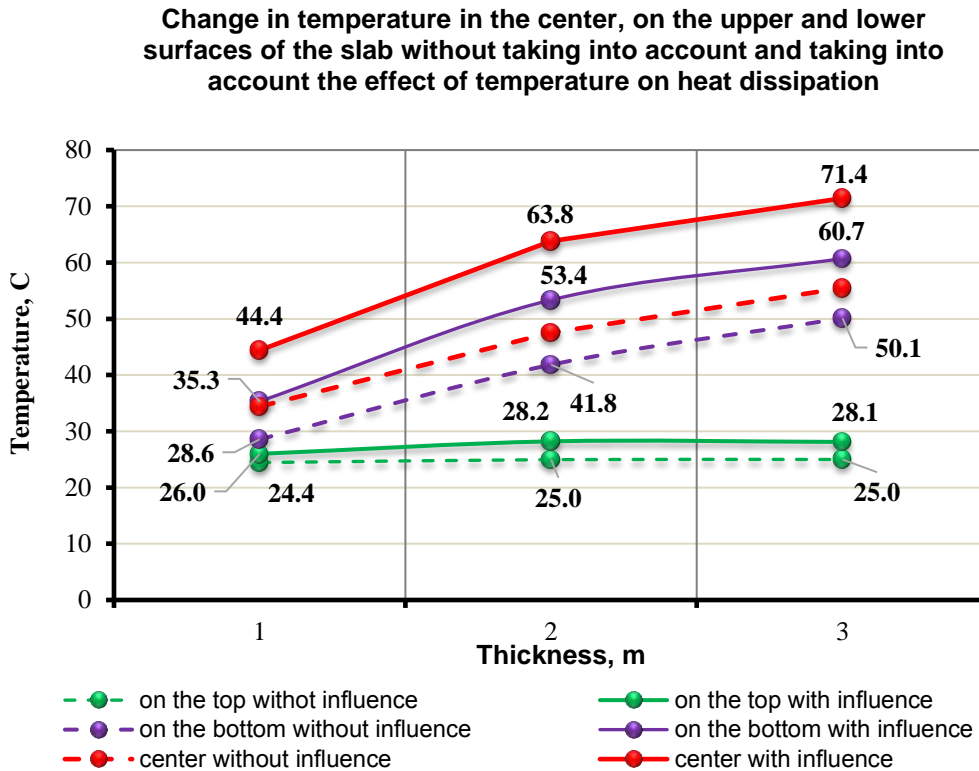


Figure 3. The graph changes the temperature in the center, on the top and bottom surfaces of the plate, depending on the thickness without taking into account and taking into account the influence of the hardening temperature on the heat dissipation

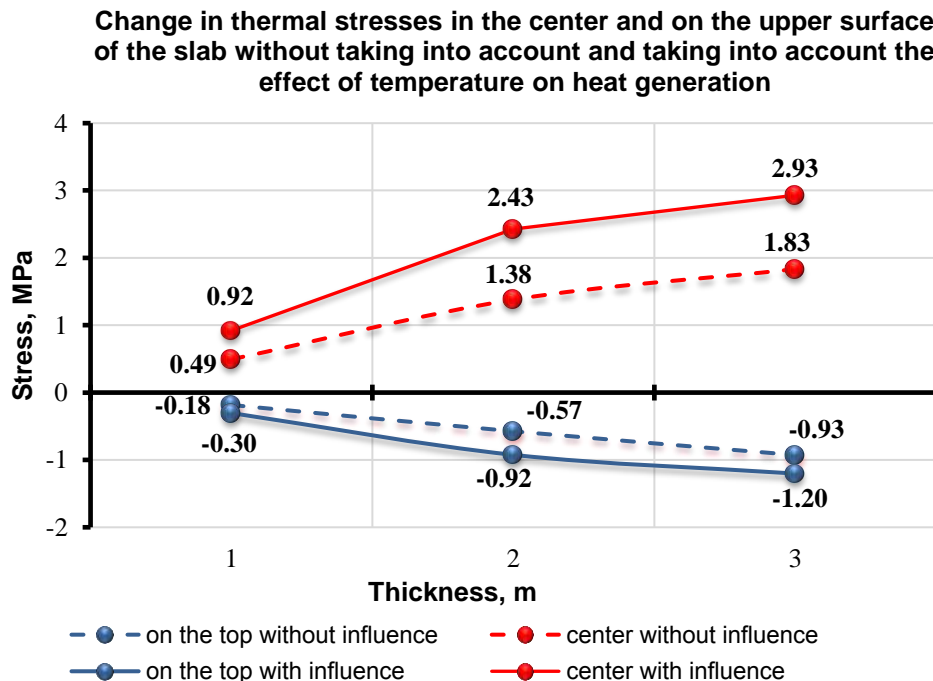


Figure 4. The graph of the dependence of the change in thermal stresses in the center and on the upper surface of the slab depending on the thickness of the slab without taking into account and the influence of the hardening temperature on the heat dissipation

In studies carried out by some authors earlier [21, 22] a calculation evaluation of the effect of hardening temperature on the thermal stressed state of massive concrete hydraulic structures was carried out. As is known, concrete mixtures used for such structures have a relatively low consumption of cement and a relatively low heat dissipation. In this paper concrete was considered with a significant cement consumption, cement also had a relatively high specific heat dissipation (concretes with similar characteristics were used for the construction of base slabs of nuclear power plants and other unique buildings and structures).

4. Conclusions

The results of the conducted experiments allow us to make following conclusions:

1. Not taking into account the effect of hardening temperature on the process of heat generation of massive concrete and reinforced concrete structures in the calculation of the thermal stressed state leads to a significant underestimation of the temperature at control points (up to 26 %) and tensile stresses (up to 43 %) on the slab surface.
2. The safe thicknesses of the surface thermal insulation, determined without taking into account the influence of temperatures, have significant deviations (upwards) from similar values obtained with such influence. Deviations were up to 92 %.
3. When the thickness of the slab is increased from 1.0 to 3.0 m, taking into account the influence of temperature leads to an increase in the maximum temperature in the body of the slab from 22 % to 52 %, and the maximum deformation of elongation on the plate surface is from 21 % to 60 %.

References

1. Vatin N.I., Nemova D.V., Rymkevich P.P., Gorshkov A.S. Influence of building envelope thermal protection on heat loss value in the building. *Magazine of Civil Engineering*. 2012. No. 8. Pp. 1–13. (rus)
2. Vatin N.I., Gorshkov A.S., Nemova D.V. Energy efficiency of envelopes at major repairs. *Construction of Unique Buildings and Structures*. 2013. No. 3(8). Pp. 1–11. (rus)
3. Petrosova D.V., Kuzmenko N.M., Petrosov D.V. A field experimental investigation of the thermal regime of lightweight building envelope construction. *Magazine of Civil Engineering*. 2013. No. 8. Pp. 31–37. (rus)
4. Nemova D.V., Vatin N.I., Gorshkov A.S., Kashabin A.V., Rymkevich P.P., Tseytin D.N. Technical and economic assessment on actions for heat insulation of external envelopes of an individual house. *Construction of Unique Buildings and Structures*. 2014. No. 8(23). Pp. 93–115. (rus)
5. Vatin N.I., Nemova D.V. Increase of power efficiency of buildings of kindergartens. *Construction of Unique Buildings and Structures*. 2012. No. 3. Pp. 1–11. (rus)
6. Korsun V., Vatin N., Korsun A., Nemova D. Physical-mechanical properties of the modified fine-grained concrete subjected to thermal effects up to 200C. *Applied Mechanics and Materials*. 2014. Vol. 633–634. Pp. 1013–1017.
7. Vatin N., Petrichenko M., Nemova D., Staritsyna A., Tarasova D. Renovation of educational buildings to increase energy efficiency. *Applied Mechanics and Materials*. 2014. Vol. 633–634. Pp. 1023–1028.
8. Korsun V., Korsun A. The influence of precompression on strength and strain properties of concrete under the effect of elevated temperatures. *Applied Mechanics and Materials*. 2015. Vol. 725–726. Pp. 469–474.
9. Semenov, K.V., Barabanshchikov, Y.G. Maintenance of thermal cracking resistance in massive concrete base slabs during winter concreting. *Construction of Unique Buildings and Structures*. 2014. No. 2(17). Pp. 125–135. (rus)
10. Aniskin N.A. Prognoz ekzotermicheskogo razogreva massivnykh betonnykh sooruzheniy [Forecast of exothermal heating of massive concrete structures]. *Vestnik MGSU*. 2009. No. 3. Pp. 216–223. (rus)
11. Nguyen Dang Zhang. *Temperaturnyy rezhim betonnykh gravitatsionnykh plotin* [The temperature regime of

Литература

1. Ватин Н.И., Немова Д.В., Рымкевич П.П., Горшков А.С. Влияние уровня тепловой защиты ограждающих конструкций на величину потерь тепловой энергии в здании // Инженерно-строительный журнал. 2012. № 8(34). С. 1–13.
2. Ватин Н.И., Горшков А.С., Немова Д.В. Энергоэффективность ограждающих конструкций при капитальном ремонте // Строительство уникальных зданий и сооружений. 2013. № 3 (8). С. 1–11.
3. Петросова Д.В., Кузьменко Н.М., Петросов Д.В. Экспериментальное исследование теплового режима легкой ограждающей конструкции в натуральных условиях // Инженерно-строительный журнал. 2013. № 8(43). С. 31–37.
4. Немова Д.В., Ватин Н.И., Горшков А.С., Кашабин А.В., Рымкевич П.П., Цейтин Д.Н. Технико-экономическое обоснование мероприятий по утеплению ограждающих конструкций индивидуального жилого дома // Строительство уникальных зданий и сооружений. 2014. № 8(23). С. 93–115.
5. Ватин Н.И., Немова Д.В. Повышение энергоэффективности зданий детских садов // Строительство уникальных зданий и сооружений. 2012. № 3. С. 1–11.
6. Korsun V., Vatin N., Korsun A., Nemova D. Physical-mechanical properties of the modified fine-grained concrete subjected to thermal effects up to 200 0C // Applied Mechanics and Materials. 2014. Vol. 633-634. Pp. 1013-1017.
7. Vatin N., Petrichenko M., Nemova D., Staritsyna A., Tarasova D. Renovation of educational buildings to increase energy efficiency // Applied Mechanics and Materials. 2014. Vol. 633-634. Pp. 1023-1028.
8. Korsun V., Korsun A. The influence of precompression on strength and strain properties of concrete under the effect of elevated temperatures // Applied Mechanics and Materials. 2015. Vol. 725-726. Pp. 469-474.
9. Семенов К.В., Барабанщиков Ю.Г. Термическая трещиностойкость массивных бетонных фундаментных плит и ее обеспечение в строительный период зимой // Строительство уникальных зданий и сооружений. 2014. № 2(17). С. 125–135.

Struchkova A.Y., Barabanshchikov Yu.G., Semenov K.S., Shaibakova Al.A. Heat dissipation of cement and calculation of crack resistance of concrete massifs. *Magazine of Civil Engineering*. 2018. No. 2. Pp. 128–135. doi: 10.18720/MCE.78.10.

- concrete gravity dams]. Cand. tech. sci. diss.. 2006. Moscow, 176 p. (rus)
12. Barabanshchikov Y.G., Semenov K.V., Shevelev M.V. Termicheskaya treshchinostoykost betona fundamentnykh plit [Thermal cracking resistance of concrete foundation mats]. *Populyarnoye betonovedeniye*. 2009. No. 1. Pp. 70–76.
 13. Vasilyev P.I., Ivanov D.A., Kononov Yu.I., Semenov K.V., Starikov O.P. Raschetnoye obosnovaniye razmerov blokov i posledovatelnosti betonirovaniya korpusa reaktora VG - 400 s proverkoj na modeli 1/5 naturalnoy velichiny [Calculation analysis of concreting blocks and VG -400 reactor shell concreting sequence using a 1/5 scale model]. *Problems of atomic science and technology*. 1988. No. 1. Pp. 62–68. (rus)
 14. Semenov K., Barabanshchikov Y. Thermal cracking resistance in massive concrete structures in the winter building period. *Applied Mechanics and Materials*. 2015. Vol. 725–726. Pp. 431–441.
 15. Kim S.G. *Effect of heat generation from cement hydration on mass concrete placement*. Civil Engineering. Master of Science Thesis. Ames: Iowa State University. 2010. 126 p.
 16. Shengxing W., Donghui H. Estimation of cracking risk of concrete at early age based on thermal stress analysis. *Journal of Thermal Analysis and Calorimetry*. 2011. Vol. 105. No. 1. Pp. 171–186.
 17. Zhang Z., Zhang X., Wang X., Zhang T., Zhang X. Merge concreting and crack control analysis of mass -concrete base slab of nuclear power plant. *Applied Mechanics and Materials*. 2011. No. 94–96. Pp. 2107–2110.
 18. Barabanshchikov Y.G., Sokolov V.A., Vasiliev A.S., Shevelev M.V. Regulirovaniye srokov skhvatyvaniya tsementa khimicheskimi dobavkami [Adjustment of cement setup time with chemical admixtures]. *ALITINFORM: Tsement, Beton, Sukhie smesi*. 2012. No. 3(25). Pp. 32–41. (rus)
 19. Barabanshchikov Y.G., Semenov K.V. Increasing the plasticity of concrete mixes in hydrotechnical construction. *Power Technology and Engineering*. 2007. Vol. 41(4). Pp. 197–200.
 20. Trapeznikov L.P. *Temperaturnaya treshchinostoykost massivnykh betonnykh sooruzheniy* [Thermal cracking resistance of mass concrete structures]. Moscow, 1986. 272 p. (rus)
 21. Malinin N.A. *Issledovaniye termonapryazhennogo sostoyaniya massivnykh betonnykh konstruksiy s peremennymi deformativnymi kharakteristikami* [Research of thermal stressed state of mass concrete structures with changing deformations characteristics]. Cand. tech. sci. diss. Leningrad, 1977. 186 p. (rus)
 22. Bredyuk V.I. *Termonapryazhennoye sostoyaniye betonnykh massivov gidrotekhnicheskikh sooruzheniy v stroitelnyy period (vliyaniye peremennykh fiziko-mekhanicheskikh kharakteristik)*. [Thermal stress state of concrete massifs of hydraulic structures in the construction period (influence of variables of physical and mechanical characteristics)]. Abstract Cand. tech. sci. diss. Leningrad, 1988. 22 p. (rus)
 23. Schackowa A., Efftig C., Gomes I. R., Patruni I. Z., Vicenzi F., Kramel C. Temperature variation in concrete samples due to cement hydration. *Applied Thermal Engineering*. 2016. Pp. 1362–1369.
 24. Larson M. *Thermal crack estimation in early age concrete - models and methods for practical application*. Division of Structural Engineering, Lulea University of Technology, Doctoral Thesis (2003) 190 p.
 25. Semenov K.V. *Temperaturnoye i termonapryazhennoye sostoyaniye blokov betonirovaniya korpusa vysokogo davleniya v stroitelnyy period* [Temperature and thermal stressed state of concreting blocks in a high pressure shell during the building period]. Cand. tech. sci. diss. Leningrad,
 10. Анискин Н.А. Прогноз экзотермического разогрева массивных бетонных сооружений // Вестник МГСУ. 2009. № 3. С. 216–223.
 11. Нгуен Данг Жанг. Температурный режим бетонных гравитационных плотин: Дис. на соиск. учен. степ. к. т. н.: Спец. 05.23.07. М., 2006. 176 с.
 12. Барабанщиков Ю.Г., Семенов К.В., Шевелев М.В. Термическая трещиностойкость бетона фундаментных плит // Популярное бетоноведение. 2009. № 1. С. 70–76.
 13. Васильев П.И., Иванов Д.А., Кононов Ю.И., Семенов К.В., Стариков О.П. Расчетное обоснование размеров блоков и последовательности бетонирования корпуса реактора VG-400 с проверкой на модели 1/5 натуральной величины // Вопросы атомной науки и техники. 1988. № 1. С. 62–68.
 14. Semenov K., Barabanshchikov Y. Thermal Cracking Resistance in Massive Concrete Structures in the Winter Building Period // *Applied Mechanics and Materials*. 2015. Vol. 725–726. Pp. 431–441.
 15. Kim S.G. Effect of heat generation from cement hydration on mass concrete placement. Civil Engineering, Master of Science Thesis. Ames: Iowa State University. 2010. 126 p.
 16. Shengxing W., Donghui H. Estimation of cracking risk of concrete at early age based on thermal stress analysis // *Journal of Thermal Analysis and Calorimetry*. 2011. Vol. 105. No. 1. Pp. 171–186.
 17. Zhang Z., Zhang X., Wang X., Zhang T., Zhang X. Merge concreting and crack control analysis of mass -concrete base slab of nuclear power plant // *Applied Mechanics and Materials*. 2011. No. 94–96. Pp. 2107–2110.
 18. Барабанщиков Ю.Г., Соколов В.А., Васильев А.С., Шевелев М.В. Регулирование сроков схватывания цемента химическими добавками // ALITINFORM: Цемент, бетон, сухие смеси. 2012. № 3(25). С. 32–41.
 19. Barabanshchikov Y.G., Semenov K.V. Increasing the plasticity of concrete mixes in hydrotechnical construction // *Power Technology and Engineering*. 2007. No. 41(4). Pp. 197–200.
 20. Трапезников Л.П. Температурная трещиностойкость массивных бетонных сооружений. М.: Энергоатомиздат, 1986. 272 с.
 21. Малинин Н.А. Исследование термонапряженного состояния массивных бетонных конструкций с переменными деформативными характеристиками: Дис. на соиск. учен. степ. к. т. н.: Спец. 05.23.01. Л., 1977. 186 с.
 22. Бредюк В.И. Термонапряженное состояние бетонных массивов гидротехнических сооружений в строительный период (влияние переменных физико-механических характеристик); Автореф. Дис. на соиск. учен. степ. к. т. н. Л., 1988. 22 с.
 23. Schackowa A., Efftig C., Gomes I.R., Patruni I.Z., Vicenzi F., Kramel C. Temperature variation in concrete samples due to cement hydration // *Applied Thermal Engineering*. 2016. Pp. 1362–1369.
 24. Larson M. Thermal crack estimation in early age concrete - models and methods for practical application. Division of Structural Engineering, Lulea University of Technology, Doctoral Thesis, 2003. 190 p
 25. Семенов К.В. Температурное и термонапряженное состояние блоков бетонирования корпуса высокого давления в строительный период: Дис. на соиск. учен. степ. к. т. н.: Спец. 05.23.01. Л., 1990. 156 с.
 26. Запорожец И.Д., Огороков С.Д., Парийский А.А. Тепловыделение бетона. М.: Стройиздат, 1966. 316 с.

Стручкова А.Я., Барабанщиков Ю.Г., Семенов К.В., Шайбакова А.А. Тепловыделение цемента и расчеты трещиностойкости бетонных массивов // Инженерно-строительный журнал. 2018. № 2(78). С. 128–135.

1990. 156 p. (rus)

26. Zaporozhets I.D., Okorokov S.D., Pariyskiy A.A.
Teplovydeleniye betona [Heat Liberation by Concrete].
Leningrad-Moscow, 1966. 316 p. (rus)

Ayyyna Struchkova,
+7(999)229-56-01; *ayyyna_struchkova93@mail.ru*

Yuriy Barabanshchikov,
+7(812)534-12-86; *ugb@mail.ru*

Kirill Semenov,
+7(921)781-19-57; *kvsemenov@bk.ru*

Albina Shaibakova,
+7(927)636-54-64; *albinashaibakova@gmail.com*

Айыына Яковлевна Стручкова,
+7(999)2295601;
эл. почта: *ayyyna_struchkova93@mail.ru*

Юрий Германович Барабанщиков,
+7(812)5341286; эл. почта: *ugb@mail.ru*

Кирилл Владимирович Семенов,
+7(921)7811957; эл. почта: *kvsemenov@bk.ru*

Альбина Айратовна Шайбакова,
+79276365464;
эл. почта: *albinashaibakova@gmail.com*

© Struchkova A.Y., Barabanshchikov Yu.G., Semenov K.S., Shaibakova Al.A., 2018

doi: 10.18720/MCE.78.11

Deformation compatibility of masonry and composite materials

Деформационная совместимость каменной кладки
с композитными материалами**V.V. Bespalov,***Peter the Great St. Petersburg Polytechnic University, St. Petersburg, Russia***D. Ucer,***Middle East Technical University, Ankara, Turkey***I.D. Salmanov,***Peter the Great St. Petersburg Polytechnic University, St. Petersburg, Russia***I.N. Kurbanov,***Saint-Petersburg Mining University, St. Petersburg, Russia***S.V. Kupavykh,***Saint-Petersburg Mining University, St. Petersburg, Russia***Студент В.В. Беспалов,***Санкт-Петербургский политехнический университет Петра Великого,**г. Санкт-Петербург, Россия***М.С., научный сотрудник Д. Ючер,***Middle East Technical University, Анкара, Турция***студент И.Д. Сальманов,****студент И.Н. Курбанов,***Санкт-Петербургский политехнический университет Петра Великого,**г. Санкт-Петербург, Россия***канд. техн. наук, ведущий инженер****С.В. Купавых***Санкт-Петербургский горный университет, г. Санкт-Петербург, Россия***Key words:** masonry; FRP; simulation; deformation compatibility; composite materials; compression-bending element**Ключевые слова:** каменная кладка; симуляция; поверхностное армирование; композитные материалы; сжато-изогнутые элементы; деформационная совместимость

Abstract. Fiber Reinforced Polymers (FRP) are commonly used nowadays for strengthening deteriorated structures. The purpose of this research was to determine the combined behavior of masonry walls and reinforcing meshes together, according to their deformation characteristics. A sample wall with average masonry parameters and seven different common polymer nets on them were modeled in Abaqus Software. Moreover, a case study wall was also modeled according to the strength values obtained from direct testing of a demolished masonry wall that was shaped as secondary blocks for reusing purposes. In addition to the analysis of this plain recovered wall, the strengthened version of it with carbon fiber polymer mesh was also modeled. The results obtained from the theoretical sample wall and the case study wall with plain and reinforced alternatives stated that; the compatibility of deformation characteristics between the wall and the reinforcing mesh is the key for combined strength behavior of the wall. Lastly, besides illustrating and discussing all the stress-strain conditions for the analyzed cases, this study also offered a formula for the detection of combined behavior in question, according to the material properties of unreinforced wall and reinforcing mesh separately. This formula is quite useful in order to decide to the suitable mesh type prior to the application.

Аннотация. Композитное поверхностное армирование обычно используются в настоящее время для усиления повреждённых конструкций. Цель исследования предполагала определение поведения кладки стен и армирующих сеток при их совместной работе с учётом их деформационных характеристик. Образец стены с усреднёнными характеристиками кладки и семь разновидностей композитного армирования были смоделированы в программном комплексе Abaqus. Кроме того, для оценки возможности применения подобной симуляции к реальным конструкциям, был произведён расчёт восстановленной каменной стены с учётом характеристик, полученных по результатам лабораторных испытаний. Учитывались случаи неармированной стены и стены с композитным поверхностным армированием. Результаты, полученные при моделировании условно принятой стены и практического случая, показали, что совместимость деформационных характеристик каменной стены и материала поверхностного армирования

Беспалов В.В., Ючер Д., Салманов И.Д., Курбанов И.Н., Купавых С.В. Деформационная совместимость каменной кладки с композитными материалами // Инженерно-строительный журнал. 2018. № 2(78). С. 136–150.

является ключевой в совместной работе всей конструкции. Также была предложена формула для определения степени деформационной совместимости в зависимости от свойств материала неармированной стены и поверхностного армирования. Определение деформационной совместимости может быть применимо при подборе вида поверхностного армирования.

1. Introduction

Unreinforced masonry has been widely used as a construction technique in the building industry throughout history. Most of these buildings are still in service and some of them require strengthening in order to adapt the structure to a new use or to fulfill the requirements of current regulations. Among the masonry structures, the most difficult ones to analyze are vaults and others under the impacts of compression and bending. Several prerequisites were proposed for calculating and evaluating the strength of such structures by the researchers [1–6] and many works were devoted to this issue [7–14]. Besides the investigations on masonry structures such as destructive, semi-destructive and non-destructive testing; there are also available formulae and tables representing the strength of masonry walls by the strength of masonry components separately. Since masonry is a composite body out of unit and mortar, the researchers state that, the most realistic strength result could be obtained when the combined behavior of masonry unit and masonry mortar is well represented [15]. Even after detecting the effective strength of a masonry structure, a new question *i.e.* suitable method for its strengthening appears.

Nowadays, one of the widely used reinforcing methods for strengthening damaged concrete and masonry structures is the use of Fiber Reinforced Polymers (FRP) in the form of plaster nets [16]. These polymers are applied as embedded meshes within the cement based plasters on the structure's surface, and are commonly available in two different geometries *i.e.* grid texture or a striped texture as illustrated in Figure 1.

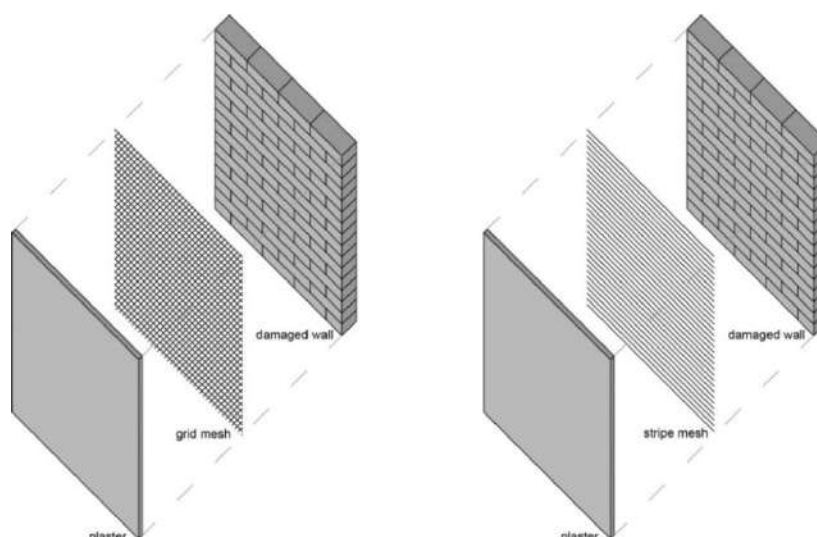


Figure 1: Grid and stripe textured FRP meshes within the plaster

The FRP nets are produced out of different materials such as carbon, glass, basalt and steel fibers in order to achieve the desired strength and compatibility with the deteriorated structures [17, 18]. Although many researchers have already focused on the relation of reinforced concrete structures and FRP based strengthening techniques, this relation is not well studied yet and hence not clear for the masonry structures. The available studies point out that a serious increase could be achieved in the strength of masonry with the help of FRP meshes [19–26]. Although, most of these studies determined the ultimate destructive loads and types of failures under various reinforcement technologies, they did not well define the comparative behavior of different reinforcing materials under one specific condition.

Lastly it was clearly shown that the performance of the strengthening system strongly depends on the accuracy of the installation, the preparation of the substrate surface and the curing condition of the plaster [20].

A significant amount of researches on FRP strengthening is devoted to their use on protecting the structures against seismic impacts [27–32]. The results show that; seismic resistance of masonry structures can be substantially improved with proper use of FRPs. On the other hand, it is a known fact

that, masonry has different behaviors under static and dynamic loads. Although many studies focused on strengthening for dynamic loads, this relation still requires to be studied in terms of static loads.

Lastly, in addition to the seismic studies, FRP strengthening can also propose opportunities in the field of reuse of construction materials. It is a known fact that, many concrete and masonry buildings are either deconstructed or demolished, though their component material still has good quality. Even though the separated material still has good quality; their re-integration as a new component can require alternative techniques in order to achieve the expected unity and strength. From this perspective, the FRP meshes appear as a featured way to sustain the unity between the recovered materials as a new component.

Besides the alternative studied explained above, the main hypothesis of this study was clarified as that; the combined behavior of strengthening intervention and masonry structure in the yielding zone is influenced more by the elastic modulus rates of the FRP and the masonry structure than the strength capacity of the FRP mesh. Therefore, in this paper deformation characteristics of a masonry structure and different types of FRP meshes as well as their combined behavior were analyzed in numerical manners. Hence, the objectives of the study can shortly be noted as follows:

- Evaluation of non-linear behavior of a masonry structure under eccentric loading, that is reinforced by different types of FRP meshes
- Comparison of different stress-strain states of this structure
- Determination of relative deformations of the FRP meshes and the adjacent masonry wall
- Determination of the impacts of FRP mesh addition, to a material reuse project as a case study

2. Methods

A masonry model was used considering its non-linear behavior for the simulation. The model was constructed in Abaqus 6.14 Software, using so-called “Extended” Finite Element Method that takes the initiation possibility of cracks and their growth, into account [33].

The simulation was carried out in a plane problem formulation. The eccentrically loaded masonry wall (under the combined action of compression and bending) was analyzed. The analytical model included a masonry wall element, concrete distribution plate [through which the load was transferred] and a composite reinforcing mesh that is rigidly connected to the masonry as illustrated in Figure 2. Under the proposed loading configuration, the expected deformation is also illustrated in the Figure.

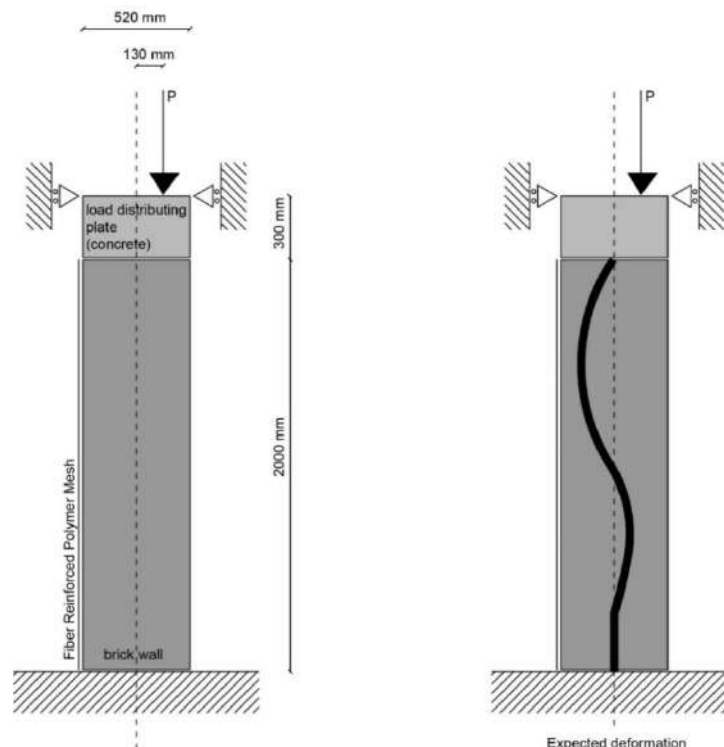


Figure 2. Schema of the masonry wall model used for the simulation

Seven models based on different FRP reinforcement types were used: Basalt grid (BFRP grid), Aramid stripe (AFRP grid), Natural fiber grid (NFRP grid), Glass fiber grid (GFRP grid), Glass fiber stripe (GFRP stripe), Carbon fiber grid (CFRP grid) and Carbon fiber stripe (CFRP stripe). Additionally, a reference model *i.e.* unreinforced (plain) masonry was obtained for the sake of comparisons. The characteristics of the materials given Table 1 were adopted from the studies of other researchers [6, 34].

Table 1. Mechanical properties of considered materials [Adapted from reference 6, 29]

Material	Modulus of elasticity,	Poisson coefficient,	Tensile strength,	Compressive strength,
	E	ν	σ_t	σ_c
	GPa	–	MPa	MPa
Basalt (grid)	85	–	400	–
Aramid (stripe)	120	–	320	–
Natural fiber (grid)	25	–	180	–
Glass fiber (grid)	70	–	280	–
Glass fiber (stripe)	105	–	250	–
Carbon fiber (grid)	230	–	350	–
Carbon fiber (stripe)	280	–	350	–
Plain Masonry	25	0.2	0.1	2

Non-linear behavior of the masonry wall under compression was specified by the piecewise approximation based on deformation characteristics of the masonry sample as shown in Figure 3, according to the data obtained from the other studies [14, 35]. When the data from these studies were used for simulation, it is found that a crack is initiated in the masonry element as soon as the tensile stress reaches to 0.1 MPa. Additionally, the stresses in the masonry element were redistributed when the crack appears.

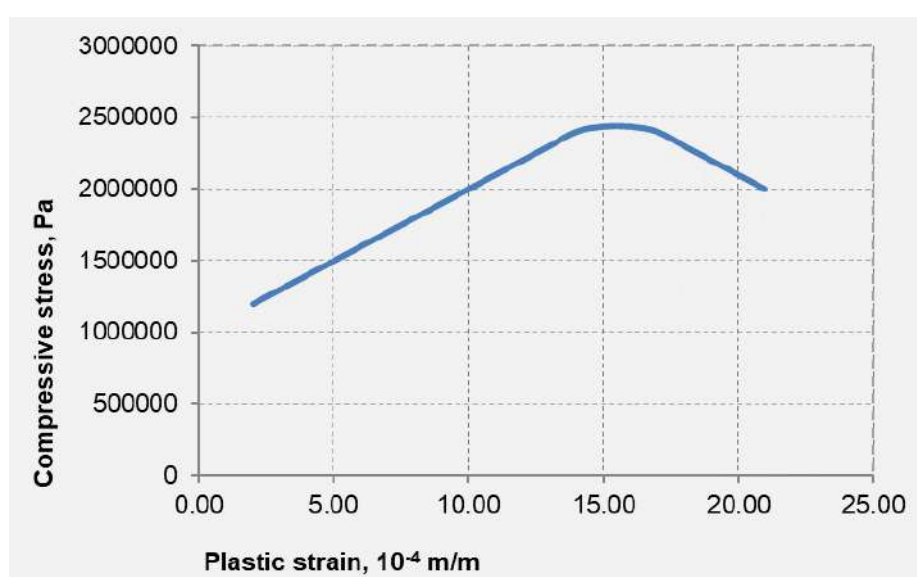


Figure 3. Plasticity diagram of the masonry wall sample

Lastly, a case simulation was completed in order to see how FRP mesh addition can add to a material reuse project. A study completed by a group of researchers offers a recovery project for the debris came out from the demolition of a brick masonry building [36]. In this study, the broken wall pieces (out of solid brick and cement based mortar) were collected from the accumulated debris and they were shaped in order to obtain prismatic blocks for compressive and shear tests as illustrated in Figure 4 and the test results were presented in Table 2.



Figure 4. Accumulated brick debris on the demolition plot, prism preparation for compression and shear test and test set-ups

Table 2. Test results of compression¹ (upper side) and shear blocks² (lower side) [31]

Prism	Area [cm ²]	Load [kN]	F _{mt sample} [kN/cm ²]	K	F _{mt corrected} [MPa]
1	408.59	575	1.41	0.75	10.55
2	401.77	435	1.08		8.12
3	436.77	432.5	0.99		7.43

Mean	8.70	sd	1.34	COV	0.15
------	------	----	------	-----	------

Prism	A ₁ +A ₂ [cm ²]	F [kN]	F _{oi} [MPa]
4	484.77	11.66	0.24
5	472.33	5.33	0.11
6	428.33	6.00	0.14

Mean	0.16
sd	0.05
COV	0.33

¹ According to the researchers of the reference study [36], compression test was done according to ASTM C1314: Standard Test Method for Compressive Strength of Masonry Prisms (2014) and K is the correction factor to convert the obtained prism results into standard cube strength. K is dependent on the proportions of the prism, the prisms for this research was 20x20x20 cms and the closest available proportion was 1:1.3 with 0.75 constant value.

² Reference study [36] states that, EN 1052-3: Methods of Test for Masonry, Part 3: Determination of Initial Shear Strength (2007) was used as shear test method.

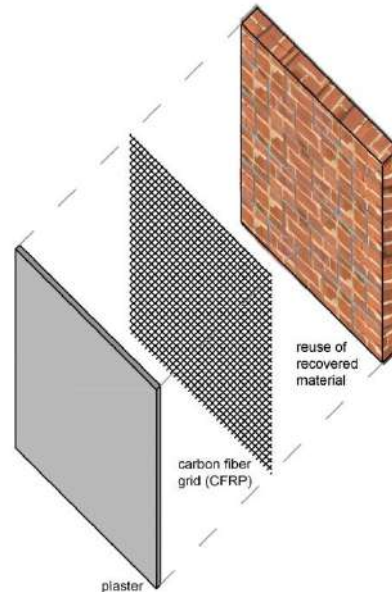


Figure 5. The schema for the material reuse case simulation

As stated in Table 2, the mean compressive strength of these blocks are 8.70 MPa while the mean shear strength for the bed mortar of them is 0.16 MPa. Although both values are quite promising in terms of reusability according to the limit definitions in the sources³, the integrity of these blocks as a new wall is a question to be answered. One featured answer is the use of FRP meshes as a plaster net for better bonding characteristics as illustrated in Figure 5, obtained according to the system noted in Figure 1. Consequently, the test results obtained from the recovered blocks presented in Table 2 were used for the simulation of a masonry wall with the addition of Carbon fiber grid (CFRP) according to the loading schema given in Figure 2. The outcomes obtained from this simulation are presented in the results section and their comparison with the default values are presented in the discussion section.

3. Results and Discussion

The results obtained from the simulations belong to the mid height of the masonry element on the compressive zone side (the wall surface without the reinforcement) as illustrated in Figure 6. The diagrams in this figure illustrate Strain, ε_{yy} , on X axis versus Stress, σ_{yy} , on Y axis. As seen in this Figure, there are sudden changes in all diagrams that are stress jumps caused by crack initiation and resultant sudden redistribution of stresses. Larger amplitude of jump with an earlier time of the crack is distinctive for FRP with a higher modulus of elasticity as the graphs of glass fiber stripe or carbon fiber grid reinforced masonry walls illustrate in Figure 6. This big-scale stress jump reflects the initiation of the main crack, sharp decrease in the cross section and local strength loss for the masonry element in the compressed zone. When the stress increases again, the jump is completed as a result of the inclusion of adjacent masonry region in plastic state. Moreover, the second jump in the diagrams reflects the occurrence of a new large crack and one more strength loss for the masonry wall. This dual crack formation is not observed in plain masonry wall and its destruction starts with the first main crack as illustrated with a model in Figure 8.

Lastly, the expected depth of cracks are shown with the stress distribution schema in Figure 7. (Embedded within Figure 6). In general, crack formations were local and took almost the same form in each FRP type in the final stage, except aramid and glass fiber stripes. In these two cases, the main crack appeared and passed through 60 % of the section.

³ The researchers of the reference study [36] concluded that, the compressive strength value obtained from the direct tests on the prisms (shaped wall sections) is higher compared to the allowable strength value indicated in related national standard [37]. This document defines the allowable masonry wall strength according to a formula based on the strengths of brick and mortar. The researchers checked the brick and mortar strengths one by one as well as wall prisms for the comparison [36]. Additionally, the researchers stated that, the shear value obtained from the tests is higher compared to the limiting value defined in Eurocode 6, Design of Masonry Structures – Part 1-1: General Rules for Reinforced and Unreinforced Masonry Structures (1996).

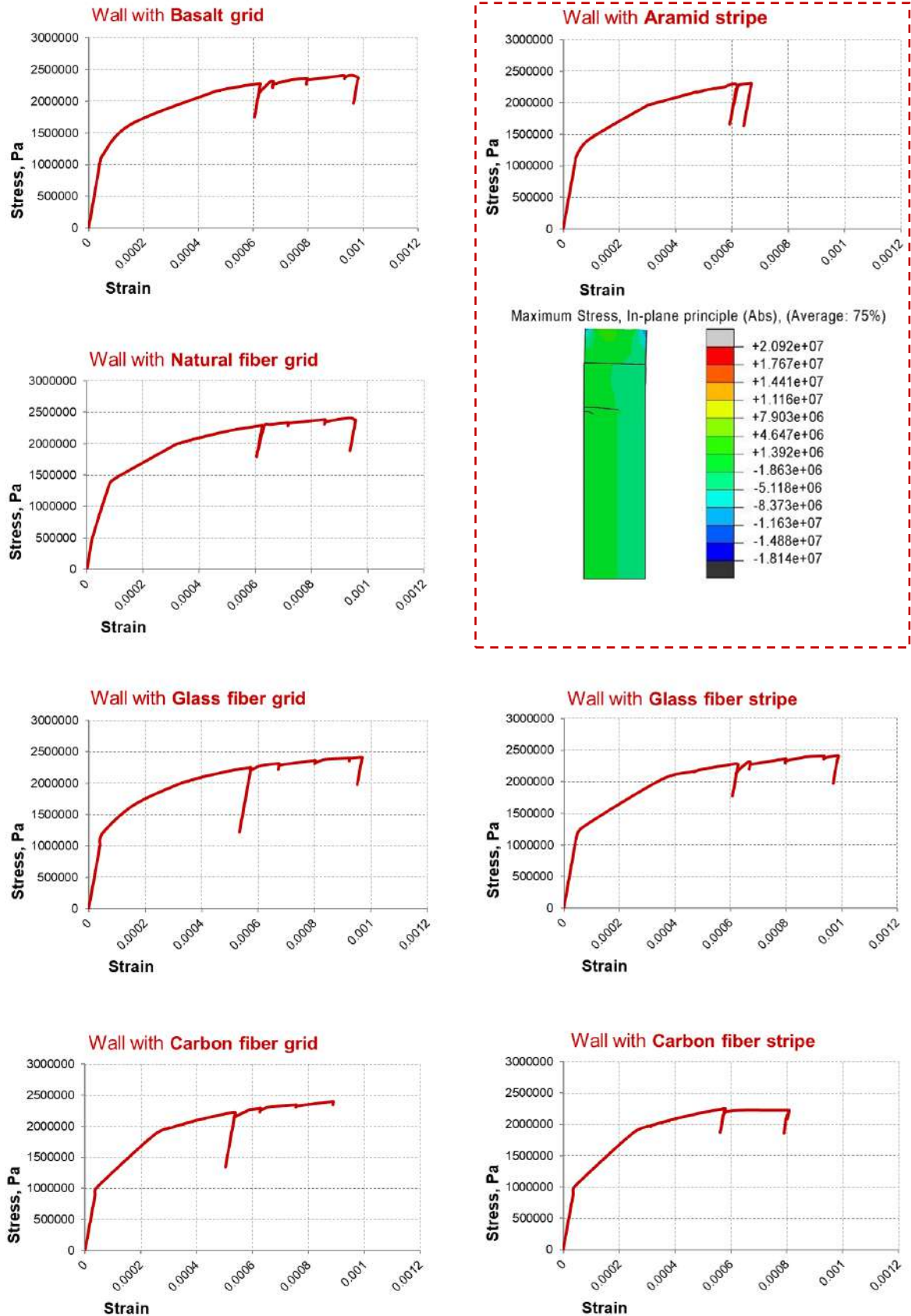


Figure 6. Stress-strain diagrams for compressive zone

Беспалов В.В., Ючер Д., Салманов И.Д., Курбанов И.Н., Купавых С.В. Деформационная совместимость каменной кладки с композитными материалами // Инженерно-строительный журнал. 2018. № 2(78). С. 136–150.

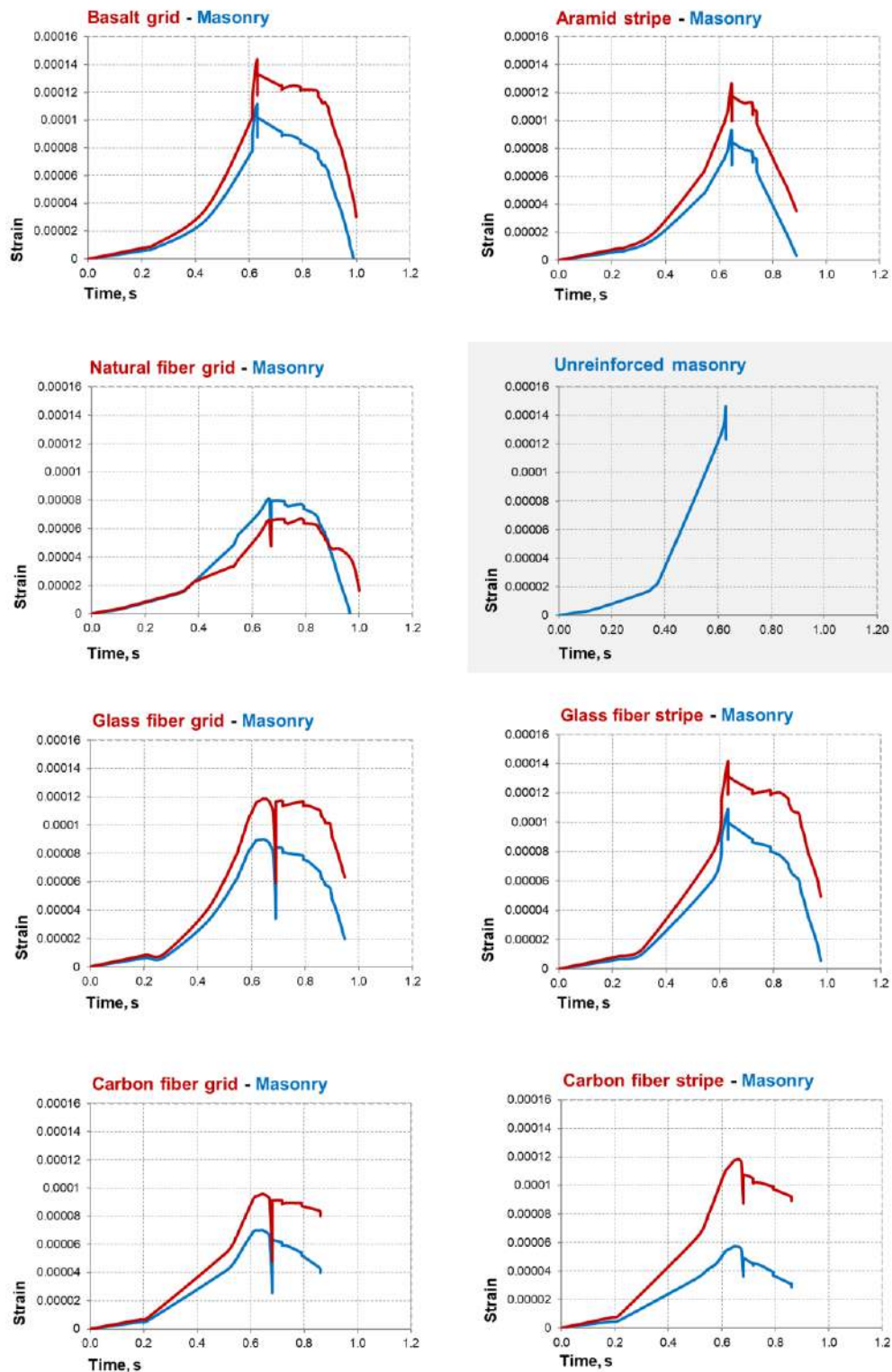


Figure 8⁴. Deformation of the FRP meshes and the adjacent masonry walls, tension zone

Diagrams showing the deformation of FRP meshes and the adjacent masonry walls in tension zone were plotted in Figure 8 to analyze the possible slippage of the mesh and its full separation from the masonry body. These diagrams reflect the deformation levels in FRP and the masonry when the load reaches to maximum.

⁴ Diagram for Natural fiber mesh reinforced wall is opposite of the others in terms of capacity comparison of the masonry wall and the reinforcement. This result is expected since this mesh type has quite low modulus of elasticity.

Lastly, the results obtained from the simulation of the case study wall *i.e.* the masonry body out of recovered wall sections is given in Figure 9. The compressive strength value that was obtained from direct test of wall prism *i.e.* 8.7 MPa was used to derive and calculate the modulus of elasticity according to the formula given below⁵:

$$\begin{aligned} E &= f_{mt} * \alpha \\ &= 8.7 * 1000 \\ &= 8700 \text{ MPa}, \end{aligned} \quad (1)$$

[37]

where $\alpha = 1000$ is elastic characteristic of masonry with mortar type M10⁶

Lastly the tensile strength of recovered masonry wall was assumed same as the sample wall (0.1 MPa), while the mean shear strength value 0.16 MPa (Table 2) was used as the modeling parameter in Software. The two diagrams plotted in this Figure illustrate the stress-strain diagrams for the unreinforced wall and its strengthened version with carbon fiber grid mesh.

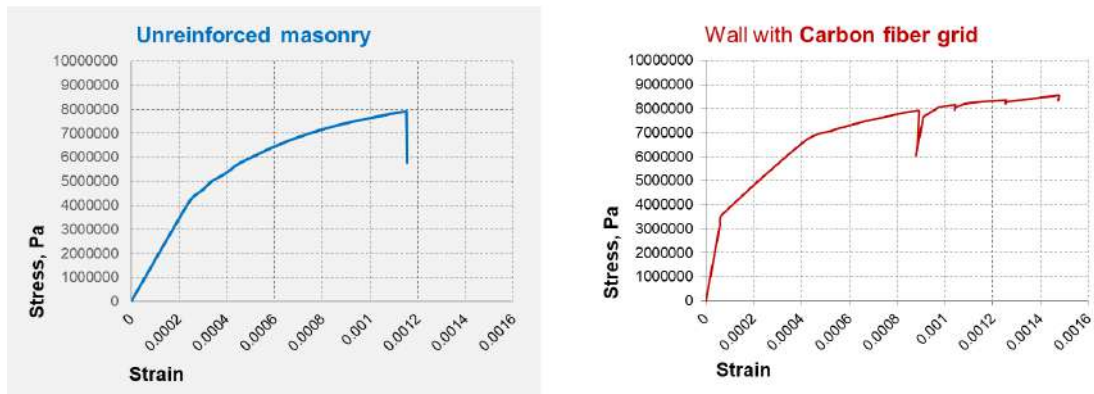


Figure 9. Stress – strain diagram of the recovered masonry wall on the left hand side and its reinforced version with CFRP grid mesh on right hand side

These two diagrams in Figure 9 illustrate that; the reinforced wall has slightly larger stress capacity *i.e.* the maximum stress for unreinforced version is about 8.0 MPa while the reinforced one can reach up to about 8.5 MPa. Additionally, the strain capacity of reinforced one reaches to 0.0015 mm while the unreinforced one is about 0.0011 mm. Moreover, the unreinforced masonry is rapidly destroyed by the crack growth in the tension zone that results in critical cross sectional reduction, which is visible with the sharp fall in the diagram, while the reinforced wall can keep the bearing capacity even after the first fall *i.e.* first main crack in the diagram as seen in Figure 9. In the reinforced case, the CFRP mesh prevents the growth of the first main crack at a certain stage that appears as a jump in the stress diagram for the reinforced wall. Since the main crack is restrained, the bearing capacity of the masonry wall slightly increases until the appearance of new cracks. These new cracks are also neutralized by the reinforcement until the fourth main crack as illustrated in Figure 10 and their reflectance as small stress jumps in Figure 9.

Lastly, when the comparative crack formations are analyzed for these two wall options, it is clear that only one single region occurs for the plain wall while this region is reduced and divided into two, for the reinforced alternative as seen in Figure 10.

In plain masonry wall case, there is no source for significant shear stress as seen in Figure 11. Additionally, the shear failure occurs in the reinforced surface of the masonry wall when the tangential stresses reaches to shear strength limit, since FRP cannot provide its full strength capacity. The FRP could provide the best performance when its modulus of elasticity is close to masonry wall, in other words the two components are compatible in terms of deformation properties.

One final aspect to be clarified is the behaviors of recovered masonry wall and the CFRP reinforcing grid mesh. Their diagrams in terms of time and deformation are given in Figure 12 below. These diagrams are presented in order to have an opinion on their compatibility as well as the

⁵ National Standard [SNIP II-22-81], (2012).

⁶ The mean compressive strength of mortar obtained from direct tests is converted into 14.13 MPa cube strength [36] and it falls into M10 type.

comparison to the sample wall and different reinforcement alternatives on it, as explained in the previous sections of this study.

Unreinforced masonry time-strain diagram here and time-strain diagram for masonry and carbon fiber grid mesh together (as the diagrams in Figure 8), the tension zone.

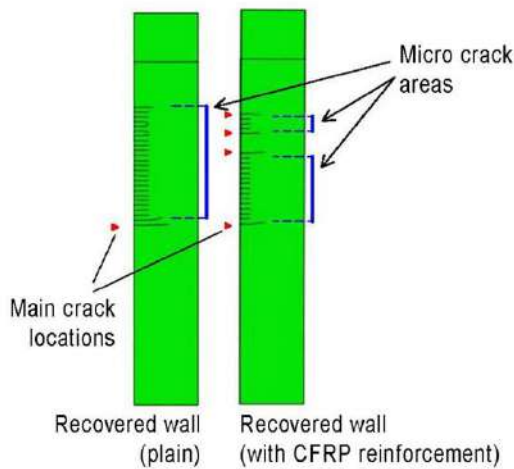


Figure 10. Simulation of cracks for recovered wall

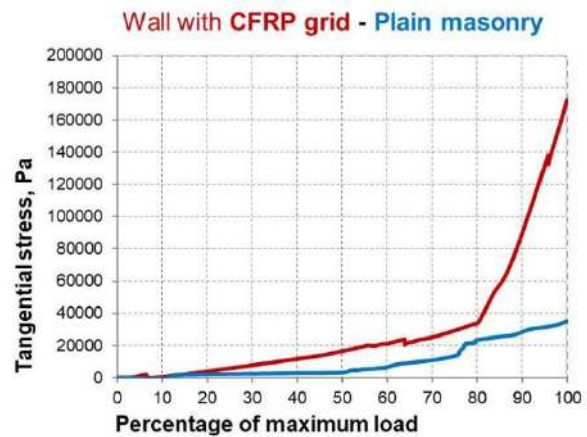


Figure 11. Tangential stress diagram for recovered wall (tension side)

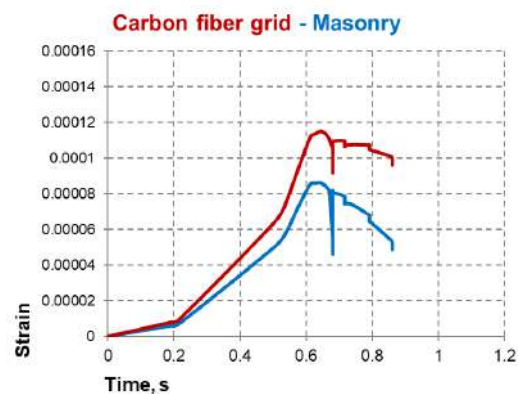
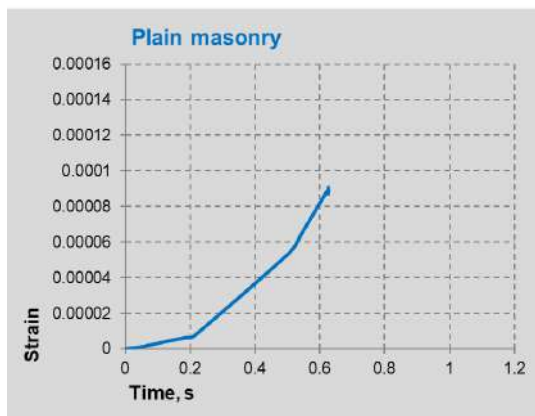


Figure 12. Deformation of recovered masonry wall on the left hand side, and Deformation of the CFPR mesh and the adjacent recovered masonry wall on the right hand side, tension zone

Following the analysis on seven different FRP meshes and their behaviors on a masonry wall sample as well as a recovery case study with and without CFRP reinforcing, all data obtained from the simulations are discussed in the following section.

All the separate stress-strain diagrams obtained from the simulation of seven different FRP meshes on the sample masonry wall are gathered in Figure 13, for the sake of comparison. The curves are of similar nature, but the difference in the appearance of spikes and the formation of the fracture cracks are clearly distinguishable in this Figure. Comparatively the earliest formation of a crack was observed in a model with carbon fiber grid reinforcement (stripe version is also one of the earliest cracks), while the latest first jump *i.e.* latest crack appeared in the basalt fiber grid reinforcing model. The first jumps of the NFRP grid and AFRP stripe reinforced masonry walls are located almost in the same point. Lastly, the largest amplitude of the jump occurred in the masonry model with GFRP grid reinforcement.

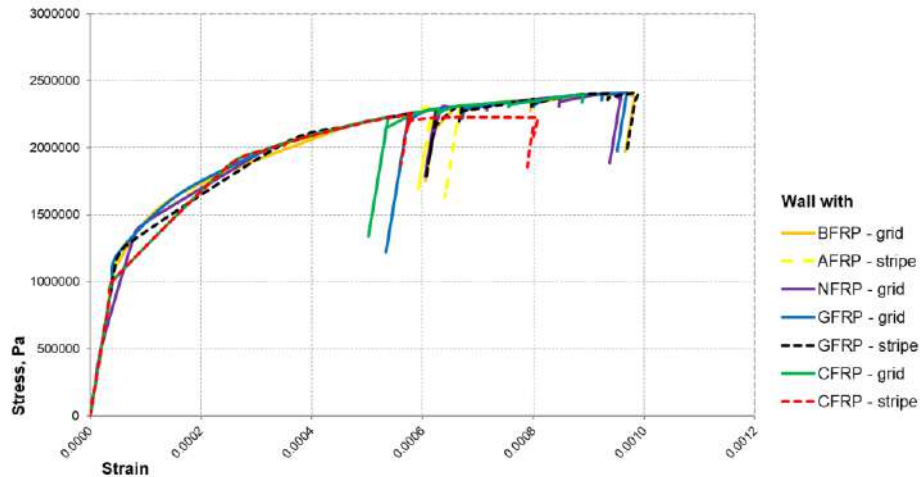


Figure 13. Stress-strain diagram of reinforced masonry alternatives in compression zone

Aramid and glass fiber stripe reinforced masonry walls experienced large cracks that are deeper than 60 % of the wall section but there is no explicit reflection of this on their stress-strain states as shown in Figure 13. This could be interpreted as that, the cracks reached to this significant depth only after the second stress jump was passed, namely; the samples reached their limits of bearing capacity on the second sharp fall. In case of aramid and glass fiber stripe, this second sharp fall resulted in fast growth of the first main crack, instead of initiation of new big crack as appeared in the other cases.

Diagrams in Figure 8 show that, the difference in deformation of the reinforcement mesh and the adjacent masonry wall reaches to significant values in some cases (as seen in pre-crack part of strain diagrams and especially in case of CFRP stripe, where strain difference grows up long before the initiation of the first main crack). As an example, the deformation of CFRP stripe mesh is twice as large as the deformation of the adjacent masonry wall, which can cause the slippage of the reinforcement from the surface. Although it is not possible to determine the relative strain difference resulting in slippage, with the help of a numerical model, where the experimental data from the real samples are compulsory; it is possible to detect the relative deformation compatibilities from the strain diagrams. Thus, the simplest expression of the deformation compatibility is the sum of the difference between relative strains of reinforcement and masonry wall; as noted in Formulae 2 and 3.

$$\alpha = \int_0^1 \Delta \varepsilon dt, \tag{2}$$

where α – Deformation compatibility;

$$\Delta \varepsilon = \left| \varepsilon^{FRP} - \varepsilon^M \right| \text{ – Strain difference of reinforcement and masonry body.}$$

Using the relative strain values can be a logical way to compare the deformation compatibility of the masonry body and the reinforcing mesh, as noted in Formula 3. The closer this value is to 1.0, the higher the relative deformation compatibility.

$$\alpha_{rel} = 1 - \left(\sum_i (|\varepsilon_i^{FRP} - \varepsilon_i^M| \times t_i) \right) \times 10^4 \tag{3}$$

where α_{rel} – relative deformation compatibility;

i – Number of calculation iterations, where the deformation of the masonry wall and the reinforcing meshes are calculated in each step;

t_i – Duration of each iteration

Lastly, relative deformation compatibility values of seven different FRP meshes, analyzed in this study were calculated according to the suggested formula above, and the results are given in Table 3.

Table 3. Deformation compatibility of different FRP meshes

Reinforcement Type	Maximum strain difference, $\Delta\varepsilon_{\max}$	Value of relative deformation compatibility, α_{rel}
BFRP (grid)	$4.63 \cdot 10^{-5}$	0.786
AFRP (stripe)	$3.51 \cdot 10^{-5}$	0.855
NFRP (grid)	$4.72 \cdot 10^{-5}$	0.898
FGRP (grid)	$4.54 \cdot 10^{-5}$	0.822
FGRP (stripe)	$4.50 \cdot 10^{-5}$	0.794
CFRP (grid)	$4.06 \cdot 10^{-5}$	0.86
CFRP (stripe)	$6.17 \cdot 10^{-5}$	0.715

As noted in Table 3, the maximum strain difference is the lowest for AFRP reinforced model whereas it is the highest for CFRP-stripe reinforced model. Additionally, relative deformation compatibility value is maximum for NFRP-stripe reinforced model, while it is minimum for CFRP reinforced model. These values can be interpreted as that, regarding the low strain difference value and comparatively high relative deformation compatibility value; AFRP features as a favorable application for strengthening the modelled sample masonry wall, among the other alternatives. On the other hand, since both values in question are the maximum ones for CFRP stripe reinforced model, this wall – reinforcement combination appear as the least suitable one. Moreover, this model also demonstrated the earliest fracture crack in stress-strain diagram, in Figure 8, which confirms the incompatibility of its components.

Table 3 indicates a large difference between the calculated values both for maximum strain values and relative deformation compatibility for reinforcing options. This deviation is a direct result of the distinct deformation diagrams of failures for reinforcing options; as already noted in Figure 8.

Lastly, the maximum strain difference and relative deformation compatibility values were calculated for the recovered masonry wall and CFRP grid reinforcement combination; according to the Formulae 2 and 3 as noted in Table 4.

Table 4. Deformation compatibility for recovered wall and carbon fiber based reinforcement combination

Reinforcement Type	Maximum strain difference, $\Delta\varepsilon_{\max}$	Value of relative deformation compatibility, α_{rel}
CFRP – grid	$5.14 \cdot 10^{-5}$	0.842

Although only one type of reinforcement was modelled for the recovered masonry wall, these two values were still obtained in order to have a broad opinion on their comparison with the sample wall models noted in Table 3. The maximum strain difference is $5.14 \cdot 10^{-5}$ where the compatibility deformation value is 0.842. When these values are compared with the values for the sample wall in Table 3, two options appear. The maximum strain value obtained from CFRP grid on the recovered wall is between the CFRP strip and the CFRP grid on the sample wall. Although the relative deformation compatibility of CFRP grid on the recovered wall is closest to the AFRP strip on the sample wall, the value from CFRP grid on the sample wall is also very close. Consequently, regarding these two parameters together, the behavior and crack formation expectation for the CFRP grid on recovered wall would be most similar to the CFRP grid reinforcement on the sample wall.

After obtaining strain difference and relative deformation compatibility values for the sample and the recovered masonry walls, the comments and summaries are presented in the following section.

4. Conclusions

The featured outcomes obtained by this study were presented and explained one by one in the following text.

1. Stress-strain state and deformation compatibility of different fiber reinforced polymer (FRP) reinforcement types for masonry walls under eccentric load were obtained.

2. Stress jump reflecting the initiation of a main crack was presented as a possible way for determining the limit bearing capacity of FRP reinforced masonry walls.

3. Different behaviors of representative masonry wall with and without FRP strengthening in the post-peak stage was determined. It was obtained that, the emergence of the main crack protects the wall from further damage and allows the strength contribution of the neighboring sections of the wall, when the reinforcement is present. On the other hand, the main crack results in the rapid destruction of the structure, if there is no reinforcement.

4. Although this outcome requires further inquiry with real experiments, the simulation model illustrated that the main cracks continue more than 60% of the wall cross section; as obtained for AFRP and GFRP stripe reinforcement cases.

5. It is shown that, the deformation diagrams of FRP meshes and the masonry wall can be used as a tool for determining their relative deformation compatibility. Additionally, this compatibility was pointed as the key element during the suitable reinforcement type selection according to the deteriorated wall in question.

6. Although the FRP reinforcing resulted in a slight strength capacity increase in the reclaimed wall alternative (case study), its main impact appeared as increasing the ductility of the wall. The wall model without reinforcement showed a brittle, sudden failure while the reinforced case could keep its unity for a while even after the failure. This is a life-saving property for the structural elements, when the case is sustaining enough time for inhabitants to escape before the failure.

7. The reinforcing mesh on the recovered wall case could have provided better shear strength behavior (since it has larger capacity) if its properties were more similar to the wall's deformation characteristics.

8. The values of maximum strain difference and the relative deformation compatibility for the CFRP reinforced, recovered wall case was closest to the CFRP stripe strengthened sample masonry wall. These approximate values are pointed as expectable behavior similarities for these two cases.

In brief, besides the 8 items noted above, the simulation software used for this study (Abaqus) showed its usefulness in terms of deformation compatibility calculations. On the other hand, the verification and refinement of the simulation results as well as combined behavior detection of masonry and reinforcement mesh (especially under compression and bending) require full scale experiments.

References

1. Bepalov V.V., Zimin S.S. The strength of masonry vaulted structures. *Construction of Unique Buildings and Structures*. 2016. No. 11(50). Pp. 37–51. (rus)
2. Zimin S.S., Kokotkova O.D., Bepalov V.V. Vault structures of historical buildings. *Construction of Unique Buildings and Structures*. 2015. No. 2(29). Pp. 57–72. (rus)
3. Zimin S.S., Bepalov V.V., Skripchenko I.V. Spandrels influence on the stress state of masonry vaults. *Obsledovanie zdaniy i sooruzhenij: problemy i puti ih resheniya: Materialy VII mezhdunarodnoj nauchno-prakticheskoy konferencii*. Izd-vo SPbGPU, 2017. Pp. 133–144. (rus)
4. Skripchenko I.V., Bepalov V.V., Lukichev S.Y., Zimin S.S. Unconventional cases of the stone vaults. *Construction of Unique Buildings and Structures*. 2017. No. 2(53). Pp. 87–95.
5. Bepalov V., Orlovich R., Zimin S. Stress-Strain State of Brick Masonry Vault with an Aperture. *MATEC Web of Conferences*. 2016. No. 53. 01009.
6. Sousa R., Guedes J., Sousa H. Characterization of the uniaxial compression behavior of unreinforced masonry–Sensitivity analysis based on a numerical and experimental approach. *Archives of Civil and Mechanical Engineering*. 2015. No. 15. Pp. 532–547.
7. Ulybin A.V., Startsev S.A., Zubkov S.V. Humidity control in the inspection of masonry structures. *Magazine of Civil Engineering*. 2013. No. 7(42). Pp. 32–39. (rus)
8. Silva B., Pappas A., Valluzzi, M.R., Porto F., Modena C. Calibration of a numerical material behaviour model for the simulation of multi-leaf stone masonry walls. *Structural Analysis of Historical Constructions*. 2012. Pp. 575–583.
9. Bisoffi-Sauve M. *Etude des ouvrages maçonnes en pierre*

Литература

1. Беспалов В.В., Зимин С.С. Прочность каменной кладки сводчатых конструкций // Строительство уникальных зданий и сооружений. 2016. № 11(50). С. 37–51.
2. Зимин С.С., Кокоткова О.Д., Беспалов В.В. Сводчатые конструкции исторических зданий // Строительство уникальных зданий и сооружений. 2015. № 2(29). С. 57–72.
3. Зимин С.С., Беспалов В.В., Скрипченко И.В. Влияние распалубок на напряженное состояние каменных сводов // Материалы VII международной научно-практической конференции (Обследование зданий и сооружений: проблемы и пути их решения). СПб.: Изд-во СПбПУ, 2017. С. 133–144.
4. Скрипченко И.В., Беспалов В.В., Лукичев С.Ю., Зимин С.С. Нетипичные случаи каменных сводов // Строительство уникальных зданий и сооружений. 2017. № 2(53). С. 87–95.
5. Bepalov V., Orlovich R., Zimin S. Stress-Strain State of Brick Masonry Vault with an Aperture // MATEC Web of Conferences. 2016. No. 53. 01009.
6. Sousa R., Guedes J., Sousa H. Characterization of the uniaxial compression behavior of unreinforced masonry–Sensitivity analysis based on a numerical and experimental approach // Archives of Civil and Mechanical Engineering. 2015. №15. Pp. 532–547.
7. Улыбин А.В., Старцев С.А., Зубков С.В. Контроль влажности при обследовании каменных конструкций // Инженерно-строительный журнал. 2013. № 7(42). С. 32–39.
8. Silva B., Pappas A., Valluzzi M.R., Porto F., Modena C. Calibration of a numerical material behaviour model for the simulation of multi-leaf stone masonry walls // Structural

Беспалов В.В., Ючер Д., Салманов И.Д., Курбанов И.Н., Купавых С.В. Деформационная совместимость каменной кладки с композитными материалами // Инженерно-строительный журнал. 2018. № 2(78). С. 136–150.

- par la méthode des éléments discrets: caractérisation et modélisation du comportement cohésif des joints. *Mécanique des structures*. Ph.D. Thesis. Université de Bordeaux. 2016. 191 p.
10. Bisoffi-Sauve M. Caractérisation et modélisation des joints de mortier dans les structures maçonnées en pierre. *34èmes Rencontres de l'AUGC*. Université de Liège, Belgique. 2016. Pp. 1–8.
 11. Villemus B. Etude des murs de soutènement en maçonnerie de pierres seches. Ph.D. Thesis. *Ecole L'institut National des Sciences Appliquées de Lyon*. 2004. 254 p.
 12. Bagneris M., Dubois F., Martin A. Numerical analysis of historical masonry structures for stone degradation diagnosis: An application to the Roman Amphitheater of Nîmes. *Digital Heritage*. 2013. Pp. 521–528.
 13. Tabbakhha M. *Multiscale methodology for vulnerability assessment of masonry structures*. Ph.D. Thesis. Ecole Centrale Paris. 2013. 241 p.
 14. Derkach V.N. *Kamennoye zapolneniye karkasnykh zdaniy: prochnost, zhestkost i silovoye vzaimodeystviye s karkasom* [Masonry filling of frame buildings: strength, stiffness and force interaction with the frame]. D.Sc Thesis. Brest, 2016. 260 p. (rus)
 15. Zubkov S.V., Ulybin A.V. and Fedotov S.D., Assessment of the mechanical properties of brick masonry by a flat-jack method. *Magazine of Civil Engineering*. 2015. No. 8. Pp. 20–29.
 16. Parghi A., Alam S. A review on the application of sprayed-FRP composites for strengthening of concrete and masonry structures in the construction sector. *Composite Structures*. 2018. No. 187. Pp. 518–534.
 17. Shaw I., Andrawes B. Repair of damaged end regions of PC beams using externally bonded FRP shear reinforcement. *Construction and Building Materials*. 2017. No. 148. Pp. 184–194.
 18. Gattulli V., Lampis G., Marcari G., Paolone A. Simulations of FRP reinforcement in masonry panels and application to a historic façade. *Engineering Structures*. 2014. No. 75. Pp. 604–618.
 19. Valluzzi M.R., Binda L., Modena C. Mechanical behaviour of historic masonry structures strengthened by bed joints structural repointing. *Construction and Building Materials*. 2005. No. 19. Pp. 63–73.
 20. Bernat-Maso E., Escrig C., Aranha C.A., Gil L. Experimental assessment of Textile Reinforced Sprayed Mortar strengthening system for brickwork wallettes. *Construction and Building Materials*. 2014. No. 50. Pp. 226–236.
 21. Shaheen E., Shrive N.G. Strengthening of masonry columns with sprayed glass fibre reinforced polymer (SGFRP). *10th Canadian Masonry Symposium*. Banff, Alberta. 2005. Pp. 1–10.
 22. McGinley W.M., Corzo A.M., Gergely J., Foster P.B., Young D.T. A design methodology for FRP systems for masonry structures. *10th Canadian Masonry Symposium*. Banff, Alberta. 2005. Pp. 34–44.
 23. Zanaz A. *Approche probabiliste d'aide au diagnostic des voûtes en maçonnerie*. Ph.D. Thesis. Université de Limoges. 2016. 208 p.
 24. Este A., Toson B., Saliba J., El Yagoubi J., Mindeguia J.-C., Martin E., Morel S. A new approach to simulate interface damage in brittle matrix composites. *Procedia Structural Integrity*. 2016. No. 2. Pp. 2456–2462.
 25. Bernat-Maso E., Escrig C., Aranha C.A. Construction Experimental assessment of Textile Reinforced Sprayed Mortar strengthening system for brickwork wallettes. *Building Materials*. 2013. No. 50. Pp. 226–236.
 26. De Santis S., De Felice G. Bond behaviour of steel reinforced grout strengthening systems applied to the extrados of masonry vaults. *Structural Analysis of Historical Constructions*. 2016. Pp. 344–350.
 27. Garmendia L., San-Mateos R., García D., Gandini A., San-José J.T., Marcos I. Retrofitting of masonry vaults with composite materials. *Structural Analysis of Historical Constructions*. 2012. Pp. 575–583.
 9. Bisoffi-Sauve M. Etude des ouvrages maçonnés en pierre par la méthode des éléments discrets: caractérisation et modélisation du comportement cohésif des joints. *Mécanique des structures*. Ph.D. Thesis. Université de Bordeaux. 2016. 191 p.
 10. Bisoffi-Sauve M. Caractérisation et modélisation des joints de mortier dans les structures maçonnées en pierre. *34èmes Rencontres de l'AUGC*. Université de Liège, Belgique. 2016. Pp. 1–8.
 11. Villemus B. Etude des murs de soutènement en maçonnerie de pierres seches. Ph.D. Thesis. Ecole L'institut National des Sciences Appliquées de Lyon. 2004. 254 p.
 12. Bagneris M., Dubois F., Martin A. Numerical analysis of historical masonry structures for stone degradation diagnosis: An application to the Roman Amphitheater of Nîmes // *Digital Heritage*. 2013. Pp. 521–528.
 13. Tabbakhha M. *Multiscale methodology for vulnerability assessment of masonry structures*. Ph.D. Thesis. Ecole Centrale Paris. 2013. 241 p.
 14. Деркач В.Н. Каменное заполнение каркасных зданий: прочность, жесткость и силовое взаимодействие с каркасом. Дисс. д.т.н. Брест, 2016. 260 с.
 15. Зубков С.В., Улыбин А.В., Федотов С.Д. Исследование механических свойств кирпичной кладки методом плоских домкратов // *Инженерно-строительный журнал*. 2015. № 8(60). С. 20–29.
 16. Parghi A., Alam S. A review on the application of sprayed-FRP composites for strengthening of concrete and masonry structures in the construction sector // *Composite Structures*. 2018. № 187. Pp. 518–534.
 17. Shaw I., Andrawes B. Repair of damaged end regions of PC beams using externally bonded FRP shear reinforcement // *Construction and Building Materials*. 2017. № 148. Pp. 184–194.
 18. Gattulli V., Lampis G., Marcari G., Paolone A. Simulations of FRP reinforcement in masonry panels and application to a historic façade // *Engineering Structures*. 2014. № 75. Pp. 604–618.
 19. Valluzzi M.R., Binda L., Modena C. Mechanical behaviour of historic masonry structures strengthened by bed joints structural repointing // *Construction and Building Materials*. 2005. № 19. Pp. 63–73.
 20. Bernat-Maso E., Escrig C., Aranha C. A., Gil L. Experimental assessment of Textile Reinforced Sprayed Mortar strengthening system for brickwork wallettes // *Construction and Building Materials*. 2014. № 50. Pp. 226–236.
 21. Shaheen E., Shrive N.G. Strengthening of masonry columns with sprayed glass fibre reinforced polymer (SGFRP) // *10th Canadian Masonry Symposium*, Banff, Alberta. 2005. Pp. 1–10.
 22. McGinley W.M., Corzo A.M., Gergely J., Foster P.B., Young D.T. A design methodology for FRP systems for masonry structures // *10th Canadian Masonry Symposium*, Banff, Alberta. 2005. Pp. 34–44.
 23. Zanaz A. *Approche probabiliste d'aide au diagnostic des voûtes en maçonnerie*. Ph.D. Thesis. Université de Limoges. 2016. 208 p.
 24. Este A., Toson B., Saliba J., El Yagoubi J., Mindeguia J.-C., Martin E., Morel S. A New Approach to Simulate Interface Damage in Brittle Matrix Composites // *Procedia Structural Integrity*. 2016. № 2. Pp. 2456–2462.
 25. Bernat-Maso E., Escrig C., Aranha C.A. Construction Experimental assessment of Textile Reinforced Sprayed Mortar strengthening system for brickwork wallettes // *Building Materials*. 2013. № 50. Pp. 226–236.
 26. De Santis S., De Felice G. Bond behaviour of steel reinforced grout strengthening systems applied to the extrados of masonry vaults // *Structural Analysis of Historical Constructions*. 2016. Pp. 344–350.
 27. Garmendia L., San-Mateos R., García D., Gandini A., San-José J.T., Marcos I. Retrofitting of masonry vaults with composite materials. *Structural Analysis of Historical Constructions*. 2016. Pp. 344–350.

- Constructions*. 2016. Pp. 351–356.
28. Wang X., Ghiassi B., Oliveira D.V. Numerical analysis of the in-plane behaviour of TRM-strengthened masonry walls. *Structural Analysis of Historical Constructions*. 2016. Pp. 365–371.
 29. Hojdis L., Krajewski P. Glass fiber grids embedded in a cement-based matrix as strengthening of masonry structures. *Structural Analysis of Historical Constructions*. 2016. Pp. 372–376.
 30. Serhal J. *Etude de la vulnérabilité des bâtiments en maçonnerie soumis à des mouvements de terrains et élaboration de critères d'évolution de leur rigidité*. Ph.D. Thesis. Université de Lorraine. 2016. 188 p.
 31. Taforel P., Dubois F., Martin A., Pagano S. Développement de formulations dynamiques adaptées à la modélisation par éléments discrets de structures maçonnées sous chargements sismiques. *10e colloque national en calcul des structures*. 2011. Pp. 1–12.
 32. Kabantsev O.V. *Nauchnyye osnovy strukturnoy teorii kamennoy kladki dlya otsenki predelnykh sostoyaniy kamennykh konstruksiy seysmostoykikh zdaniy* [Scientific basis for the structure theory of masonry for the assessment of limit states of masonry structures for earthquake-resistant buildings]. D.Sc Thesis. Moscow, 2016. 358 p. (rus)
 33. Martin A., Esnault J.-B., Massin P. About the use of standard integration schemes for X-FEM in solid mechanics plasticity. *Computer Methods in Applied Mechanics and Engineering*. 2014. Pp. 283–293.
 34. *Geometrical and Mechanical properties of the hemp FRP composite*. [Electronic resource]. System requirements: AdobeAcrobatReader. URL: http://www.fidiaglobalservice.com/eng/materiali_schede/FIDHEMP20UNIDIR2024020HS40.pdf (accessed: 19.10.2017).
 35. Pelà L. *Continuum damage model for nonlinear analysis of masonry structures*. Ph.D. Thesis. Universitat Politècnica de Catalunya. 2009. 299 p.
 36. Ucer D., Ulybin A., Zubkov S., Elias-Ozkan S.T. Analysis on the mechanical properties of historical brick masonry after machinery demolition. *Construction and Building Materials*. 2018. No. 161. Pp. 186–195.
 37. *SNIP [II-22-81], Building Regulations for Stone and Reinforced Masonry Structures*, Central Institute of Standard Design [CNIISK Institute], Moscow, [1987], 2012.
- composite materials // *Structural Analysis of Historical Constructions*. 2016. Pp. 351–356.
28. Wang X., Ghiassi B., Oliveira D.V. Numerical analysis of the in-plane behaviour of TRM-strengthened masonry walls // *Structural Analysis of Historical Constructions*. 2016. Pp. 365–371.
 29. Hojdis L., Krajewski P. Glass fiber grids embedded in a cement-based matrix as strengthening of masonry structures // *Structural Analysis of Historical Constructions*. 2016. Pp. 372–376.
 30. Serhal J. *Etude de la vulnérabilité des bâtiments en maçonnerie soumis à des mouvements de terrains et élaboration de critères d'évolution de leur rigidité*. Ph.D. Thesis. Université de Lorraine. 2016. 188 p.
 31. Taforel P., Dubois F., Martin A., Pagano S. Développement de formulations dynamiques adaptées à la modélisation par éléments discrets de structures maçonnées sous chargements sismiques // *10e colloque national en calcul des structures*. 2011. Pp. 1–12.
 32. Кабанцев О.В. *Научные основы структурной теории каменной кладки для оценки предельных состояний каменных конструкций сейсмостойких зданий*. Дис. д.т.н. Москва, 2016. 358 с.
 33. Martin A., Esnault J.-B., Massin P. About the use of standard integration schemes for X-FEM in solid mechanics plasticity // *Computer Methods in Applied Mechanics and Engineering*. 2014. Pp. 283–293.
 34. *Geometrical and Mechanical properties of the hemp FRP composite*. [Электронный ресурс]. Сист. требования: AdobeAcrobatReader. URL: http://www.fidiaglobalservice.com/eng/materiali_schede/FIDHEMP20UNIDIR2024020HS40.pdf (дата обращения: 19.10.2017).
 35. Pelà L. *Continuum damage model for nonlinear analysis of masonry structures*. Ph.D. Thesis. Universitat Politècnica de Catalunya. 2009. 299 p.
 36. Ucer D., Ulybin A., Zubkov S., Elias-Ozkan S.T. Analysis on the mechanical properties of historical brick masonry after machinery demolition // *Construction and Building Materials*. 2018. No. 161. Pp. 186–195.
 37. СП 15.13330.2012 «Актуализированная редакция СНиП II-22–81* Каменные и армокаменные конструкции».

Vladimir Bepalov,
+7(981)785-08-99; chanchullero@yandex.ru

Deniz Ucer,
+7(981)956-03-45; deucer@metu.edu.tr

Ildus Salmanov,
+7(911)843-34-26; ildussalmanov@gmail.com

Israfil Kurbanov,
+7(962)715-11-17; Israfil-kurbanov@mail.ru

Svetlana Kupavykh,
+7(812)328-86-74;
Siniavina_SV@pers.spmi.ru

Владимир Владимирович Беспалов,
+7(981)785-08-99;
эл. почта: chanchullero@yandex.ru

Дениз Ючер,
+7(981)956-03-45; эл. почта: deucer@metu.edu.tr

Ильдус Динисламович Сальманов,
+7(911)843-34-26;
эл. почта: ildussalmanov@gmail.com

Исрафил Низамович Курбанов,
+7(962)715-11-17;
эл. почта: Israfil-kurbanov@mail.ru

Купавых Светлана Викторовна
+7(812)328-86-74;
эл. почта: Siniavina_SV@pers.spmi.ru

© Bepalov V.V., Ucer D., Salmanov I.D., Kurbanov I.N., Kupavykh S.V., 2018

doi: 10.18720/MCE.78.12

Silica fumes of different types for high-performance fine-grained concrete

Микрокремнеземы различных типов для высокопрочных мелкозернистых бетонов

A.S. Rassokhin,
A.N. Ponomarev,
Peter the Great St. Petersburg Polytechnic University, St. Petersburg, Russia
O.L. Figovsky,
International Nanotechnology Research Center Polymate, Migdal Haemek, Israel

Аспирант А.С. Рассохин,
канд. техн. наук, профессор
А.Н. Пономарев,
Санкт-Петербургский политехнический университет Петра Великого, г. Санкт-Петербург, Россия
д-р техн. наук, директор О.Л. Фиговский,
International Nanotechnology Research Center Polymate, г. Мигдаль ха-Эмек, Израиль

Key words: silica fume; fine grained concrete; modified concrete; nanocarbon; comparison of properties

Ключевые слова: микрокремнезем; мелкозернистый бетон; модифицированный бетон; наноглерод; сравнение свойств

Abstract. One of the most often and successfully applied admix as a part of the modified concrete is active amorphous silica fume. The increased practical interest in this admix has led to emergence in the market of various producers and also to emergence of different types (brands) of the silica fume produced from various raw materials with use of various technologies. At the same time their makeup, dispersion and content of silicone dioxide drastically ranges. It takes toll on results of use of such admixes in relation to the same recipes of concrete mixtures. The research is focused on the experimental study of the most useful types of active silica fume and the comparison of results of their using in fine-grained concrete. Results of these researches have shown a dependence of properties of the modified concrete on the content of active silica fume and from degree of its dispersion. The best results had silica fumes produced as the accompanying product by silicon production and including some additional quantity of particles of nanodimensional carbon.

Аннотация. Одна из наиболее часто и успешно применяемых добавок в составе модифицированных бетонов – активный аморфный микрокремнезем. Однако повышенный практический интерес к этой добавке привел к появлению на рынке различных производителей и, что более существенно, к появлению различных видов (марок) микрокремнеземов, получаемых из различного сырья с использованием различных технологий. При этом заметно варьируется их состав, дисперсность и содержание собственно диоксида кремния. Это не может не сказываться на результатах использования таких добавок применительно к одним и тем же рецептурам бетонных смесей. Настоящая работа посвящена экспериментальному исследованию нескольких, наиболее распространенных в настоящее время видов активного микрокремнезема и сопоставлению результатов их применения в мелкозернистых бетонах. Результаты этих исследований показали зависимость характеристик модифицируемых бетонов от содержания активного микрокремнезема и, особенно, от степени его дисперсности. Наилучшие результаты были получены для микрокремнеземов, получаемых, как сопутствующий продукт при производстве кремния и содержащего некоторое дополнительное количество частиц наноразмерного углерода.

1. Introduction

Active silica fume is an important part of many high-strength and special concrete now that has led to emergence in the market of various producers and also to emergence of different types of active silica fumes. It affects properties of the product. From the analysis of literature, it is visible that active silica fume was initially used only as means for increase in strength characteristics of the modified concrete

Рассохин А.С., Пономарев А.Н., Фиговский О.Л. Микрокремнеземы различных типов для высокопрочных мелкозернистых бетонов // Инженерно-строительный журнал. 2018. № 2(78). С. 151–160.

and cement economy [1–5]. A little later, it has become clear, that the use of this admix allows to improve also rheological and technological properties of concrete [6, 7] and, along with a plasticizing agent, to provide effective water reduction and increase in durability (frost resistance) of the created concrete. The first detailed contributions about results of comparative researches of properties of fine-grained concrete with the silica fumes containing various amount of silicon belong to the beginning of the 90th years [8–14]. Industrial production of silica fume for use in construction has reached mass proportions so far. The statutory enactments use of active silica fume and other mineral and organo-mineral microadmixes to concrete have been developed [15–20]. And new combinations of silica fumes not only with plasticizing agents, but also with some new types of nanocarbon have been developed [21–25]. All this does relevant this research to find out the best materials in the market. The main research task is the detailed comparative study of the quality of silica fume of various producers and effects of their application in recipes, first of all, of fine-grained concrete because use of the modified fine-grained concrete all-time increases [26–32].

2. Methods

As the studied types of silica fume in this research have been studied:

- amorphous silica fume MKU-85 (compact) productions of JSC Kuznetskiye ferrosplavy containing 82-87% of SiO₂;
- amorphous silica fume MKU-95 (compact) productions of JSC Kuznetskiye ferrosplavy
- amorphous silica fume MKU-95 productions of PJSC Rusal;
- amorphous silica fume MD1 productions of pilot production of INRTU [33];
- amorphous silica fume with nanocarbon MD2 productions of pilot production of INRTU [33];
- amorphous silica fume with mark MK 17-42 productions of PJSC Rusal.

For research of extent of influence of dispersion of silica fume on properties of the modified concrete have been used methods of mechanical (spherical and planetary mills) and ultrasonic dispergating (the density of the power of ultrasonic machining is from 3 to 5 VA/cm³). The size distribution of silica fume before additional dispergating and after additional dispergating was controlled on a laser granulometr "Mastersizer" productions of Malvern Instruments Ltd.

The test recipe of fine-grained concrete is:

- Portland Cement CEM I 42.5 N, production of JSC Mordovtsement (content of free alkalis (in terms of Na₂O) doesn't exceed 0.85% of masses).....18.82 % of masses;
- Washed-out river sand with the fineness modulus 0.5.....66.42 % of masses;
- Silica fume of different studied types3.32 % of masses;
- Water of mixing as per GOST Standard 23732-2011 [21].....11.44 % of masses;

The prepared concrete mixes were filled in standard forms with the sizes of 100x100x100 mm (time of vibration is 30 seconds) in number of 6 pieces for each type of the test mix and for every curing period. Form stripping was carried out on the second day. The tests of control samples for compressive breaking strength as per Russian State Standard GOST 10180-90 [22] on a hydraulic press PSU – 50A (the certificate on checking No. 0028982 of March 09, 2017) were carried out for 2, 3, 7, 14, 17, 21 and 28 days.

3. Results and Discussion

Characteristic results of additional dispergating of silica fume MKU-85 by mechanical methods (in spherical and planetary mills) are presented on Figure 1.

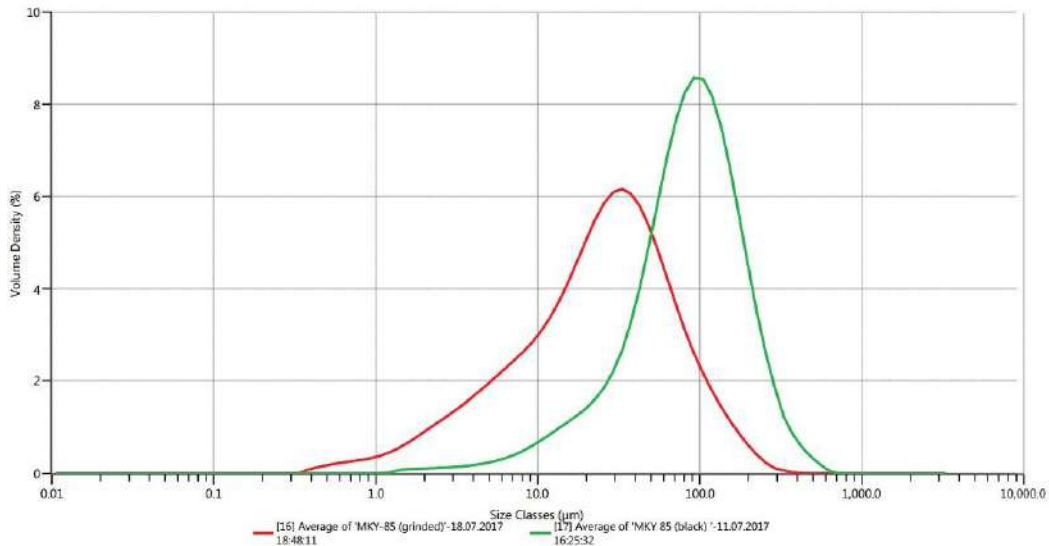


Figure 1. Size distribution of particles of initial MKU-85 and MKU-85 after additional mechanical dispersing

On the graphics (Figure 1) it is distinctly noticeable that particles that size less than 1 micron are practically absent in initial MKU-85 and that the quantity of particles that size less than 10 microns don't exceed 4.5 % of masses. After an additional mechanical dispersing the quantity of particles with sizes less than 10 microns already exceeds 26 % of masses. Also, the fraction begins to be shown by sizes less than 1 micron.

The results of the additional dispersing of silica fume MD2 with admixes of carbon nanoparticles (up to 0.5 %) are presented in Figure 2.

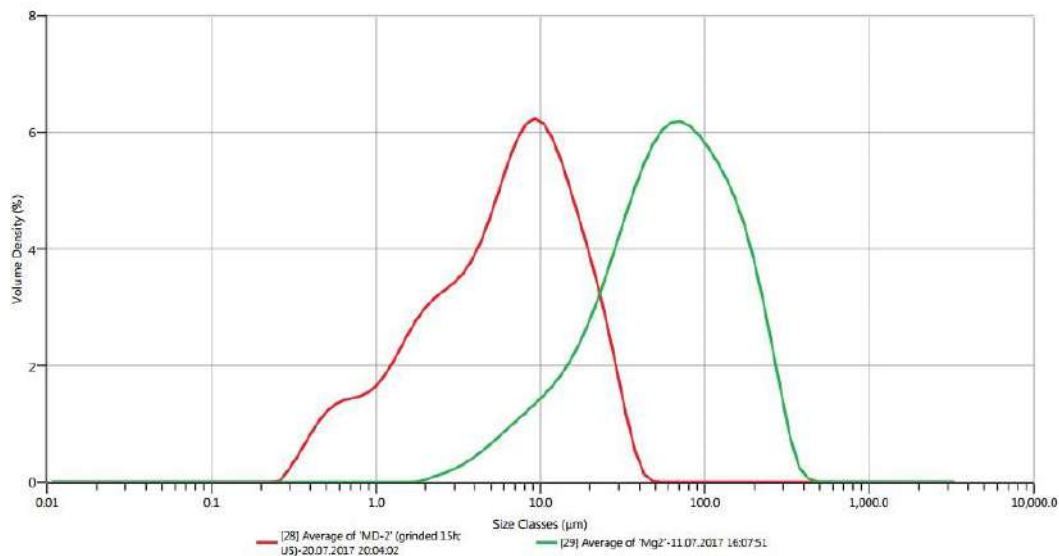


Figure 2. Particle size distribution of initial MD2 and MD2 after additional mechanical dispersing

Here it is impressive to see that particles that size less than 1 micron are completely absent as a part of MD2 before additional dispersing and a quantity of particles with a size of less than 10 microns is available no more than 6.8% of masses. The results are obtained by the weight of the spectra recorded on a dense cardboard. After dispersing the situation changes the quantity of particles with a size of less than 10 microns is available already more than 65 % of masses. Also, there are particles with a size of less than 1 micron in the quantity of about 10.5 % of masses.

The results of additional ultrasonic dispersing of the particles of silica fume MKU-85 which have undergone intensive mechanical dispersing show some displacement of this distribution towards increase in quantity of particles of the smaller sizes (Figure 3).

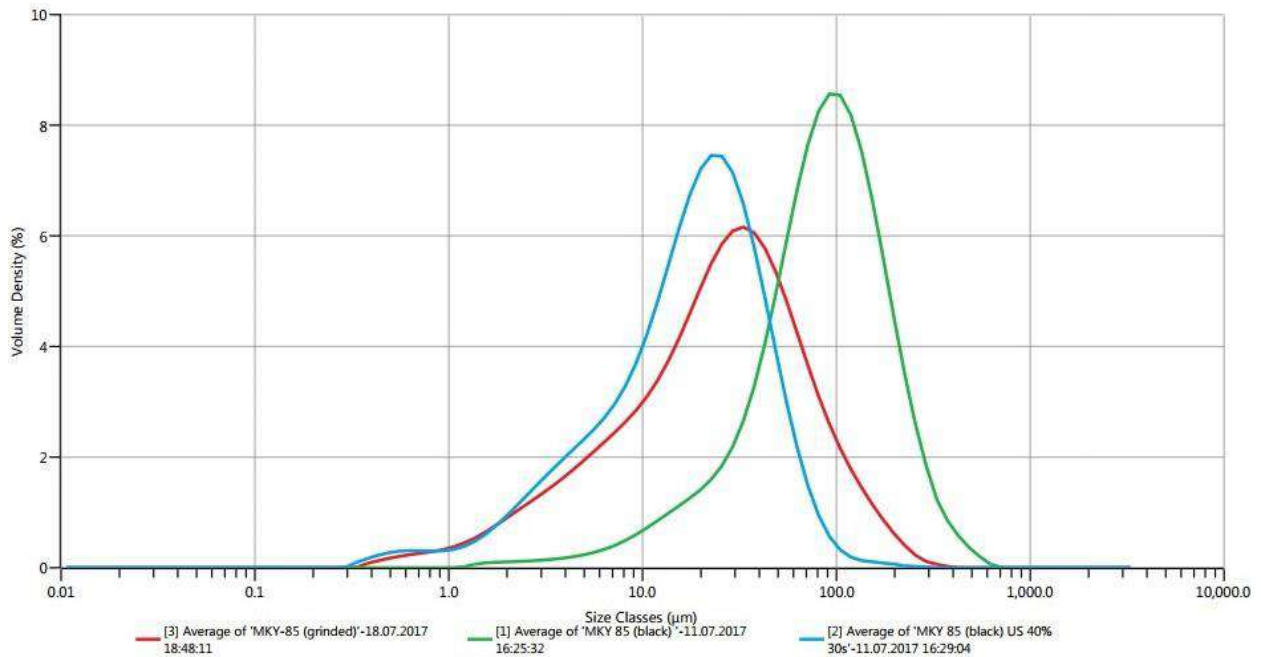


Figure 3. Particle size distribution of silica fume MKU-85 pre- and post of ultrasonic and mechanical dispersing

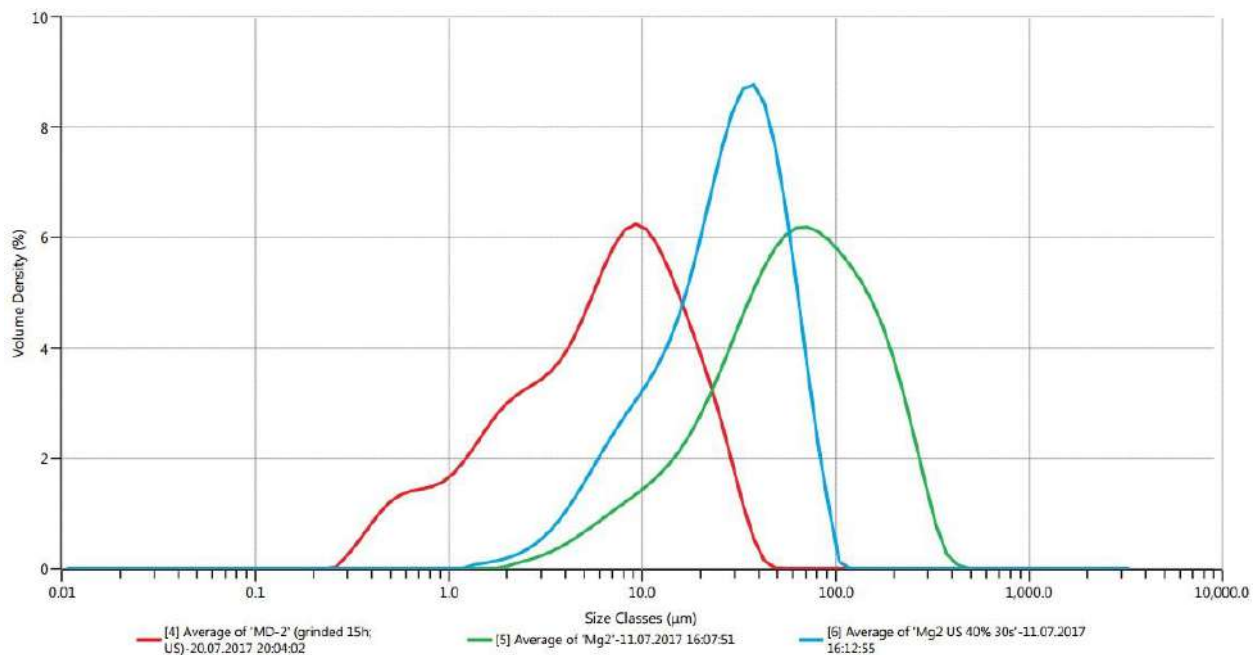


Figure 4. Particle size distribution of silica fume MD-2 pre- and post of ultrasonic and mechanical dispersing

The results of the ultrasonic dispersing for the MD-2 are in an interval between size distribution of initial silica fume and size distribution of the silica fume particles which have been mechanically dispersed (Figures 3 and 4).

It is possible to interpret such differences proceeding from the fact that as a part of the MD-2 there are carbon nanoparticles which promote aggregation of silica fume particles at enough high concentration of silica fume in dispersion.

Nevertheless, the main interest is represented by the obtained results at determining of compressive breaking strength of samples of the fine-grained concrete modified by different types of the silica fumes which are different not at least because of the structure dispersion. The obtained results on various curing periods of concrete samples are given in the Tables 1–7.

Table 1. Comparative properties of the test samples of fine-grained concrete modified by different types of silica fumes (curing period is 2 days)

Type of silica fume	Properties of concrete	Compressive breaking strength, MPa, 2 days	Density, g/cm ³	Strength-to-density ratio
	Check sample, without silica fume	8.1	2.26	3.58
	Sample with MKU-85	11.15	2.19	5.09
	Sample with MKU-85 with additional dispergating	8.1	2.24	3.61
	Sample with MKU-95	11.1	2.24	4.95
	Sample with MKU-95 with additional dispergating	7.85	2.17	3.62
	Sample with MKU-95* productions of PJSC Rusal	13.65	2.26	6.04
	Sample with MD-2	10.1	2.27	4.45
	Sample with MD-2 with additional dispergating	7.35	2.21	3.33
	Sample with mark 17-42 of PJSC Rusal	13.55	2.26	6.0

Table 2. Comparative properties of the test samples of fine-grained concrete modified by different types of silica fumes (curing period is 3 days)

Type of silica fume	Properties of concrete	Compressive breaking strength, MPa, 3 days	Density, g/cm ³	Strength-to-density ratio
	Check sample, without silica fume	12.15	2.245	5.41
	Sample with MKU-85	15.15	2.21	6.85
	Sample with MKU-85 with additional dispergating	11.1	2.21	5.02
	Sample with MKU-95	15.45	2.26	6.84
	Sample with MKU-95 with additional dispergating	10.9	2.2	4.95
	Sample with MKU-95* productions of PJSC Rusal	17.3	2.25	7.69
	Sample with MD-2	14.15	2.25	6.29
	Sample with MD-2 with additional dispergating	10.1	2.22	4.55
	Sample with mark 17-42 of PJSC Rusal	14.7	2.14	6.87

Table 3. Comparative properties of the test samples of fine-grained concrete modified by different types of silica fumes (curing period is 7 days)

Type of silica fume	Properties of concrete	Compressive breaking strength, MPa, 7 days	Density, g/cm ³	Strength-to-density ratio
	Check sample, without silica fume	17.25	2.25	7.67
	Sample with MKU-85	29.51	2.2	13.41
	Sample with MKU-85 with additional dispergating	27.15	2.2	12.34
	Sample with MKU-95	23.4	2.24	10.45
	Sample with MKU-95 with additional dispergating	28.2	2.22	12.7
	Sample with MKU-95* productions of PJSC Rusal	31.9	2.235	14.27
	Sample with MD-2	21.2	2.245	9.44
	Sample with MD-2 with additional dispergating	29.75	2.215	13.43
	Sample with mark 17-42 of PJSC Rusal	27.1	2.125	12.75

From the Tables 1-3 it is absolutely visible that silica fumes MKU-85, MKU-95 with additional dispergating, MKU-95*, MD-2 with additional dispergating and MK 17-42 lean toward to attainment of the early strength of the check samples. It will be possible to discuss the possible reasons of such a fact after an analysis of all data on a curing period of an attainment of maximum strength, which will be specified in the subsequent Tables 4–7.

Table 4. Comparative properties of the test samples of fine-grained concrete modified by different types of silica fumes (curing period is 14 days)

Type of silica fume	Properties of concrete	Compressive breaking strength, MPa, 14 days	Density, g/cm ³	Strength-to-density ratio
	Check sample, without silica fume	23.2	2.23	10.4
	Sample with MKU-85	33.41	2.2	15.18
	Sample with MKU-85 with additional dispergating	35.65	2.195	16.24
	Sample with MKU-95	26.1	2.225	11.73
	Sample with MKU-95 with additional dispergating	33.9	2.19	15.48
	Sample with MKU-95* productions of PJSC Rusal	35.31	2.23	15.83
	Sample with MD-2	24.42	2.24	10.9
	Sample with MD-2 with additional dispergating	37.2	2.23	16.68
	Sample with mark 17-42 of PJSC Rusal	32.7	2.125	15.39

Table 5. Comparative properties of the test samples of fine-grained concrete modified by different types of silica fumes (curing period is 17 days)

Type of silica fume	Properties of concrete	Compressive breaking strength, MPa, 17 days	Density, g/cm ³	Strength-to-density ratio
	Check sample, without silica fume	25.0	2.225	11.23
	Sample with MKU-85	35.0	2.05	17.05
	Sample with MKU-85 with additional dispergating	37.1	2.195	16.9
	Sample with MKU-95	27.65	2.21	12.51
	Sample with MKU-95 with additional dispergating	36.35	2.17	16.75
	Sample with MKU-95* productions of PJSC Rusal	36.72	2.225	16.5
	Sample with MD-2	25.05	2.235	11.2
	Sample with MD-2 with additional dispergating	41.0	2.2	18.63
	Sample with mark 17-42 of PJSC Rusal	33.15	2.12	15.62

Tables 4 and 5 equally fix the dominating strength enhancement on the compression for control samples with an admix of MKU-85, of MKU-85 with an additional dispergating, of MKU-95 with an additional dispergating, of MKU-95 productions of PJSC Rusal, as also of MD-2 with an additional dispergating.

On the basis of the data it is possible to mention the availability of a not really big but stable effect of an air entrainment, which is characteristic for silica fumes MKU-85, MKU-95 and MK 17-42 regardless of their dispersion degree.

Table 6. Comparative properties of the test samples of fine-grained concrete modified by different types of silica fumes (curing period is 21 days)

Type of silica fume	Properties of concrete	Compressive breaking strength, MPa, 21 days	Density, g/cm ³	Strength-to-density ratio
	Check sample, without silica fume	26.1	2.225	11.73
	Sample with MKU-85	36.41	2.2	16.55
	Sample with MKU-85 with additional dispergating	38.82	2.19	17.72
	Sample with MKU-95	28.73	2.21	13.0
	Sample with MKU-95 with additional dispergating	38.15	2.17	17.58
	Sample with MKU-95* productions of PJSC Rusal	39.55	2.225	17.77
	Sample with MD-2	27.9	2.235	12.48
	Sample with MD-2 with additional dispergating	43.15	2.2	19.61
	Sample with mark 17-42 of PJSC Rusal	34.55	2.12	16.29

Table 7. Comparative properties of the test samples of fine-grained concrete modified by different types of silica fumes (curing period is 28 days)

Type of silica fume	Properties of concrete	Compressive breaking strength, MPa, 18 days	Density, g/cm ³	Strength-to-density ratio
Check sample, without silica fume		27.9	2.225	11.23
Sample with MKU-85		38.27	2.195	17.43
Sample with MKU-85 with additional dispergating		40.35	2.19	18.42
Sample with MKU-95		30.2	2.21	13.66
Sample with MKU-95 with additional dispergating		39.6	2.165	18.29
Sample with MKU-95* productions of PJSC Rusal		40.42	2.225	18.17
Sample with MD-2		29.12	2.233	13.1
Sample with MD-2 with additional dispergating		44.24	2.197	20.13
Sample with mark 17-42 of PJSC Rusal		36.13	2.116	17.07

Summarizing the experimental data obtained in the research on the comparison of 8 types of active silica fume manufactured now in the Russian Federation, it is possible to draw the following main conclusions:

– the best results on late terms of concrete maturity had silica fume MD2 with additional dispergating (with additive of nanodisperse carbon of 0.5 % of masses, productions of pilot production of INRTU). The increase of strength of the fine-grained concrete by it referred of control sample modified without admixes has made 58.5 %.

The most air-entering properties has shown silica fume with mark 17–42 productions of PJSC RUSAL. Its air-entering property at concentration of admix in 3.32 % of masses referring the mass of concrete mix (17.6 % of masses referring the mass of cement) was from 3.4 % to 6.6 %.

Some of the made available samples of silica fumes (from our point of view) were retained or transported to the test location in breach of temperature-humidity conditions, in particular samples of silica fume MD-1, which have been rejected. It has led to an increase in amount of sorption humidity and to partial loss of activity. However, as it was revealed, except reduction of the sizes of particles at additional dispergating there is almost a complete recovery of admix activity.

Besides of the comparison of properties of fine-grained concrete modified by silica fumes of different types this research confirms earlier conducted researches in the field.

This research like other [1–9, 17] shows increase in durability of concrete when using silica fume.

Also, there is a confirmation of improvement of properties of silica fume at increase in its dispersion which has been made in the article [17].

This research confirms improvement of properties of silica fume at addition of microamount of nanodimensional carbon that has been investigated in the research [28].

4. Conclusions

The main result of the research can be considered the comparison of several, best known types of active silica fumes manufactured in the Russian Federation in the recent years. All tested types of active silica fumes were suitable for an improvement of strength (and also rheological) properties of fine-grained concrete. The use of the studied types of silica fumes in quantity up to 17.6 % of the mass of cement brings in an increase in strength properties of control samples of fine-grained (sand) concrete at a size from 29.5 % to 58.5 %. The shared use of these admixes with a plasticizing agent of perspective generations promises much more impressive results that forms the basis for continuation of this research. From all studied samples the best results were shown by the silica fume MD-2 productions of pilot production of INRTU activated by microamount of nanodimensional carbon.

5. Acknowledgement

The authors would like to express their gratitude to the staff of the Centre for Innovative Technologies of Composite Nanomaterials, who has helped in researches of the size distribution of particles of silica fumes and to the staff of IRGTU, who have samples of new types of silica fumes.

References

1. Kapriyelov S.S., Sheynfeld A.V., Krivoborodov Yu.R. Influence the structure of the cement stone with the silica fume and super plasticizer additives on the properties of concrete. *Concrete and reinforced concrete*. 1992. No. 7. Pp. 4–7.
2. Batrakov V., Kapriyelov S., Sheinfeld A. influence of different types of silica fume having varying silica content on the microstructure and properties of concrete // *Fourth int. conf. on fly ash, silica fume, slag and natural pozzolans in concrete, Istanbul, Turkey. Proceedings*. 1992. Pp. 943–964.
3. Holland T.C. Working with silica fume in ready-mixed concrete - USA Experience // *CANMET/ACI. Third International Conference. Trondheim. Norway. Proceedings*. 1989. Vol. 2. Pp. 763–781.
4. Kapriyelov S.S., Batrakov V.G., Sheynfeld A.V. A new generation of modified concretes: real state and perspective. *Concrete and reinforced concrete*. 1999. No. 6. Pp. 6–10.
5. Kim J.-E., Park W.-S., Jang Y.-I., Kim S.-W., Kim S.W., Nam Y.-H., Kim D.-G., Rokugo K. Mechanical properties of energy efficient concretes made with binary, ternary, and quaternary cementitious blends of fly ash, blast furnace slag, and silica fume. *International Journal of Concrete Structures and Materials*. 2016. Vol. 10. Pp. 97–108.
6. Adekunle S., Ahmad S., Maslehuddin M., Al-Gahtani H. J. Properties of SCC prepared using natural pozzolana and industrial wastes as mineral fillers. *Cement and Concrete Composites*. 2015. Vol. 62. Pp. 125–133.
7. Ramanathan P., Baskar I., Muthupriya P., Venkatasubramani R. Performance of self-compacting concrete containing different mineral admixtures. *Journal of Civil Engineering*. 2013. Vol. 17. No. 2. Pp. 465–472.
8. Dinakar P., Sahoo P.K., Sriram G. Effect of metakaolin content on the properties of high strength concrete. *International Journal of Concrete Structures and Materials*. 2013. Vol. 7. No. 3. Pp. 215–223.
9. Baldino N., Gabriele D., Lupi F.R., Seta L., Zinno R. Rheological behaviour of fresh cement pastes: Influence of synthetic zeolites, limestone and silica fume. *Cement and Concrete Research*. 2014. Vol. 63. Pp. 38–45.
10. Larsen L.O., Naruts V.V. Self-compacting concrete with limestone powder for transport infrastructure. *Magazine of Civil Engineering*. 2016. No. 8. Pp. 76–85.
11. Rakhimov R.Z., Rakhimova N.R., Gaifullin A.R. Influence of the addition of dispersed fine polymineral calcined clays on the properties of Portland cement paste. *Advances in Cement Research*. 2017. No. 1(29). Pp. 21–32.
12. Suraneni P., Weiss J. Examining the pozzolanicity of supplementary cementitious materials using isothermal calorimetry and thermogravimetric analysis. *Cement and Concrete Composites*. 2017. Vol. 83. Pp. 273–278.
13. Mueller F.V., Wallevik O.H., Khayat K.H. A new homogeneity assessment concept applied to evaluate selfconsolidation and segregation stability of self-consolidating concrete. *Proceedings pro100: 8th International RILEM Symposium on Self-Compacting Concrete – SCC*. 2016.
14. Da Silva P.R., De Brito J. Experimental study of the porosity and microstructure of self-compacting concrete (SCC) with binary and ternary mixes of fly ash and limestone filler. *Construction and Building Materials*. 2015. Vol. 86. Pp. 101–112.
15. Da Silva P.R., De Brito J. Durability performance of

Литература

1. Kapriyelov S.S., Sheynfeld A.V., Krivoborodov Yu.R. Influence the structure of the cement stone with the silica fume and super plasticizer additives on the properties of concrete. *Concrete and reinforced concrete*. 1992. № 7. Pp. 4–7.
2. Batrakov V., Kapriyelov S., Sheinfeld A. influence of different types of silica fume having varying silica content on the microstructure and properties of concrete // *Fourth int. conf. on fly ash, silica fume, slag and natural pozzolans in concrete, Istanbul, Turkey. Proceedings*. 1992. Pp. 943–964.
3. Holland T.C. Working with silica fume in ready-mixed concrete - USA Experience // *CANMET/ACI. Third International Conference. Trondheim. Norway. Proceedings*. 1989. Vol. 2. Pp. 763–781.
4. Kapriyelov S.S., Batrakov V.G., Sheynfeld A.V. A New Generation of Modified Concretes: real state and perspective // *Concrete and reinforced concrete*. 1999. № 6. Pp. 6–10.
5. Kim J.-E., Park W.-S., Jang Y.-I., Kim S.-W., Kim S.W., Nam Y.-H., Kim D.-G., Rokugo K. Mechanical properties of energy efficient concretes made with binary, ternary, and quaternary cementitious blends of fly ash, blast furnace slag, and silica fume // *International Journal of Concrete Structures and Materials*. 2016. Vol. 10. Pp. 97–108.
6. Adekunle S., Ahmad S., Maslehuddin M., Al-Gahtani H. J. Properties of SCC prepared using natural pozzolana and industrial wastes as mineral fillers // *Cement and Concrete Composites*. 2015. Vol. 62. Pp. 125–133.
7. Ramanathan P., Baskar I., Muthupriya P., Venkatasubramani R. Performance of self-compacting concrete containing different mineral admixtures // *Journal of Civil Engineering*. 2013. Vol. 17. № 2. Pp. 465–472.
8. Dinakar P., Sahoo P.K., Sriram G. Effect of metakaolin content on the properties of high strength concrete // *International Journal of Concrete Structures and Materials*. 2013. Vol. 7. № 3. Pp. 215–223.
9. Baldino N., Gabriele D., Lupi F.R., Seta L., Zinno R. Rheological behaviour of fresh cement pastes: Influence of synthetic zeolites, limestone and silica fume // *Cement and Concrete Research*. 2014. Vol. 63. Pp. 38–45.
10. Ларсен О.А., Наруть В.В. Самоуплотняющийся бетон с карбонатным наполнителем для объектов транспортной инфраструктуры // *Инженерно-строительный журнал*. 2016. № 8(68). С. 76–85.
11. Rakhimov R.Z., Rakhimova N.R., Gaifullin A.R. Influence of the addition of dispersed fine polymineral calcined clays on the properties of Portland cement paste // *Advances in Cement Research*. 2017. № 1(29). Pp. 21–32.
12. Suraneni P., Weiss J. Examining the pozzolanicity of supplementary cementitious materials using isothermal calorimetry and thermogravimetric analysis // *Cement and Concrete Composites*. 2017. Vol. 83. Pp. 273–278.
13. Mueller F.V., Wallevik O.H., Khayat K.H. A new homogeneity assessment concept applied to evaluate selfconsolidation and segregation stability of self-consolidating concrete // *Proceedings pro100: 8th International RILEM Symposium on Self-Compacting Concrete – SCC*. 2016.
14. Da Silva P.R., De Brito J. Experimental study of the porosity and microstructure of self-compacting concrete (SCC) with binary and ternary mixes of fly ash and limestone filler // *Construction and Building Materials*. 2015.

Rassokhin A.S., Ponomarev A.N., Figovsky O.L. Silica fumes of different types for high-performance fine-grained concrete. *Magazine of Civil Engineering*. 2018. No. 2. Pp. 151–160. doi: 10.18720/MCE.78.12.

- selfcompacting concrete (SCC) with binary and ternary mixes of fly ash and limestone filler. *Materials and Structures*. 2016. Vol. 49. No. 7. Pp. 2749–2766.
16. Nemarov A., Lebedev N., Kondrat'ev V., Korniyakov M., Karlina A.I. Theoretical and experimental research of parameters of pneumatic aerators and elementary cycle flotation. *International Journal of Applied Engineering Research*. 2016. No. 20. Pp. 10222–10226.
 17. Kiski S.S., Ponomarev A.N., Ageev I.V., Cun Ch. Modification of the fine-aggregate concrete by high disperse silica fume and carbon nanoparticles containing modifiers. *Advanced Materials Research*. 2014. Vols. 941–944. Pp. 430–435.
 18. Kondrat'ev V.V., Nemchinova N.V., Ivanov N.A., Ershov V.A., Sysoev I.A. New production solutions for processing silicon and aluminium production waste. *Metallurgist*. 2013. № 5-6. Pp. 455–459.
 19. Kondrat'ev V.V., Ershov V.A., Shakhrai S.G., Ivanov N.A., Karlina A.I. Formation and utilization of nanostructures based on carbon during primary aluminum production. *Metallurgist*. 2016. No. 60(7-8). Pp. 877–882.
 20. Kuz'min M.P., Kondrat'ev V.V., Larionov L.M., Kuz'mina M.Yu., Ivanchik N.N. Possibility of preparing alloys of the al-si system using amorphous microsilica. *Metallurgist*. 2017. Vol. 61. No. 1-2. Pp. 86–91.
 21. Kondrat'ev V.V., Balanovskii A.E., Ivanov N.A., Ershov V.A., Korniyakov M.V. Evaluation of the effect of modifier composition with nanostructured additives on grey cast iron properties. *Metallurgist*. 2014. No. 5-6. Pp. 377–387.
 22. Kondrat'ev V.V., Nebogin S.A., Sysoev I.A., Gorovoy V.O., Karlina A.I. Description of the test stand for developing of technological operation of nano-dispersed dust preliminary coagulation. *International Journal of Applied Engineering Research*. 2017. Vol. 12. No. 22. Pp. 12809–12813.
 23. Ivanchik N., Kondrat'ev V., Chesnokova A. Use of the nanosilica recovered from the finely dispersed by-product of the electrothermal silicon production for concrete modification. *Procedia Engineering*. 2016. No. 150. Pp. 1567–1573.
 24. Nemarov A., Lebedev N., Kondrat'ev V., Korniyakov M., Karlina A.I. Theoretical and experimental research of parameters of pneumatic aerators and elementary cycle flotation. *International Journal of Applied Engineering Research*. 2016. Vol. 11. No. 20. Pp. 10222–10226.
 25. Petrovskaja V.N., Kondrat'ev V.V., Nemarov A.A., Petrovskij A.A. Uglerodnyye nanotrubki v proizvodstve kristallicheskogo kremnija [Carbon nanotubes in production of crystal silicon]. *Jekologija i promyshlennost' Rossii*. 2017. No. 1. Pp. 17–23. (rus)
 26. Korsun V.I., Vatin N.I., Korsun A.V., Nemova D.V. Physical-Mechanical Properties of the Modified Fine-Grained Concrete Subjected to Thermal Effects up to 200°C. *Applied Mechanics and Materials*. 2014 Vols. 633-634. Pp. 1013–1017.
 27. Ponomarev A., Knezević M., Vatin N., Kiski S., Ageev I. Nanosize scale additives mix influence on the properties of the high performance concretes. *Journal of Applied Engineering Science*. 2014. No. 12(3). Pp. 227–231.
 28. Nizina T.A., Ponomarev, A.N., Balykov, A.S., Pankin, N.A. Fine-grained fibre concretes modified by complexed nanoadditives. *International Journal of Nanotechnology*. 2017. No. 14(7-8). Pp. 665–679.
 29. Cherkashin A.V., Pykhtin K.A., Begich Y.E., Sherstobitova P.A., Koltsova T.S. Mechanical properties of nanocarbon modified cement. *Magazine of Civil Engineering*. 2017. No. 72(4). Pp. 54–61.
 30. Akimov L., Ilenko N., Mizharev R., Cherkashin A., Vatin N., Chumadova L. Composite concrete modifier CM 02-10 and its impact on the strength characteristics of concrete. Vol. 86. Pp. 101–112.
 15. Da Silva P.R., De Brito J. Durability performance of selfcompacting concrete (SCC) with binary and ternary mixes of fly ash and limestone filler // *Materials and Structures*. 2016. Vol. 49. № 7. Pp. 2749–2766.
 16. Nemarov A., Lebedev N., Kondrat'ev V., Korniyakov M., Karlina A.I. Theoretical and experimental research of parameters of pneumatic aerators and elementary cycle flotation // *International Journal of Applied Engineering Research*. 2016. № 20. Pp. 10222–10226.
 17. Kiski S.S., Ponomarev A.N., Ageev I.V., Cun Ch. Modification of the fine-aggregate concrete by high disperse silica fume and carbon nanoparticles containing modifiers // *Advanced Materials research*. 2014. Vols. 941–944. Pp. 430–435.
 18. Kondrat'ev V.V., Nemchinova N.V., Ivanov N.A., Ershov V.A., Sysoev I.A. New production solutions for processing silicon and aluminium production waste // *Metallurgist*. 2013. № 5-6. Pp. 455–459.
 19. Kondrat'ev V.V., Ershov V.A., Shakhrai S.G., Ivanov N.A., Karlina A.I. Formation and utilization of nanostructures based on carbon during primary aluminum production // *Metallurgist*. 2016. № 60(7-8). Pp. 877–882.
 20. Kuz'min M.P., Kondrat'ev V.V., Larionov L.M., Kuz'mina M.Yu., Ivanchik N.N. Possibility of preparing alloys of the al-si system using amorphous microsilica // *Metallurgist*. 2017. Vol. 61. № 1–2. Pp. 86–91.
 21. Kondrat'ev V.V., Balanovskii A.E., Ivanov N.A., Ershov V.A., Korniyakov M.V. Evaluation of the effect of modifier composition with nanostructured additives on grey cast iron properties // *Metallurgist*. 2014. № 5–6. Pp. 377–387.
 22. Kondrat'ev V.V., Nebogin S.A., Sysoev I.A., Gorovoy V.O., Karlina A.I. Description of the test stand for developing of technological operation of nano-dispersed dust preliminary coagulation // *International Journal of Applied Engineering Research* ISSN 0973-4562. 2017. Vol. 12. № 22. Pp. 12809–12813.
 23. Ivanchik N., Kondrat'ev V., Chesnokova A. Use of the nanosilica recovered from the finely dispersed by-product of the electrothermal silicon production for concrete modification // *Procedia Engineering*. 2016. № 150. Pp. 1567–1573.
 24. Nemarov A., Lebedev N., Kondrat'ev V., Korniyakov M., Karlina A.I. Theoretical and experimental research of parameters of pneumatic aerators and elementary cycle flotation // *International Journal of Applied Engineering Research*. 2016. Vol. 11. № 20. Pp. 10222–10226.
 25. Петровская В., Кондратьев В., Немаров А., Петровский А. Углеродные нанотрубки в производстве кристаллического кремния // *Экология и промышленность России*. 2017. № 1(21). Pp. 17–23.
 26. Korsun V.I. Vatin N.I. Korsun A.V., Nemova D.V. Physical-mechanical properties of the modified fine-grained concrete subjected to thermal effects up to 200 °C // *Applied Mechanics and Materials*. 2014. Vols. 633–634. Pp. 1013–1017.
 27. Ponomarev A., Knezević M., Vatin N., Kiski S., Ageev I. Nanosize scale additives mix influence on the properties of the high performance concretes // *Journal of Applied Engineering Science*. 2014. № 3(12). Pp. 227–231.
 28. Nizina, T.A., Ponomarev, A.N., Balykov, A.S., Pankin, N.A. Fine-grained fibre concretes modified by complexed nanoadditives // *International Journal of Nanotechnology*. 2017. № 14(7-8). Pp. 665–679.
 29. Черкашин А.В., Пыхтин К.А., Бегич Я.Э., Шерстобитова П.А., Кольцова Т.С. Механические свойства наноуглеродного цемента // *Инженерно-строительный журнал*. 2017. № 4(72). С. 54–61.
 30. Akimov L., Ilenko N., Mizharev R., Cherkashin A., Vatin N., Chumadova L. Composite concrete modifier CM 02-10 and

- MATEC Web of Conferences. 2016. No. 53.
31. Frolov A., Chumadova L., Cherkashin A., Akimov L. Prospects of use and impact of nanoparticles on the properties of high-strength concrete. *Applied Mechanics and Materials*. 2014. Pp. 584–586, 1416–1424.
32. Shishkin A., Shishkina A., Vatin N. Low-shrinkage alcohol cement concrete. *Applied Mechanics and Materials*. 2014. Pp. 917–921.
33. Kondratiev V.V., Govorkov A.S., Kolosov A.D., Gorovoy V.O., Karlina A.I. The development of a test stand for developing technological operation "Flotation and separation of MD2. the deposition of nanostructures MD1" produce nanostructures with desired properties. *International Journal of Applied Engineering Research*. 2017. Vol. 12. No. 22. Pp. 12373–12377.
- its impact on the strength characteristics of concrete // MATEC Web of Conferences. 2016. № 53.
31. Frolov A., Chumadova L., Cherkashin A., Akimov L. Prospects of use and impact of nanoparticles on the properties of high-strength concrete // *Applied Mechanics and Materials*. 2014. Pp. 584-586, 1416-1424.
32. Shishkin A., Shishkina A., Vatin N. Low-shrinkage alcohol cement concrete // *Applied Mechanics and Materials*. 2014. Pp. 917–921.
33. Kondratiev V.V., Govorkov A.S., Kolosov A.D., Gorovoy V.O., Karlina A.I. The development of a test stand for developing technological operation "Flotation and separation of MD2. the deposition of nanostructures MD1" produce nanostructures with desired properties // *International Journal of Applied Engineering Research*. 2017. Vol. 12. № 22. Pp. 12373–12377

Aleksandr Rassokhin,
+7(911)526-68-59; rassokhinaleksandr@gmail.com

Andrey Ponomarev,
+7(911)929-35-22; 9293522@gmail.com

Oleg Figovsky,
+97(250)577-99-20; figovsky@gmail.com

Александр Сергеевич Рассохин,
+7(911)526-68-59;
эл. почта: rassokhinaleksandr@gmail.com

Андрей Николаевич Пономарев,
+7(911)929-35-22;
эл. почта: 9293522@gmail.com

Олег Львович Фиговский,
+97(250)577-99-20;
эл. почта: figovsky@gmail.com

© Rassokhin A.S., Ponomarev A.N., Figovsky O.L., 2018

doi: 10.18720/MCE.78.13

The temperature waves motion in hollow thick-walled cylinder

Распространение температурных волн в пустотелом толстостенном цилиндре

O.D. Samarin,
National Research Moscow State University of
Civil Engineering, Moscow, Russia

Канд. техн. наук, доцент О.Д. Самарин,
Национальный исследовательский
Московский государственный
строительный университет, Москва,
Россия

Key words: hollow cylinder; thermal conductivity equation; finite-difference scheme; temperature wave; temperature profile; cylindrical symmetry

Ключевые слова: полый цилиндр; уравнение теплопроводности; конечно-разностная схема; температурная волна; профиль температуры; цилиндрическая симметрия

Abstract. A hollow cylinder with thick walls is one of the most complex objects to calculate the unsteady temperature field, so this field is the least studied. However, such objects are found in many modern constructions of systems of generation and distribution of heat. In the proposed article it deals with the study of propagation of temperature waves in the wall of the hollow cylinder after a sudden temperature change of the internal environment, fuses-causes upon termination of the movement or circulation of the heated stream. The algorithm of calculation of temperature fields numerically is shown using an explicit finite-difference scheme of high accuracy in conditions of cylindrical symmetry with boundary conditions of the first kind. The results of calculations of the penetration depth of the temperature wave according to the considered algorithm, depending on the time since the start of heat exposure and their comparison with the existing data for one-dimensional case are given for the implementation of the identification obtained mathematical model. Calculated radial profiles of relative temperature in the cylinder wall within the temperature waves in dimensionless coordinates and the analytical approximation relations for the description of these profiles are presented. The results are compared with the existing analytical solution for an unlimited array in rectangular coordinates and it is marked that the common results are found regardless of the material and geometry of the cylinder, as well as of temperatures of inner and outer environment. Presented dependences are invited to apply for the analytical evaluation of the minimum temperature on the inner surface of the heated cylindrical structures that will allow the use of engineering methods to verify compliance with industrial safety requirements.

Аннотация. Полый цилиндр с толстыми стенками является одним из наиболее сложных объектов для расчета нестационарного температурного поля, поэтому такое поле является наименее изученным. Вместе с тем подобные объекты встречаются во многих современных конструкциях систем генерации и распределения теплоты. В предлагаемой работе рассматривается исследование распространения температурной волны в стенке полого цилиндра при скачкообразном изменении температуры внутренней среды, возникающем при прекращении движения или циркуляции нагретого потока. Показан алгоритм расчета температурного поля численным методом с помощью явной конечно-разностной схемы повышенной точности в условиях цилиндрической симметрии при граничных условиях первого рода. Приведены результаты вычисления глубины проникновения температурной волны по рассмотренному алгоритму в зависимости от времени с момента начала теплового воздействия и их сопоставление с существующими данными для одномерного случая для осуществления идентификации получаемой математической модели. Представлены рассчитанные радиальные профили относительной температуры в стенке цилиндра в пределах температурной волны в безразмерных координатах и предложены аналитические аппроксимационные зависимости для описания данных профилей. Полученные результаты сопоставлены с имеющимся аналитическим решением для неограниченного массива в прямоугольных координатах и отмечена общность найденных результатов независимо от материала и геометрии цилиндра, а также температур внутренней и наружной среды. Представленные зависимости предложено применять для аналитической оценки минимальной температуры на внутренней поверхности цилиндрических

нагреваемых конструкций, что позволит использовать инженерные методы проверки выполнения требований промышленной безопасности.

1. Introduction

The proposed work has unsteady state temperature field of hollow thick-wall cylinder at a single heat exposure as target of research.

The task of research of unsteady state conduction in bodies of various geometric forms has been investigated for quite a long time. Most such investigations come from a solution of differential equation of heat transfer in solids, known as Fourier [1–2]. For the last time, due to development of computing tools, the center stage is taken by numerical methods of its solution obtaining, if required, approximation analytical dependences [2–3]. In most cases, though, they belong to one-dimensional case, or the consideration is performed in rectangular coordinates. This, though, corresponds to prevailing part of actually met tasks, and also not only in unsteady, but also in steady state [3]. In condition of cylindrical symmetry the most developed are the issues of heating and cooling of solid or thin-wall cylinders [1–2]. At the same time in some applications the calculation of unsteady state temperature field of hollow cylindrical structures with thick walls is of interest. But even in fundamental monograph [1] corresponding solution is not provided. For the last time there arise a set of publications, where such issues are considered both analytically and numerically. But the results obtained by the authors, as a rule, are extremely complicated for application in engineering practice [4, 5, 10, 15, 17, 18] or, otherwise, are too rough [12]. Others relate to specific options of structures, applied in limited fields and functioning in specific conditions, for example, under supercritical modes [9], in nuclear power industry [14] or composite materials production [6–8, 11, 13], and in the presence of phase transitions [16, 19], or fuel combustion processes [20].

Thus, the relevance of the proposed research lies in the need of finding sufficiently accurate and physically based, but at the same time acceptable for engineering use variations of the temperature of the heated cylindrical structures in emergency conditions. For example, it can be useful when resolving the issue about beginning of condensate formation at internal surfaces of smoke stacks when boiler unit is stopped or at outer surface of heat insulation of heat pipelines when heat supply is switched off. One can in general note that these tasks mainly bear a relation to safety, both industrial and connected with human livelihood. The obtained results can be applied in this case for quite wide range of power facilities of such structure.

The target of the work is the calculation of unsteady temperature field at discontinuous variation of environment temperature at internal surface of cylinder. The tasks of the research will be:

- development of algorithm realizing a finite difference scheme of resolving an equation of heat conduction in cylinder wall;
- obtaining of analytical dependences for a depth of penetration of temperature wave and temperature at internal surface of cylinder on the results of approximation of program generation results.

2. Methods

Figure 1 shows the scheme of cylinder under consideration and some conventional symbols. Main of them are R and r_0 – correspondingly outer and inner radius, m.

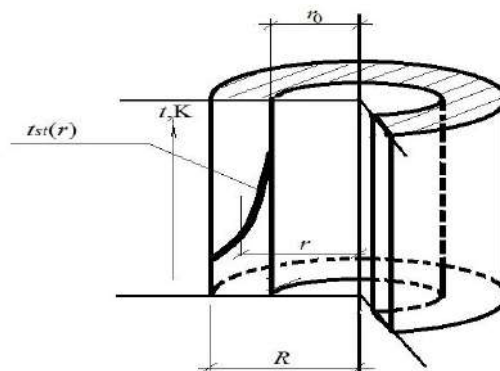


Figure 1. Scheme of hollow cylinder and steady state temperature field in its wall

In this case in cylinder wall a steady state temperature field $t_{st}(r)$ of logarithmic type is set. It can be calculated in a usual way [1, 2]. Its typical character is also shown at Figure 1. For convenience of further narration and to achieve maximum collectivity of the obtained results it is convenient to pass to a relative non-dimensional temperature θ . It can be defined according to the equation:

$$\theta = \frac{t - t_{ex}}{t_{in} - t_{ex}}, \quad (1)$$

where t_{ex} and t_{in} – correspondingly environment temperatures, K, from outer side of cylinder and inside its chamber. Then the differential equation of unsteady state conduction for cases of cylindrical symmetry can be written in the following way [1–2]:

$$\frac{\partial \theta}{\partial \tau} = a \left[\frac{\partial \theta}{r \partial r} + \frac{\partial^2 \theta}{\partial r^2} \right], \quad (2)$$

where $a = \frac{\lambda}{c\rho}$ – coefficient of chamber wall material temperature conductivity, m^2/s ; λ – its heat conductivity $W/(m \cdot K)$; c and ρ – specific heat capacity, $J/(kg \cdot K)$, and density, kg/m^3 ; t , s – time moment for which θ value is calculated; r – radial coordinate (see figure 1). Solution in this case will show current deviation of temperature field from initial steady state.

This equation in the simplest case can be tried to investigate at boundary conditions of first order, i.e. consider that $\theta = 1$ at $r = r_0$ and $\theta = 0$ at $r = R$. This just corresponds to the mode of non-continuous variation of heat current at switching off or, vice versa, switching on of heat supply. Then at a first approximation the actual value θ at internal surface of chamber can be calculated, if we input an additional cylindrical layer. Its thickness can be defined from conditions of internal heat exchanging, on account of equality of thermal resistance of such layer to actual resistance of heat exchange:

$$\delta_0^* = r_0 \left(\exp\left(\frac{\lambda}{\alpha_0 r_0}\right) - 1 \right) = r_0 \left(\exp\left(\frac{1}{Bi_0}\right) - 1 \right), \quad (3)$$

where α_0 – coefficient of convective heat exchange to internal surface, $W/(m^2 \cdot K)$;

$Bi_0 = \frac{\alpha_0 r_0}{\lambda}$ – non-dimensional criterion Bio for this surface. It is easy to see that at big values Bi_0 thickness of additional layer with sufficient preciseness can be determined as λ/α , and for flat wall too. Then actual radius r_0 , for which $\theta = 1$ is fixed, is obtained from actual by reduction by value δ_0^* . The same is actual radius R of outer surface, where $\theta = 0$ is maintained, will be increased by thickness δ^* . It can be calculated according to (3), but instead r one shall use R , and as α_0 a corresponding coefficient of outer heat exchange will be used.

To resolve the equation (2) one can use numerical methods. The main importance in this case is the preciseness of the obtained result, and volume of the used memory and amount of performed operations is not critical due to high computational resources of modern computing devices. So the explicit finite-difference scheme appears to be advantageous due to its simplicity for programming. Then temperature value in i -th mesh point in $j+1$ -st time moment can be calculated according to equation:

$$t_{i,j+1} = Fo_{\Delta} \left(\frac{2i-1}{2i-2} t_{i+1,j} + \left(\frac{1}{Fo_{\Delta}} - 2 \right) t_{i,j} + \frac{2i-3}{2i-2} t_{i-1,j} \right). \quad (4)$$

Here $t_{i,j}$, $t_{i-1,j}$ and $t_{i+1,j}$ – value of temperature in j -th moment of time in i -th mesh and neighboring on the left and on the right (mesh numeration from chamber axle in direction of outer surface);

$Fo_{\Delta} = \frac{a\Delta\tau}{(\Delta r)^2}$ – non-dimensional local criterion of Fourier, where $\Delta\tau$, s , and Δr , m – correspondingly steps on time and coordinate, representing parameters of finite-differentiate scheme. As it is known [1],

[2], the adopted scheme is concurred at $For_{\Delta} \leq 1/2$. So in calculations they selected the value $For_{\Delta} = 1/6$, providing improved accuracy of approximation – of 4-th order on space and 2-nd – on time coordinate.

3. Results and Discussion

For analysis and interpretation of results of calculations it is required first of all to note that from general theoretical considerations, including dimensional analysis method, it arises that the depth of penetration of temperature wave into the depth of material Δ , m, shall be increased with the flow of time in general as $\Delta = k\sqrt{a\tau}$ [1]. Of course, within the frames of the applied phenomenological model, providing the basis of derivation of differential equation of heat conductivity, specific level of coefficient k will always be an issue of some reasonable agreement. Really, as a result of supposition about infinitely big speed of spreading heat in a substance, the values θ appear to be different from zero at any r for each moment $t > 0$. That is why it is required to stipulate, what the calculated value θ will be equal to at the boundary of the area of penetration of temperature wave. If we accept for this case $\theta = 0.01$, series of sources gives value $k = 3.6$. In this case the approximation of results of numerical calculations allows with good accuracy to consider $k = 3.75$. Some deviation from known data can be explained, apparently, with the fact that in this case we investigate the case of cylindrical symmetry. Figure 2 shows the results of calculations according to scheme (4) for correlation $r_0/R = 0.7$ with the help of the program developed by author for computing device at algorithm language *Fortran*.

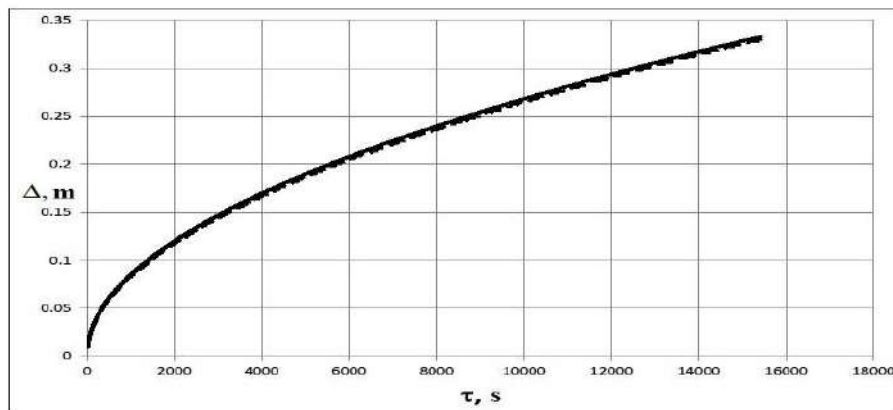


Figure 2. Dependence Δ from τ according to data of numerical calculation (dot line) and its approximation in the form of $\Delta = 3.75\sqrt{a\tau}$ for $r_0/R = 0.7$

The calculated non-dimensional profile of temperature on chamber profile web within the limits of the layer with thickness Δ at the value of Fourier criterion, related to the outer chamber radius $For_R = \frac{a\Delta\tau}{R^2} = 5 \cdot 10^{-4}$, is shown at Figure 3 with dots. Here parameter δ is a difference $(r - r_0)$, i.e. distance along chamber radius from its internal surface. At other For_R of the same order the results differ only in the within the limits of thickness of approximating lines.

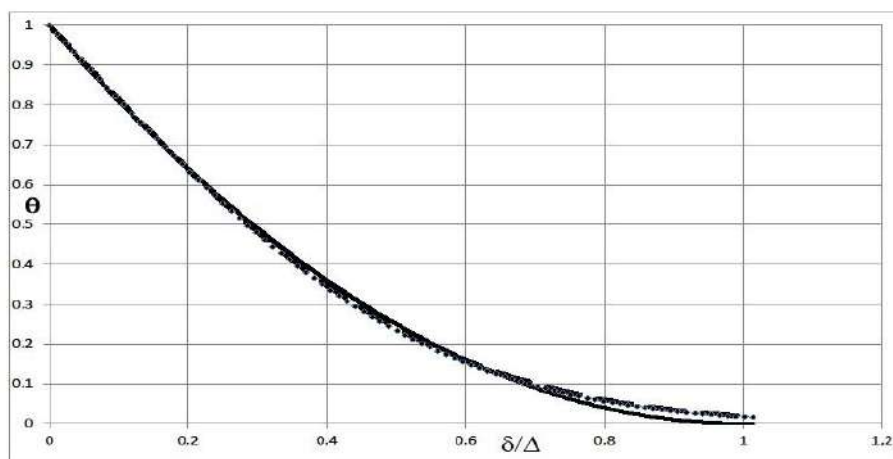


Figure 3. Non-dimensional temperature field in chamber wall at small For_R

The calculated curve is well approximated with the following dependency:

$$\theta = \left(1 - \frac{\delta}{\Delta}\right)^2 = \left(1 - \frac{\delta}{k\sqrt{a\tau}}\right)^2 = \left(1 - \frac{1}{k\sqrt{Fo_{\delta}}}\right)^2, \quad (5)$$

Here $Fo_{\delta} = \frac{a\tau}{\delta^2}$ – Fourier criterion, related to the current distance δ . The plot of the obtained expression is shown at figure 3 with full line. It is easy to see that taking into account the easiness of this formulae and meaning an inadvertent error, which is entered when passing to a finite-differentiate scheme, this solution can be acknowledged as quite successful. The condition of its application is, naturally, performance of inequation $r_0 + \delta < R$. It can be compared with theoretical solution for spreading of temperature wave in non-limited single-dimension array [1]:

$$\theta = 1 - \operatorname{erf}\left(\frac{\delta}{n\sqrt{a\tau}}\right) = 1 - \operatorname{erf}\left(\frac{1}{n\sqrt{Fo_{\delta}}}\right), \quad (6)$$

where erf – special function of errors, and numerical coefficient $n = 2$. Calculations show that for approximation of results of program calculations the dependency (6) is also useful on condition that parameter n will be taken in the amount of $2.27 = 1 + 4/\pi$. Corresponding plot is provided at figure 3 with dot line. This coincidence additionally confirms the fairness of obtained solution. Like in the case of coefficient k when determining Δ , the deviation on n can be explained by cylindrical symmetry. Correlations (5)-(6) are written in non-dimensional form. So they are general, regardless actual values t_{ex} and t_{in} , of definite material of chamber walls and correlation r_0/R , at least, at $r_0/R > 0.5$, for which numerical calculations were performed. These results are in principle agreed also with data which were previously obtained by author for another structure geometry [21–23], and, as it was previously noted, with theoretical considerations, provided in [1–2]. Besides, general view of the calculated temperature fields corresponds to results of some other authors, for example [16], and their found analytical description finds out analogies in theoretical solutions from other sources, in particular [14, 17].

To illustrate the practical use of the ratio (5) and its comparison with other solutions, we calculate the cooling of the brick chimney with the parameters $r_0 = 0.6$ m, $R = 1$ m at an initial flue gas temperature $t_{in} = 120^\circ\text{C}$ and the outside air temperature $t_{ex} = -25^\circ\text{C}$. In this case, the $r_0/R > 0.5$ condition is met. For brickwork $\lambda = 0.81$ W/(m·K), $c = 880$ J/(kg·K), $\rho = 1800$ kg/m³, so $a = 5.11 \cdot 10^{-5}$ m²/s. Since we are primarily interested in the temperature on the inner surface of the chimney t_s in terms of estimating the time of condensation of water vapor, for the actual value of r_0 , which is fixed $t_{in} = 120^\circ\text{C}$, we accept, as it was mentioned above, the value of $\delta_0^* = r_0 - \lambda\alpha$. The factor α at a given radius of the tube and the speed of movement of gases about 12 m/s will be near 21 W/(m²·K), then $\delta_0^* = 0.039$ m, $r_0 = 0.561$ m and the t_s is still defined at $r = 0.6$ m. In the calculations it was taken into account that in the considered mode the value θ , as it was already noted, shows the deviation of the current dimensionless temperature from the initial stationary distribution $t_{st}(r)$, therefore it was initially calculated the value of t_{st} on the inner surface of the chimney. In this case it is equal to 104 °C. In Figure 4 the dependence of the t_s from τ , constructed according to the formula (5), is shown by a solid line. The dotted line in figure 4 shows also the results of calculations using the analytical solution in the form of a series of data [24], and the dash – also on the analytical solution in the form of a series of [17]. As an example, we can cite a series of [24] with some changes corresponding to the peculiarities of the problem under consideration and the symbols accepted in this paper:

$$\theta = \frac{1}{4 \ln(R/r_0)} \left(-0.5772 + \ln\left(\frac{4a\tau}{r^2}\right) + \frac{r^2}{4a\tau} - \frac{r^4}{64a^2\tau^2} + \dots \right), \quad (7)$$

where -0.5772 is the Euler's constant.

It can be noted that the coincidence of the curves in figure 4 is close enough both in quality and quantity. In all cases, the decrease of value t_s over time occurs practically by the same law, which in the considered time interval can be approximated by hyperbolic (5) or logarithmic [17, 24] dependence from τ . We can notice that, in general, the decrease of t_s looks somewhat sharper when calculating by (5)

and smoother when calculating by analytical solutions in the form of series. However the difference lies within the accuracy of engineering calculation and the deviation lies within the accuracy of the engineering calculation, but the expression (5) is much easier in structure and is available for use in engineering practice.

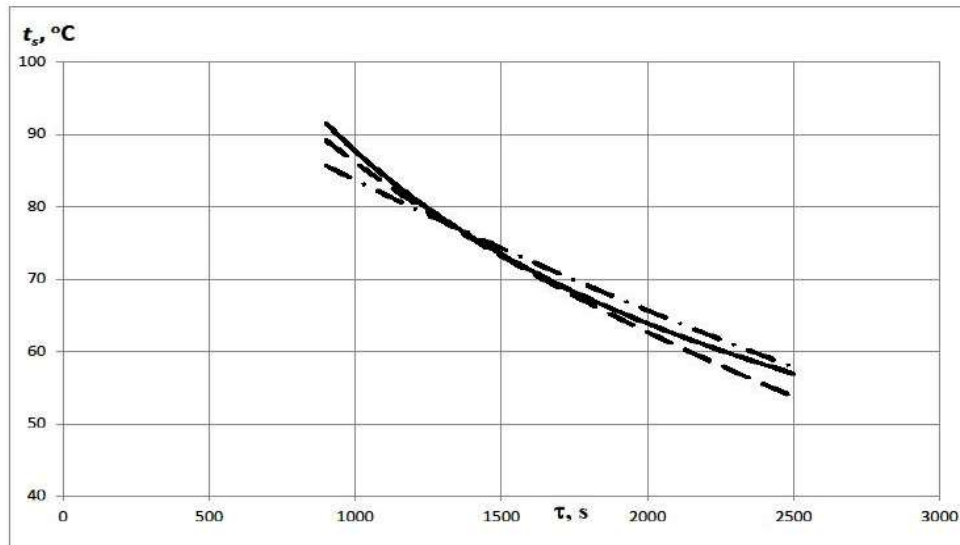


Figure 4. Dependence of the temperature on the inner surface of the cooling chimney from the value τ

4. Conclusion

1. It is noted that the speed of spreading of temperature wave in cylindrical wall complies to the same conformities that is in one-dimensional case, but with another proportional coefficient.
2. It was found that correlation of inner and outer radius of hollow chamber does not influence at the character of temperature field in the area of temperature wave, at least, at $r_0/R > 0.5$.
3. It is proved that the radial temperature profile in the wall of the hollow cylinder when $r_0/R > 0.5$ within the temperature wave propagation is described with good accuracy by quadratic dependence or with the use of an error function similar to a flat wall.
4. It is shown that the rate of temperature change over time at a fixed point in the cylinder wall within the temperature wave is sufficiently well approximated by hyperbolic dependence into which the expression for θ passes at $r = \text{const}$.
5. It is proved that the error in the use of formulas obtained in the paper in comparison with the results of numerical calculations and existing analytical solutions in the form of series lies within the accuracy of engineering calculations.
6. It is proposed to apply correlations obtained in the research for analytical estimation of minimal temperature at inner surface of cylindrical heated structures, primarily when resolving the issue about beginning of condensate formation at internal surfaces of smoke stacks when boiler unit is stopped or at outer surface of heat insulation of heat pipelines when heat supply is switched off, which will allow applying not only program, but also engineering methods of checking execution of industrial safety requirements.
7. It is noted that the ratio r_0/R , typical for modern designs of chimneys and thermal insulation of pipelines, allows to use the found formulas for θ when assessing the cooling time of their surfaces.
8. It is shown that the cooling rate of the inner surface of the smoke stack of a typical design, calculated in accordance with the found dependencies, before condensation of water vapor from flue gases of a standard composition is limited to tens of minutes which determine the available time for repair.

References

1. Carslaw H.S., Jaeger J.C. *Conduction of heat in solids*. Oxford University Press, USA, 1986. 520 p.
2. Kuvshinov Yu.Ya. *Energoberezheniye v sisteme obespecheniya mikroklimata zdaniy* [Energy saving in the building microclimate system]. Moscow : MSUCE – ASV Publ. 2010. 320 p. (rus)
3. THERM. Two-Dimensional Building Heat-Transfer Modeling [Electronic resource]. System requirements: Windows 7. URL: <https://windows.lbl.gov/software/therm/therm.html> (date of treatment: 04.03.2017).
4. Shokouhmand H., Ghaffari S. Investigation of cooling process of a high-temperature hollow cylinder in moving induction heat treatment. *Journal of Thermal Science and Engineering Applications*. 2012. Vol. 4. No. 1. Pp. 011002.
5. Kalynyak B. M. Fredholm equations of the second kind for radial stresses aimed at the determination of the thermoelastic state of an inhomogeneous hollow long cylinder. *Journal of Mathematical Sciences*. 2015. Vol. 205. No. 5. Pp. 659–666.
6. Norouzi M., Birjandi A. K., Rahmani H., Joneidi A. A. A general exact analytical solution for anisotropic non-axisymmetric heat conduction in composite cylindrical shells. *International Journal of Heat and Mass Transfer*. 2016. Vol. 93. Pp. 41–56.
7. Norouzi M., Shariati M., Rezaei Niya S.M., Karimi Demneh M., Naghavi M.S., Kayhani M.H. Exact solution of unsteady conductive heat transfer in cylindrical composite laminates. *Journal of Heat Transfer*. 2012. Vol. 134. No. 10. Pp. 101301.
8. Shevchuk V. A. Nonstationary one-dimensional problem of heat conduction for a cylinder with a thin multi-layer coating. *Journal of Mathematical Sciences*. 2012. Vol. 184. No. 2. Pp. 215–223.
9. Brunner G. Heat transfer. *Supercritical fluid science and technology*. 2014. No. 5. Pp. 228–263.
10. Horikiri K., Yao Y., Yao J. Modelling conjugate flow and heat transfer in a ventilated room for indoor thermal comfort assessment. *Building and Environment*. 2014. No. 77. Pp. 135–147.
11. Yun T.S., Jeong Y.J., Han T.-S., Youm K.-S. Evaluation of thermal conductivity for thermally insulated concretes. *Energy and Buildings*. 2013. No. 61. Pp. 125–132.
12. Gabrielaitiene I. Numerical simulation of a district heating system with emphases on transient temperature behavior. *Proceedings of the 8th International Conference «Environmental Engineering»*. Vilnius : VGTU Publishers, 2011. Vol. 2. Pp. 747–754.
13. Akimov I.A., Akimov A.I., Karakulina E.O. Issledovaniye teploperedachi v mnogosloynnykh cilindricheskikh izdeliyakh na pervom etape proizvodstva kompozicionnykh materialov [Investigation of heat transfer in multy-layer cylindrical products at the first step of production of composite materials]. *Scientific and technical herald of the Volga region*. 2015. No. 2. Pp. 68–72. (rus)
14. Loginov V.S., Parpiev A.T. Nestacionarnye temperaturnye rezhimy pologo cilindricheskogo aktivnogo elementa i paroperegrevatelya v parogeneratorе [Non-stationary thermal regimes of the hollow cylindrical active element and the vapor superheater in the vapor generator]. *Herald of the Sholom-Aleihem Amur State Univ*. 2013. No. 2(13). Pp. 90–97. (rus)
15. Eliseev V. N., Tovstonog V. A., Borovkova T.V. Algoritm resheniya obobshchennoy zadachi nestacionarnoy teploprovodnosti [Solution Algorithm of Generalized Non-Stationary Heat Conduction Problem in the Bodies of Simple Geometric Shapes]. *Herald of the Bauman Moscow State Tech. Univ., Mech. Eng.* 2017. No. 1. Pp. 112–128. (rus)

Литература

1. Carslaw H.S., Jaeger J.C. *Conduction of heat in solids*. Oxford University Press, USA, 1986. 520 p.
2. Кувшинов Ю.Я. Энергосбережение в системе обеспечения микроклимата зданий. М.: МГСУ - Изд-во Ассоциации строительных вузов. 2010. 320 с.
3. THERM. Two-Dimensional Building Heat-Transfer Modeling [Электронный ресурс]. Систем. требования: Windows 7. URL: <https://windows.lbl.gov/software/therm/therm.html> (дата обращения: 04.03.2017).
4. Shokouhmand H., Ghaffari S. Investigation of cooling process of a high-temperature hollow cylinder in moving induction heat treatment // *Journal of Thermal Science and Engineering Applications*. 2012. Vol. 4. № 1. Pp. 011002.
5. Kalynyak B. M. Fredholm equations of the second kind for radial stresses aimed at the determination of the thermoelastic state of an inhomogeneous hollow long cylinder // *Journal of Mathematical Sciences*. 2015. Vol. 205. № 5. Pp. 659–666.
6. Norouzi M., Birjandi A. K., Rahmani H., Joneidi A. A. A general exact analytical solution for anisotropic non-axisymmetric heat conduction in composite cylindrical shells // *International Journal of Heat and Mass Transfer*. 2016. Vol. 93. Pp. 41–56.
7. Norouzi M., Shariati M., Rezaei Niya S. M., Karimi Demneh M., Naghavi M. S., Kayhani M. H. Exact solution of unsteady conductive heat transfer in cylindrical composite laminates // *Journal of Heat Transfer*. 2012. Vol. 134. № 10. Pp. 101301.
8. Shevchuk V. A. Nonstationary one-dimensional problem of heat conduction for a cylinder with a thin multi-layer coating // *Journal of Mathematical Sciences*. 2012. Vol. 184. № 2. Pp. 215–223.
9. Brunner G. Heat transfer // *Supercritical fluid science and technology*. 2014. № 5. Pp. 228–263.
10. Horikiri K., Yao Y., Yao J. Modelling conjugate flow and heat transfer in a ventilated room for indoor thermal comfort assessment // *Building and Environment*. 2014. № 77. Pp. 135–147.
11. Yun T.S., Jeong Y.J., Han T.-S., Youm K.-S. Evaluation of thermal conductivity for thermally insulated concretes // *Energy and Buildings*. 2013. № 61. Pp. 125–132.
12. Gabrielaitiene I. Numerical simulation of a district heating system with emphases on transient temperature behavior // *Proceedings of the 8th International Conference «Environmental Engineering»*. Vilnius : VGTU Publishers. 2011. Vol. 2. Pp. 747–754.
13. Акимов И.А., Акимов А.И., Каракулина Е.О. Исследование теплопередачи в многослойных цилиндрических изделиях на первом этапе производства композиционных материалов // *Научно-технический вестник Поволжья*. 2015. № 2. С. 68–72.
14. Логинов В.С., Парпиев А.Т. Нестационарные температурные режимы полого цилиндрического активного элемента и пароперегревателя в парогенераторе // *Вестник Приамурского государственного университета им. Шолом-Алейхема*. 2013. № 2(13). С. 90–97.
15. Елисеев В.Н., Товстоног В.А., Боровкова Т.В. Алгоритм решения обобщенной задачи нестационарной теплопроводности в телах простой геометрической формы // *Вестник МГТУ им. Н.Э. Баумана. Сер. Машиностроение*. 2017. С. 112–128.
16. Остапенко В.В., Лукьянов А.В., Дремов В.В. Модель работы кожухотрубного аккумулятора теплоты фазового перехода на основе решения задачи Стефана // *Вестник Воронежского государственного*

16. Ostapenko V.V., Lukjanov A.V., Dryomov V.V. Model' raboty kozhukhotrubnogo akkumulyatora teploty fazovogo perekhoda na osnove resheniya zadaci Stefana [Model of work tube type phase transition heat accumulator by solving the Stephan problem]. *Herald of the Voronezh State Tech. Univ.* 2014. Vol. 10. No. 5. Pp. 89–93. (rus)
17. Vidin U.V., Ivanov D.I. Priblizhenny metod rascheta nestacionarnogo temperaturnogo polya v polom cilindre [The approximate method of calculation of the non-stationary temperature field in a hollow cylinder]. *Herald of the Murmansk State Tech. Univ.* 2013. Vol. 16. No. 1. Pp. 40–42. (rus)
18. Liu C.-S. An integral equation method to recover non-additive and non-separable heat source without initial temperature. *International Journal of Heat and Mass Transfer.* 2016. Vol. 97. Pp. 943–953.
19. Bahadori A., Vuthaluru H. B. Simple method for estimation of unsteady state conduction heat flow with variable surface temperature in slabs and spheres. *International Journal of Heat and Mass Transfer.* 2010. Vol. 53. No. 21–22. Pp. 4536–4542.
20. Li Y., Kong S.-C. Coupling conjugate heat transfer with in-cylinder combustion modeling for engine simulation // *International Journal of Heat and Mass Transfer.* 2011. Vol. add.
21. Samarín O.D. *Teplofizika. Energoberezeniye. Energoeffektivnost'* [Thermal physics. Energy saving. Energy efficiency]. Moscow : ASV Publishers, 2014. 296 p. (rus)
22. Parfentyeva N., Samarín O., Lushin K., Paulauskaite S., Valancius K. Temperature efficiency of rotary heat recovery units in ventilation and air conditioning. *Proceedings of 8th conference «Environmental Engineering».* Vilnius : VGTU Publishers, 2011. Vol. 2. Pp. 799–801.
23. Samarín O.D., Fedorchenko Yu.D. Vliyaniye regulirovaniya sistem obespecheniya mikroklimata na kachestvo podderzhaniya vnutrennikh meteoparametrov [The influence of microclimatic systems control on the quality of the maintenance of the internal meteorological parameters]. *Herald of the Moscow State Univ. of Civil Engineering.* 2011. No. 7. Pp. 124–128. (rus)
24. Podledneva N.A., Krasnov V.A., Magomadov R.S. Opredeleniye koeffitsientov teploprovodnosti i temperaturoprovodnosti za odin opyt metodom lineynogo istochnika teploty postoyannoy moshchnosti [Determination of coefficients of heat conductivity and heat diffusivity for one experience by a method of a linear source of heat of constant power]. *Herald of Astrakhan State Technical University.* 2013. No. 2. Pp. 50–55. (rus)
- технического университета. 2014. Т. 10. № 5. С. 89–93.
17. Видин Ю.В., Иванов Д.И. Приближенный метод расчета нестационарного температурного поля в полой цилиндрической трубе // Вестник Мурманского государственного технического университета. 2013. Т. 16. № 1. С. 40–42.
18. Liu C.-S. An integral equation method to recover non-additive and non-separable heat source without initial temperature // *International Journal of Heat and Mass Transfer.* 2016. Vol. 97. Pp. 943–953.
19. Bahadori A., Vuthaluru H. B. Simple method for estimation of unsteady state conduction heat flow with variable surface temperature in slabs and spheres // *International Journal of Heat and Mass Transfer.* 2010. Vol. 53. No. 21–22. Pp. 4536–4542.
20. Li Y., Kong S.-C. Coupling conjugate heat transfer with in-cylinder combustion modeling for engine simulation // *International Journal of Heat and Mass Transfer.* 2011. Vol. add.
21. Самарин О.Д. *Теплофизика. Энергосбережение. Энергоэффективность.* М.: Изд-во АСВ, 2014. 296 с.
22. Парфентьева Н., Самарин О., Лущин К., Паулаускайте С., Валанциус К. Температурная эффективность ротационных теплообменников в вентиляции и кондиционировании // *Proceedings of 8th conference «Environmental Engineering».* Vilnius : VGTU Publishers, 2011. Vol. 2. Pp. 799–801.
23. Самарин О.Д., Федорченко Ю.Д. Влияние регулирования систем обеспечения микроклимата на качество поддержания внутренних метеопараметров // Вестник МГСУ. 2011. № 7. С. 124–128.
24. Подледнева Н.А., Краснов В.А., Магомедов Р.С. Определение коэффициентов теплопроводности и температуропроводности за один опыт методом линейного источника теплоты постоянной мощности // Вестник Астраханского государственного технического университета. 2013. № 2. С. 50–55.

Oleg Samarín,
+7(916)107-77-01; samarin-oleg@mail.ru

Олег Дмитриевич Самарин,
+7(916)107-77-01;
эл. почта: samarin-oleg@mail.ru

© Samarín O.D., 2018

doi: 10.18720/MCE.78.14

Adaptive finite-element models in structural health monitoring systems

Адаптивные конечноэлементные модели в системах мониторинга зданий и сооружений

A.M. Belostotsky,
P.A. Akimov,
StadyO Research & Engineering Centre,
Moscow, Russia
O.A. Negrozov,
N.O. Petryashev,
S.O. Petryashev,
S.V. Sherbina,
National Research Moscow State Civil
Engineering University, Moscow, Russia
D.K. Kalichava,
ООО "Pixar", Moscow, Russia
T.B. Kaytukov,
Russian Academy of Architecture and
Construction Sciences, Moscow, Russia

Д-р техн. наук, генеральный директор
А.М. Белостоцкий,
д-р техн. наук, заместитель директора
по науке П.А. Акимов,
ЗАО "Научно-исследовательский центр
СтаДиО", Москва, Россия
ассистент О.А. Негрозов,
инженер Н.О. Петряшев,
инженер С.О. Петряшев,
инженер С.В. Щербина,
Национальный исследовательский
Московский государственный
строительный университет, Москва,
Россия,
канд. техн. наук, генеральный директор
Д.К. Каличава,
ООО "ПИКСАР", Москва, Россия,
канд. техн. наук, заместитель главного
ученого секретаря Т.Б. Кайтуков,
Российская академия архитектуры и
строительных наук, г. Москва, Россия

Key words: structural health monitoring; finite element method; adaptive models; unique buildings; seismometric approach; standing wave method; natural frequencies

Ключевые слова: мониторинг строительных конструкций; метод конечных элементов; адаптивные модели; уникальные здания и сооружения; сейсмометрический подход; метод стоячих волн; собственные частоты

Abstract. The design and construction of unique buildings, facilities and complexes of "modern" architectural forms and constructive solutions in Russia began less than 20 years ago in the conditions of a shortage of national design codes and experience of such construction. Thus these objects were not provided with proper scientific and technical support and structural health monitoring (SHM) systems. Generally only the instrumental monitoring system, based on results of finite element analysis and comparison with measured data allows performing planning activities to prepare for and respond to changes in state of critical structures and drawing conclusions about the actual state and the possibility of further safe operation of the building. Theoretical foundations of methodology of such SHM have been developed. Parameterized finite element models of buildings, special algorithm of adaptation (calibration) in accordance with results of measurements, methodology of measurements of natural frequencies and modal shapes and algorithm of structural evaluation are proposed in this paper. So-called "start" finite element model is normally developed to study the load-bearing capacity of the current version of the project. Parameterized "monitoring-oriented" three-dimensional dynamic finite element model for each significant stage of life cycle of the building (the stages of construction and operation) is constructed or modified, verified and adapted in accordance with the measured data. The main criterion for the adaptation is the correspondence of calculated and measured spectrum of the natural frequencies and mode shapes in the entire frequency range, significant for the assessment of system-wide changes and for identification – localization of possible defects.

Белостоцкий А.М., Акимов П.А., Негрозов О.А., Петряшев Н.О., Петряшев С.О., Щербина С.В., Каличава Д.К., Кайтуков Т.Б. Адаптивные конечноэлементные модели в системах мониторинга зданий и сооружений // Инженерно-строительный журнал. 2018. № 2(78). С. 169–178.

Аннотация. Расчетное обоснование, проектирование и строительство уникальных зданий, сооружений и комплексов «современных» архитектурных форм и конструктивных решений в Российской Федерации начинались менее двадцати лет назад в условиях дефицита национальной нормативной документации и опыта подобного строительства, в результате чего не были обеспечены надлежащим научно-техническим сопровождением и мониторингом соответствующих несущих конструкций. Вообще, лишь система инструментального мониторинга, построенная на основе анализа результатов конечноэлементного моделирования в сопоставлении с данными измерений, позволяет выполнять планирование мероприятий по подготовке и реагированию на изменения состояния ответственных конструкций, сделать выводы о фактическом состоянии и возможности дальнейшей безопасной эксплуатации здания (сооружения). Теоретические основы соответствующей методики разработаны и представлены в настоящей статье. Описываются параметризованные конечноэлементные модели зданий, алгоритм их адаптации (калибровки) по данным инструментальных наблюдений, методика измерения собственных частот и форм колебаний, подход к оценке несущей способности для фактического состояния объекта. «Стартовая» конечноэлементная модель используется, как правило, для обоснования несущей способности актуального проектного варианта. Для каждой значимой стадии «жизненного цикла» здания (этапы строительства и эксплуатации) строится, модифицируется (актуализируется), верифицируется и адаптируется по текущим данным инструментальных наблюдений параметризуемая пространственная динамическая «мониторинговая» конечноэлементная модель. Основным адаптационным критерием здесь принимается соответствие расчетного и измеренного спектра собственных частот и форм колебаний во всем диапазоне частот, значимом как для оценки общесистемных изменений, так и идентификации-локализации возможных дефектов.

1. Introduction

The main target of research of this paper is unique buildings, facilities and complexes of “modern” architectural forms and constructive solutions. The design and construction of unique buildings, facilities and complexes of “modern” architectural forms and constructive solutions in Russia began less than 20 years ago in the conditions of a shortage of national design codes and experience of such construction.

The systematic process of observing, tracking and logging data over a period of time in order to characterize the health state of structures and to detect any possible change due to damage occurrence is referred to as structural health monitoring (SHM) [1]. SHM is nowadays a field of great concern. The main aim of SHM is to prevent and avoid fatal structural damages through the determination of stresses and deformations (i.e. displacements) of whole structure or a specific component. It is clear that external loads and boundary conditions should be previously identified [2].

Due to the above-mentioned reasons, unique buildings, facilities and complexes in Russia were not provided with proper scientific and technical support and SHM systems [3]. Corresponding consequences of this situation include, in particular, inadequacy of the structural analysis and the poor quality of the construction works [4, 5]. The problem of SHM (at the construction and operation stages) takes on special significance, the importance of which has already been recognized by designers, builders and specialists of supervisory organizations [6, 7]. However, there is no algorithm for the solution of this problem in the Russian design codes. Besides, SHM systems of erected unique buildings and structures exist, as a rule, only on papers, approved by the Russian State Expertise [8].

In the last decades, SHM technology has emerged creating an exciting new field within various branches of engineering. This technology integrated remote sensing [9], smart materials, and computer based knowledge systems to allow civil engineers see how built up structures are performing over time. Since the emergence of this technology, it became more and more useful for large infrastructures, such as bridges, buildings, tunnels, pipelines, offshore platforms, wind turbines, and railway infrastructure where performance is critical but onsite field test is difficult or even impossible [10, 11]. Besides, the request for damage detection by means of non-destructive methods is greatly increasing in order to reduce the maintenance costs and to increase the safety level of the structures [12].

As is known, there are four basic methods of instrumental monitoring at the present time: geodetic measurements; geotechnical monitoring the state of foundation; measuring loads and strains in the substructure and superstructure; dynamic (seismometric) approach [13–15]. Special mention should go to seismometric method that allows investigator to explore the whole building and to identify significant changes in the load-bearing structures without instrumental actions and visual inspections of each structure [16, 17]. The experiments on real objects confirmed the potential of this method, however, revealed a number of problems [18, 19]. It is necessary to note complex specify of unique buildings and

advantages of seismometric method in the context of the monitoring problems (high dimensionality and variability (relative to loads, masses and stiffness) of object; difficulty of corresponding instrumental measurements (online access to the majority of load-bearing structures in residential and other premises is difficult or impossible [17]).

Instrumental monitoring of unique buildings without corresponding correct and adequate “monitoring-oriented” mathematical and computer models has random nonsensical nature and therefore it is not of practical interest. These “monitoring-oriented” models (several models or parameterized one) have a number of specific differences from the conventional design models, which are normally used to justify design decisions (input of real (actual measured instead of design) physical and mechanical parameters of construction materials (steel, concrete, reinforcement etc.) and geometry of structures; input of real (actual measured instead of design) loads; inclusion of non-bearing structures (dividing walls, facades, etc.) in static and dynamic operation of structures under weak “background” loads; modelling of work of several joints in accordance with schemes, different from design ones (for example, elastic restraint instead of hinge joint); adaptability (calibration, “learning”) of model in accordance with data obtained from instrumental measurements (including detected defects).

The main objective of this paper is the development of correct adaptive finite element models in SHM systems of unique buildings. Thus, the following tasks are solved:

1. Formulation of basic theoretical foundations of advanced methodology of structural health monitoring.
2. Development of parameterized finite element models of buildings (so-called “design” and “monitoring-oriented” models).
3. Adaptation (calibration) of finite element models in accordance with results of measurements.
4. Introduction of effective technology of measurements of natural frequencies and modal shapes.
5. Introduction of correct approach to structural evaluation in real situation of building.
6. Approbation of advanced methodology of structural health monitoring.

2. Methods

2.1. Formulation of basic theoretical foundations of advanced methodology of structural health monitoring

Block diagram and content of developed computational and experimental methodology of structural health monitoring dealing with load-bearing structures of unique buildings, is presented in Figure 1.

So-called “start” (“design”) finite element model is normally developed to study the load-bearing capacity of the current version of the project. Parameterized “monitoring-oriented” three-dimensional dynamic finite element model for each significant stage of life cycle of the building (the stages of construction and operation) is constructed or modified, verified and adapted in accordance with the measured data. The main criterion for the adaptation is the correspondence of calculated and measured spectrum of the natural frequencies and mode shapes in the entire frequency range, significant for the assessment of system-wide changes and for identification – localization of possible defects.

Computational assessment of load-bearing capacity of structures is carried out in accordance with design codes with the use of “design” and “monitoring-oriented” finite element models based on design and measured parameters of structures, foundation, loads etc. Basic peculiarities of components of proposed methodology of structural health monitoring are discussed in the distinctive paper.

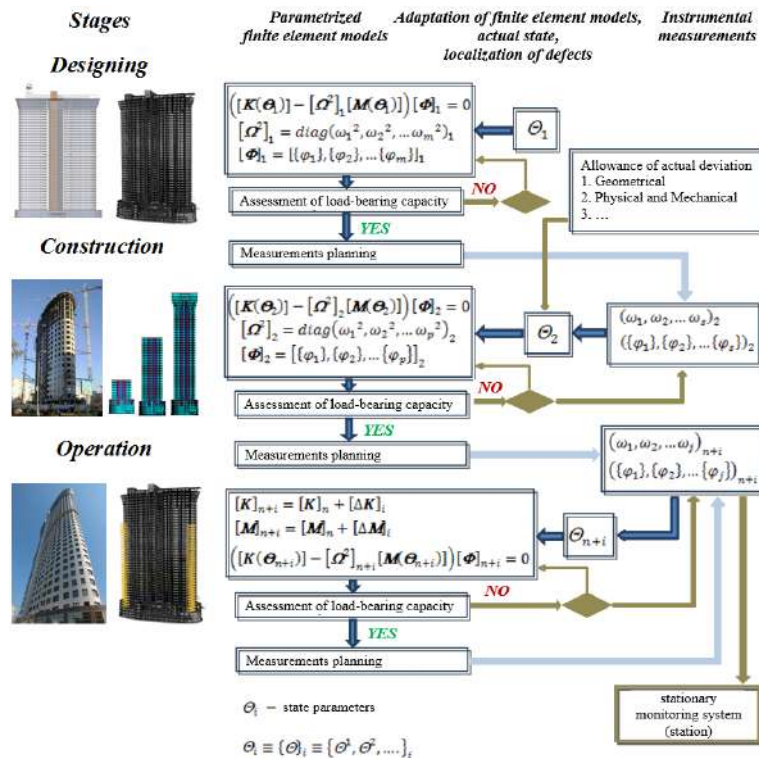


Figure 1. Block diagram and content of developed computational and experimental methodology of structural health monitoring dealing with load-bearing structures of unique buildings

2.2. Parameterized finite element models of buildings (“design” and “monitoring-oriented” models)

Three-dimensional shell-beam finite element model (models) of coupled systems “foundation – building” are normally constructed for strain-stress state analysis and load-bearing capacity of actual design version. It is so-called “start” (“design”) model for subsequent parameterization and adaptation.

Vector of parameters of model has the form

$$\theta_l = \{\theta\}_l = \{\theta_1 \theta_2 \theta_3 \dots\}_l, \tag{1}$$

where l is the number of stage of construction and operation ($l = 1, 2 \dots$) with corresponding instrumental SHM.

Vector (1) can contain the following measured parameters, which normally differ from design ones: θ_1 is dynamic parameters of foundation; θ_2 is physical and mechanical parameters of construction materials (concrete, reinforcement, steel, etc.); θ_3 is geometrical parameters of load-bearing structures (particularly eccentricities and inclinations of walls and columns; θ_4 is measured loads and impacts; θ_5 is stiffness and mass of nominally non-bearing structures (dividing walls, façade structures), included in dynamic operation of structures under weak “background” loads; θ_6 is modeling of structural behavior of several joints in accordance with schemes, different from design ones (for instance, elastic restraint instead of hinge).

Well-known methods of construction of three-dimensional shell-beam dynamic finite element models [20, 21] with allowance for above mentioned factors are realized. Thus, the reduction of the actual class of the concrete in comparison with the project one are taken into account by corresponding reduction in the modulus of elasticity, deviations of the geometric positions of the columns, walls and other load-bearing elements are taken into account by introduction of so-called “rigid inserts” allowing displacement of the elements in the plan, and their inclination.

The most problematic is the allowance for stiffness of dividing walls (especially located inside apartment) and façade structures included in the dynamic operation of the system for the operation stages, under weak background loads. We can use “integrated” approach (a proportional increase of stiffness of the vertical load-bearing structures), and introduction of each non-bearing structure with

reduced dynamic stiffness in finite element model (this approach can substantially (at times) increase computational dimension of the model).

Partial eigenvalue problem is formulated and solved for parameterized finite element model (computing of natural frequencies ω_i and mode shapes $\{\varphi_i\}$) of dynamic system has the form

$$[K(\theta_l)][\Phi] = [\Omega^2][M(\theta_l)][\Phi], \quad (2)$$

where

$$[\Phi] = [\{\varphi_1\} \dots \{\varphi_n\}]; [\Omega^2] = \text{diag}(\omega_1^2 \dots \omega_n^2); \quad (3)$$

$[K(\theta_l)]$ is the global stiffness matrix of system; $[M(\theta_l)]$ is the global mass matrix of system.

The following parameters (criteria) of the solution of partial eigenvalue problem can be used: the number ($\leq n$) of computing lower natural frequencies and mode shapes; frequency range (from Ω_1 to Ω_2), within which all natural frequencies (mode shapes) must be computed; frequency range (from Ω_1 to Ω_2), and the number of computing lower natural frequencies and forms within this range.

If the frequency range is given, shift σ of stiffness matrix within triangulation procedure and eigenvalue analysis must be done. Recommended value of this shift σ can be defined by formula

$$\sigma = -0.5 \cdot (\Omega_1^2 + \Omega_2^2). \quad (4)$$

In accordance with recommendations from [4] the most advanced and competitive methods of solution of generalized and partial eigenvalue problems (subspace iteration method, and block Lanczos method) can be used as basic methods. Numerous computational experiments (including samples with "contrasting" ill-conditioned systems and systems with multiple eigenvalues) showed reliability and efficiency of current implementations of these methods. Experience has proven that Lanczos method had undeniable advantages in high speed of computing of the given number of eigenvalues and eigenvectors for practical problems (of high dimension; up to 10 million of unknowns (dynamic degrees of freedom)) of finite element analysis of unique buildings.

2.3. Adaptation (calibration) of finite element models in accordance with results of measurements

Two main groups of approaches are used for adaptation of finite element models in accordance with results of dynamic monitoring data: "intuitive-engineering" approaches and mathematically formalized approaches. The first group of approaches, which is the most popular at this time in Russia, leaves wide scope for interpretation of the calculated and measured dynamic characteristics. We should note the most severe and challenging approach from the second group, which is based on numerical solution of incorrect inverse problems by Tikhonov regularization method. It should be noted that algorithms and software, enabling identification of the actual status and localization of defects for simple linear-elastic structures (beam and plate on elastic (Winkler) foundation, frame, framework etc.) have been already developed.

Let's consider one of the versions of corresponding algorithm based on solution of nonlinear optimization problem (i.e. minimization of objective function):

$$\min_{\theta} \Pi(\theta) = \frac{1}{2} \sum_{i=1}^{N_{md}} a_i \|\varphi_i - \hat{\varphi}_i\|^2 \text{ on condition that } R(\theta) \geq 0. \quad (5)$$

Sensitivity function is defined by formula

$$\Pi_{,\theta} = \sum_{i=1}^{N_{md}} a_i \|\varphi_i - \hat{\varphi}_i\| \varphi_{i,\theta}; \quad \varphi_{i,e} = - \sum_{i \neq j}^{N_{md}} \frac{\varphi_i^T K_{,\theta} \varphi_j}{(\lambda_i - \lambda_j) \varphi_i^T M \varphi_i} \varphi_i \quad (i \neq j) \quad (6)$$

Regularization has the form

$$\min_{\theta} \Pi(\theta) = \frac{1}{2} \sum_{i=1}^{N_{md}} a_i \|\varphi_i - \hat{\varphi}_i\|^2 + \frac{\beta}{2} \|K(\theta) - K(\theta_0)\|^2 \text{ on condition that } R(\theta) \leq 0, \quad (7)$$

where $\theta = \{\theta\} = \{\theta_1 \theta_2 \theta_3 \dots\}$ is previously user-defined vector of parameters of model; α is weight coefficients; φ_i and $\hat{\varphi}_i$ are computered and measured natural mode shapes; $R(\theta)$ is constrain with respect to parameters; λ_i is computered eigenvalues (angular frequencies squared); θ_0 is initial state; β is parameter of regularization; K is the global stiffness matrix; M is the global mass matrix.

It is necessary to note specific requirements to accuracy of structural design and instrumental measurements (including modal analysis in corresponding significant frequency range).

2.4. Technology of measurements of natural frequencies and modal shapes

As follows from the common engineering sense and confirmed by formal above-mentioned mathematical manipulations, seismometric method of measurement should provide reasonable accuracy of computing of not only lower total-system performance natural frequencies [22] and mode shapes but also natural frequencies and mode shapes corresponding to local deviations of state of structure (including structural failures). Besides, efficiency and economic competitiveness are also provided.

Analysis of available sources showed that so-called standing wave method, proposed by Professor A.F. Emanov, is fully consistent with these principles and criteria. Standing wave field, different from other waves by coherence property in time, is always formed in closed spaces. Standing waves extraction from recorded wave fields on filtering basis by coherence in time and conversion of nonsimultaneous observations in simultaneous standing waves records in studied objects forms the basis of standing wave method. The method performs well in study of self-induced buildings vibrations. Amplitudes and phases maps of standing waves in set of natural frequencies fully characterize object and allow to determine not only seismic stability, but realize physical state diagnostics at a constructional elements level. In microzoning the standing wave method performs well as direct research method of resonant properties of section. As a result of standing wave method use we have set of section natural frequencies and vibration amplification maps. On the basis of maps of standing wave phases a resonance type is simply set. The resonances, formed as multiples between horizontal boundaries, have the same close phase on area, whereas in lenses and block mediums horizontal resonances may appear characterized by banded change of areal phase. Combination of high-accuracy study of resonant properties of areas and buildings provides a new echelon of accuracy in seismic risk assessment [4, 15, 18].

Russia already has positive experience of using this method to determine the dynamic characteristics of dams, bridges and buildings. However, there is no such experience for high-rise buildings, complexes and long span structures. It is planned to fill this gap in research on real objects.

2.5. Structural evaluation in real situation of building

Analysis of stress-strain state and load-bearing capacity of structures is carried out in accordance with the design codes and corresponding criteria with the use of finite element model comprising parameters of "monitoring-oriented" and design models.

Static and dynamic (including seismic) stress-strain state for stage number l can be obtained after solution of system of linear algebraic equations. In particular, we have displacement equations of equilibrium

$$[K(\theta_l)]\{u\}_1 \dots \{u\}_m = \{F(\theta_l)\}_1 \dots \{F(\theta_l)\}_m \quad (8)$$

and displacement equations of motion

$$[M(\theta_l)]\{\ddot{u}\} + [C(\theta_l)]\{\dot{u}\} + [K(\theta_l)]\{u\} = \{F(\theta_l)\}. \quad (9)$$

Stability analysis (computing of lower critical loads λ_i and modes of buckling φ) can be done as a result of solution of partial eigenvalue problem

$$[K(\theta_l)]\{\Phi\} = [\Lambda][K_G(\theta_l)]\{\Phi\}, \quad (10)$$

where

$$\{\Phi\} = \{\{\varphi_1\} \dots \{\varphi_n\}\}; \quad [\Lambda] = \text{diag}(\lambda_1 \dots \lambda_n). \quad (11)$$

This enables the additional (as compared with the dynamic model), the properties, namely, parameters of foundation, stiffness and loads (set of parameters θ_l). The model is complemented by data measures within SHM.

The proposed approach allows verification of results of progressive collapse analysis at each stage of SHM based on the actual state of the object.

Planning for measurement at the current stage of SHM should be done with the use of results of the previous stage. Thus, the detection of “suspicious” of natural frequencies and mode shapes requires installation of a sufficient number of sensors for the measurements for the qualitative identification of these frequencies and shapes. However it should be noted that for most SHM applications, the number of available sensors for monitoring is usually significantly less than the number of potential monitoring locations.

3. Results and Discussion

We considered so-called Evolution Tower as a vital object for approbation of proposed methodology of SHM. One of the most ambitious skyscraper projects in Moscow, Evolution Tower is part of the Moscow International business center Moscow City. The impressive design of this 255 meters high skyscraper, its well-developed facilities and efficient state-of-the-art engineering services form most comfortable conditions for work and rest (Figure 2).

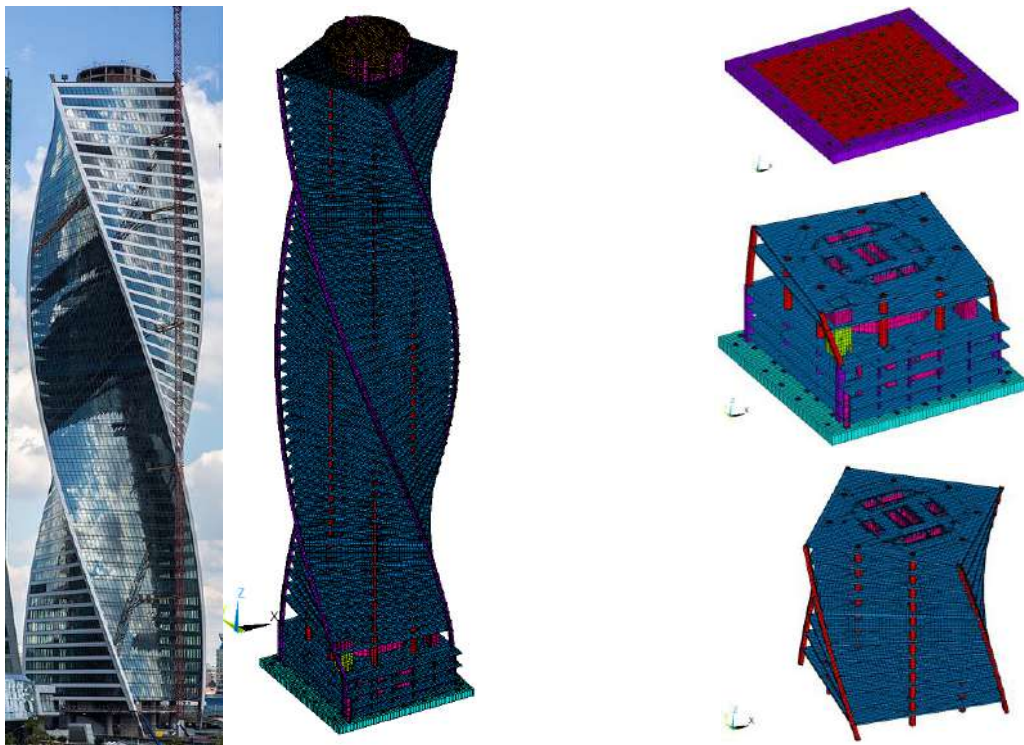


Figure 2. Evolution tower. Building and corresponding finite element models

Basing on the files of the research activity customer in the form of AutoCAD and the set of drawings in the software ANSYS, a “design” shell-beam finite element model (FE model) of a building was constructed (Figure 1). Then basing on the “design” (ideal) model another two models were developed: “actual no. 1” – finite element model of an object, in which the deviations of piles from the designed positions were taken into account, that were found out as a result of investigation; “actual no. 2” – finite element model of an object, in which the deviations of walls from the designed positions were taken into account, that were found out as a result of investigation.

In frames of verification of finite element models the natural frequencies and vibrational modes of the considered system were estimated (for “design” and “actual no. 1” models), which means almost most informative test tasks were solved, which, from the one hand, integrate many factors and parameters of the design models, and, from the other, allow detecting their difference. Thus determined natural frequencies and vibration modes of the building were expectable characteristic (for the objects of a similar type) in quality and quantity senses (in terms of natural frequencies spectrum and systemic forms), which allowed making a conclusion on the correctness and adequacy of the created finite element models to the “design” variant of the building (“actual no. 1” model is dynamically equivalent to the “design” one).

The comparative analysis of the corresponding results for “design” and “actual” finite element models revealed the slight “sensitivity” of the stress-strain state parameters, which predetermine the

reliability of the bearing structures (piles, columns and walls), to the considered deviations of the columns and walls from the designed positions, detected as a result of the investigations. It was established, that the design reinforcement of the piles and walls generally possesses an essential reserve compared to the corresponding design parameters for “design” and “actual” models.

Basing on the results of the investigations the authors made a conclusion on the correspondence of the design parameters of the stress-strain state and reliability of the bearing structures of a high-rise building to the specified criteria of stability and deformability at set actual deviations of the reinforced concrete structures from the designed positions, detected as a result of field measurements (account for eccentricities and vertical deviations [17, 20]).

The obtained results of the mathematical simulation of a building – static displacements, natural frequencies and vibration modes – may (и as authors believe, should) be used at developing and implementing the program and methods of monitoring the state of the foundation and bearing structures of a building on all the stages of its operating life [4, 23, 24].

4. Conclusion

Generally the finite element method (FEM) method is nowadays a very powerful computer aided simulation technique, allowing the user to study any kind of problem virtually without limitation in model size and complexity.

Finally we can formulate the main results.

1. Formulation of basic theoretical foundations of advanced methodology of structural health monitoring is presented
2. Parameterized finite element models of buildings (so-called “design” and “monitoring-oriented” models) are proposed.
3. Algorithm of adaptation (calibration) of finite element models in accordance with results of measurements is described.
4. Effective technology of measurements of natural frequencies and modal shapes and correct approach to structural evaluation in real situation of building are introduced.
5. The results of the approbation of advanced methodology of SHM were very satisfactory and were discussed in this paper. Since the investigated cases are taken from real structures, it can be concluded that the proposed advanced methodology can be a valuable tool for SHM.
6. Thus only the instrumental monitoring system, based on results of finite element analysis and comparison with measured data allows performing planning activities to prepare for and respond to changes in state of critical structures and drawing conclusions about the actual state and the possibility of further safe operation of the building.

As we have already mentioned, the monitoring of building structures is rather complicated due to complex relationship between various loads and structural members. However, if the proposed advanced methodology of SHM is developed, it will have a positive effect on the maintenance of structures.

5. Acknowledgements

The Reported study was funded by Government Program of the Russian Federation “Development of science and technology” (2013-2020) within Program of Fundamental Researches of Ministry of Construction, Housing and Utilities of the Russian Federation and Russian Academy of Architecture and Construction Sciences, the Research Projects 7.1.1, 7.1.2 and 7.4.17”.

References

1. Masciotta M.-G., Ramos L.F., Lourenco P.B. The importance of structural monitoring as a diagnosis and control tool in the restoration process of heritage structures: A case study in Portugal. *Journal of Cultural Heritage*. 2017, <http://dx.doi.org/10.1016/j.culher.2017.04.003>.
2. Papa U., Russo S., Lamboglia A., Del Core G., Iannuzzo G. Health structure monitoring for the design of an Innovative UAS fixed wing through inverse finite element method (iFEM). *Aerospace Science and Technology*. 2017, <http://dx.doi.org/10.1016/j.ast.2017.07.005>.

Литература

1. Masciotta M.-G., Ramos L.F., Lourenco P.B. The importance of structural monitoring as a diagnosis and control tool in the restoration process of heritage structures: A case study in Portugal // *Journal of Cultural Heritage*. 2017, <http://dx.doi.org/10.1016/j.culher.2017.04.003>.
2. Papa U., Russo S., Lamboglia A., Del Core G., Iannuzzo G. Health structure monitoring for the design of an Innovative UAS fixed wing through inverse finite element method (iFEM) // *Aerospace Science and Technology*. 2017.

Belostotsky A.M., Akimov P.A., Negrozov O.A., Petryashev N.O., Petryashev S.O., Sherbina S.V., Kalichava D.K., Kaytukov T.B. Adaptive finite-element models in structural health monitoring systems. *Magazine of Civil Engineering*. 2018. No. 2. Pp. 169–178. doi: 10.18720/MCE.78.14.

3. Belostotskiy A.M., Akimov P.A. Obzorno-analiticheskoye issledovaniye normativno-metodicheskoy literatury v oblasti monitoringa zdaniy i sooruzheniy [Review and analysis of design codes and methodological literature in the field of structural health monitoring]. *International Journal for Computational Civil and Structural Engineering*. 2016. No. 2(12). Pp. 42–64.
4. Belostotskiy A.M., Akimov P.A. Adaptive finite element models coupled with structural health monitoring systems for unique buildings. *Procedia Engineering*. 2016. No. 153. Pp. 83–88.
5. Belostotskiy A.M., Akimov P.A., Kaytukov T.B., Petryashev N.O., Petryashev S.O., Negrozov, O.A. Strength and stability analysis of load-bearing structures of Evolution tower with allowance for actual positions of reinforced concrete structural members. *Procedia Engineering*. 2016. No. 153. Pp. 95–102.
6. Brownjohn J.M.W. Structural health monitoring of civil infrastructure. *Philosophical Transactions of the Royal Society A*. 2007. No. 1851(365). Pp. 589–622.
7. Belostotskiy A.M., Akimov P.A., Afanasyeva I.N., Kaytukov T.B. Contemporary problems of numerical modelling of unique structures and buildings. *International Journal for Computational Civil and Structural Engineering*. 2017. No. 2(13). Pp. 9–34.
8. Belostotskiy A.M., Akimov P.A. Nauchno-issledovatel'skiy tsentr StaDiO. 25 let na fronte chislennogo modelirovaniya [25-th Anniversary of scientific research centre StaDyO]. *International Journal for Computational Civil and Structural Engineering*. 2016. No. 1(12). Pp. 9–34. (rus).
9. Suhaimi S.A., Azemi S.N., Jack S.P. Evolution of structural health monitoring. *Journal of Built Environment, Technology and Engineering*. 2016. No. 1. Pp. 76–80.
10. Kim J.-T., Sim S.-H., Cho S., Yun C.-B., Min J. Recent R&D activities on structural health monitoring in Korea. *Structural Monitoring and Maintenance*. 2016. No. 1(3). Pp. 91–114.
11. Ryu H.-H., Kim J.-S., Choi E.-G., Lee S.-H. Preliminary design of structural health monitoring for high-rise buildings. *International Journal of High-Rise Buildings*. 2017. No. 3(6). Pp. 279–284.
12. Mordini A., Savov K., Wenzel H. The finite element model updating: A powerful tool for structural health monitoring. *Structural Engineering International*. 2007. No. 4. Pp. 352–358.
13. Brownjohn J.M., Pan T.C., Deng X. Correlating dynamic characteristics from field measurements and numerical analysis of a high rise building. *Earthquake Engineering & Structural Dynamics*. 2000. No. 29(4). Pp. 523–543.
14. Novikov P.I. Identifying Real Stiffness Properties of Structural Elements of Adapted Finite-Element Models of Buildings and Structures - Part 1: Problem Setting. *Applied Mechanics and Materials*. 2014. No. 670-671. Pp. 732–735.
15. Yemanov A.F., Krasnikov A.A. Primeneniye metoda stoyachikh voln dlya issledovaniy seysmoizolirovannykh zdaniy [The use of standing waves method in study of seismically isolated buildings]. *Voprosy inzhenernoy seysmologii*. 2015. No. 4(42). Pp. 37–64. (rus)
16. Chang P.C., Flatau A., Liu S.C. Review paper: Health monitoring of civil infrastructure. *Structural Health Monitoring*. 2003. No. 2(3). Pp. 257–267.
17. Zhou H.Z. Recent advances in research on damage diagnosis for civil engineering structures. *China Civil Engineering Journal*. 2003. No. 36(5). Pp. 105–110.
18. Krasnikov A.A., Yemanov A.F., Bakh A.A. Otsenka polnoty konechnoelementnykh modeley inzhenernykh sooruzheniy po eksperimentalnym dannym metoda stoyachikh voln [Finite element model of engineering structures
3. Белостоцкий А.М., Акимов П.А. Обзорно-аналитическое исследование нормативно-методической литературы в области мониторинга зданий и сооружений // *International Journal for Computational Civil and Structural Engineering*. 2016. № 2(12). С. 42–64.
4. Belostotskiy A.M., Akimov P.A. Adaptive finite element models coupled with structural health monitoring systems for unique buildings // *Procedia Engineering*, 2016. № 153. Pp. 83–88.
5. Belostotskiy A.M., Akimov P.A., Kaytukov T.B., Petryashev N.O., Petryashev S.O., Negrozov, O.A. Strength and stability analysis of load-bearing structures of Evolution tower with allowance for actual positions of reinforced concrete structural members // *Procedia Engineering*. 2016. № 153. Pp. 95–102.
6. Brownjohn J.M.W. Structural health monitoring of civil infrastructure // *Philosophical Transactions of the Royal Society A*. 2007. № 1851(365). Pp. 589–622.
7. Белостоцкий А.М., Акимов П.А., Афанасьева И.Н., Кайтуков Т.Б. Contemporary problems of numerical modelling of unique structures and buildings // *International Journal for Computational Civil and Structural Engineering*. 2017. № 2(13). С. 9–34.
8. Белостоцкий А.М., Акимов П.А. Научно-исследовательский центр СтаДиО. 25 лет на fronte численного моделирования // *International Journal for Computational Civil and Structural Engineering*. 2016. № 1(12). С. 9–34.
9. Suhaimi S.A., Azemi S.N., Jack S.P. Evolution of structural health monitoring // *Journal of Built Environment, Technology and Engineering*. 2016. № 1. Pp. 76–80.
10. Kim J.-T., Sim S.-H., Cho S., Yun C.-B., Min J. Recent R&D activities on structural health monitoring in Korea // *Structural Monitoring and Maintenance*. 2016. № 1(3). Pp. 91–114.
11. Ryu H.-H., Kim J.-S., Choi E.-G., Lee S.-H. Preliminary design of structural health monitoring for high-rise buildings // *International Journal of High-Rise Buildings*. 2017. № 3(6). Pp. 279–284.
12. Mordini A., Savov K., Wenzel H. The finite element model updating: A powerful tool for structural health monitoring // *Structural Engineering International*. 2007. № 4. Pp. 352–358.
13. Brownjohn J.M., Pan T.C., Deng X. Correlating dynamic characteristics from field measurements and numerical analysis of a high rise building // *Earthquake Engineering & Structural Dynamics*. 2000. № 29(4). Pp. 523–543.
14. Novikov P.I. Identifying Real Stiffness Properties of Structural Elements of Adapted Finite-Element Models of Buildings and Structures - Part 1: Problem Setting // *Applied Mechanics and Materials*. 2014. № 670-671. Pp. 732–735.
15. Еманов А.Ф., Красников А.А. Применение метода стоячих волн для исследований сейсмоизолированных зданий // *Вопросы инженерной сейсмологии*. 2015. № 4(42). С. 37–64.
16. Chang P.C., Flatau A., Liu S.C. Review paper: Health monitoring of civil infrastructure // *Structural Health Monitoring*. 2003. № 2(3). Pp. 257–267.
17. Zhou H.Z. Recent advances in research on damage diagnosis for civil engineering structures // *China Civil Engineering Journal*. 2003. № 36(5). Pp. 105–110.
18. Красников А.А., Еманов А.Ф., Бах А.А. Оценка полноты конечноэлементных моделей инженерных сооружений по экспериментальным данным метода стоячих волн // *Интерэкспо Гео-Сибирь*. 2017. № 4(2). С. 179–184.
19. Friswell M.I., Mottershead J.E., Ahmadian H., Experimental test data: Parameterization and regularization // *Transactions of the Royal Society of London, Series A*,

Белостоцкий А.М., Акимов П.А., Негрозов О.А., Петряшев Н.О., Петряшев С.О., Щербина С.В., Каличава Д.К., Кайтуков Т.Б. Адаптивные конечноэлементные модели в системах мониторинга зданий и сооружений // *Инженерно-строительный журнал*. 2018. № 2(78). С. 169–178.

- completeness assessment by standing waves method experimental data]. *Interespo Geo-Sibir*. 2017. No. 4(2). Pp. 179–184. (rus)
19. Friswell M.I., Mottershead J.E., Ahmadian H., Experimental test data: Parameterization and regularization. *Transactions of the Royal Society of London, Series A, Special Issue on Experimental Modal Analysis*. 2001. No. 359(1778). Pp. 169–186.
 20. Ebrahimian H., Astroza R., Conte J.P. De Callafon R.A. Nonlinear finite element model updating for damage identification of civil structures using batch Bayesian estimation // *Mechanical Systems and Signal Processing*. 2017. No. 84(B). Pp. 194–222.
 21. Kefal A., Tessler A., Oterkus E. An enhanced inverse finite element method for displacement and stress monitoring of multilayered composite and sandwich structures. *Composite Structures*. 2017. No. 179, Pp. 514–540.
 22. Sartorato M., De Medeiros R., Vandepitte D., Tita V. Computational model for supporting SHM systems design: Damage identification via numerical analyses. *Mechanical Systems and Signal Processing*. 2017. No. 84(A). Pp. 445–461.
 23. Ursos M.E., Tingatinga E.A., Longalong R.E. A finite element based method for estimating natural frequencies of locally damaged homogeneous beams. *Procedia Engineering*. 2017. No. 199. Pp. 404–410.
 24. Zhong R., Zong Z., Niu J., Liu Q., Zheng P. A multiscale finite element model validation method of composite cable-stayed bridge based on Probability Box theory. *Journal of Sound and Vibration*. 2016. No. 370. Pp. 111–131.

Alexander Belostotsky,
+7(499)706-88-10; amb@stadyo.ru

Pavel Akimov,
+7(499)706-88-10; pavel.akimov@gmail.com

Oleg Negrozov,
+7(958)819-64-30; genromgsu@gmail.com

Nikolay Petryashev,
+7(499)929-50-17; stadyo@stadyo.ru

Sergey Petryashev,
+7(499)929-50-17; petsero@mail.ru

Sergey Sherbina,
+7(499)929-50-17; serg_msk89@mail.ru
Dmitry Kalichava,
+7(495)120-04-05; 2109962@gmail.com

Taymuraz Kaytukov,
+7(495)625-81-53; tkaytukov@gmail.com

Александр Михайлович Белостоцкий,
+7(499)706-88-10; эл. почта: amb@stadyo.ru

Павел Алексеевич Акимов,
+7(499)706-88-10;
эл. почта: pavel.akimov@gmail.com

Олег Александрович Негрозов,
+7(958)819-64-30;
эл. почта: genromgsu@gmail.com

Николай Олегович Петряшев,
+7(499)929-50-17; эл. почта: stadyo@stadyo.ru

Сергей Олегович Петряшев,
+7(499)929-50-17; эл. почта: petsero@mail.ru

Сергей Викторович Щербина,
+7(499)929-50-17;
эл. почта: serg_msk89@mail.ru

Дмитрий Котэвич Каличава,
+7(495)120-04-05;
эл. почта: 2109962@gmail.com

Таймураз Батразович Кайтуков,
+7(495)625-81-53;
эл. почта: tkaytukov@gmail.com

© Belostotsky A.M., Akimov P.A., Negrozov O.A., Petryashev N.O., Petryashev S.O., Sherbina S.V., Kalichava D.K., Kaytukov T.B., 2018



ПОЛИТЕХ
Санкт-Петербургский
политехнический университет
Петра Великого

Инженерно-строительный институт
Центр дополнительных профессиональных программ

195251, г. Санкт-Петербург, Политехническая ул., 29,
тел/факс: 552-94-60, www.stroikursi.spbstu.ru,
stroikursi@mail.ru

Приглашает специалистов проектных и строительных организаций,
не имеющих базового профильного высшего образования
на курсы профессиональной переподготовки (от 500 часов)
по направлению «Строительство» по программам:

П-01 «Промышленное и гражданское строительство»

Программа включает учебные разделы:

- Основы строительного дела
- Инженерное оборудование зданий и сооружений
- Технология и контроль качества строительства
- Основы проектирования зданий и сооружений
- Автоматизация проектных работ с использованием AutoCAD
- Автоматизация сметного дела в строительстве
- Управление строительной организацией
- Управление инвестиционно-строительными проектами. Выполнение функций технического заказчика

П-02 «Экономика и управление в строительстве»

Программа включает учебные разделы:

- Основы строительного дела
- Инженерное оборудование зданий и сооружений
- Технология и контроль качества строительства
- Управление инвестиционно-строительными проектами. Выполнение функций технического заказчика и генерального подрядчика
- Управление строительной организацией
- Экономика и ценообразование в строительстве
- Управление строительной организацией
- Организация, управление и планирование в строительстве
- Автоматизация сметного дела в строительстве

П-03 «Инженерные системы зданий и сооружений»

Программа включает учебные разделы:

- Основы механики жидкости и газа
- Инженерное оборудование зданий и сооружений
- Проектирование, монтаж и эксплуатация систем вентиляции и кондиционирования
- Проектирование, монтаж и эксплуатация систем отопления и теплоснабжения
- Проектирование, монтаж и эксплуатация систем водоснабжения и водоотведения
- Автоматизация проектных работ с использованием AutoCAD
- Электроснабжение и электрооборудование объектов

П-04 «Проектирование и конструирование зданий и сооружений»

Программа включает учебные разделы:

- Основы сопротивления материалов и механики стержневых систем
- Проектирование и расчет оснований и фундаментов зданий и сооружений
- Проектирование и расчет железобетонных конструкций
- Проектирование и расчет металлических конструкций
- Проектирование зданий и сооружений с использованием AutoCAD
- Расчет строительных конструкций с использованием SCAD Office

П-05 «Контроль качества строительства»

Программа включает учебные разделы:

- Основы строительного дела
- Инженерное оборудование зданий и сооружений
- Технология и контроль качества строительства
- Проектирование и расчет железобетонных конструкций
- Проектирование и расчет металлических конструкций
- Обследование строительных конструкций зданий и сооружений
- Выполнение функций технического заказчика и генерального подрядчика

По окончании курса слушателю выдается диплом о профессиональной переподготовке
установленного образца, дающий право на ведение профессиональной деятельности

